SPOLEČNOST-
ARMÁDA-
TECHNOLOGIE-
ŽIVOTNÍ
PROSTŘEDÍ

2017

Sborník 14. odborného semináře

Materiály a technologie ve výrobě speciální techniky

pořádaný pod záštitou firem

NITECH výroba a.s.
nitridační technologie, plazmová nitridace

mt.eu měřicí technika - morava
messtechnik - moravia
measurement technic - moravia

OLYMPUS

1. června 2017
UO Brno, ulice Šumavská 4, budova č. 8
Brno

Organizují

BVV Veletrhy Brno

Veletrhy Brno, a. s.

TnUAD v Trenčíne Fakulta špeciálnej techniky

Univerzita obrany Katedra strojírenství

ISBN: 978-80-7231-420-1

Již tradiční, XIV. odborný seminář "Materiály a technologie ve výrobě speciální techniky", se koná jako součást účasti AČR na veletrhu IDET 2017 ve dnech 31. 5. - 2. 6. 2017 v Brně, v České republice.

XIV. odborný seminář svým zaměřením na problematiku materiálů a technologií výroby speciální techniky, vytváří prostor pro výměnu zkušeností z oblasti výzkumu, vývoje a výroby speciální techniky včetně zabezpečení její jakosti. V těchto oblastech se řeší celá řada nových problémů a výměna zkušeností je jedním z prostředků jak přispět k rozvoji technické úrovně a kvality materiálního vybavení AČR a interoperabilitě s ostatními armádami NATO.

Všechny dodané příspěvky v anglickém, českém a slovenském jazyce jsou publikovány ve sborníku konference na CD. Anglicky psané příspěvky vybrané organizačním výborem budou publikovány v časopise MANUFACTURING TECHNOLOGY, v databázi SCOPUS.

Obsah:

Heat affected zone after cutting and welding of armoured high strength steels

Igor Barényi[1]
[1]Faculty of Special Technology, Alexander Dubcek University of Trencin. Pri Parku 19, 911 05 Trenčín. Slovak Republic. E-mail: igor.barenyi@tnuni.sk

Armox steels are armoured ultra-high strength martensitic steels with the usage in special technology. The steels are produced in the form of forged semiproducts as sheets and plates. These sheets are cut and mostly welded in a way to made the final product. The paper deals with heat affection of selected Armox steels after their cutting by plasma and laser and their welding with using MAG welding method where critical degradation of mechanical properties could occur in heat affected zone after application of these technologies. Experimental samples made of Armox 500 steel with using of these thermal based technologies are studied in the paper for evaluating selected heat affected zone parameters.

Keywords: high strength steel, martensite, tempering, armoured steel, hardness, microstructure

1 Introduction

The Armox steels are group of armoured middle alloyed steels with martensitic structure, heat treated on very high strength and hardness as well as good toughness. These properties result from specific production process of the steel where most important steps are minimizing of H, N and O content by the vacuum furnace and heat treatment consist of quenching with very rapid cooling and low tempering at temperatures about 150÷200 °C. If the final steel is exposed to the temperature above the 200°C some phase transformations take place in the microstructure and the degradation of mechanical properties needed for the steel usage occurs. These conditions are typical for secondary processing of the steel as are cutting or welding.

There are published several studies about microstructure changes of carbon or low alloyed steels after welding or plasma or laser cutting in scientific literature [1, 2]

Heat affected zone (HAZ) after the cutting by these processes could be classified to three different areas according that knowledge [3, 4]:

1. Surface area with full recrystallization to the austenite and back to pearlite, bainite or martensite (temperature range from A_3 to the solidus). The depth of this area is relatively low (about 50 μm) and depends on chemical composition of steel and parameters of used cutting process as are cutting speed or heat input. If martensitic transformation occurs in the area it may cause the internal stresses and consequently the crack creation.
2. Area with partial recrystallization (temperature range from A1 to A3) where the heating up period is very short and therefore the autenitization is just partial. There is new phase created as a result of partial austenitization beside origin microstructure phases. The amount of new phase decreases in relation to distance from surface. In contrast to full recrystallization area in surface layer, the heatig up temperature of this area is not so high and followed cooling is not so rapid. Therefore, the new created phases are more in steady state (bainitic or pearlitic type). The depth of this area is about 500 μm.
3. Transition area between HAZ and core material (heating up below A1) where any essential phase transformation is not present. Processes known from basics of tempering process take place in steels with martensitic structure. Morphology of martensite is changed from tetragonal to cubic tempered martensite, transformation of the residual austenite occurs and cementite and other carbides are created. This area could reach the depth of several millimetres from surface.

The first step of structure changes in area 1 and 2 is full or partial austenitizing of origin structure. The simplified model with equilibrium state of the strucure is mostly used to describe austenitizing but equilibrium pealitic structure is very rare in real steels because most of them are used in quenched state with martensitic structure as Armox steel are. Therefore, the austenitizing of these steels starts with more complex reverse martensitic transformation.

The reverse transformation mechanism of martensite to austenite and the volume fraction of created austenite have been studied in some steels by means of dilatometry, transmission electron microscopy and X-ray diffraction. It can be diffusion as well as difusionless process. The determining factors are temperature and heating rate. Below a heating rate of 10 $°C \cdot s^{-1}$ the reverse transformation of martensite to austenite occurs by diffusion, whereas it occurs by a diffusionless shear mechanism above 10 $°C \cdot s^{-1}$ s. After reversion treatment at low temperatures, filmlike austenite is observed along martensite lath boundaries, while reversion treatment at high temperatures produces granular austenite inside the martensite laths in addition to filmlike retained austenite. The volume fraction of austenite increases with increasing of reversion treatment temperature [5].

After partial or full austenizing in the form of reversrse martensitic transformation repeard standard transformation of austenite to martensite one of other transformation phases as bainite or pearlite according to cooling condition, when the temepraature in HAZ area starts to decrease. Therefore the final structure of areas of HAZ sffected by this means can be very complex and consist of many phases.

2 Material and Methods

Armox 500 ultra high strengh martensitic steel i sused for experiment. Armox steels are mainly used as a armor material and protection for vehicles, mobile containers and other components in armament as well as civil applications. Ballistic resistance of these steels are given by combination of high hardness and strength with optimal value of toughness in a view of materials characteristics. Armox steel were used in Slovakia for construction of Aligator army vehicle body, demining system Bozena or mobile army containers for modular communication system Mokys. Scientific research and development in production of those steels allows to reduce active thickness of armor on 50 % with the same ballistic resistance.

Basic mechanical characteristics and chemical composition of the Armox 500 steel are described in the table 1. Showed mechanical properties were evaluated on base unaffected material by standard tensile strength test (EN ISO 6892-1), Charpy impact test (EN ISO 148-1) and Brinell hardness test (EN ISO 6506-1). Chcemical composition was measured by spectral analyzer Spectrolab Jr CCD.

Tab. 1 Chemical composition and mechanical properties of examined steel Armox 500 [6]

Chemical composition [wt. %]	**C**	**Si**	**Mn**	**P**	**S**	**Cr**	**Ni**	**Mo**	**B**
	0,27	**0,23**	**1,10**	**0,014**	**0,009**	**0,81**	**1,58**	**0,7**	**0,004**

Mechanical properties	**Tensile strength R_m [MPa]**	**Yield strength $R_{p0.2}$ [MPa]**	**Toughness KCU [J]**	**Hardness [HBW]**	**Elongation A_5 [%]**
	1638	**1422**	**25**	**516**	**9**

Basic microstructure of this steel is shown in fig. 1. The microstructure consists of tempered martensite with assumed small amount of retained austenite. There are observed some carbides as a product of tetragonal martensite transformation to cubic tempered martensite during tempering.

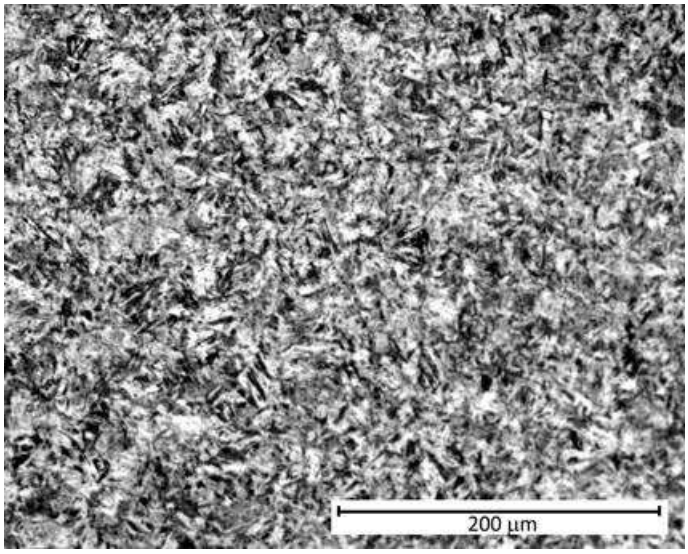

Fig. 1 Basic microstructure of Armox 500 steel

The objects of experiment are samples of Armox steel with heat affected zone (HAZ) after cutting by laser and plasma thermal processes and welded by using of MAG (Metal inert gas) arc welding. The basic parameters of all three used processes are shown in table 1, table 2 and table 3. Heat affected zones after application of these thermal processes were evaluated by microhardness Vicker's test on samples with three thickness – 4, 5 and 8 mm.

Tab. 2 Basic parameters of used laser cutting process

Thickness [mm]	**Laser Output [W]**	**Frequency [Hz]**	**Cutting speed [m.min^{-1}]**
4	**1900**	**10000**	**3,1**
5	**3200**	**10000**	**2,9**
8	**3200**	**10000**	**2,9**

Tab. 3 Basic parameters of used plasma cutting process

Thickness [mm]	Voltage [V]	Current [A]	Cutting speed [m.min^{-1}]	Plasma gas: O_2
4	120	30	0,9	
5	125	45	0,85	Supplementary gas: O_2 / N_2
8	130	50	0,55	

Tab. 4 Basic welding parameters of used MAG method

Current [A]	Voltage [V]	Polarity	Wire feed rate [m·min^{-1}]	Filler material
145÷155	27-29	= (+)	15-16	Thermanit X

3 Heat affected zone after cutting processes

There were measured the microhardness profile in cross setion to the cut face on three group of experimental samples with three difrent thickness. Course of microhardnes of Armox steel with thickness 5 mm cut by plasma and laser is shown in fig. 2 as an example whereby corresponding microstructures of HAZ are in fig. 3 and fig. 4. All measured microhardness courses have the chracteristic shape with three basic areas of heat affected zone:

- increase of hardness in narrow area close under the cut face (heating up to the temperature in austenite area and rapid cooling);
- decrease of hardness with minimum in depth about 0,5÷1 mm under the cut face (uncontrolled tempering of origin martensitic structure);
- slow increase of microhardness to the value of basse material hardness.

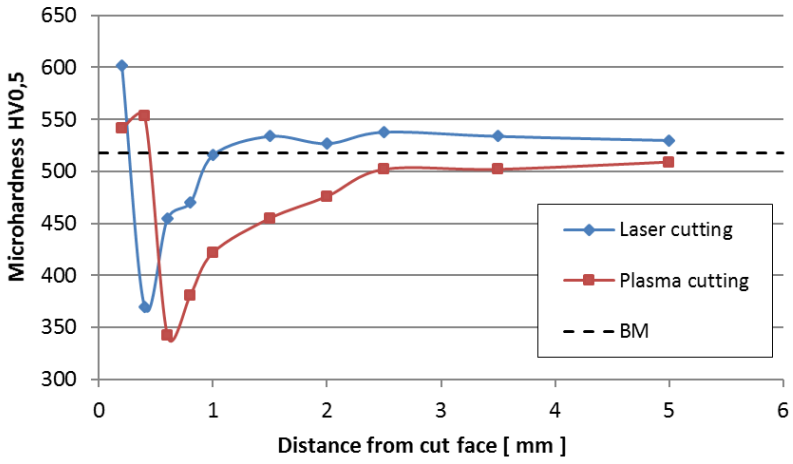

Fig. 2 Course of microhardness in cross section to the cut face for Armox 500 steel with thickness 5 mm cut by plasma and laser

The width of uncontolled tempering area is bigger in case of plasma cutting. This process uses lower cutting speeds and plasma arc is greater heat input source than laser beam. The width of uncontrolled tempering area also depends to cut thickness because lower cutting speed and more power output is required for cutting of bigger thicknesses.

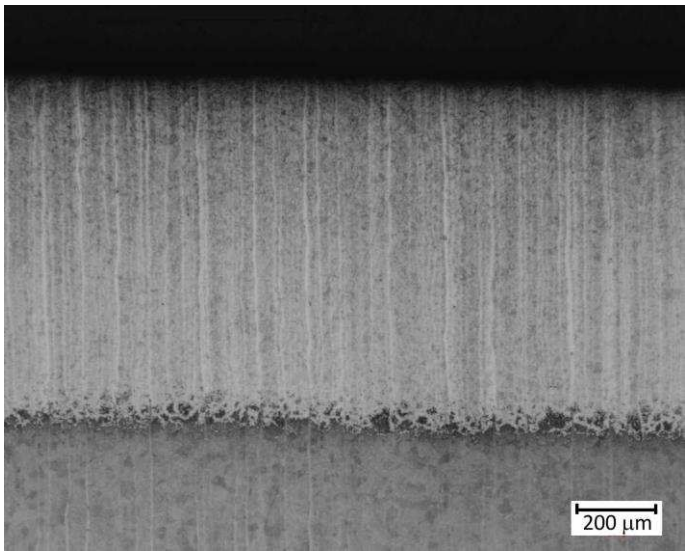

Fig. 3 HAZ of Armox 500 steel with 5 mm thickness cut by laser

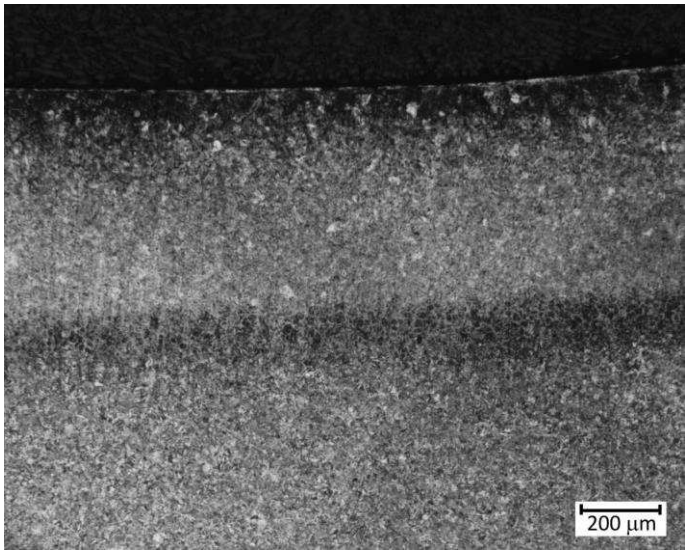

Fig. 4 HAZ of Armox 500 steel with 5 mm thickness cut by plasma

Also, depths of heat affected zones were measured from microhardnes courses and avereaged values for all three material thicknesess are shown in table 5. The values of depth are determined by modified method for hardened surface based on limitet hardness as a criterion for reading the depth value from hardness course. Morover, the part of hardness courses where the hardness slowly increases is used only for depth of HAZ evaluating. The hardness of base material is considered as the limit hardness.

The percentage decrease of hardness in minimal point of microhardness course in relation to the base material hardness is also calculated and shown in table 6. The values proved the decrease about 20÷40 % of base material hardness in critical area of heat affected zone. The decrease is more noticeable in plasma cutting than laser cutting.

Tab. 5 Depths of HAZ for laser and plasma cutting

Thickness [mm]	**Depth of heat affected zone [mm]**	
	Laser cutting	**Plasma cutting**
4	**0,77**	**2,40**
5	**1,06**	**2,63**
8	**3,30**	**4,80**

Tab. 6 Percentage decrease of hardness in minimal point of microhardness course in relation to the base material

Thickness [mm]	Percentage decrease of hardness in minimal point of microhardness course in relation to the base material [%]	
	Laser cutting	Plasma cutting
4	18,1	26,2
5	28,6	34,0
8	37,1	40,4

4 Heat affected zone after MAG welding

There is shown course of microhardness across the weld joing of Armox 500 steel made by MAG welding in fig. 5. Some characteristic areas of welding joint are noticeable in the course. Zone with highest decrease of microhardness (a) in the center of the weld joint which is about 5÷6 mm wide and almost completely consists of filler material only. Mechanical properties of this part correspond to used consumable properties and is not consodered as a parrt of heat affected zone. The choice of welding consumable material for Armox steel is a separate problem. High strength ferritic cosumable material or less strength but tougher autenitic material with higher resitance agains hydrogen craks and with lower density of internal stresses could be chosen. Even the high strength consublable is used, it's strength is still less than base material. Therefore, the weld metal area is the weakest part of weld joint.

Next characteristic zone of the course is the area with increased hardness with comparison to the base material hardness. This is the area with full recrystallization and consequent repeard martensitic transformation what results to the high hard martensitic needle structure with residual austenite (fig. 6). The wide of this area is relatively narrow (1÷1,5 mm).

Last characteristic area (c) is typical for rapid decreasing of hardness and the slow increase to the value of base material hardness. It is the area with uncontrolled tempering and relative decrease of hardness in the area is about 30 % for Armox 500 steel in comparison to the base material hardness. Microstructure of the area (fig. 7) is consisted of ferritic – carbidic mixture with lighter boundaries borders.

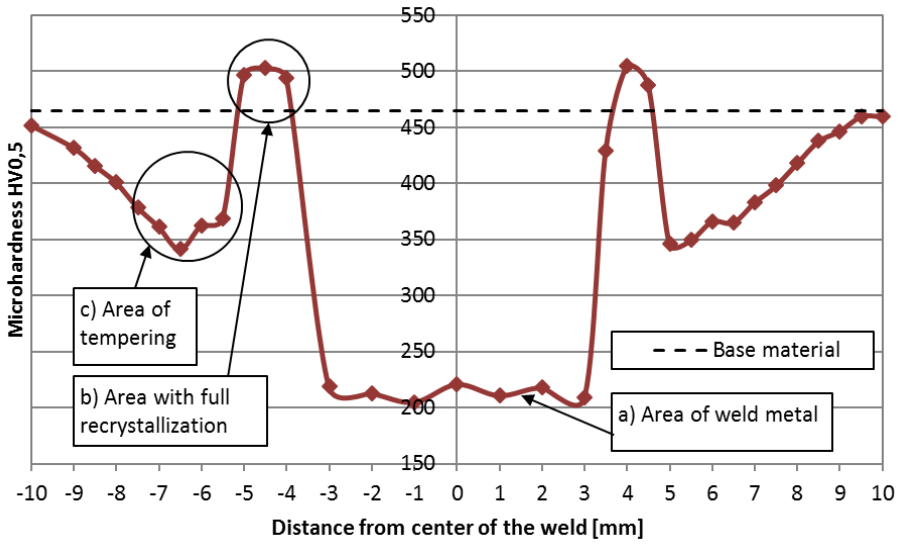

Fig. 5 Course of microhardness across the weld joint of Armox 500 steel made by MAG welding

Last characteristic area (c) is typical for rapid decreasing of hardness and the slow increase to the value of base material hardness. It is the area with uncontrolled tempering and relative decrease of hardness in the area is about 30 % for Armox 500 steel in comparison to the base material hardness. Microstructure of the area (fig. 7) is consisted of ferritic – carbidic mixture with lighter boundaries borders.

Showed course of microhardness and the corresponding width of HAZ according to total thickness of samples proved that Armox 500 steel has high sensitivity of heat affection by welding.

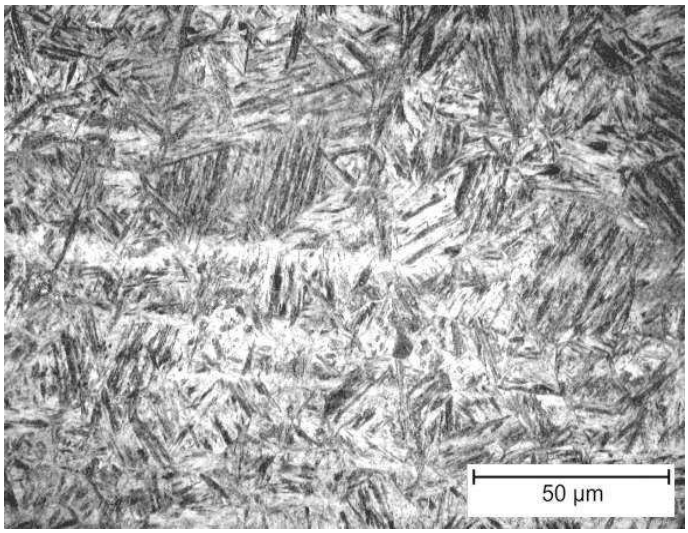

Fig. 6 Microstructure of HAZ area with full recrysrtallization

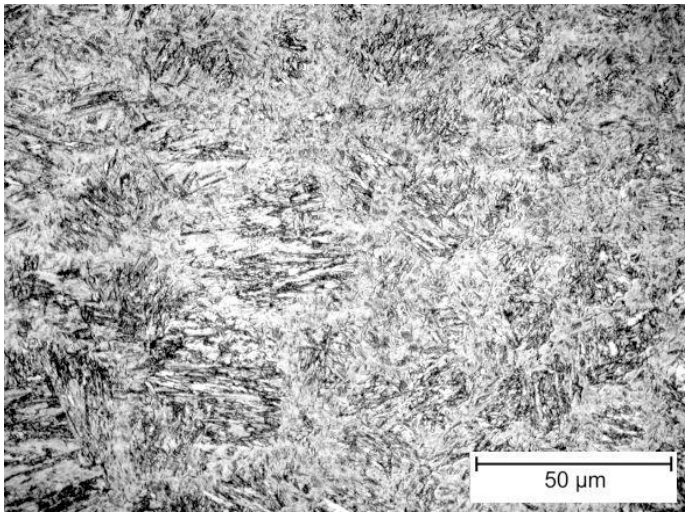

Fig. 7 Microstructure of HAZ area with uncontrolled tempering

5 Conclusions

The processing of ultra high strength martensitic steels Armox with using the processes based on thermal transfer causes the formation of significant heat affected zone. The width of the HAZ depends on heat input brought to the processed material which is a function of specific welding or cutting parameters.

Described influence may affect final quality of processed product with smaller intersections mainly. Due to these reasons is advisable to cut Armox materials by using of the water jet cutting process which is without the heat affection in principle. Welding of Armox is more problematic because the heat transfer is essential to made the weld joint. Optimizing of welding parameters considering heat input could help to minimize heat affection. Also, some progressive welding method could be used besides conventional arc welding methods as is friction stir welding that using lower welding temperatures. However, FSW of Armox steel could be difficult due to its very high hardness.

Acceptance of these recommendations supports the increasing of reliability and safety of products made of Armox steels as are civil and army car protection, building protection or mobile army containers construction.

Acknowledgement

This work was supported by the Slovak Research and Development Agency under the contract No. APVV-15-0710.

References

[1] BELHADJ, A., BAUDOUIN, P., HOUBAERT, Y. (2002). Simulation of the HAZ and magnetic properties of laser cut non-oriented electrical steels, Journal of Magnetism and Magnetic Materials, Volume 248, Issue 1, July 2002, Pages 34-44, ISSN 0304-8853, http://dx.doi.org/10.1016/S0304-8853(02)00064-1.

[2] RAGU NATHAN, S. et al. (2015). Effect of welding processes on mechanical and microstructural characteristics of high strength low alloy naval grade steel joints. Defence Technology. Elsevier B.V, No. 3. ISSN 2214-9147.

[3] HATALA, M. (2005). The Principle of Plasma Cutting Technology and Six Fold plasma cutting. In: Fascicle Mechanics, Tribology, Machine Manufacturing Technology, vol. XIX,. ISSN 1224-3264

[4] HÍREŠ, O., HATALA, M. (2009). Cutting of material by laser beam. TnUAD v Trenčíne, ISBN 978-80-8075-365-8.

[5] SEOK-JAE, L. YONG-MIN a YOUNG-KOOK L. (2009). Reverse transformation mechanism of martensite to austenite. Materials Science and Engineering A. Elsevier, No. 515, s. 32-37. ISSN 0921-5093.

[6] BARÉNYI, I. (2017). Changes of material characteristics of high strength martensitic steels at their cutting and welding / Scientific monograph, TnUAD, 2017. - 131 s.

Evaluation of tribological features of polymeric materials

Lenka Bartošová[1]
[1]Faculty of Special Technology, Alexander Dubcek University of Trencin. Pri Parku 19, 911 05 Trenčín. Slovak Republic. E-mail: lenka.bartosova@tnuni.sk

The paper deals with effects of radiation by accelerated electrons on a tribological feature, particularly a friction factor. The friction process can be evaluated through a friction factor, which is influenced by a size of load, sliding speed, temperature, surface roughness and other operational parameters. The measured values of the friction factor were taken with UMT TriboLAB device at Faculty of Special Technology at Alexander Dubcek´s Trencin University in Trencin. The paper also deals with a study of effects of ratiation through accelerated electrons on sliding features of polymeric materials. It informs about possible netting of polymeric materials through ionising radiation. It examines an effect on radiation through accelerated electrons on sliding features of polymeric materials. In the second part, it describes an experiment evaluation assessing sliding features of a basic and irradiated materials. Finally it evaluates an effect of irradiation on features of some chosen materials.

Keywords: Wear, polymers, radiation mesh netting, friction

1 Introduction

Recently the polymer materials have been applied more often in different industries. This is due to their easy process ability, low weight, corrosion resistance and especially its affordability. Large role pertains to the possibility of improving their properties by irradiation, in such a way the conventional polymers get closer through their newly acquired properties to others, highly durable materials. Tribology is an interdisciplinary science that solves the problems of friction, wear and lubrication with a relative motion of two surfaces. [1] Ionizing irradiation is irradiation that when transiting through an environment it results in its ionization. That means that from initially electrically neutral atoms it forms positive and negative atoms. According to the nature of the ionization process the ionizing radiation can be divided into direct ionizing and indirectly ionizing one. Directly ionizing one is formed by charged particles (electrons, positrons, protons, particles α and β), with sufficient kinetic energy to cause ionisation. Indirectly ionizing irradiation is formed by non-charged particles (photons, neutrons). These particles do not ionize the environment, but when interacting with it, they release the secondary, directly ionizing particles. The ionisation is then caused by those secondary particles. [2]. According to the behaviour of electric and magnetic fields we distinguish α rays, ß rays and γ-rays. A radiation is made up of helium nuclei. β radiation consists of fast electrons or positrons with a large scale of energies (up to 16,6 MeV). There are two types of such irradiation namely the β+ irradiation and β-. Radiation γ is electromagnetic radiation with a very short wavelength (10^{-11}-10^{-13} m), formed by photons - particles without charge, which differs only in their energy. Radiation netting is a technology using beta or gamma radiation for improving the mechanical, chemical and thermal properties of the plastic materials. The principle of radiation netting is a bombing of molecules with accelerated electrons or gamma rays. This energy is absorbed by the irradiated material; there is formation of free radicals which interact sequentially to form the desired connection among adjacent chains – a needed network. Netting of polymer materials with accelerated electrons is performed using an electron accelerator, wherein the hot cathode emits electrons which are accelerated in an electromagnetic field.

Fig. 1 UMT TriboLAB Tribological device

UMT TriboLAB (Fig.1) is a fully electronic, universal testing equipment intended to carry the nano, micro and macro tribological and mechanical testing of different types of materials. It has a synchronized combination of linear and rotational movement of the different axes (x, y, z), which makes it suitable for use for different types of tests such as Ball / Pin-on-Disk, Block-on-Ring, Ball / pin-on-plate indentation and scratch tests. The tests can be carried out in the control chamber at a temperature of -40 ° C to 1000 ° C, relative humidity 5 to 95%, under vacuum, with lubricants.

2 Experiment to asses sliding features of a basic and irradiated material

The samples of materials provided by the TechPlasty Žilina, Ltd. Company were used for an experiment – namely PET – polyetyleneterefthalate, PTFE – polytetraphluoretylene and PE2000C – high molecular weight polyethylene modified with glass microspheres. Irradiation of testing samples was performed with a linear electron accelerators UELR-5-1S at a workplace of the University Centre of electron accelerators of the Slovak Medical University (SMU UCEA) in Trencin. The UELR-5-1S accelerator is assigned to perform various radiation technological processes and radiation sterilization using a beam of electrons accelerated in the developed zone and also to carry out research work in these areas. [4]

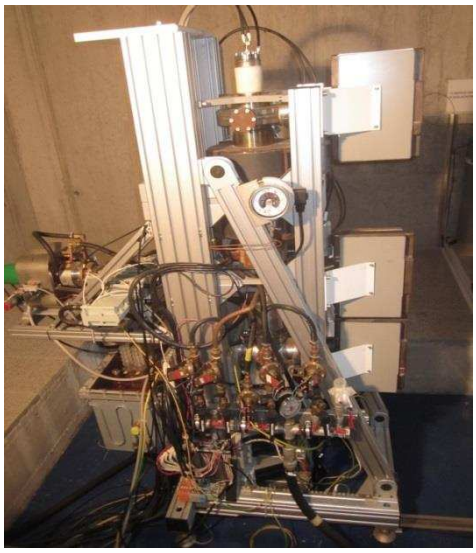

Fig. 2 UELR–5-1S accelerator

The testing samples were irradiated with accelerated electrons doses of 33 kGy, 129 kGy to 300 kGy. Experimental evaluation of the sliding properties of irradiated and non-irradiated materials was carried out on the universal tribological UMT TriboLAB testing facility in a laboratory of the Faculty of Special Technology. Specifically, the friction factor was defined for particular materials before and after irradiation through a Ball-on-Flat method. The measurement was performed on 12 pieces of samples (4 pieces of PET, 4 pieces of PTFE, 4 pieces of PE2000C) namely from each kind of material 1 piece of each non-irradiated material as well as 1 piece of irradiated ones by doses of 33 kGy, 129 kGy a 300 kGy. For each sample, two measurements were made with a different time. For a measurement No.1 the time of measurement was 60 sec. and for the measurement Nr. 2 the time of measurement was chosen 120 s. During the measurement the measuring device was taking the measurements every one hundredth of a second. During the measurement No.1 (60 sec) we obtained 6000 values and during the measurement Nr.2 (120 sec) 12 000 values. These values are then adjusted through the Dixon test. It's a test aiming to exclude the minimum or maximum values in the data set. For its implementation, the values are arranged by size in an ascending order. This test is performed regarding the fact, that a representative of the group will be the arithmetic average along with a standard variation and their calculation is sensitive to extreme values. After having excluded extreme valued, we calculated the arithmetic mean and a standard variation using the weighted form.

Arithmetic average:

$$\overline{x} = \frac{\sum_{i=1}^{n} x_i . n_i}{n} \tag{1}$$

where: x_i – the measured values of the friction factor,
n_i – absolute multiplicity of particular values,
n – a total number of measurements.

Standard variation:

$$\sigma = \sqrt{\frac{\sum_{i=1}^{n}(x_i - \bar{x})^2 . n_i}{n}} \tag{2}$$

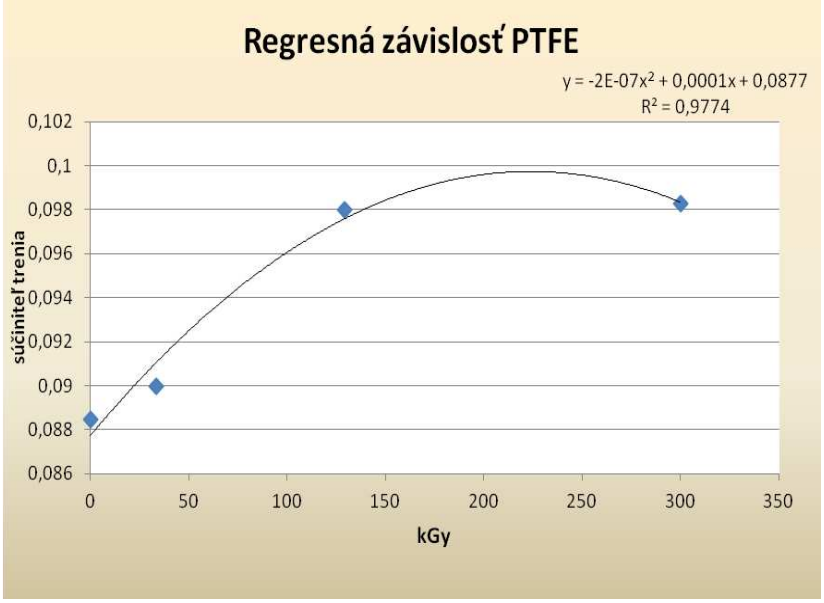

Fig. 3 Graph of a PTFE regression correlation

The graph (Fig.3) shows the quadratic regression correlation between the friction factor and radiation doses (33 kGy, 129 kGy a 300 kGy). Input variables are the individual doses of radiation and the output variable is the mean value of a friction factor. If a sample has not been irradiated, such sample is considered as an etalon. It results from a given graph that with an increasing value of the irradiation, the value of a friction factor increases as well, namely up to the value 250 kGy, then a value of a friction factor will decrease. We defined this value of radiation using first derivative of the obtained quadratic correlation.

$$y = -2 \cdot 10^{-7} \cdot x^2 + 0{,}0001 \cdot x + 0{,}0877$$

$$y' = -4 \cdot 10^{-7} \cdot x + 0{,}0001 = 0 \quad \Rightarrow \quad x = \frac{-0{,}0001}{-4 \cdot 10^{-7}} = 250$$

Value of a determination factor is 97.74%, which is a high correlation between input and output variables.

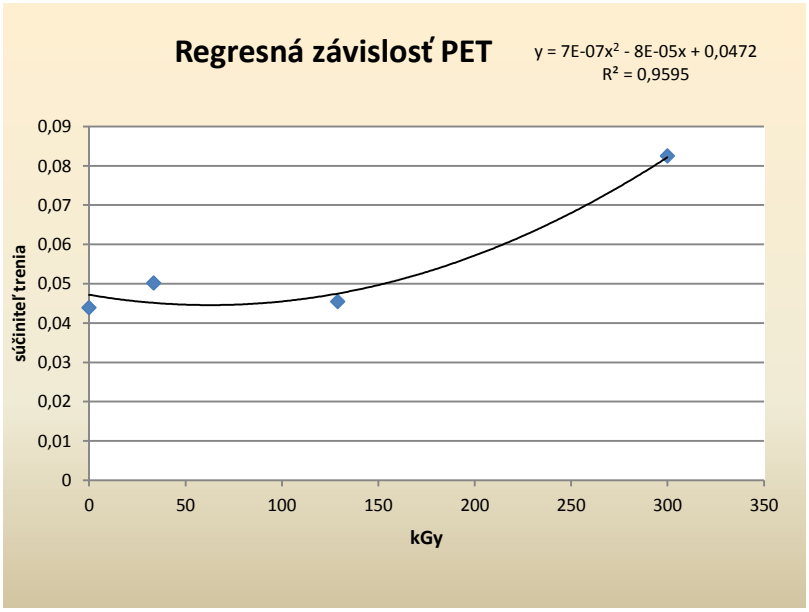

Fig. 4 Graph of a regression relation PET

The graph (Figure 4) shows that with increasing radiation value, the value of a coefficient at first decreases and then

gradually increases. Its value decreases up to a 57,143 kGy radiation dose. The determination coefficient is equal to 95,95%, that is a high correlation between input and output variables.

$$y = 7 \cdot 10^{-7} \cdot x^2 - 8 \cdot 10^{-5} x + 0{,}0472$$

$$y' = 14 \cdot 10^{-7} \cdot x - 8 \cdot 10^{-5} = 0 \quad \Rightarrow \quad x = \frac{8 \cdot 10^{-5}}{14 \cdot 10^{-7}} = 57{,}143$$

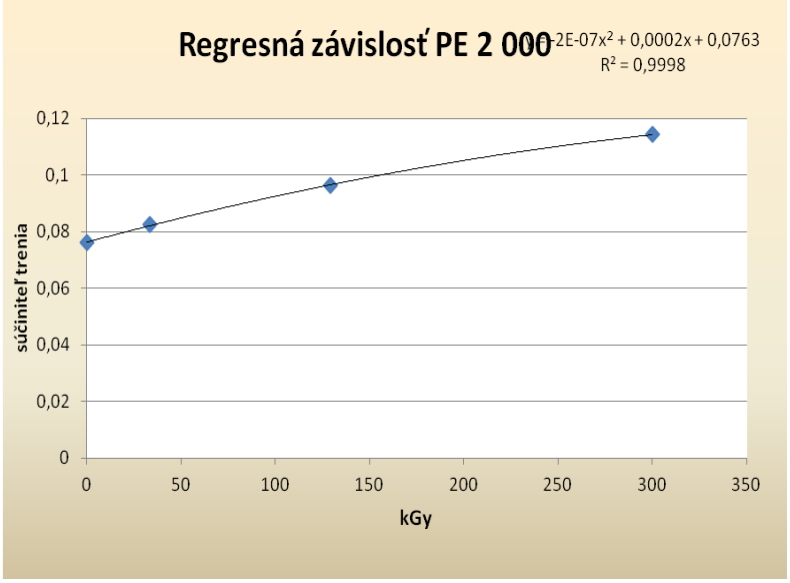

Fig. 5 Graph of regression relation PE2000C

It results from a given (Fig.5) graph, that the increasing value of irradiation will gradually increase the value of the friction factor. Due to the quadratic correlation and a shape of a parabola we find the maximum value of irradiation using derivation of a regression function. For this value the friction factor will be still increasing.

$$y = -2 \cdot 10^{-7} \cdot x^2 + 0{,}0002x + 0{,}0763$$

$$y' = -4 \cdot 10^{-7} \cdot x + 0{,}0002 = 0 \quad \Rightarrow \quad x = \frac{-0{,}0002}{-4 \cdot 10^{-7}} = 500$$

The determination factor equals 99,98%, that is a high correlation between an input and output parameter.

3 Conclusion

The paper deals with the effect of irradiation with accelerated electrons on the tribological property, which is the friction factor. The friction process can be evaluated through a friction factor, which is affected by the load, a sliding speed, temperature, surface roughness and other operating parameters.

The values of a friction factor were measured with the UMT TriboLAB tribological device at the Faculty of Special Technology at the Trencin University of Alexander Dubcek in Trencin. The materials PTFE, PET and PE2000C were used. 4 samples were measured for each material, whereby one sample was not irradiated; the second one was irradiated with a dose of 33 kGy, the third sample with 129 kGy and the fourth with 300 kGy. The irradiation of the samples was performed with a UELR-5-1S linear accelerator of electrons at a working place of the University centre of electron accelerators at the Slovak medical university in Trencin.

Subsequently two measurements were made on each sample, the first one lasted 60 sec, the second one 120 seconds. The value of a measurement was recorded within one hundredth of a second. These values were statistically processed using the Dixon´s test and through a computation of a location characteristics, represented through an arithmetical average and through a variability represented by a standard variation. By applying a regression analysis through a quadratic correlation, it was found that in the studied types of materials, that with increasing doses of irradiation the friction factor increases or decreases.

Acknowledgement

This work was supported by the Slovak Research and Development Agency under the contract No. APVV-15-0710.

References

[1] BLAŠKOVIČ, P.- BALLA, J.- DZIMKO, M. 1990. Tribológia. 1. vyd. Bratislava: ALFA, 1990. 360 s. ISBN 80-05-00633-0.

[2] ŠVEC, J. 2005. Radioaktivita a ionizující záření. 1. vyd. Ostrava: Sdružení požárniho a bezpečnostního inženýrství v Ostravě, 2005. 36 s. ISBN 80-866-3462-0.

[3] Charakteristiky ionizujícího záření. [online]. 2011. [cit. 2016-03-20]. Dostupné na internete: <http://fbmi.sirdik.org/1-kapitola/13/131.html>.

[4] Interné materiály UCEA SZU Trenčín

[5] POŠTA, J. – DVOŘÁK, M. – VESELÝ, P. 2002. Degradace strojních součástí. [online]. 1 vyd. Praha: Česká zemědělská univerzita, Technická fakulta, 2002. 67 s. [cit. 2016-03-02]. Dostupné na internete: <http://degradace.tf.czu.cz/>. ISBN 80-213-0967-9.

[6] DUCHÁČEK, V. 2006. Polymery, výroba, vlastnosti, zpracování, použití. 2 vyd. Praha: Vysoká škola chemicko-technologická v Praze, 2006. 280 s. ISBN 80-7080-617-6.

[7] DANĚK, M. a kolektív 2015. Radiačné sieťovanie – metóda zlepšovania vlastností polymérov. [online]. © 2009 – 2016. [cit. 2013-04-02]. Dostupné na internete:<http://www.plasticportal.sk/sk/radiacne-sietovanie-metoda-zlepsovania -vlastnosti-polymerov-1-cast/c/2641>.

[8] Interné materiály TechPlasty, s.r.o. Žilina

[9] AUSPERGER, A. 2015. Technológie zpracování plastů. Svitavy: Střední odborní učiliště Svitavy, 2015. ISBN 978-80-88058-77-9.

[10] LAHUČKÝ, D. – HOLLÝ, S. – ŠTEININGEROVÁ, J. 2009. Tribológia, tribotechnika. Trenčín: Trenčianska univerzita Alexandra Dubčeka v Trenčíne, 2009. ISBN 978-80-8075-429-7.

[11] SMETANOVÁ, S. 2016. Vplyv ožarovania urýchlenými elektrónmi na klzné vlastnosti vybraných materiálov. Trenčín. Diplomová práca.

Riziká a ich vplyv na kvalitu produktov špeciálnej techniky

Risks and their impact on the quality of specialty products

Viliam Cibulka[1]
[1]Fakulta špeciálnej techniky, Trenčianska univerzita Alexandra Dubčeka v Trenčíne, Pri parku 19, 91106 Trenčín, Slovensko, E-mail: viliam.cibulka@tnuni.sk

V príspevku je predstavený postup hodnotenia rizík kvality produktov špeciálnej techniky, ktorý zohľadňuje novelizované požiadavky na riziká podľa ISO STN EN 31000:2011 a ISO STN EN 9100:2015 v kontexte s používanými súbormi štandardov noriem AQAP a novelizovaných noriem rady STN ISO. Aplikovaním tohto postupu sa dosahujú lepšie odhady a spôsob analýzy a hodnotenia rizík (známych, ale i skrytých) v dodávkach produktov špeciálnej techniky pre odberateľov. Efektívnym postupom sa javí budovanie databáz rizík pre jednotlivé druhy špeciálnej techniky, čo umožňuje dosahovať lepšie výsledky pri kontrole dodávanej kvality produktov špeciálnej techniky.

Kľúčové slová: riziko, kvalita, norma, postup hodnotenia, databáza

1 Úvod

Riadenie rizík procesov výroby v organizácii je to základná a nevyhnutná podmienka pre jej existenciu a úspešné fungovanie na trhu. Týka sa to i organizácií, ktoré dodávajú produkty špečiálnej techniky. Dôsledné riadenie priebehu rizík umožňuje dosiahnutie plánovaných cieľov a tiež predchádzať ich nežiaducim vznikom. Aplikovaním takéhoto postupu v organizácii sa vytvárajú podmienky na dosiahnutie väčšej dôvery u zamestnancov podniku, ale hlavne u zákazníkov, odberateľov. Rovnako umožňuje navrhnúť správne rozhodnutia, vrátane efektívnejšieho využitia času na riešenie rizík a tiež zdrojov na zabezpečenie plánovaných cieľov. Čo je dôležité, aplikovanie riadenia rizík redukuje rizikový potenciál organizácie a tiež procesy a priebehy rizík sú pri jeho aplikovaní efektívnejšie.

Pre oblasť riadenia rizík sa využíva norma STN EN ISO 31000:2011 [14], ako celosvetový štandard pre všetky predpokladané aplikácie, je základná a záväzná pre všetky organizácie. Pri jej implementovaní je potrebné zohľadniť veľkosť a druhy jednotlivých potenciálnych rizík v organizáciách. Norma je integrovateľná do existujúcich systémov riadenia a podnikových procesov, vrátane existujúcej organizačnej štruktúry organizácie. V súčasnosti jej zásady sa požadujú uplatňovať i v novo zavádzanej norme STN ISO 9001:2015 [12], v ktorej sa kladie dôraz na nepretržitý jej preventívny charakter vo všetkých jej oblastiach zamerania. Zároveň sa uskutočňuje i revízia normy STN ISO 14001:2015 [11] z hľadiska jednoduchšieho aplikačného integrovania s normou STN ISO 9001:2015 a tiež proaktívnych iniciatív na ochranu životného prostredia, zohľadnenia životného cyklu produktov a služieb a environmentálnych aspektov.

Základom „filozófie“ riadenia rizík (obr. 1) podľa STN ISO 31000:2011 sú dva paralelné procesy a to komunikácia a konzultovanie a monitorovanie a kontrolovanie. Tým sa dosahuje oveľa výkonnejšie riadenie rizík procesov. Proces *„monitorovanie a kontrolovanie“ je kontrolný proces, ktorý riadenie rizík procesov zabezpečuje a kontroluje pomocou indikátorov, ukazovateľov alebo porovnávacích (kvalitatívnych) hodnôt. Takýmto spôsobom sa dosahuje vyššia úroveň kontrolovateľnosti a porovnateľnosti rizík procesov v rámci riadenia rizík.*

Proces „komunikovanie a konzultovanie“ zabezpečuje, že takto realizované riadenie rizík zahrňuje tiež proces učenia. Tento proces slúži všetkým záujmovým skupinám v organizácii. Pre úspešné riadenie rizík je dôležité, že poznatky všetkých pracovníkov, čiže interných záujmových skupín sú zohľadňované. *Tiež očakávania a priania externých záujmových skupín, čiže zákazníkov, obchodných partnerov, spoločností ovplyvňujú tento proces a sú stredobodom pozornosti riadenia rizík podľa STN EN ISO 31000.*

Proaktívny charakter zamerania normy STN ISO 31000 umožňuje, že riadenie rizík sa viac zameriava na zabezpečovanie funkcií včasného varovania. Známe sú preventívne opatrenia, ktoré umožňujú rizikám včas predchádzať, ako napr. ich eliminovaním, substitúciou alebo ich znižovaním (redukovanie). V spojení s funkciami včasného varovania sa vhodne proaktívne dopĺňajú. Čo znamená to, že riziká je možne ešte pred ich vznikom úspešne zvládnuť.

Zavedenie systému manažérstvo rizík v organizácii vytvára podmienky na [7]:

- zvýšenie pravdepodobnosti dosiahnutia podnikateľských zámerov a cieľov,
- zlepšenie využitia príležitostí,
- zvýšenú dôveru zákazníkov, pracovníkov a zainteresovaných strán,
- vytvorenie spoľahlivého základu pre prijímanie rozhodnutí a plánovanie,
- zvýšenie efektívnosti umiestnenia a využívania zdrojov,
- zlepšenie efektívnosti procesov vo výrobe,
- zlepšenie prevencie strát a manažérstva udalostí,

- minimalizovanie strát,
- zlepšenie organizačnej a procesnej výkonnosti.

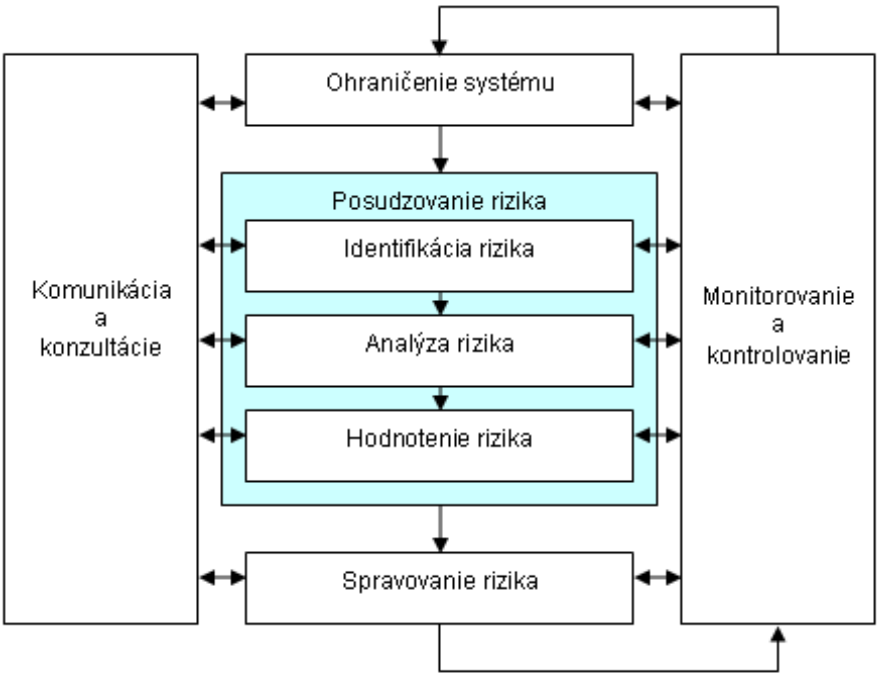

Obr. 1 Proc*esy riadenia rizík podľa ISO 31000* [14]

2 Postupy riadenia rizika dodávok produktov špeciálnej techniky

Produkty určené na zaistenie obrany štátu sú svojim charakterom vysoko špecifické. Vstupom Slovenskej republiky do NATO je zabezpečovanie kvality produktov dodávaných pre potreby rezortu obrany riadené štandardizačnou dohodou NATO STANAG 4107 „Vzájomné uznávanie štátneho overovania kvality a použitie spojeneckých publikácií na kvalitu AQAP", zákonom NR SR č. 11/2004 Z. z. o obrannej štandardizácii, kodifikácii a štátnom overovaní kvality a spojeneckými publikáciami zmluvného typu AQAP.

Pri obstarávaní produktov pre rezort obrany je zmluvný dodávateľ povinný splniť termíny, podmienky a požiadavky kontraktu a nepretržite udržiavať systém manažérstva kvality podľa prv definovaných podmienok v predchádzajúcej kapitole tohto príspevku. Overovanie kvality produktov je tiež zabezpečované štátnou organizáciou (úradom) a uskutočňuje sa na úrovni štátneho overovania kvality produktov. Pri overovaní kvality produktov sa aplikujú nasledovné súbory štandardov AQAP noriem, v ktorých sú postavené požiadavky v porovnaní so štandardnými ISO normami na podstatne vyšej úrovni, t. zn. i z hľadiska potenciálneho rizika kvality dodávky špeciálnej techniky.

Súbor štandardov AQAP radu 2000 obsahuje politiku, zásady, pokyny a zmluvné požiadavky NATO na overovanie kvality, ktoré zahŕňa i norma STN EN ISO 9001:2015. V tejto ISO norme sú definované požiadavky v systéme manažérstva kvality, vrátane povolených výnimiek. Tento nový prístup, ktorý je uvedený v tejto norme vyvolal nárast požiadaviek na štandardy NATO rady AQAP. Súčasťou zásad tohto štandardu je i napr. princíp stupňovitého rozvrhnutia požiadaviek na overovanie kvality, čo znamená, že na produkty s nízkym výskytom rizík sa požiadavky na overovanie kvality nezvyšujú, zatiaľ čo pre produkty s vyšším výskytom rizík sa nariaďuje rozsiahlejšie a náročnejšie overovanie kvality. Zásady definované v štandardoch AQAP radu 2000 obsahujú základné zásady integrovaného systémového prístupu v rámci organizácie k dosahovaniu kvality produktov a služieb počas celého životného cyklu.

AQAP-2110 - Požiadavky NATO na overovanie kvality pri návrhu, vývoji a výrobe [4]. Štandard obsahuje požiadavky na dodávateľa, ktoré pri vhodnom používaní poskytujú istotu, že dodávateľ je spôsobilý dodávať produkty vyhovujúce zmluvným požiadavkám odberateľa. Využitie tohto štandardu sa uplatňuje v zmluve (kontrakte) vtedy, ak sú požiadavky definované formou funkčných a technických požiadaviek a dodávateľ je zodpovedný za návrh, vývoj a výrobu. Súčasťou tohto štandardu je napr. Dodatok NATO, „Dodávateľ musí vytvoriť, dokumentovať, zaviesť, posudzovať a efektívne zlepšovať ekonomický systém, nevyhnutný k plneniu zmluvných požiadavkou, v zhode s týmto štandardom, ktorý zahŕňa požiadavky STN EN ISO 9001:2015“. Útvar štátneho overovania kvality má právo žiadať od dodávateľa objektívny dôkaz, že tento systém vyhovuje požiadavkám tohto štandardu a že je efektívny. Dôkaz môže byť overený formou posudzovania procesov (dokumentácia) alebo formou certifikácie (prvá, druhá alebo tretia strana). Ďalšie špecifické požiadavky NATO vyplývajúce z tohto štandardu sa môžu týkať napr. spoľahlivosti

a udržiavateľnosti produktu, vrátane procesov jeho návrhu. Tieto musí dodávateľ dokladovať príslušnou dokumentáciou a prv uvedené procesy musia byť komplexne riadené, vrátane dokumentácie od subdodávateľov.

AQAP 2120 - Požiadavky NATO na overovanie kvality pri výrobe [5]. Základný cieľ tohto štandardu je rovnaký ako pre AQAP-2110, pretože je zameraný opäť na dodávateľa. Tzn., že obsahuje požiadavky, ktoré pri vhodnom používaní poskytujú istotu, že dodávateľ je spôsobilý dodávať produkty vyhovujúce zmluvným požiadavkám odberateľa.

Ako špecifické požiadavky vyplývajúce zo štandardu NATO je možné uviesť napr. „Dodávateľ alebo subdodávateľ musia poskytnúť objektívny dôkaz, že v priebehu plánovania zohľadňujú riziká a tiež procesy identifikovania rizík, analýzy rizík, riadenia rizík a eliminovania rizík. Všetky prv uvedené procesy vzťahujúce sa na riziká sú priebežne aktualizované". K prv uvedeným špecifickým požiadavkám patrí tiež ďalšia špecifikácia štandardu NATO, čo znamená, že „Dodávateľ musí zabezpečiť vytvorenie komunikačného kanála s útvarom pre ŠOK (Štátne overovanie kvality) alebo organizáciou štátnej správy alebo organizáciou NATO. Dodávateľ musí oznámiť prv uvedeným odberateľom zmeny, ktoré ovplyvňujú kvalitu produktu alebo systému manažmentu kvality. Zároveň dodávateľ musí zabezpečiť prenos potrebných požiadaviek vyplývajúcich zo zmluvy s odberateľom k subdodávateľovi takým spôsobom, že sa odvoláva na stanovené požiadavky zo zmluvy, vrátane príslušných platných štandardov v krajine. Vo všetkých druhoch dokumentácií spojených s nákupom musí dodávateľ upozorniť, že požiadavky tejto zmluvy môžu byť podrobené skúmaniu útvarom ŠOK. Zároveň dodávateľ musí zabezpečiť, že všetky zmluvné požiadavky, vrátane dodatkov NATO, budú súčasťou procesov interných auditov. Dodávateľ musí informovať zástupcov ŠOK a ďalších odberateľov o nedostatkoch zistených v priebehu interného auditu, pokiaľ to nie je s nimi odsúhlasené inak. Úlohou dodávateľa je tiež navrhnutie a zavedenie dokumentovaných postupov, ktoré identifikujú, riadia a vylučujú všetky nezhodné produkty.

Toto sú len niektoré ukážky z uvedenej normy, ktoré dokumentujú vyššiu náročnosť AQAP noriem v porovnaní s ISO normami, obvykle používanými pri overovaní kvality vo výrobe.

AQAP 2131 - Požiadavky NATO na overovanie kvality pri výstupnej kontrole [6]. Účelom tohto štandardu je špecifikovať a zabezpečiť útvaru ŠOK a/alebo odberateľom práva prístupu k dodávateľovi takým spôsobom, aby výstupná kontrola, vykonávaná dodávateľom poskytla objektívny dôkaz, že produkt vyhovuje požiadavkám podľa zmluvy. Povinnosťou je použiť tento štandard pre všetky procesy dodávateľa, ktoré sú nevyhnutné k naplneniu požiadaviek vyplývajúcich zo zmluvy, ak sú takéto uvádzané v zmluve. Dodávateľ v rámci vykonávania výstupnej kontroly musí vykonať všetky druhy nevyhnutných kontrol a skúšok na produkte, ktoré umožňujú preukázanie zhody s požiadavkami vyplývajúcimi zo zmluvy. Musí udržovať postačujúce záznamy o kontrolách a skúškach, ktoré zabezpečujú preukázanie zhody produktu s požiadavkami vyplývajúcimi zo zmluvy.

STANAG 4174 - Spojenecká publikácia pre spoľahlivosť a udržiavateľnosť [10]. Táto publikácia poskytuje základ pre dosiahnutie vysokého stupňa pohotovosti a požadovaného úspechu pri zabezpečovaní (obstarávaní) vojenského materiálu, vrátane špeciálnej techniky. Zameraná je hlavne pre programy spolupráce pri obstarávaní majetku v NATO, ale nie je výlučne orientovaná iba naň. Pre spoľahlivosť a nadväzujúce činnosti sa v plnom rozsahu používa štandard SAE JA 1000 (Štandard pre program spoľahlivosti). Pre udržiavateľnosť a nadväzujúce činnosti sa v plnom rozsahu používa štandard SAE JA 1010 (Štandard pre program udržiavateľnosti). Podmienky uvedené v tomto dokumente sú platné pre ľubovoľný vojenský materiál uvedený v zmluve alebo v nákupnej objednávke. Tento štandard nevylučuje používanie ďalších štandardov za predpokladu, že bude zachovaný zmysel (podmienky a požiadavky) tohto štandardu. Vo všetkých etapách programu spoľahlivosti a udržiavateľnosti platí tento štandard. Vzťahuje sa na všetky druhy obstarávania, či už vyplývajúce z činností návrhu a vývoja, z činností výroby, z existujúcich zásob materiálov (napr. obchodný tovar) alebo z ich kombinovania.

Tento štandard opisuje zmluvné ustanovenia pre plnenie požiadaviek na bezporuchovosť a udržiavateľnosť, na návrh plánov spoľahlivosti a udržiavateľnosti v prevádzke. Charakterizuje tiež ako posudzovať spoľahlivosť a udržiavateľnosť počas prevádzkovania výzbroje a techniky, ale tiež ako ich v priebehu prevádzky zlepšovať. Súčasťou tohto štandardu je zoznam príslušných metód vhodných pre jednotlivé druhy procesov. Obsah štandardu je určený členom projektových tímov, pracovníkom logistiky alebo iným pracovníkom rezortu obrany, ale hlavne a vrcholovým manažérom dodávateľských organizácií z priemyslu. Zdôrazňuje zodpovednosť dodávateľov (výrobcov), ale zároveň i užívateľov za poskytovanie potrebných údajov z prevádzky.

Nepretržité posudzovanie spoľahlivosti a udržiavateľnosti je dôležité, ako z obchodného, tak i z funkčného hľadiska. Umožňuje efektívne manažovanie nákladov vojenského materiálu počas jeho životného cyklu. Zásady definované v štandarde sa aplikujú počas etáp obstarávania a prevádzky v programoch NATO pre výzbroj a techniku. Sú určené všetkým vrcholovým manažérom (projektov a riadiacim procesy prevádzky), zodpovedným za spoľahlivosť a udržiavateľnosť v organizácii. Tieto sú špecifikované formou ukazovateľov bezporuchovosti, udržiavateľnosti, testovateľnosti, skladovateľnosti alebo pomocou špecifických ukazovateľov, napr. pravdepodobnosť splnenia úlohy alebo stredná doba medzi poruchami, stredná doba na opravu, rýchlosť nájdenia poruchy a jej identifikácia pre testovateľnosť.

Požiadavky na spoľahlivosť a udržiavateľnosť sú kvantitatívne definované vo všetkých požadovaných dokumentoch hlavne z dôvodov:

- potreby stanovenia dosiahnuteľnej úrovne v prevádzkových podmienkach,
- definovania požiadaviek pre dodávateľa,
- potreby ich preukazovania na konci riešenia jednotlivých etáp návrhu a výroby.

V požadovanej dokumentácii sa musí zabezpečiť ich sledovateľnosť vo väzbe na všetky rozhodnutia, ktoré požiadavky sú nimi ovplyvňované a tieto sa musia dokumentovať.

Úlohou štátneho overovania kvality [15] je vhodným plánovaním činností vykonávaných v rámci výkonu štátneho overovania kvality v maximálnej miere znížiť pravdepodobnosť vzniku identifikovaných rizík produktov alebo rizík výrobcu produktu alebo dodávateľa produktu pri realizácii dodávok na účely obrany, čo predpokladá v plnom rozsahu požiadavky vyplývajúce STN EN ISO 31000:2011 , ale tiež STN ISO 9001: 2015. Z toho dôvodu sa buduje databanka potenciálnych rizík jednotlivých produktov špeciálnejtechniky, aby sa efektívnejším spôsobom predchádzalo ku vzniku potenciálnych rizík. Koncepcia plánovania štátneho overovania kvality je zameraná na dohľad nad systémom manažérstva kvality výrobcu produktu, procesmi realizácie a skúšok produktu za účelom preukázania zhody produktu so zmluvnými požiadavkami na kvalitu.

3 Záver

Cieľom príspevku je predstaviť postup hodnotenia rizík kvality produktov špeciálnej techniky, ktorý zohľadňuje novelizované požiadavky na riziká podľa ISO STN EN 31000:2011 a ISO STN EN 9100:2015 v kontexte s používanými súbormi štandardov noriem AQAP a novelizovaných noriem rady STN ISO. Aplikovaním tohto postupu sa umožňuje zlepšiť odhady a spôsob analýzy a hodnotenia rizík (známych, ale i skrytých) v dodávkach produktov špeciálnej techniky pre odberateľov. Dôležité je návrhy postupov opatrení aplikovať v reálnom čase, pretože vývoj rizík je dynamický proces. Manažéri rizika sú zodpovedný za to, že sa vzniknuté riziká efektívnym a účinným spôsobom zvládnu. Manažér rizika musí ich preto nepretržite monitorovať, zmierňovať a zaisťovať sa proti ním. Efektívným postupom sa javí budovanie databáz rizík pre jednotlivé druhy špeciálnej techniky, čo umožňuje dosahovať lepšie výsledky pri kontrole dodávanej kvality produktov špeciálnej techniky.

References

[1] AQAP 2000, NATO Policy On An Integrated Systems Approach To Quality Through The Life Cycle , Edition 3, 2009, 30 s.

[2] AQAP 2050, NATO Project Assessment Model, Edition 1, September 2003, 69 s.

[3] AQAP 2105 NATO Anforderungen fuer Qualitätsmanagementpläne, 2. Ausgabe, November 2009, 14 s.

[4] AQAP 2110, NATO Quality Assurance Requirements For Design, Development And Production, Edition 3, 2009, 20 s.

[5] AQAP-2120, NATO Quality Assurance Requirements For Production, Edition 3, 2009, 19 s.]

[6] AQAP-2131, NATO Quality Assurance Requirements For Final Inspection, Edition 2, 2006, 9 s.

[7] CIBULKA, V., Riadenie kvality, Vydavateľstvo Trenčianska univerzita Alexandra Dubčeka v Trenčíne, 2015,

[8] ISBN 978-80-8075-681-9, 235 s.

[9] CIBULKA, V., Systémy riadenia kvality, 1. vyd., Trenčín : TnUAD, 2015, CD ROM, ISBN 978-80-8075-708-3, 254 s.

[10] MONJAU, G., Risikomanagement , Teil 1, 2, 3, 4, 5, http://www.perspektivemittelstand.de/ Risikomanagement, 2007.

[11] STANAG 4107, Mutual Acceptance Of Government Quality Assurance And Usage Of The Allied Quality Assurance Publications (AQAP), Edition 8, 2007, 12 s.

[12] Slovenský obranný štandard AQAP 2105 – Požiadavky NATO na plány kvality dodávateľa, Vydanie 1,

[13] Máj 2007, Úrad pre obrannú štandardizáciu, kodifikáciu a štátne overovanie kvality, Trenčín, 13 s.

[14] STN EN ISO 9001 Systémy manažérstva kvality, Požiadavky (ISO 9001: 2015), Slovenský ústav technickej normalizácie, Bratislava, 2016

[15] STN EN ISO 14 001:2015, Systémy environmentálneho manažérstva, Požiadavky s pokynmi na použitie, Slovenský ústav technickej normalizácie, Bratislava, 2016

[16] STN ISO 31000:20011, Manažérstvo rizika, Zásady a návod, Slovenský ústav technickej normalizácie, Bratislava

[17] Úrad pre obrannú štandardizáciu, kodifikáciu a štátne overovanie kvality so sídlom v Trenčíne, Výročná správa za rok 2013, 49 s.

[18] Úřad pro obrannou standardizaci, katalogizaci a státní ověřování jakosti, odbor strategie státního ověřování jakosti, Státní ověřování jakosti (SOJ) – všeobecně, http://www.ossoj.army.cz/soj.htm

[19] VARCHALOVÁ, T., DUBOVICKÁ, L., Nový manažment rizika, Iura Edition spol. s r. o., Bratislava, 2008,

ISBN 978-80-8078-191-0, 196 s.

Analysis of weld joint of DX51D steel with $AlMg_3$ alloy made by CMT welding method

David Dobrocky[1], Petr Dostal[2], Michal Sustr[2], Zdenek Pokorny[1]
[1]Department of Mechanical Engineering, Faculty of Military Technology, University of Defence, Kounicova 65, 662 10 Brno. Czech Republic. E-mail: david.dobrocky@unob.cz, zdenek.pokorny@unob.cz
[2]Institute of Technics and Automotive Transport, Faculty of AgriSciences, Mendel University in Brno. Zemedelska 1/1665, 613 00 Brno. Czech Republic. E-mail: pet.d@seznam.cz, sete.mike@gmail.com

The combination of steel and aluminum as a constructional material brings many benefits. Steel is characterized by strength and is suitable for components exposed to high stress. Aluminum is light and is suitable for less stressed parts. However, for technical and economic reasons, the arc welding of these materials has not been possible for a long time. The development of the technology that allows welding of steel with aluminum is linked to the requirements of the automotive industry. This is a process known as CMT – Cold Metal Transfer and refers to the low energy transition of the droplet during MIG/MAG welding. In this so-called "welding soldering", the base steel material is not melted, but merely wetted, whereas in the case of aluminum, a melt weld is formed. The advantage of this process is the lower heat input and consequently considerably less heat deformation. This paper deals with the analysis of the welded joint of the DX51D steel sheet with the Aluzinc layer and the $AlMg_3$ alloy sheet made by CMT welding using the digitized inverter welding power from Fronius company. An $AlSi_5$ welding wire of Ø 1.2 mm was chosen as an additive material. The used technology has led to the formation of a weld with a considerable porosity of the weld metal.

Keywords: CMT welding, steel DX51D, Aluzinc, Aluminum alloy $AlMg_3$, Porosity, $AlSi_5$

1 Introduction

At present, combinations of the specific properties of different materials promise interesting perspectives. The combination of materials imparts to the respective components or product the required properties of multiple materials, Sun et al. (2017). This kind of joints was previously possible only by mechanical means or as glued joints. But the greatest attention today is devoted the thermal joining of materials with different properties. The center of gravity is steel and aluminum joints. Aluminum joining with steel through the CMT process opens new design and technological possibilities, Gungor et al. (2014). It is mainly used in the automotive industry where is focused on weight reduction and increasing safety due to targeted strength improvement, Hagara (2000), Larsson (2003). Based on the different properties of steel and aluminum, their joints can provide optimal utility properties, Feng et al. (2009). The CMT process differs from other thermal techniques, such as MIG/MAG, WIG, or laser welding, in a few important parameters, by lower heat input to the welding and controlled reversible wire movement. The process brings about 20 – 30% less heat than MIG/MAG welding. CMT welding which was originated from the development of the of MIG/MAG welding branch, Schierl (2005), Talalaev et al. (2012), is based on controlled near-wire transfer of welded material, Kah et al. (2013). The result is a very uniform weld. This is one of the preconditions for joining aluminum and steel. Another requirement when using the CMT method is a material – the steel sheet must be galvanized, Zhang et al. (2009), Cao et al. (2014). The advantage of CMT welding is high bridgeability without the need for a welding pad, minimal welding deformation due to low heat input, highly stable arc, practically zero spatter and minimum finishing works, Schierl (2005). However, with the welding method being evaluated, we can encounter some welding problems and defects, e.g. the porosity of the weld metal, Ahsan et al. (2016), Cong et al. (2015), and the formation of segregation cracks during solidification, Rush et al. (2010).

The paper deals with the evaluation of the welded joint of DX51D steel with the Aluzinc layer and the $AlMg_3$ aluminum alloy formed by CMT welding. Both materials in the form of a 1 mm thick sheet metal were welded with overlapping, using a 1.2 mm thick $AlSi_5$ alloy welding wire. The Aluzinc layer on the steel sheet surface is formed of alloy from aluminum and zinc. Welding was carried out according to the conditions and parameters mentioned in Table 1.

Tab. 1 – Conditions and parameters of the welding process

Type of weld joint	Overlapped joint
Additional material	Welding wire Ø 1.2 mm, $AlSi_5$
Protective gas	100% Ar
Protective gas flow	14 $l \cdot min^{-1}$
Welding current	100 – 110 A
Welding voltage	19 V
Welding speed	0.5 $m \cdot min^{-1}$/8.3 $mm \cdot s^{-1}$

The weld joints created by the CMT method were performed on a welding machine from Fronius company. The entire welding process was digitally controlled, including the reverse motion of the wire, which took place at a frequency

of 70 Hz. Chemical analysis of weld metals was performed by a spark optical emission spectrometer Q4 Tasman. The metallographic samples of the welds were prepared using MTH Micron 150 metallographic saw and Struers Labopol 60 grinder. Metallographic analysis was performed on the Olympus DSX100 opto-digital microscope and Olympus GX51 metallographic microscope. The microhardness measurement was performed by the Leco LM247AT automated hardness tester. The evaluated weld joint exhibited considerable porosity in the weld metal.

2 Experimental methods

2.1 Analysis of chemical composition

To analyze the chemical composition was used the Tasman Q4 spark optical emission spectrometer and the corresponding standards were selected based on the measured material (standard for steel, standard for aluminum alloy). The results of the chemical analysis of the steel sheet are shown in Table 2. Table 3 shows the results of the chemical analysis of the aluminum alloy sheet.

Tab. 2 – Chemical composition of DX51D steel [wt. %]

C	Si	Mn	P	S	Cr	Mo	Ni	Cu	Al
0.068	0.013	0.323	<0.005	<0.15	0.0065	<0.01	0.0067	0.06	0.026

Tab. 3 – Chemical composition of $AlMg_3$ alloy [wt. %]

Si	Fe	Cu	Mn	Mg	Cr	Ni	Zn	Ti	Al
0.144	0.406	0.016	0.220	2.792	0.115	0.0023	0.023	0.027	96.22

2.2 Metalographic analysis

The cuts of welds were prepared using the MTH Micron 150 precision metallographic saw, then were casted into methylacrylate Duracryl Plus self-curing resin, and after curing, they were hand grinded on the Struers Labopol 60 metallographic grinder. Grinding was performed on Hermes abrasive paper with a particle size of 80 – 4000 μm. The polishing of the samples was carried out on the Leco Brown Technotron abrasive cloth using a Leco diamond slurry with a particle size of 1 μm. A velvet polishing disc and a diamond suspension with a particle size of 0.5 μm were used to a finish polishing. 2% Nital was used to induce the steel sheet structure, the aluminum alloy was etched by immersion in NaOH and the surface of the sample was wipeded with a cotton swab soaked in a solution of 95% H2O + 5% HF. The structure of weld metal (AlSi5) was induced by HF. Macroscopic images were taken on an Olympus DSX100 optical microscope, the microstructure was evaluated using the Olympus GX51 inverted metallographic microscope.

2.3 Measurement of microhardness

The microhardness measurement was performed by the Leco LM247AT automatic hardness tester. Measurement was done in 5 rows, 20 indentations, by Vickers method with load 50 g (HV 0.05). The principle of microhardness measuring the transition area on the contact of steel sheet – the weld metal is shown in Fig. 1 (a). The principle of microhardness measuring of the transition area of contact of weld metal – Aluminum alloy is shown in Fig. 1 (b). The red arrow shows the direction of measurement.

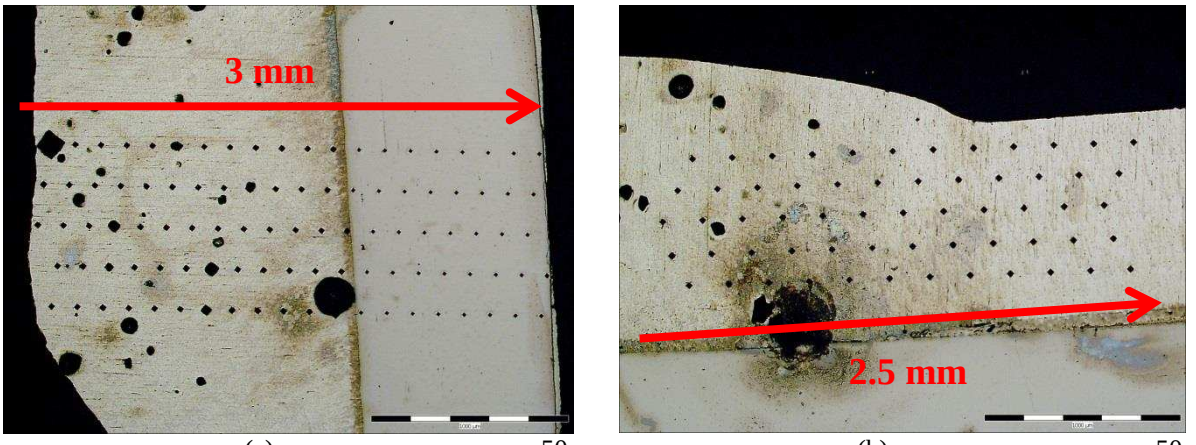

(a) 50x (b) 50x

Fig. 1 Indentations after microhardness measurement. Measurement of the transition area at the contact of DX51D steel–weld metal $AlSi_5$ (a) and contact of $AlMg_3$ alloy–weld metal$AlSi_5$ (b)

3 Results and discussion

The picture of weld with the description of the individual parts is shown in Fig. 2 (a). Fig. 2 (b) documents the

cross-sectional of the weld also with the description of the individual parts of the weld and visible numerous porosity in the weld metal. The porosity of the weld metal is documented in Figures 3 (a) and 3 (b). The formation of gas cavities and pores in CMT welding may be related to the absorption of gases by aluminum. The creation of gas cavities is most often caused by hydrogen, which is soluble in aluminum. Weld metal absorbs hydrogen, which diffuses through the entire volume of the welding bath. When cooling the weld metal, the solubility of hydrogen decreases. Because the cooling rate is high during welding, it is not enough to exclude all hydrogen from the liquid metal, hydrogen is staying there and forming gas cavities. When welding the CMT, the protective atmosphere is made up of 100% argon, so it is possible that the gas cavities creation is also join with presence of argon. Cais et al. (2014) documents the porosity in the case of pressurized die casting alloys AlSi7Mg0.3, which is created by the presence of hydrogen according to the equation:

$$2\ Al + 3\ H_2O = Al_2O_3 + 3\ H_2 \tag{1}$$

Overheating of the aluminum melt causes excessive oxides formation. During aluminum melting process, each temperature rise of 10 ° C above the melting point results in an increase of the gases in the melt by 0.1%, Wierzbicka (1998), Michna et al. (2011), Žydek et al. (2010). According to a similar mechanism, welding pores can also be formed during the CMT welding process.

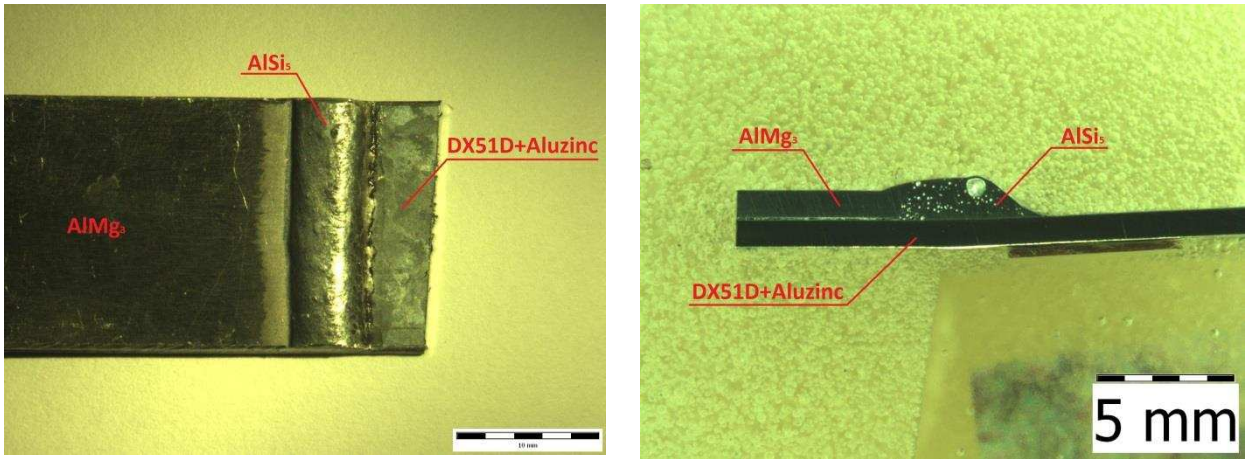

(a) 3.15x (b) 6.25x

Fig. 2 A weld image with a description of the main parts (a) and a cross section of the weld (b)

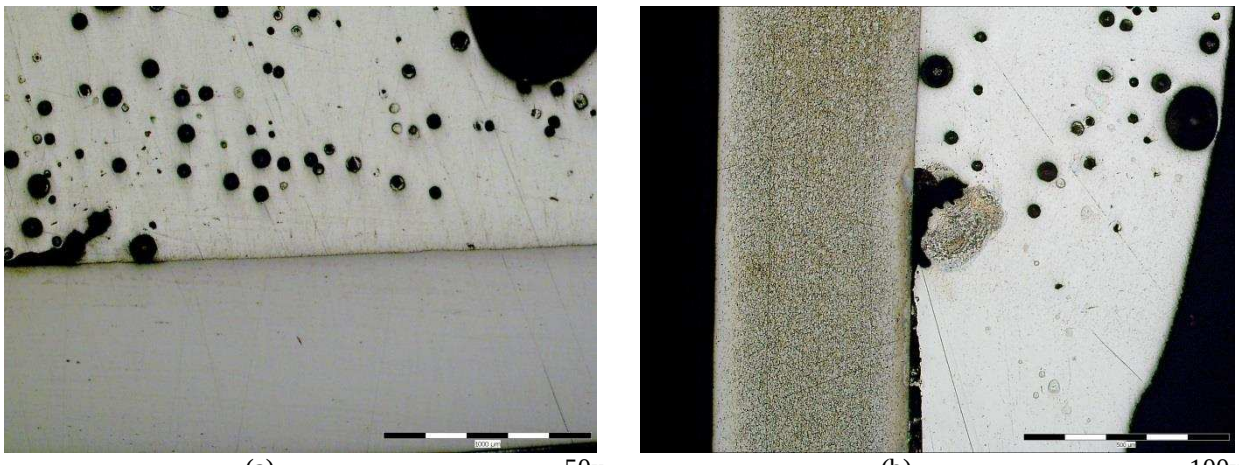

(a) 50x (b) 100x

Fig. 3 Porosity in transition area of weld metal $AlSi_5$ – DX51D steel (a) and in transition area of $AlMg_3$ alloy – weld metal $AlSi_5$ (b)

The metallographic analysis of the metal sheet with an aluzinc layer is documented in Fig. 4 (a) and Fig. 4 (b). The core structure of the steel sheet consists of ferrite with a lamellar perlite. The aluzinc layer, which has a defined chemical composition of 55% aluminum, 43.4% zinc and 1.6% silicon, was applied to the steel sheet by a continuous hot-dip process, which corresponds to a significant heat-affected area of the base material under the aluzinc layer. The microstructure of the aluminum alloy $AlMg_3$ is shown in Fig. 5 (a). In the structure of the aluminum alloy, Mg_2Al_3 phase exclusion regions are visible. With less magnification, the aluminum alloy linearity is evident, as is visible from Fig. 5 (b). The metallographic analysis of the $AlSi_5$ weld metal is documented in Figure 6 (a). With smaller magnification, individual grains of aluminum alloy having a considerable size are visible, as shown in Figure 6 (b). The coarse grain structure may reduce the strength and plasticity of the weld metal. The microstructure in the transition zone of steel

sheet - weld metal is documented in Fig. 7 (a). A thin layer of the intermetallic phase is visible on the contact of steel with weld metal, which is better visible at higher magnification; see Fig. 7 (b). The grains of steel are enlarged in contact area with the weld metal, which can again lead to deterioration of the mechanical properties of the weld joint. In the case of the transition zone aluminum alloy-weld metal they are visible the sharp grain boundaries, see Fig. 8 (a). With greater magnification of the transition area which is shown in Figure 8 (b), it is evident that the precipitating particles have been gradually softened and that the sharp grain boundaries have decreased.

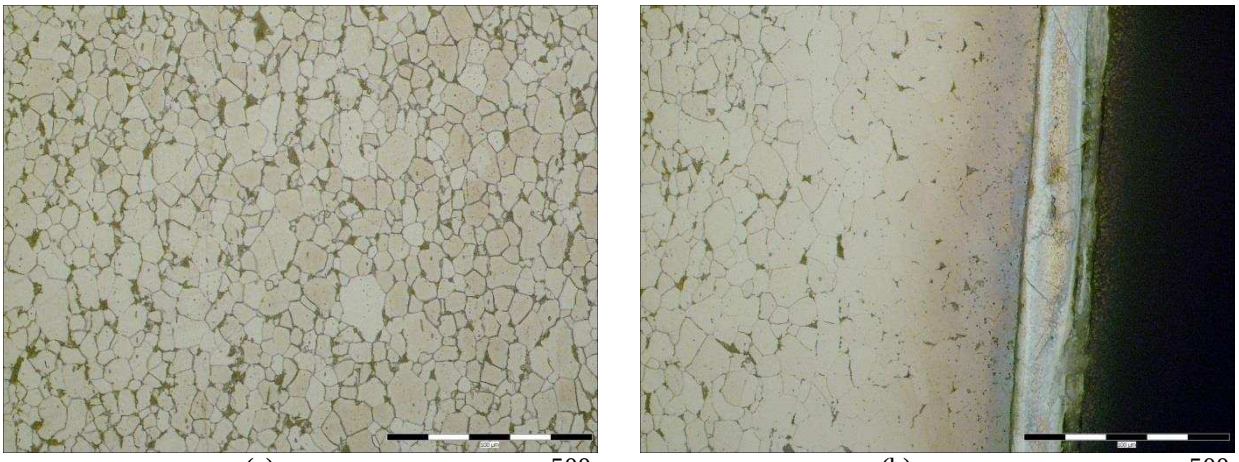

(a) 500x (b) 500x

Fig. 4 Microstructure of steel sheet (a) and aluzinc layer on steel surface (b)

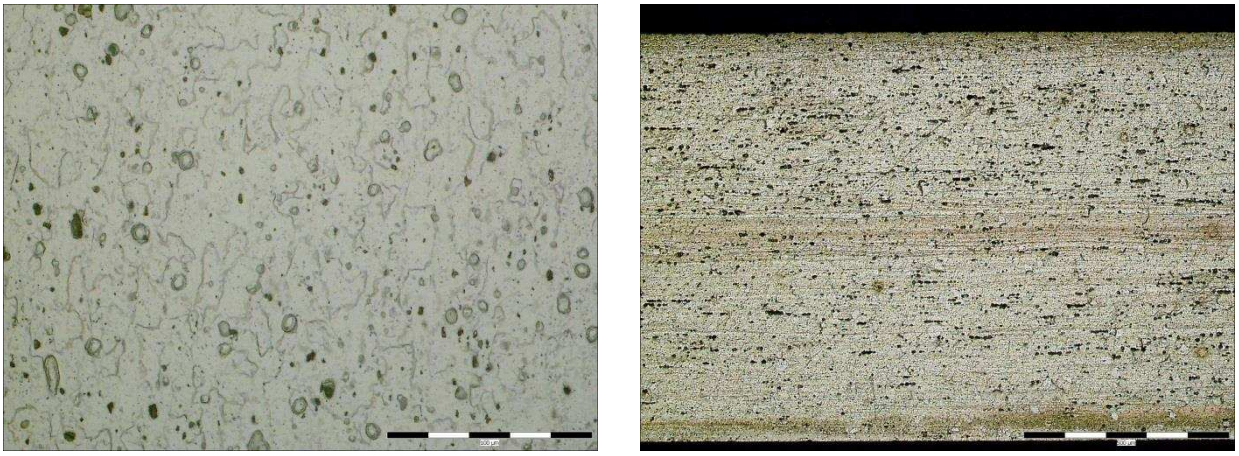

(a) 500x (b) 100x

Fig. 5 Microstructure of aluminum alloy (a) and its visible linearity (b)

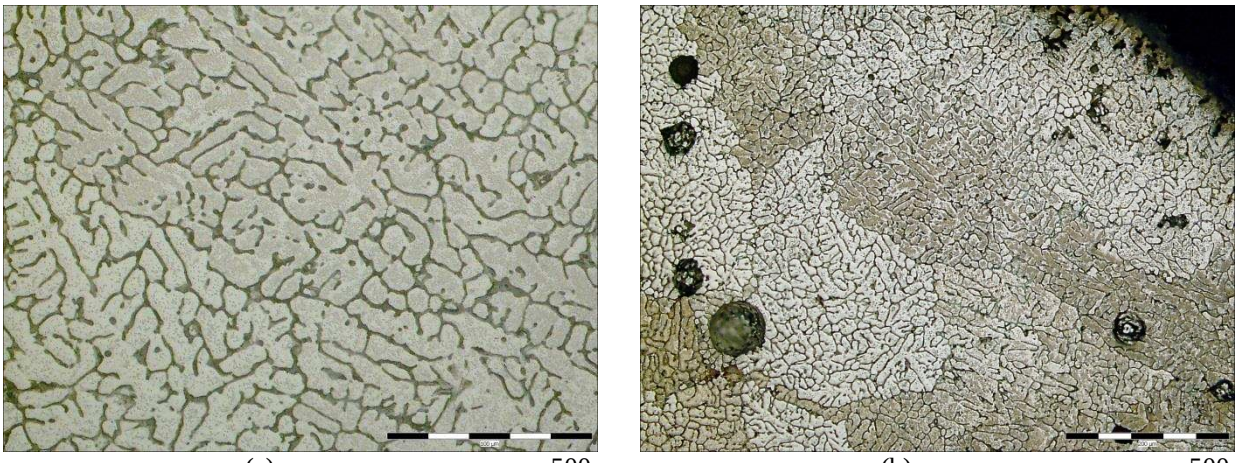

(a) 500x (b) 500x

Fig. 6 The weld metal microstructure (a) and the visible grains of the $AlSi_5$ additional material (b)

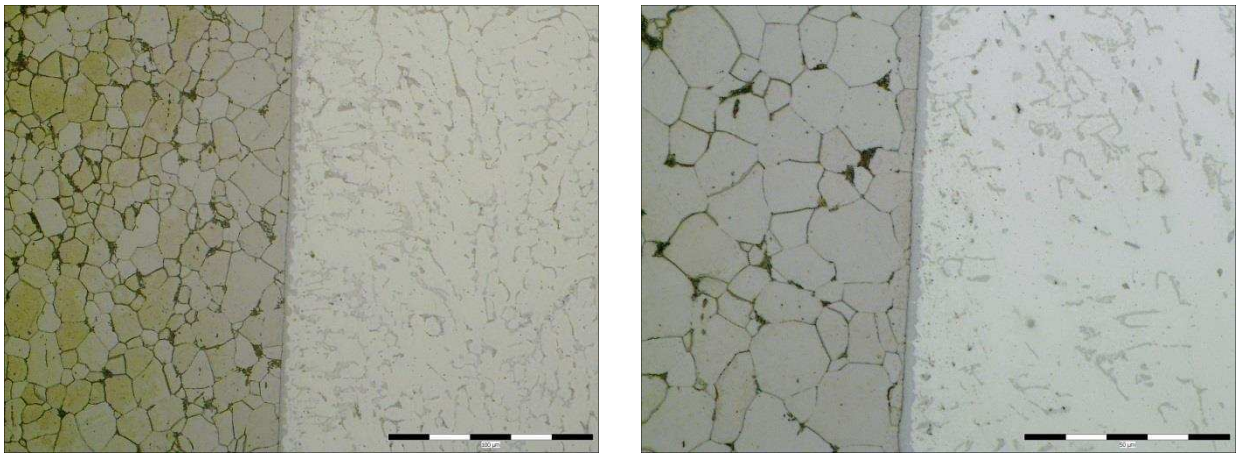

(a) 500x (b) 1000x

Fig. 7 Microstructure of transition area of DX51D steel – AlSi5 weld metal (a) and visible layer of intermetallic phase (b)

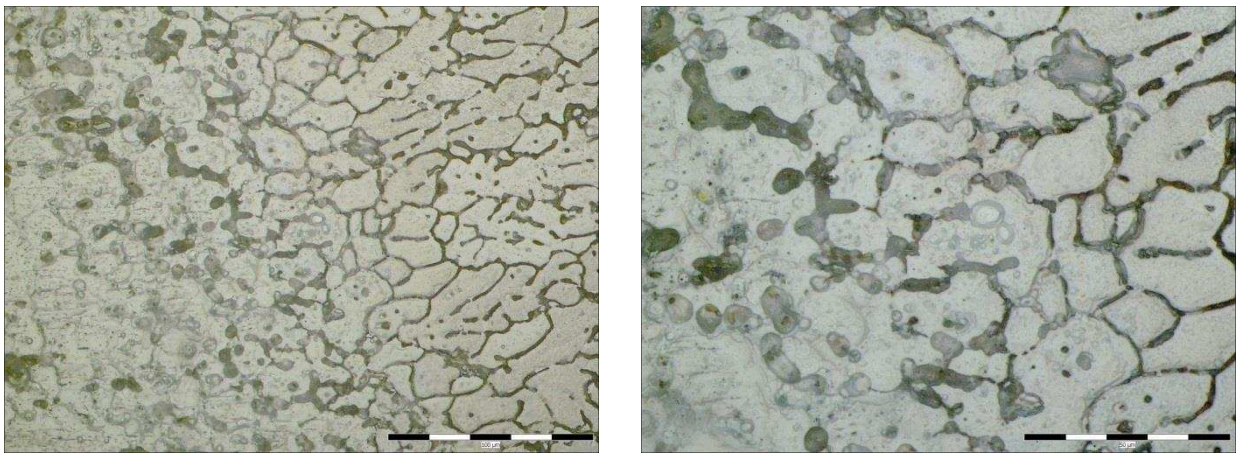

(a) 500x (b) 1000x

Fig. 8 Microstructure of transition area $AlMg_3$ aluminum alloy – $AlSi_5$ weld metal (a) and area of grain refinement (b)

The microhardness measurement results show differences in microhardness of individual weld joint materials. Fig. 9 documents the results of microhardness measurements in transition area of weld metal – steel sheet. The results show that the microhardness of the weld metal is about 80 HV0.05, and there is a sharp transition to a steel sheet with a microhardness of about 180 HV0.05. The heat-affected area is not visible from the process of microhardness measurement. When measuring the microhardness at the transition area weld metal - aluminum alloy, the higher value of microhardness of the weld metal (about 80 HV0.05) is evident, as compared to the aluminum alloy (about 70 HV0.05), which is evident from Fig. 10. The transition area is not characterized by a more pronounced microhardness variation, from which it can be concluded that a welded joint has perfectly bonded the weld metal to the aluminum sheet. This was confirmed by metallographic analysis.

4 Conclusion

CMT belongs between arc-welding with a melting electrode in an inert gas, most commonly argon, which originates from MIG / MAG welding. When welding by CMT, the electric arc melts the wire electrode and the base material of the aluminum alloy. Usually there is no melting of the steel sheet. In this method, fusion welding of aluminum alloy is combined with hard brazing of steel sheet, the so-called overlapped joint. When welding two heterogeneous materials, one encounters a problem in the difference in physico-chemical properties. Weldability is greatly complicated by the limited solubility of both metals. The technological difficulty of welding is considerable, especially the intermetallic phases at the interface of both metals must be avoided. The effort is to bring as little heat to the joint as possible, shorten the welding process itself, reduce diffusion and intermetallic phase formation, in particular by selecting a suitable additive material. For the welding of selected materials, an additional $AlSi_5$ material was chosen, which very well compensates for the susceptibility of the weld metal to heat cracking and limits the formation of intermetallic phases. The evaluated welds exhibited slight deformations. The macrophotography shows a quality weld, without spraying, with a minimal heat-affected area. Metallographic analysis documents the considerable porosity of the weld metal. Between the weld metal and the steel sheet there is a thin layer of the intermetallic phase and the area of the coarse grain of the steel.

The transition phase of the aluminum sheet and the weld metal was characteristic by area of fine grain of the weld metal. The results of the measurement of the microhardness of the transition region did not show any fluctuations in the microhardness values, i.e. no wider heat-affected area was created. In the transition steel sheet – weld metal, a sharp transition in microhardness values, which indicates the sharp interface of the solder joint, is visible. In the transition area, the aluminum alloy – weld metal exhibits microhardness similar to the two materials which is result of a welded joint with a diffusion bond between the two materials. The article confirmed the suitability of the CMT method for welding two heterogeneous materials. However, it should be remembered that even with this method, weld defects can occur which must be detected which was confirmed also in this work.

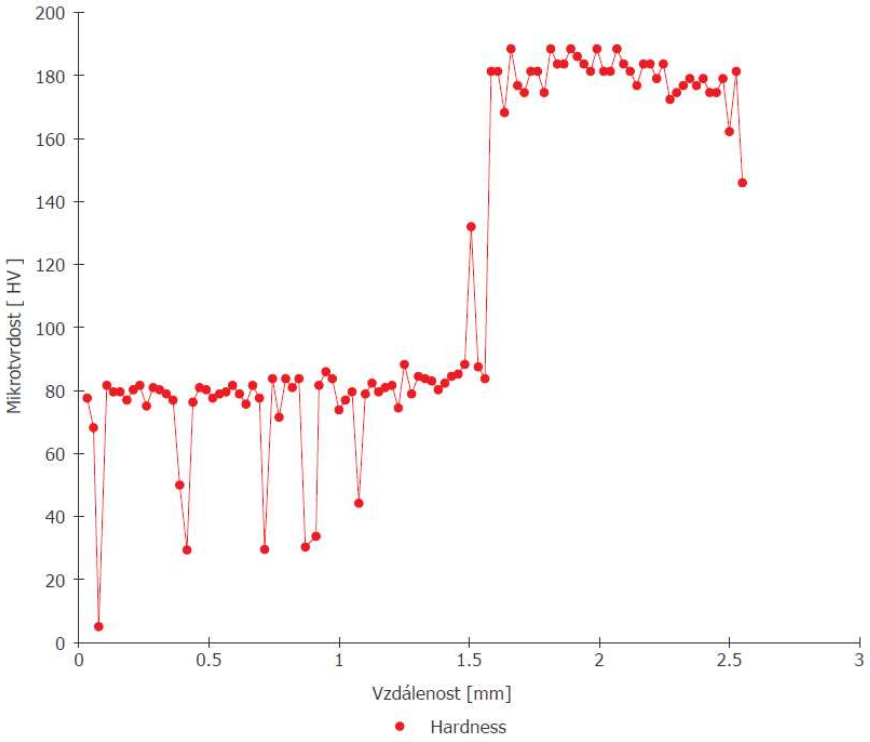

Fig. 9 Microhardness measurement of the transition area of steel sheet – weld metal

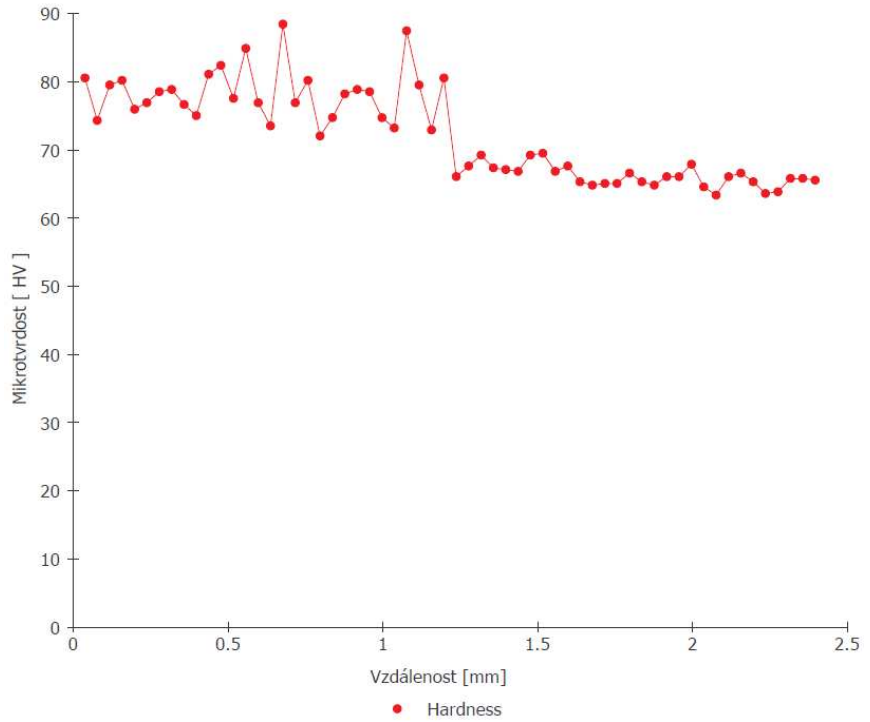

Fig. 10 Measurement of microhardness of the transition area of aluminum sheet – weld metal

Acknowledgement

The paper was prepared with the support of the Project for the Development of the Organization *"DZRO K 201"* and by the Specific research project 2016 of the Department of Mechanical Engineering *"SV16-216"*.

References

[1] SUN, Q.J., LI, J.Z., LIU, Y.B., LI., B.P., XU, P.W., FENG, J.C. (2017). Microstructural characterization and mechanical properties of Al/Ti joint welded by CMT method – Assisted hybrid megnetic field. In: Materials and Design, Vol. 116, pp. 316 – 324.

[2] GUNGOR, B., KALUC, E., TABAN, E., SIK, A. (2014). Mechanical and microstructural properties of robotic Cold Metal Transfer (CMT) welded 5083-H111 and 6082-T651 aluminum alloys. In: Materials and Design, Vol. 54, pp. 207 – 211.

[3] HAGARA, K. (2000). Strength properties of aluminum/aluminum and aluminum/steel joints for light weighting of automotive body. In: Weld. World, Vol. 44, No. 4, pp. 23 – 27.

[4] LARSSON, J.K. (2003). Overview of joining technologies in the automotive industry. In: Weld. Res. Abroad, Vol. 49, No. 6/7, pp. 29 – 45.

[5] FENG, J.C., ZHANG, H.T., HE, P. (2009). The CMT short-circuiting metal transfer proces and its use in thin aluminium sheets welding. In: Mater. Des., Vol. 30, No. 5, pp. 1850 – 1852.

[6] SHIERL, A. (2005). The CMT proces – a revolution in welding technology. In: Weld. World, Vol. 9, No. 38.

[7] TALALAEV, R., VEINTHAL, R., LAANSOO, A., SARKANS, M., (2012). Cold metal transfer (CMT) welding of thin sheet metal product. In: Estonian Journal of Engineering, Vol. 13, No. 3, pp. 243 – 250.

[8] KAH, P., SUORANTA, R., MARTIKAINEN, J. (2013). Advanced gas metal arc welding processes. In: J. Adv. Manuf. Technol., Vol. 67, pp. 655 – 674.

[9] ZHANG, H.T., FENG, J.C., HE, P., ZHANG, B.B., CHEN, J.M., WANG, L. (2009). The arc characteristics and metal transfer behaviour of cold metal transfer and its use in joining aluminium to zinc-coated steel. In: Mater. Sci. Eng., Vol. A 499, No. 1, pp. 111 – 113.

[10] CAO, R., FENG, Z., LIN, Q., CHEN, J.H. (2014). Study on cold metal transfer welding – brazing of titanium to cooper. In: Mater. Des., Vol. 56, No. 4, pp. 165 – 173.

[11] AHSAN, M.R.U., KIM, Y.R., KIM, C.H., KIM, J.W., ASHIRI, R., PARK, D. (2016). Porosity formation mechanisms in cold metal transfer (CMT) gas metal arc welding (GMAW) of zinc coated steels. In: Science and Technology of Welding and Joining, Vol. 21, No. 3, pp. 209 – 215.

[12] CONG, B., DING, J., WILLIAMS, S. (2015). effect of arc mode in cold metal transfer proces on porosity of additively manufactured Al-6.3%Cu alloy. In: Int. J. Adv. Manuf. Technol., Vol. 76, No. 9. pp. 1593 – 1606.

[13] RUSH, M.T., COLEGROVE, P.A., ZHANG, Z., COURTOT, B. (2010). An investigation into cracking in nickel-base superalloy repair welds. In: Advanced Materials Research, Vol. 89 – 91, pp. 467 – 472.

[14] CAIS, J., WEISS, V., SVOBODOVA, J. (2014). Realtion between Porosity and Mechanical Properties of Al-Si Alloys Produced by Low-Pressure Casting. In: Archives of Foundry Engineering, Vol. 14, No. 1, pp. 97 – 102.

[15] WIERZBICKA, B. (1998). Krystalizacja stopów Al-Cu w procesie szybkiego chlodzenia. In: Archives of Foundry Engineering, No. 38, pp. 143 – 150.

[16] MICHNA, Š., NÁPRSTKOVÁ, N., LUKÁČ, I. (2011). Mechanical Properties Optimization of Al-Si12CuMgNi Alloy by Heat during Annealing. In: Archives of Foundry Engineering, Vol. 11, No. 4, pp. 163 – 166.

[17] ŽYDEK, A., KAMIENIAK, J., BRASZCZYŃSKA-MALIK, K.N. (2010). Microstructural stability of Mg-5Al-0.4Mn-3RE alloy Treatment. In: Mettalofizika i Noveishie Teknologii, Vol. 11.

Possibility for improving damage tolerance of integral structure by high strength bonded straps

Vaclav Jetela[1], Josef Klement[1], Petr Augustin[1]
[1]Faculty of Mechanical Engineering, Brno University of Technology. Technicka 2896/2, 616 69 Brno. Czech Republic.
E-mail: vaclav.jetela@vutbr.cz, klement@fme.vutbr.cz, augustin@fme.vutbr.cz

Integral stringer panels can attain weight reduction in a primary aircraft structures, but does not contain physical barriers for fatigue crack growth. One of the promising technique for prolonging fatigue life are bonded crack retarders made of materials with high stiffness. Experimental study was done on two specimens with different geometries. The straps consisted of high strength corrosion resistant steel AISI 301 was adhesively bonded to an aluminium alloy 2024-T351 Center-Cracked Tension (CCT) specimens fabricated by a high-speed machining process to promote fatigue crack growth retardation. Specimens were tested at constant amplitude load. The study concludes that the fatigue crack growth life can be significantly improved.

Keywords: Bonded crack retarder, Damage tolerance, Fatigue crack growth, Integral structure, Strap

1 Introduction

Integrally stiffened structures preserve minimum section size in highly loaded applications. This main advantage leads to weight reduction of aircraft structure [1]. Unfortunately, integral structures have poor crack growth properties. Fatigue crack growth (FCG) in proximity of a stiffener will not be delayed compared to a built-up structure. Crack propagates directly into a stiffener [2]. Bonded crack retarders (BCR) provide an additional safety element in terms of damage tolerance increase.

2 Main findings of previous studies

In 1989 Schijve [3] concluded that BCR are much more effective than riveted retarders. In terms of low fatigue sensitivity, high ultimate strength and low specific density he suggested ARALL retarders as the most effective solution.

The study of Li and Zhang [4] based on numerical calculations showed that BCRs made of carbon/epoxy are more effective in transferring load from base material than Ti-alloy retarders.

Boscolo et al. [5] done many experiments with retarders made of carbon/epoxy, glass/epoxy, GLARE and Ti-alloy. They also developed new modeling technique comprising disbond behavior. Influence of size, weight and location were investigated according to fatigue crack growth.

Irving et al. [6] presented at ICAF 2011 the results of study focused on BCRs made of GLARE, Ti-alloy, Al-alloy and carbon/epoxy. GLARE and Al-alloy BCRs were most effective in fatigue crack growth retardation during constant amplitude loading up to 60MPa. Under variable amplitude loading GLARE maintained its effectiveness as a strap material.

Molinari et al. [7] developed analytical tool named LEAF to predict damage tolerance properties of stiffened structure. They concluded that BCR with higher width to thickness ratio are more effective in retardation.

3 Mechanisms and requirements

Secondary bending: Due to unsymmetrical configuration of panel stiffened with BCRs, secondary bending will occur. Secondary bending has the negative consequence on FCG [8].

Disbonding: When the crack passes under BCR, a progressive disbond starts at the bonded interface. The straps can still carry the load but are less effective because of the lack of shear transfer capability [4]. Disbonding promotes negative contribution to FCG. Disbonding effect can be influenced by using high strength adhesive or advisable surface pretreatment methods. BCRs made of cross-ply laminates are recommended for weaker adhesives, because a complete disbond can be retarded. For tougher adhesives, the best stacking sequence is the unidirectional layup provided that under the load spectrum the strap does not disbond completely [5].

Stiffening: Two parts made of dissimilar materials are bonded together and loaded by a tension. Same displacement should be maintained. The part made of material with higher elastic modulus (e.g. BCR) transfer more load than the part made of material with lower elastic modulus. Consequently, the BCR transfer load from the substrate. However, BCR with higher stiffness could promote disbond failure [9].

Bridging: BCR restrain the crack tip opening by the restraining forces, reduction of the stress intensity factor is obtained [9]. Restraining forces depend on the strip stiffness between the edges of the delaminated area of the BCR [3]. Bridging has a favorable effect to FCG.

Thermal residual stresses: When the coefficients of thermal expansion between BCR and substrate deviates, thermal residual stress (TRS) will occur. The level of thermal residual stress is related to environment temperature. In order to maintain self-equilibrium in a structure, the residual stresses act together [8]. Tensile TRS induced in the sheet is bal-

anced by compressive TRS induced in stiffening element. Compressive thermal residual stress can negatively affect fatigue life [10].

Fatigue sensitivity: When the crack passes the BCR, crack nucleation occurs in adjacent BCR made of fatigue sensitive material. Crack nucleation can promote failure of the BCR in the future, resulting in shorter fatigue life. This behavior was observed in experiments with sheet and BCR made of same material, the Al-alloy [3].

4 Specimen description

Tests were carried out on the CCT specimens with three different geometries. Dimensions of CCT specimens are presented in Fig. 1. First, the referential (bare) Specimen 1 without grooves and BCRs was tested. The capability of retarding the crack growth was examined for the Specimen 2 with one steel layer and Specimen 3 with two steel layers. Bonded crack retarder cross sections are mentioned in Fig. 2. The CCT specimens were high-speed milled from a sheet made of 2024-T351 aluminium. The material at the location of BCR (Specimen 2, 3) was removed because the steel has high density. Potential weight increase in the specimens was partly compensated. Mechanical properties and chemical compositions of substrate, BCR and adhesive are shown in Tab. 1, 2.

Fig. 1 CCT specimen shape. BCRs was bonded to grooves with length 210 mm and depth 0.4 mm. Dimensions in mm.

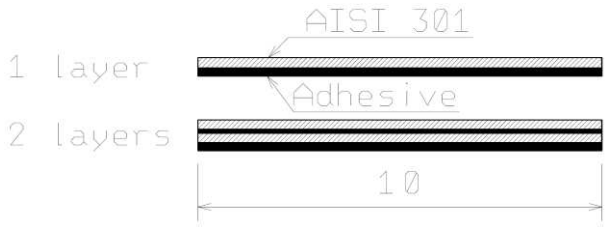

Fig. 2 Bonded crack retarder cross sections. Dimension in mm.

Substrate surface pretreatment: The surface was degreased with an acetone and FPL etched in the bath composed of 6.4 % $Na_2Cr_2O_7$*$2H_2O$, 23.4 % H_2SO_4 and 70.2 % H_2O (weight fraction). FPL etching duration was 4 hours at ambient temperature. Finally, the substrate was rinsed in a water and blow-dried with 45 °C air.

Strap surface pretreatment: The straps were cut out of a sheet made of 0.255 mm thick AISI 301 corrosion resistant steel and degreased with an acetone. After that, the straps were immersed in a solution containing 12.5 % HF, 40.8 % H_2O, and 46.7 % HNO_3 for 20 minutes at ambient temperature. At the end, the straps were rinsed in a water and blow-dried with 45 °C air.

Adhesive bonding: In both cases, the straps were bonded onto the specimen surface by the two-component Araldite® 2011 structural adhesive. The Specimen 2 with one steel layer was cured for 24 hours at ambient temperature and for 30 minutes at 80 °C.

The straps were bonded onto the Specimen 3 surface in a several following steps. First, two steel straps were bonded together and cured. An excessive adhesive layer on the outer surfaces of the bonded straps was removed. The bonded straps were degreased with an acetone and immersed in the solution containing H2O, HF and HNO3 for 20 minutes at ambient temperature. Finally, the bonded straps consisted of two steel layers were bonded onto the substrate and cured. Same curing process was used as in the first case.

Tab. 1 Mechanical and thermal properties of substrate, bonded crack retarder and adhesive

			2024-T351[a]	AISI 301	Araldite® 2011
Young's elastic modulus	E	[GPa]	72.4	185[b]	-
Shear modulus	G	[GPa]	-	-	0.9[e]
Poisson's ratio	ν	[-]	0.33	0.27[c]	-
Thickness	t	[mm]	2	0.255	0.2[f] / 0.2[g] / 0.1[h]
Density	ρ	[g/cm^3]	2.77	8[d]	1.05[e]
CTE (20°C)	α	[10^{-6}/K]	23	17[d]	-
Ultimate Tensile Strength	Rm	[MPa]	470	1635[b]	-
Yield Strength	$Rp_{0.2}$	[MPa]	325	1508[b]	-
Elongation	A	[%]	20	2.1[b]	-
Shear Strength	τ	[MPa]	-	-	15 - 18[i]

Tab. 2 Chemical composition of substrate and bonded crack retarder material

	Si	C	Fe	Cu	Mn	Mg	Cr	Ni	Zn
2024-T351[a]	0.5	-	0.5	3.8 - 4.9	0.3 - 0.9	1.2 - 1.8	0.1	-	0.25
AISI 301[c]	1	0.15	-	-	2	-	16.0 - 18.0	6.0 - 8.0	-

[a] ASM INTERNATIONAL HANDBOOK COMMITTEE. (1990). Properties and selection: Nonferrous alloys and special-purpose materials.ASM International, Netherlands.
[b] DYMÁČEK, P., KLEMENT, J. (2011). Properties and manufacturing of steel-C/epoxy fiber-metal laminates. In: Proceedings of the Fourth Seminar on Recent Research and Design Progress in Aeronautical Engineering and its Influence on Education: Part II, pp. 47-52. Institute of Aeronautics and Applied Mechanics, Warsaw.
[c] (2001). Stainless Steel - Grade 301. AZo Materials. In: Atlas Speciality Metals, Australia
[d] ASM INTERNATIONAL HANDBOOK COMMITTEE. (1990). Properties and Selection: Irons, Steels, and High-Performance Alloys. ASM International, Netherlands.
[e] (1994). *Araldite® 2011 (AW106 + HW953U): Dvoukomponentní konstrukční lepidlo na bázi epoxidové pryskyřice*. pp. 1. Vantico, Vídeň.
[f] Specimen 2; thickness between strap and substrate
[g] Specimen 3; thickness between strap and substrate
[h] Specimen 3; thickness between steel layers
[i] Lap shear strength test: AISI 301 + 2024-T351

5 Fatigue crack growth test and results

Specimens were subjected to a crack propagation test with subsequent parameters: σ_h = 60 MPa, R = 0.1 and f = 15 Hz. Crack length was periodically measured by a microscope with a metric scale on both sides of the specimen. The cyclic load was applied until final failure of the specimen. During the crack propagation test no crack initiation was observed in the BCRs. Steel straps broke (Specimen 2) or disbond (Specimen 3) shortly after the substrate failure.

Crack lengths were plotted as a function of the number of cycles, see Fig. 3. Fatigue life of the specimen with one steel layer was increased by a factor of 1.4 and fatigue life of the specimen with two steel layers was increased by a factor of 1.9. BCRs led only to a slight weight increase of 4.7 % in Specimen 2 and 9.3 % in Specimen 3.

6 Future work

The results of this paper will be compared to another possibilities promoting the fatigue crack growth retardation. A study of the influence of crack retarders prepared by a cold spray technology and an autoclave technology on fatigue crack growth is expected. The most promising technology will be applied onto full-scale integral panel and resulting increase in fatigue crack growth life will be compared to bare integral panel, which was tested during the DaToN project [11].

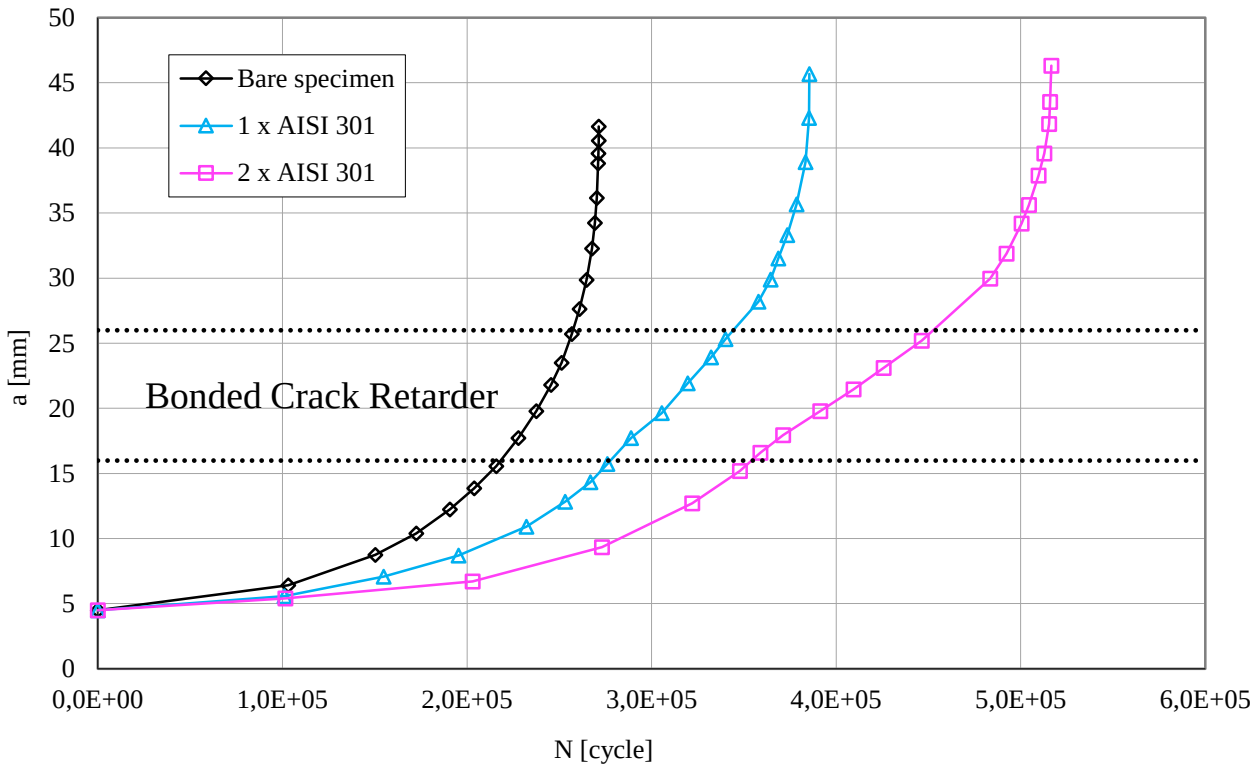

Fig. 3 Crack propagation curves: CCT specimens with two different strap geometries

Acknowledgement

The research leading to these results has received funding from the MEYS under the National Sustainability Programme I (Project LO1202).

References

[1] NIU, M. (1989). Airframe structural design, pp. 261. Conmilit Press Ltd., Hong Kong.

[2] NESTRENKO, G. (2000). Comparison of damage tolerance of integrally stiffened and riveted structures, pp. 6. ICAS Congress, Harrogate.

[3] SCHIJVE, J. (1990). Crack stoppers and arall laminates. In: Engineering Fracture Mechanics, Vol. 37, No. 2, pp. 405-421. Pergamon Press, New York.

[4] ZHANG, X., LI, Y. (2005). Damage Tolerance and Fail Safety of Welded Aircraft Wing Panels. In: AIAA Journal, Vol. 43, No. 7, pp. 1613 – 1623. American Institute of Aeronautics and Astronautics, Reston.

[5] BOSCOLO, M., ALLEGRI, G., ZHANG, X. (2008). Design and Modelling of Selective Reinforcements for Integral Aircraft Structures. In: AIAA Journal, Vol. 46, No. 9, pp. 2323 – 2331. American Institute of Aeronautics and Astronautics, Reston.

[6] IRVING, P., ZHANG, X., DOUCET, J., et al. (2011). Life Extension Techniques for Aircraft Structures – Extending Durability and Promoting Damage Tolerance through Bonded Crack Retarders. In: ICAF 2011 Structural Integrity: Influence of Efficiency and Green Imperatives (J. Komorowski, (Ed.)), pp. 753 – 770. Springer, Dordrecht.

[7] MOLINARI, G., MENEGHIN, I., MELEGA, M., TROIANI, E. (2012). Parametric damage tolerance design of metallic aeronautical stiffened panels. In: The Aeronautical Journal, Vol. 166, No. 1182, pp. 815-831. Royal Aeronautical Society, London.

[8] SCHIJVE, J. (2009). Fatigue of structures and materials, pp. 519. Springer, Berlin.

[9] ZHANG, X., BOSCOLO, M., FIGUEROA-GORDON, D., et al. (2009). Fail-safe design of integral metallic aircraft structures reinforced by bonded crack retarders. In: Engineering Fracture Mechanics, Vol. 76, No. 1, pp. 114 – 133. Pergamon Press, New York.

[10] MENEGHIN, I., IVETIC, G., TROIANI, E. (2011). Analysis of Residual Stress Effect on Fatigue Crack Propagation in Bonded Aeronautical Stiffened Panels. In: Material Science Forum, Vol. 681, pp. 236 – 242. TTP. Switzerland.

[11] LANCIOTTI, A., LAZZERI, L., POLESE, C., et al. (2011). Fatigue crack growth in stiffened panels, integrally machined or welded (LBW or FSW): The DaToN project common testing program. In: SDHM Structural Durability and Health Monitoring, Vol. 7, No. 3, pp. 211 – 230. Tech Science Press, Duluth.

Materials for mechanical seals in military applications

Ivan Kopecký*, Danka Rakúsová*, Peter Lipták*

* Faculty of Special Technology, Trenčín University of A. Dubček in Trenčín Pri parku 19, 91105 Trenčín, e-mail: ivan.kopecky@tnuni.sk
† Faculty of Special Technology, Trenčín University of A. Dubček in Trenčín Pri parku 19, 91105 Trenčín, e-mail: danka.rakusova@tnuni.sk
† Faculty of Special Technology, Trenčín University of A. Dubček in Trenčín Pri parku 19, 91105 Trenčín, e-mail: peter.liptak@tnuni.sk

The mechanical seals are parts of equipment in petrol stations [1] as a part of standard pumps, in sewage systems, in water treatment pumps. They are adaptable to water pumps, chemical pumps and general rotary equipments as well as for corrosiveness equipments (sulfuric acid, hydrochloric acid, nitric acid). They are suitable for heavy pollution, others for vacuum and high pressure interchange equipment. The material, the mechanical seals are produced from, depends on their application. Therefore the question of kind and quality of material for mechanical seals is not a simple one. A bad choice of material for mechanical seals significantly reduces a lifecycle of all expensive equipment [2].

Keywords: mechanical seals, application conditions, temperature, pressure, standard materials

Fig. 1 Water treatment facility

1 Introduction to Mechanical seals

A mechanical seal is simply a method of containing a fluid within a vessel (typically pumps) where a rotating shaft passes through a stationary housing or, occasionally where the housing rotates around the shaft [3]. When sealing a centrifugal pump, the challenge is to allow a rotating shaft to enter the "wet" area of the pump, without allowing large volumes of pressurized fluid to escape. To address this challenge there needs to be a seal between a shaft and the pump housing that can contain the pressure of the process being pumped and withstand the friction caused by the shaft rotating.

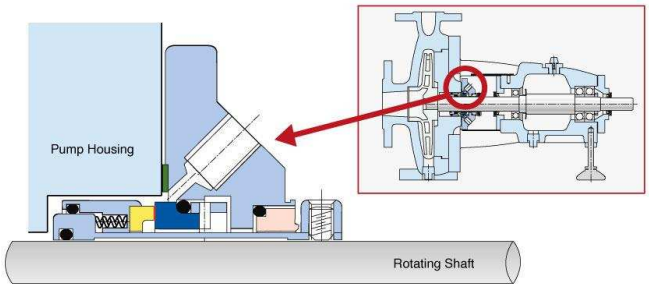

Fig. 2 Mechanical sealing

1.1 Traditional Methods

Fig. 3 Gland Packing

Before examining how mechanical seals function it is important to understand other methods of forming this seal. One such method still widely used is Gland Packing. Gland packing is a rope like material that is packed around the shaft - physically stuffing the gap between the shaft and the pump housing. Gland packing is still commonly used in many applications, however increasingly users are adopting mechanical seals for the following reasons:

- The friction of the shaft rotating wears away at the packing over time, which leads to increased leakage until the packing is adjusted or re-packed.
- The friction of the shaft also means that packing also needs to be flushed with large volumes of water in order to keep it cool [4].
- Packing needs to press against the shaft in order to reduce leakage – this means that the pump needs more drive power to turn the shaft, wasting energy.
- Because packing needs to contact the shaft it will eventually wear a groove into it, which can be costly to repair or replace.

Mechanical seals are designed to overcome these drawbacks.

2 Design

A basic mechanical seal contains three sealing points.

The stationary part of the seal is fitted to the pump housing with a static seal –this may be sealed with an o-ring or gasket clamped between the stationary part and the pump housing.

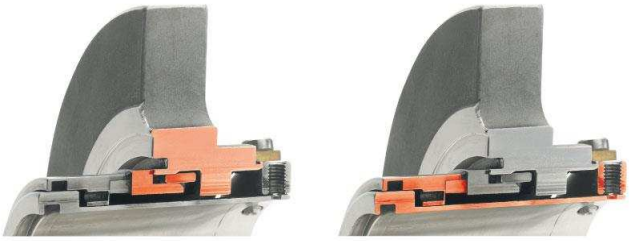

Fig. 4 Mechanical seal – a stationary and rotating parts.

The mechanical seal itself is the interface between the static and rotary portions of the seal. One part of the seal, either to static or rotary portion, is always resiliently mounted and spring loaded to accommodate any small shaft deflections, shaft movement due to bearing tolerances and out-of-perpendicular alignment due to manufacturing tolerances.

A. A Sealing Points

While two of the sealing points in a seal design are simple static seals, the seal between the rotating and stationary members needs a little more consideration. This primary seal is the basis of all seal design and is essential to its effectiveness.

The primary seal is essentially a spring loaded vertical bearing - consisting of two extremely flat faces, one fixed, one rotating, running against each other. The seal faces are pushed together using a combination of hydraulic force from the sealed fluid and spring force from the seal design [5]. In this way a seal is formed to prevent process leaking between the rotating (shaft) and stationary areas of the pump.

The surfaces of the seal faces are super-lapped to a high degree of flatness; typically 2-3 Helium light-bands (0.00003" / 0.0008mm)[6].

If the seal faces rotated against each other without some form of lubrication they would wear and quickly fail due to face friction and heat generation. For this reason some form of lubrication is required between the rotary and stationary

seal face; this is known as the fluid film.

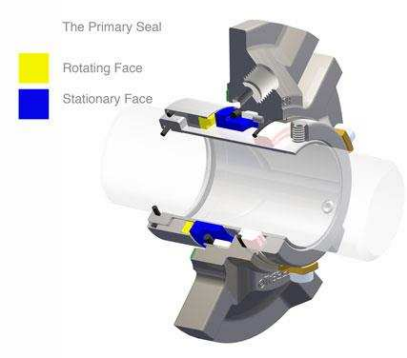

Fig. 5 The primary seal

B. The Fluid Film

In most mechanical seals the faces are kept lubricated by maintaining a thin film of fluid between the seal faces. This film can either come from the process fluid being pumped or from an external source. The need for a fluid film between the faces presents a design challenge – allowing sufficient lubricant to flow between the seal faces without the seal leaking an unacceptable amount of process fluid, or allowing contaminants in between the faces that could damage the seal itself. This is achieved by maintaining a precise gap between the faces that is large enough to allow in a small amounts of clean lubricating liquid but small enough to prevent contaminants from entering the gap between the seal faces.

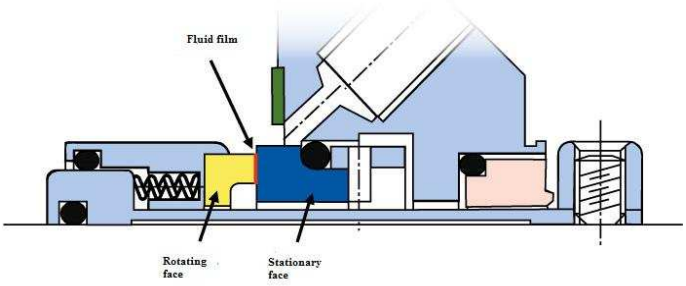

Fig. 6 Elements of a seal.

The gap between the faces on a typical seal is as little as 1 micron – 75 times narrower than a human hair. Because the gap is so tiny, particles that would otherwise damage the seal faces are unable to enter, and the amount of liquid that leaks through this space is so small that it appears as vapor – around ½ a teaspoon a day on a typical application. This micro-gap is maintained using springs and hydraulic force to push the seal faces together, while the pressure of the liquid between the faces (the fluid film) acts to push them apart.

III. Production pressures can lead to mechanical seal failure

- Misalignment
- Dry Running (caused by no flow through a seal)
- Solids and abrasion
- Vibration caused by cavitation

Mechanical seals fail for two reasons:
-The seal face is open
- A part becomes damaged

The problem of oversized pumps
Discharge recirculation
-You start to re-circulate the fluid in the pump
-This changes the fluid velocity
-This changes the fluid pressure and lead to hydraulic imbalance
-This leads to vibration and damage to the mechanical seal

C. Leakage

When we talk about leakage we are referring to visible leakage of the seal. This is because as detailed above, a very thin fluid film holds the two seal faces apart from each other. By maintaining a micro-gap a leak path is created making it impossible for a mechanical seal to be totally leak free. What we can say, however, is that unlike gland packing, the

amount of leakage on a mechanical seal should be so low as to be visually undetectable.

Leakage can occur at any time throughout the life of the mechanical seal. To troubleshoot leaking seals effectively it is helpful to know just when the leakage starts. This is the advantage of being able to troubleshoot a running pump, or one that is still hooked up to its piping. By noting the type of leakage and when the leakage occurs, we can do a more thorough job of analyzing any seal failure. In addition to leakage it is needed to look for other symptoms that are visible to the trained troubleshooter.

The Fig. 7 shows different types of leakage in the following diagram of a stationary seal design in an API gland and installed on a jacketed pump.

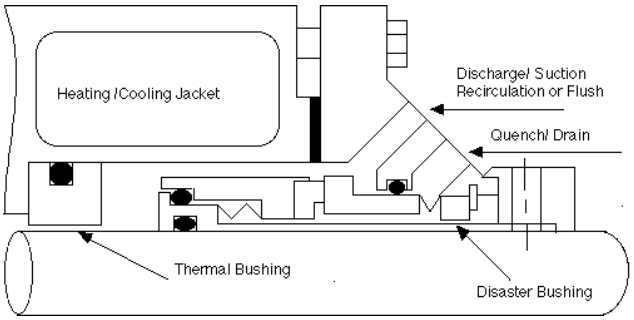

Fig. 7 Types of leakage

The leakage occurs while the pump is both running and stopped.

The leakage can be detected visually, by odor, or by instrumentation. A strobe light can sometimes be used to determine its location.

III. SOME POSSIBLE PLACES AND REASONS FOR LEAKING DURING OPERATION ARE:

At the lapped faces. Since they are a wearable surface the leak will probably get either better or worse. It should never remain constant. The leak started because:

The outside springs in a dual cartridge seal were painted during routine maintenance.

The spring load has been reduced because of thermal growth, axial thrust, or impeller adjustment.

The seal was set-screwed to a hardened shaft and the set screwa have vibrated loose.

One or both of the seal faces is not flat. Solid tungsten carbide and silicon carbide faces are often lapped flat on only one side. Check to see if the face has been installed backwards.

The dynamic elastomer has swollen up and seized the spring loaded face; preventing it from remaining in contact with the stationary face.

The product has prevented the lapped seal faces from remaining in contact.

Dirt has gotten into the sliding components.

- The product has crystallized.
- The product solidified or became very viscous.
- The product is vaporizing across the seal faces, expanding and blowing them open.

At the static and dynamic elastomer locations.

This type of leak tends to remain constant and will often stop when the small opening clogs up with solids. The leak can be caused by a damaged rubber part, or damage on the surface where the elastomer seals. In some instances the elastomer is not seated properly. It twisted because of either poor installation, excessive shaft movement, or high pressure extrusion.

At the gland gasket. This is the easiest leak to detect because it's very visible and does not change with shaft rotation.

Between the shaft sleeve and the shaft.

This is a common problem with double ended pumps, where the sleeve is used to position the impeller and there is no method of sealing the sleeve against the impeller.

Between the seal face and its metal holder.

The leakage frequently increases, as the product temperature increases, because the metal face holder has an expansion rate three times that of the carbon face.

Through fretting damage

- The damage is caused by spring loaded dynamic o-rings, Teflon wedges, chevrons, U- cups etc.
- You can't miss the frett marks. They'll be located on the pump shaft, pump sleeve, or inner sleeve of the mechanical seal.
- The seal leaks only when the pump is running.
- The stationary face has been over tightened against the stuffing box face causing it to go out of flat. Statically the carbon will readjust to the distorted hard face and not leak.
- The clamping is not equal and opposite across the static seal face. Checking for different width gaskets at the front and rear of the static face is needed. Again, the carbon will readjust and stop leaking when the shaft is not turning.
- Between the face and holder.
- The holder heats up and expands faster than the pressed in face. The leak will begin when the metal holder comes up to temperature. Metal expands three times faster than a typical seal face.
- Cryogenic (cold) service will harden the elastomer. Need to check for the lower temperature limit of the elastomer being selected.
- Misalignment between the pump and the driver.
- The shaft is bending and not allowing the seal to move freely. This occurs if the pump is operating off of its best efficiency point and the shaft is not small enough to resist the bending.
- The product is vaporizing across the seal faces.
- Cavitation, slip stick, harmonic, or some other type of vibration is bouncing the faces open, need to check the lugs or drive pins for sign of excessive wear.
- The seal was installed without enough compression, or the impeller was adjusted after the seal was installed and thermal expansion of the shaft is opening the faces.
- A discharge recirculation line is aimed at the seal faces, or some other critical point and the faces are being forced open.
- A non- concentric seal, bad sleeve installation, or an out of balance rotating assembly is causing the rotating portion of the seal to run off the stationary face.
- A bent shaft can cause the rotating portion of the seal to run off the stationary face.
- The rotating portion of the seal is hitting a stationary object. Need to look for:
- A protruding gasket or fitting.

A foreign object that has worked its way into the stuffing box area.
A stationary portion of the rotating equipment, such as a close fitting bushing.
At elevated temperature the product thins out (the viscosity decreases) and is leaking through an elastomer. It will not leak at the cooler temperature when the product viscosity is higher.
High temperature is causing the lapped seal face to go out of flat.

3 Materials

Quality of material plays the vital role in operation of the mechanical seal. High quality sealing products include Oring, rotary seals (PTFE oil seals, oil seals, Vrings), static seals (packing, spiral wound gasket, metallic gasket, flexible graphite gasket, bonded seals), hydraulic seals (rod seals, hydraulic seals, piston seals, U-ring/U-cup), hydraulic scrapers, hydraulic wear rings, pneumatic seals.

Considering the working conditions, repaired seals can be upgraded by replacing carbon faces with silicon carbide or tungsten carbide[7]. When the seals are being repaired, they are to be cleaned, inspected for factory tolerance, faces are to be replaced (if required) otherwise lapped, new springs, new elastomer (rubber boot or o-rings), new set screw, new setting clips, (if cartridge seal), lapped to industry standard (within 2 helium light bands).

4 Conclusion

Mechanical seal engineering focuses on increasing the longevity of the primary seal faces by ensuring a high quality of lubricating fluid, and by selecting appropriate seal face materials for the process being pumped.

Acknowledgment

This publication was created in the frame of the project Research of a technological base for draft of application of renewable sources of energy in practice, ITMS code 26220220083, of the Operational Program Research and

Development funded from the European Fund of Regional Development.

References

[1] D**.** Rakusova, " Need for mechanical protection of Gabcikovo ship lock", 2015. In: Recent advances on mechanics, materials, mechanical engineering and chemical engineering: Proceedings of the international conference on mechanics, materials, mechanical engineering and chemical engineering Barcelona, Spain. - Sofia : Institute for Natural Sciences and Engineering, 2015. - ISBN 978-1-61804-295-8. - p.88-97.

[2] J. Balla, Z. Krist, Ich Le Cong: Infantry fighting vehicle in case of burst firing, 2015. In: International Conference on Military Technologies : ICMT 2015. - Brno : University of Defence, 2015. - ISBN 978-80-7231-976-3. - p.3-8, CD ROM.

[3] P. Liptak, J. Stodola, D. Rakusova: Methodology of risk analysis: In: University review. - ISSN 1339-5017. - Vol.8, No.3-4(2014), p.90-93.ty review. - ISSN 1339-5017. - Vol.8, No.3-4(2014), p. 90-93.

[4] A.V. Aliev, J. V. Merzliakov, P. Lipták, I. Kopecký: Ochlaždenie konstrukcii gazoperekačivajuščego agregata 2016. In: Medzinárodná vedecká konferencia o vojenských a špeciálnych technológiách 2016 : ICMT-2016. Zborník príspevkov. - Trenčín : TnUAD, 2016. - ISBN 978-80-8075-743-4. - s.244-248, CD ROM

[5] A. V. Aliev, A. V. Volochin, V. A. Volochin, P. Lipták, I. Kopecký: Predochraniteľnyj klapan dlja zapornogo protivovybrosovogo oborudovanija 2016. In: Medzinárodná vedecká konferencia o vojenských a špeciálnych technológiách 2016 : ICMT-2016. Zborník príspevkov. - Trenčín : TnUAD, 2016. - ISBN 978-80-8075-743-4. - s.234-237, CD ROM.

[6] O. V. Mišenkova, D. S. Blinov, P. Lipták, I. Kopecký: Modelirovanie raboty gazogeneratora pri vychode na kvazistacionarnyj režim 2016. In: Medzinárodná vedecká konferencia o vojenských a špeciálnych technológiách 2016 : ICMT-2016. Zborník príspevkov. - Trenčín : TnUAD, 2016. - ISBN 978-80-8075-743-4. - s.238-243, CD ROM.

[7] P. Lipták, I. Kopecký, P. Radič: The possibilities for improving the properties of materials by plasma nitriding 2016. In: Transport means 2016 : 20th international conference. Part III. - Kaunas : Kaunas University of Technology, 2016. - ISSN 1822-29

Mechanical and tribological features of the 31CrMoV9 steel after plasma nitriding

Michal Krbata[1], Vojtech Hruby[1], Danka Rakusova[1]
[1]Faculty of Special Technology, Alexander Dubcek University of Trencin. Pri parku 19, 911 06 Trencin. Slovak Republic. E-mail: michal.krbata@tnuni.sk, mkrbata@gmail.com, Tel: +421 7400 265

The paper deals with a change of mechanical features and wear after plasma nitriding of the 31CrMoV9 structural steel having a broad range of application in special equipment mainly in aircraft engines. Plasma nitriding was performed at a temperature of 500 °C for 10 hours period in a standard N2 /H2 atmosphere with 1:3 gases ratio. Microstructure, phase structure, thickness of a nitriding layer and surface roughness of samples were measured with optical microscopes and a profilemeter. Verification of a chemical composition was carried out on the BAS TASMAN Q4 device. Wear resistance was measured on a general BRUKER UTM 3 tribometer, through a, "pin on disc" method. The results of experiments have shown that plasma nitriding process, significantly improves the mechanical properties of selected materials.

Keywords: plasma nitriding, microhardness, friction coefficient, pin on disc,

1 Introduction

The 31CrMoV9 structural steel is suitable for plasma nitriding process due to its chemical composition. This steel has a broad range of application for production of complex engine parts. Tribology of these parts plays an important role in their functionality and lifetime. Tribological problems can often be solved with a surface finish. Plasma nitriding, with regard to many advantages unlike common kinds of nitriding found an increasing industrial application [1]. The main problem of nitridations in salt bathes is connected with a toxicity of cyanide salts. Traditional gaseous nitriding requires a longer time for treatment to obtain a needed nitridation depth. Direct current of plasma nitriding (DCPN) has been recently one of conventional treatment of a surface finish being used in industry aiming to improve mechanical features and wear resistance of mechanical engineering materials [7]. Various layers may rise on a surface due to a plasma nitriding. These layers are classified by composition of particular phases. With respect to a steel composition, its layer is mainly composed of ferrous nitrides (γ'-Fe_4N or ε-$Fe_{2-3}N$) and nitrides of alloying elements [1-3].
Research studies showed that a microstructure of a nitriding layer can be affected with a change of parameters of a nitriding process, as temperature, time and plasma composition of the gas. Changes in a microstructure of nitriding layer effect mechanical and tribological features of the material, as surface hardness, wear resistance and endurance strength [3, 4]. For a diffusion controlled growth, a thickness of a nitriding layer increases with temperature and nitridation time. [4-6]. However a maximum surface hardness is achieved only at a certain nitridation time and temperature. Previous studies showed that a chemical potential of nitrogen is important a plasma nitriding of steels.

2 Experiment

The samples were standardized, hardened at 850 °C into oil and tempered at 550 °C temperature aiming to achieve optimal mechanical features. Process of a plasma nitriding was carried out on the Rubig 60/60 device. The parameters of a plasma nitriding were chosen so that a nitriding layer is reached as thick and as hard as possible, Tab. 1.
Thermally treated and surface finished steel samples were numerically marked. Chemical composition of given steel was verified through a BAS TASMAN Q4 device and subsequently it was compared with the DIN 31CrMoV9 technical standard Tab. 2.

Measurements of micro hardness and thickness of a nitriding diffusion layer were taken on each sample through a Vickers method. Impressing of a diamond pyramid under vertex angle of136º is essence of the method. The LECO M400H microhardnessmeter will be used to verify and to compare achieved results before and after plasma nitriding. The load force will be 0, 5 N and force action time in accordance with DIN 50190 standard will be 10 sec. The measurements of micro hardness will be taken on a cross-section of a nitrided sample, upright from a surface to the material core. The achieved values on hardness will be displayed as a function of a distance from a surface. Thickness of a nitride layer will be taken on 18 imprints and 5 imprints in the material core. Limit value in terms of this standard is a hardness value, designated as limit hardness GH) and it is indicated as the Vickers hardness and it applies:
GH=average measured value in a core + 50 HV (rounded to 10HV).

Metallographic analysis is based on a polishing of samples and a subsequent etching with Nital. Etching of samples brings up their microstructures. We make out matallographical pictures of all samples with the Olympus GX51 optical matallographical microscope. With the microscope we can monitor a size of a white layer as well as an approximated size of a diffusion layer. Then we can assess a resulting structure of a diffusion layer as well as a basic material.
Roughness of surface was measured on the Talisurf CCI Lite 3D device. All samples had been grinded on a magnetic grinder with 0,001mm precision before plasma nitriding and marking. Surface roughness was measured before and after plasma nitriding aiming to define changes of roughness.

Measurement of wear was executed on the BRUKER UTM 3 device using,, pin of disc“method. This method is based on imprinting a firmly gripped body in a ball shape into a testing material in a disc shape, being rotated with constant revolutions. The testing ball was made of the 440-C stainless steel with a 6,35 mm diameter and 746 HV hardness. The measurements were taken from 6 samples at 3 loads and three measurement radiuses. The Measurement radiuses for each sample are shown in Tab. 3.

Pressure [mbar]	Voltage [V]	Atmosphere PN	Temperature PN [°C]	Time PN [hour]
2,8	700	N2 / H2 1/3	500	10

Tab. 1 The parameters of plasma nitriding

Element	C	Si	Mn	P	S	Cr	Mo	V
DIN Standard	0,27 -0,34	max 0,40	0,40 -0,70	max 0,025	max 0,035	2,30 -2,70	0,15 -0,25	0,10 -0,20
BAS Tasman Q4	0,34	0,39	0,69	-	0,034	2,38	0,21	0,20

Tab. 2 Chemical composition 31CrMoV9 steel [in wt. %]

Identifications of the samples	Heat treatment	Turning radius	Load [N]	Rotation speed [rpm]	Measuring time [min]
1	Quenching	19	50	250	20
		21	50		
		23	50		
2	Quenching	19	100	250	20
		21	100		
		23	100		
3	Quenching	19	150	250	20
		21	150		
		23	150		
4	Plasma nitriding	19	50	250	20
		21	50		
		23	50		
5	Plasma nitriding	19	100	250	20
		21	100		
		23	100		
6	Plasma nitriding	19	150	250	20
		21	150		
		23	150		

Tab. 3 Measurement parameters for tribology

3 Results

3.1 Metallographic structure

There is a microstructure of the 31CrMoV9 steel in the Fig. 1a in a treated condition and after having etched 2% Nital and it was assessed as a sorbitic one (martensite tempered to a high temperature). An average micro hardness had a value of 420 HV. We suppose that in a structure there is a residual austenite; however it was not metallographically proved. After plasma nitriding on a metallographic section there were expressly visible and measurable only thicknesses of white layers. There is a coherent and relatively even white layer of nitrides on the samples surface. Under a white layer there is a diffusion layer, composed of highly tempered martensite and nitrous ferrite.

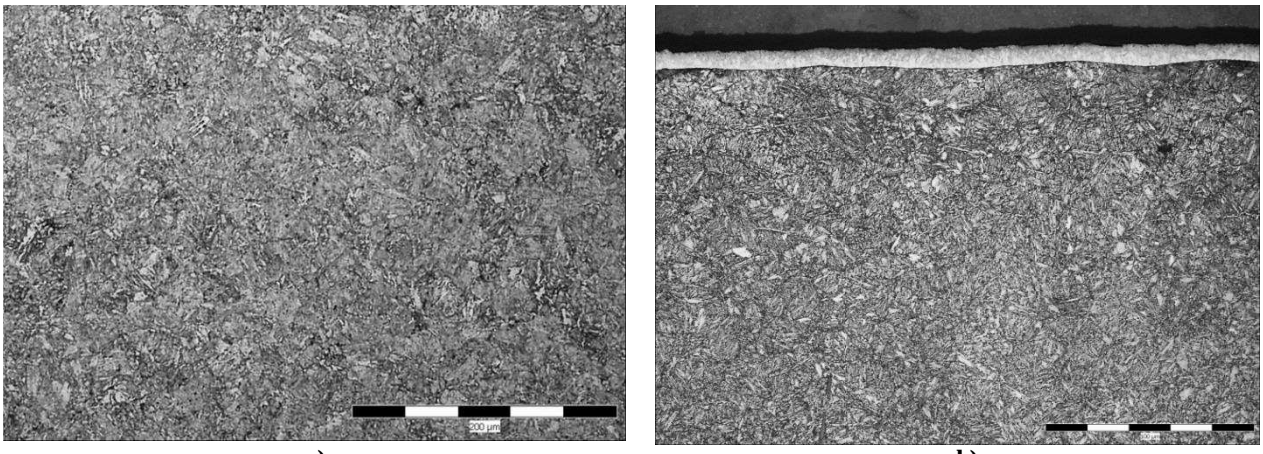

a) **b)**

Fig. 1 Cross-sectional microstructure

The white layer with an average thickness 5,6 μm was created at the plasma nitriding temperature of 500 °C and nitriding period of 10 hours (Fig. 1b). Micro structurally in this case a diffusion layer is distinguishable from a core and it consists of highly tempered martensite (a prevailing component). We can notice that all samples have indications of a nitriding netting being formed in a diffusion layer (Fig. 1a).

3.2 Profiles of micro hardness and a depth of steel nitriding layers

The Tab. 4 was developed from the measurement results, where thicknesses of particular diffusion layers of steels are documented. In the Tab. 4 there are also displayed the values of thicknesses of white layers on particular samples. From the table it is obvious that the results are the same for thickness of nitriding layer as well as for the white layer. At the sample 6 a minimum increase of a diffusion layer is visible, which shows no significant change in subsequent measurements. We can note that all samples had passed through plasma nitriding process at the same conditions and a risen diffusion layer is the same on all samples.

Identification of the sample	Thickness of diffusion lay-er[mm]	Thickness of white layer [mm]
4	**0,20**	**5,6**
5	**0,21**	**6,4**
6	**0,20**	**5,9**

Tab. 4 The results of thickness diffusion and white layers

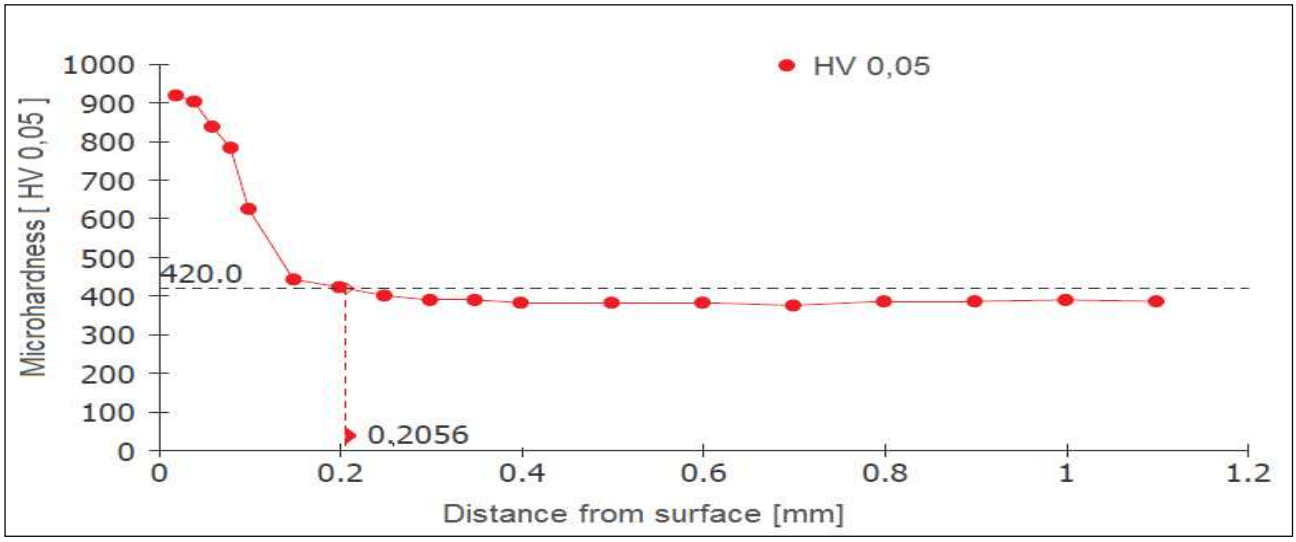

Fig. 2 Micro hardness depth profile sample No. 4

3.3 Surface roughness

Qualitative data on roughness are shown in Graph. 1. Surface roughness on all samples that had passed through a plasma nitriding process, deteriorated in average by 23 % comparing with samples without plasma nitriding. This deterioration was caused by a dedusting process and due to a rise of a new nitride surface layer.

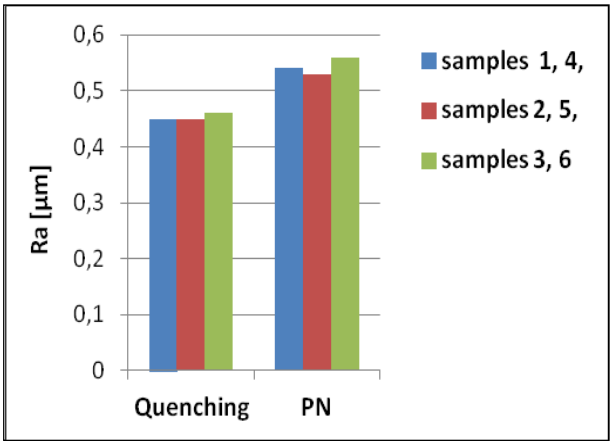

Graph. 1 Surface roughness Ra 31CrMoV9 before and after plasma nitriding

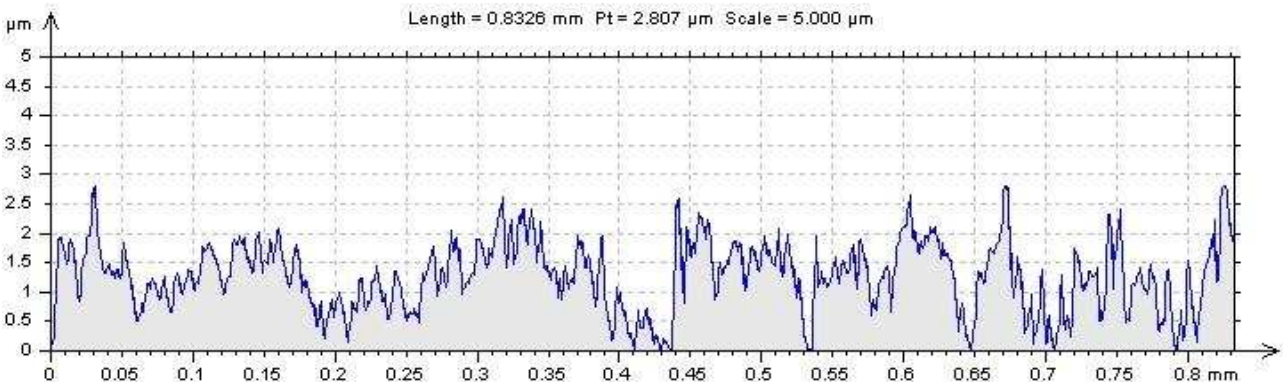

Fig. 3 *2D profile steel 31CrMoV9 without application of plasma nitriding; Ra 0,45µm*

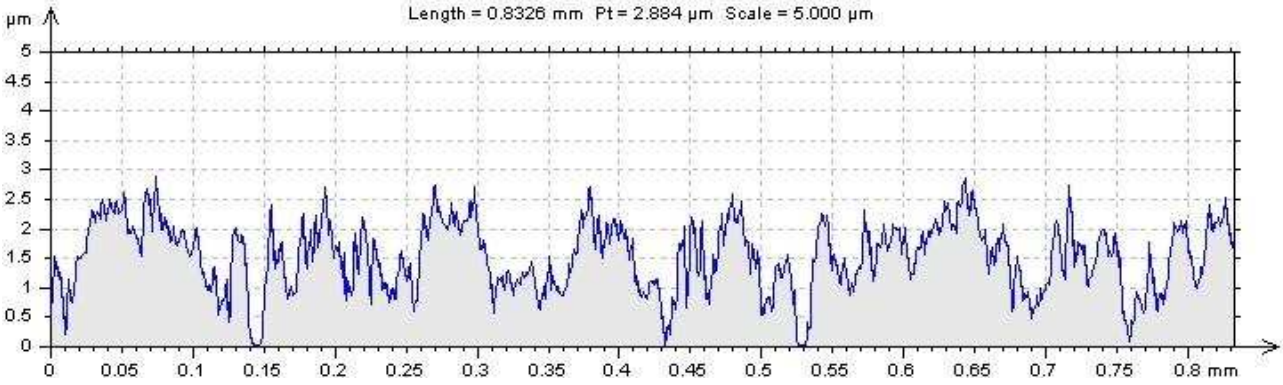

Fig. 4 *2D profile of the steel 31CrMoV9 nitrided at 500 °C and time of 10 hours; Ra* 0,54 *µm*

3.4 Wear resistance

The results on wear before and after plasma nitriding are shown in the Fig. 5. In the picture we can distinctly see different traces after wearing. The wear shown in the picture a), points at a high rate of wear, as this sample had passed only through a basic type of a thermal treatment. For the next samples b), c), d), a significant improvement of a surface profile occurred and these samples were plasma nitrided and they featured with much higher quality of surface. We can make a comparison in the Graph. 2 among all measurements of wear at different load parameters and different radiuses of rotation.

The depth of wear was measured with profile meter and the results are displayed on a plot in the Graph. 3. Each measurement of a depth was taken on four different places and subsequently an average depth of an imprint was

defined. The results expressly point at excellent mechanical features of plasma nitrided samples, as their depth of the imprint was ranging only in several micrometers comparing with tempered samples.

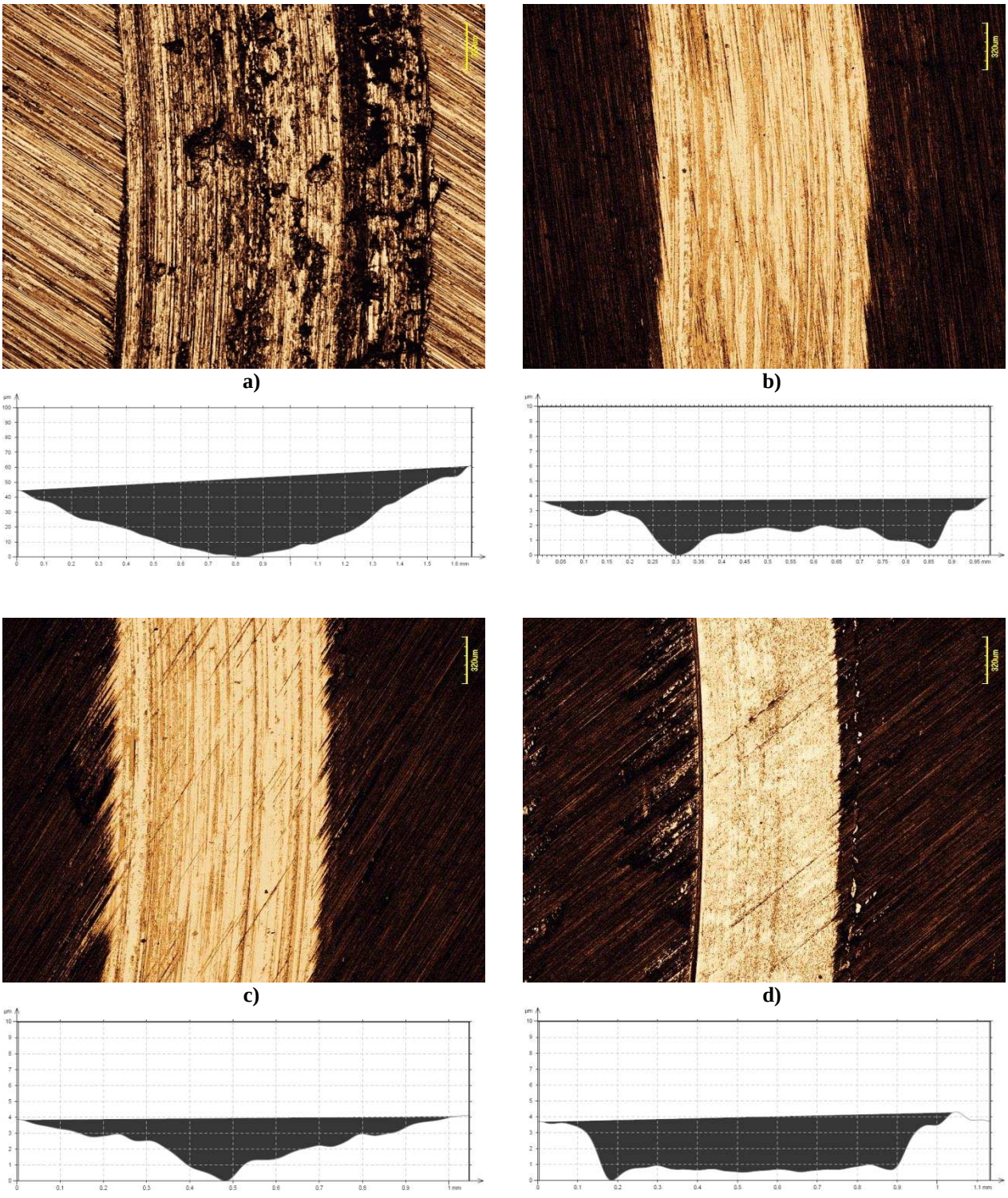

Fig. 5 Surface profiles of wear and depth tracks a) before PN, COF 0,59 μm, h 0,44 μm, b) after PN, COF 0,42 μm, h 3,8 μm, c) COF 0,40 μm, h 3,9 μm, d) COF 0,39 μm, h 4,1 μm

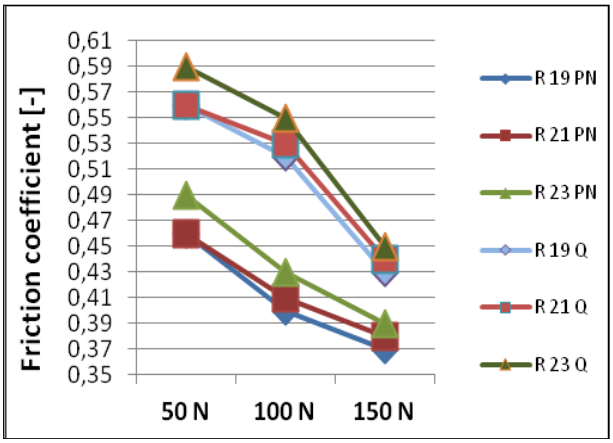

Graph. 2 Comparison of friction coefficient for all samples

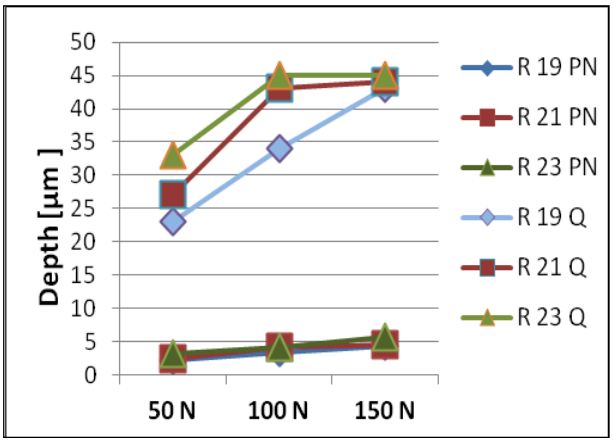

Graph. 3 Comparison indention depth in all samples

4 Conclusion

All measurements were focused on a study of the 31CrMoV9 structural nitride steel. Plasma nitriding was carried out at standard conditions and parameters were chosen in such a way to achieve the best possible diffusion layer. The research brought us some valuable information about mechanical features of the 31CrMoV9 steel. From a study of a microstructure and based on results the following conclusions can be made:

- The 31 CrMoV9 structural steel is suitable for a plasma nitriding process due to is chemical composition and the results of micro structure point at a rise of a diffusion layer of 6,1 mm thickness, mainly composed of ε-phase (Fe2-3N).
- A surface hardness of tempered samples had a value of 390 HV, it increased after plasma nitriding in average to a value of 1000 HV, i.e. we can note, that plasma nitriding significantly increases a surface hardness and so the lifetime as well, as the majority of degradation processes start spreading from the surface into the material core.
- Material roughness before nitriding process was ranging on the level of 0,45 µm, after plasma nitriding the surface quality got worse by 23 % to the value of 0,54 µm. Such deterioration is caused by a dedusting process, when the nitride cations bombard a material surface and subsequently atoms of various elements, being on a material surface are shot out.
- Resistance to wear plays one of the most important roles in a material lifecycle. Plasma nitriding process significantly decreases a friction coefficient. The friction coefficient decreased at plasma nitrided samples comparing with samples that had passed only a basic thermal treatment at all three loads. The same results are obtained from an imprint depth, left by a measuring ball. These findings are connected with a rise of a hard diffusion layer on a surface after a plasma nitriding process.

From the results of the experiment we can state that a plasma nitriding improves a quality of mechanical features of the 31CrMoV9 steel except of material roughness. It brings a great benefit in area of improvement of tribological

features of materials as well as their application in various sectors of mechanical engineering industry.

References

[1] O. Öztürka, O. Onmuya, D.L. Williamson, Surf. Coat. Technol. 196 (2005) 341–348.

[2] M. Keddam, Appl. Surf. Sci. 254 (2007) 2276–2280.

[3] A.K. Sinha, Physical Metallurgy Handbook, McGraw-Hill, New York, 2003

[4] A. Alsaran, A. Çelik, C. Çelik, Surf. Coat. Technol. 160 (2002) 219–226.

[5] F. Mahboubi, K. Abdolvahabi, Vacuum 81 (2006) 239–243.

[6] S.Y. Sirin, K. Sirin, E. Kaluc, Mater. Charact. 59 (2008) 351–35.

[7] C. Zhao, C.X. Li, H. Dong, T. Bell, Surf. Coat. Technol. 201 (2006) 2320–2325.

Mechanical Properties of Low-alloy (50CrV4 + QT) Steel after Plasma Nitriding

Mariana Kuffová[1],
[1]Department of Mechanical Engineering, Armed Forces Academy of Gen. M. R. Stefanik, Demanova 393, 031 06 Liptovsky Mikulas. Slovakia. E-mail: mariana.kuffova@aos.sk

Nitriding is a very effective method to increase the lifetime of constructive materials and tools by improving material properties, e.g. enhancing surface hardness, improving wear resistance (abrasive, adhesive, erosive, cavitation), reducing a friction coefficient, increasing a fatigue limit or corrosion resistance. The paper focuses on a low-alloyed steel 50CrV4 + QT after plasma nitriding. The low – alloyed (manganese – chromium - vanadium) steel is commonly used after heat treatment – quenching and tempering – QT (.7). This steel is widely used for highly loaded machines and parts of road vehicles: crankshafts of diesel engines, shafts of driving gears, connecting shafts, pins, springs, axle shafts and piston rods. A comparison of the surface hardness of the plasma nitrided sample and the samples that remained plasma untreated presents increases of 76% (HV1 after 5 hour nitriding) and 71% (HV1 after 20 hour nitriding), 135% (HV5 after 5 hour nitriding), and 107% (HV10), respectively, in plasma-treated samples. The enhancing effect of plasma-nitriding on the fatigue limit was thus confirmed attaining an improvement of 44% (5 hour plasma nitriding) and 57% (20 hour plasma nitriding).

Keywords: low-alloy steel 50CrV4+QT; plasma nitriding; hardness; tensile strength; yield strength; fatigue limit

1 Introduction

Nitriding is a very effective method to increase the lifetime of constructive materials and tools by improving material properties, e.g. enhancing surface hardness, improving wear resistance (abrasive, adhesive, erosive, cavitation), reducing a friction coefficient, increasing a fatigue limit or corrosion resistance. As a result, the nitriding process develops nitrides of iron in the diffusion layer inside the nitride material [1]. Nitriding is usually applied to the heat-treated material, i.e. after the chemical-thermal processing [2, 3, 4]. In order to avoid low durability and low reliability of components as a result of premature wear caused by friction, incidence of fatigue processes, corrosion, a number of other operational impacts [5] or insufficient attention given to mutual adjustment of multiple treatment processes [6], optimisation of design and conditions of technological processes, e.g. quenching [7], tempering [8], grinding [9], thermomechanical treatment [10], and others, are considered to be essential. This is even more pertinent to materials which are exposed to extreme loads. Any damage to such a component spreads from its surface or areas immediately below the surface. In order to increase service life of these components it is necessary to develop treatments that help improve the surface properties. Various approaches have been scrutinised to address this problem. For example, Mizukami et al. [11] attempted to improve the fatigue strength of components by tensile overloading prior to use. Singh and Mondal [12] examined the influence of quenching and tempering processes and the intensity of shot peening on the abrasive wear response of medium carbon SAE-6150 steel. Several years ago, Zenker et al. [13] published a comprehensive review on research and development in the combination of electron beam and laser beam surface processing with thermochemical surface treatment (nitriding, nitrocarburising, boronising) or PVD/CVD hard protective coating using different classes of steels (C45; 31CrMoV9; 50CrV4; 100Cr6; X100CrMoV5-1, X155CrVMo 12-1, X220CrVMo13-4). The authors also discussed the relationship between treatment conditions, process parameters and structure, composition and properties of layers, basic and composite materials.

2 Experimental material

As an experimental material, steel 50CrV4 was used. The low – alloyed (manganese – chromium - vanadium) steel is commonly used after heat treatment – quenching and tempering – QT (.7). Optimal diameter for that heat treatment is 80 mm. Welding of steel is difficult. Hot shaping is good. Machining after soft annealing is good. This steel is widely used for highly loaded machines and parts of road vehicles: crankshafts of diesel engines, shafts of driving gears, connecting shafts, pins, springs, axle shafts and piston rods. Steel is suitable for quenching and tempering and contains chemical elements which predetermine it to the chemical – thermal treatment, plasma nitriding.

Chemical composition is depicted in Table 1 and the microstructure is shown in Fig. 1.

Tab. 1 Chemical composition of low –alloyed steel 50CrV4 + QT

50CrV4+QT	**Chemical composition [wt.%]**								
	C	**Mn**	**Si**	**P**	**S**	**Cr**	**Ni**	**V**	**Cu**
Analysis	0.49	0.54	0.19	0.023	0.017	1.02	0.06	0.11	0.13

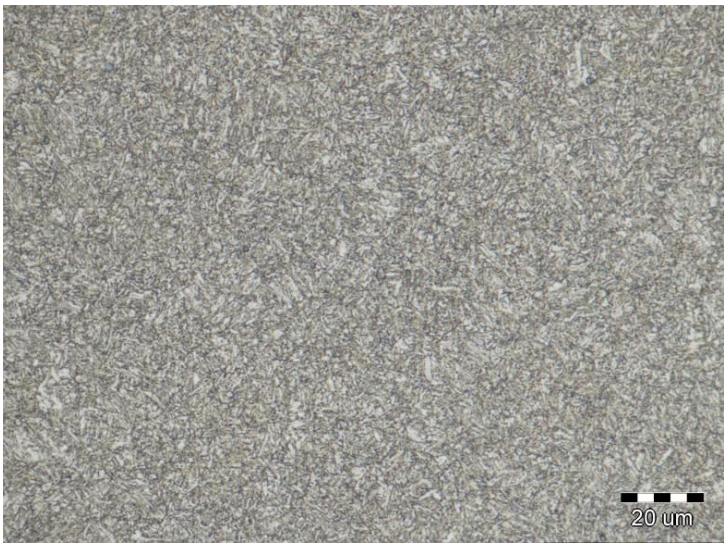

Fig. 1 Microstructure of low – alloyed steel 50CrV4+QT, magnified 1000x, etch. 2 % Nital

Microstructure of basic material steel 50CrV4+QT is created by heterogeneous structure formed by fine martensite and retained austenite as well as tempered martensite. Metallographic samples were observed by using the optic microscope OLYMPUS GX 51 and software ANALYSIS.

The measurement of non-metallic inclusions volume was obtained in accordance with STN ISO 4967. There was used the B method with determining area 0.50 mm^2 with magnitude 100x. Number of determining fields was N = 10. We have observed only inclusions of type A (fine sulphides) depicted in Figure 2. Experimental results are shown in Table 2.

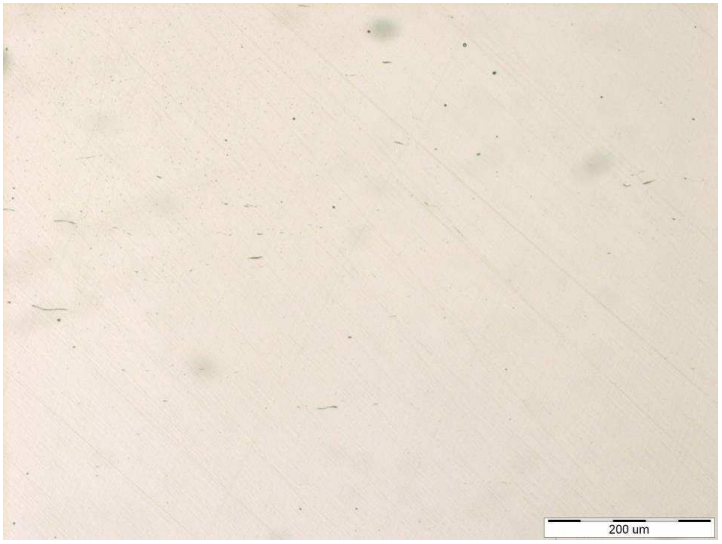

Fig. 2 Inclusions in microstructure of steel 50CrV4+QT

Tab. 2 Inclusion size and purity index

Part	Distance measured part – edge [mm]	Inclusion		Index	
		length [µm]	width [µm]	coarse	fine
1	**edge**	204	2.70	0	1.5
2	**1**	129	1.00	0	1.5
3	**2**	120	1.74	0	1
4	**3**	297	2.90	0	2
5	**4**	253	2.69	0	1.5
6	**5**	132.3	2.73	0	1.5
7	**6**	80	2.70	0	1
8	**7**	308	2.80	0	2
9	**8**	172	2.80	0	1.5
10	**9**	135.5	2.71	0	1.5

Plasma nitriding of low – alloyed steel 50CrV4 + QT was carried out on the nitriding device RÜBIG PN 60/60. Applied parameters of plasma nitriding are shown in Table 3.

Tab. 3 Parameters of plasma nitriding

	Temperature [°C]	**Gases H_2:N_2 [l/hour]**	**Time [hours]**	**Pressure [Pa]**	**Voltage [V]**	**Pulse time [µs]**
De-dusting	480	20:2	0.5	80	800	100
Plasma nitriding No. 1	500	24:8	5	280	530	100
Plasma nitriding No. 2	500	24:8	20	280	530	100

After plasma nitriding, nitriding layer was formed in the surface layer of steel 50CrV4+QT. Nitriding layer consists of the white layer and diffusion layer. Structures after 5 and 20 hours are shown in Fig. 3a,b.

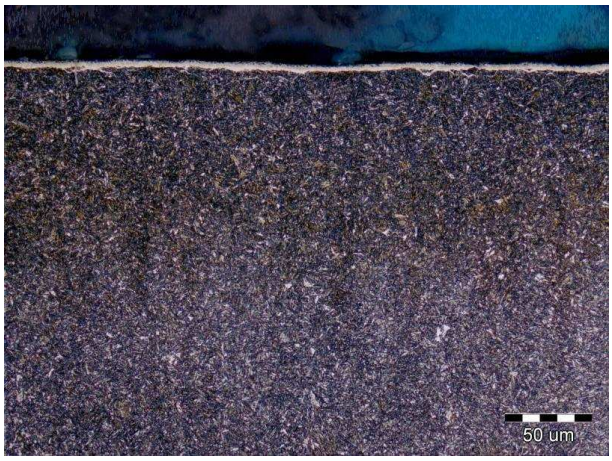

a)

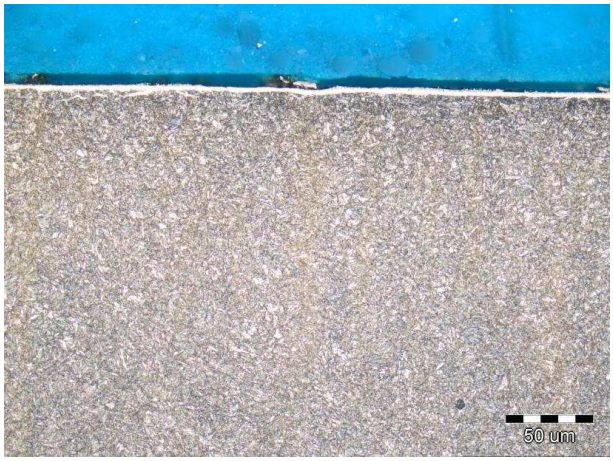

b)

Fig. 3 Microstructure of steel 50CrV4+QT after plasma nitriding, magnified 500x, etch. 2 % Nital, a – after 5 hours, b – after 20 hours

Accordings to Fig. 3 and measured values (Tab. 4) bigger white layer thickness was created on samples which were exposed to plasma nitriding within 5 hours.

Tab. 4 White layer thickness

Material	**Exposure time [hours]**	**Average white layer thickness [µm]**
50CrV4+QT	5	4.22
	20	3.72

3 Mechanical properties evaluation

Both types of samples, untreated and plasma nitrided underwent a Vickers surface hardness test, tensile test and the rotating bending test.We obtained from the tests the mechanical properties of untreated and plasma nitrided samples: tensile strenght, yield strenght, hardness, micro-hardness and fatigue limit.

Hardness measurement was carried out in laboratories of University in Trencin using experimental device INSTRON Wolpert Testor. Values of surface hardness of 50CrV4 +QT as well as after plasma nitriding are shown in Table 5.

Tab. 5 Surface hardness of 50CrV4+QT and after plasma nitriding

State	HV1	HV5	HV10
untreated	503	442	446
nitrided 5 hours	887	1022	945
nitrided 20 hours	860	1039	924

Micro-hardness across the nitriding layer was determined by using Vickers method in accordance with Standard EN ISO 6507-1 [9]. According to the Standard DIN 50190 [10], the micro-hardness of core GH as well as nitriding layer thickness Nht were determined. As an experimental device LECO ML 247 AT was used. Measured values are shown in Table 6 and depicted in Fig. 4.

Tab. 6 Micro-hardness of the core and nitriding layer thickness

Plasma nitriding	Hardness of core		
	GH [HV0.05]	GH+50 [HV0.05]	Nht [mm]
5 hours	399	450	0.193
20 hours	408	460	0.212

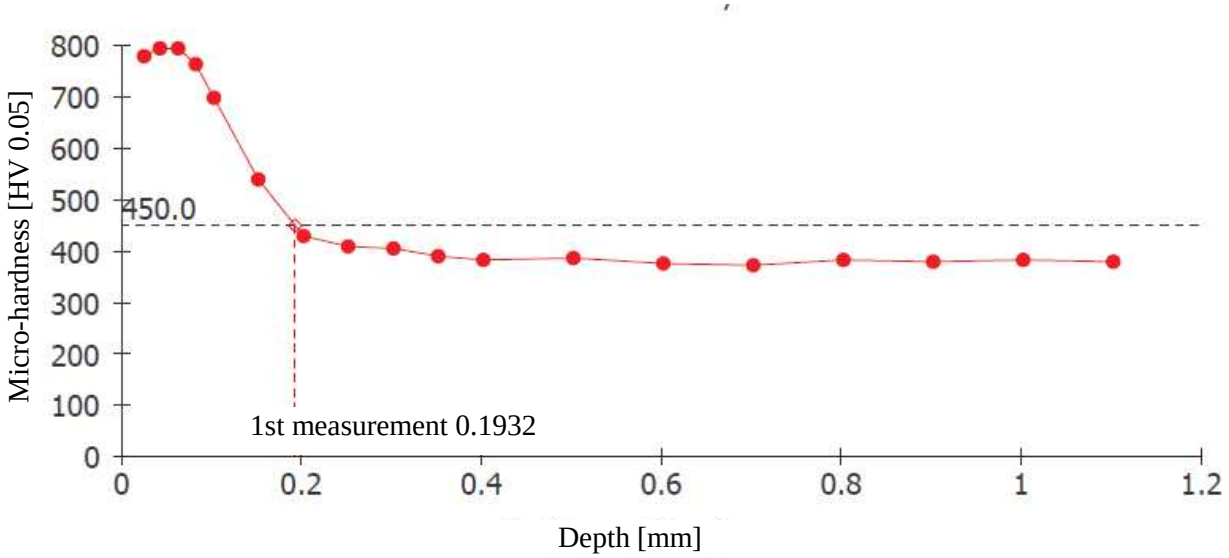

a)

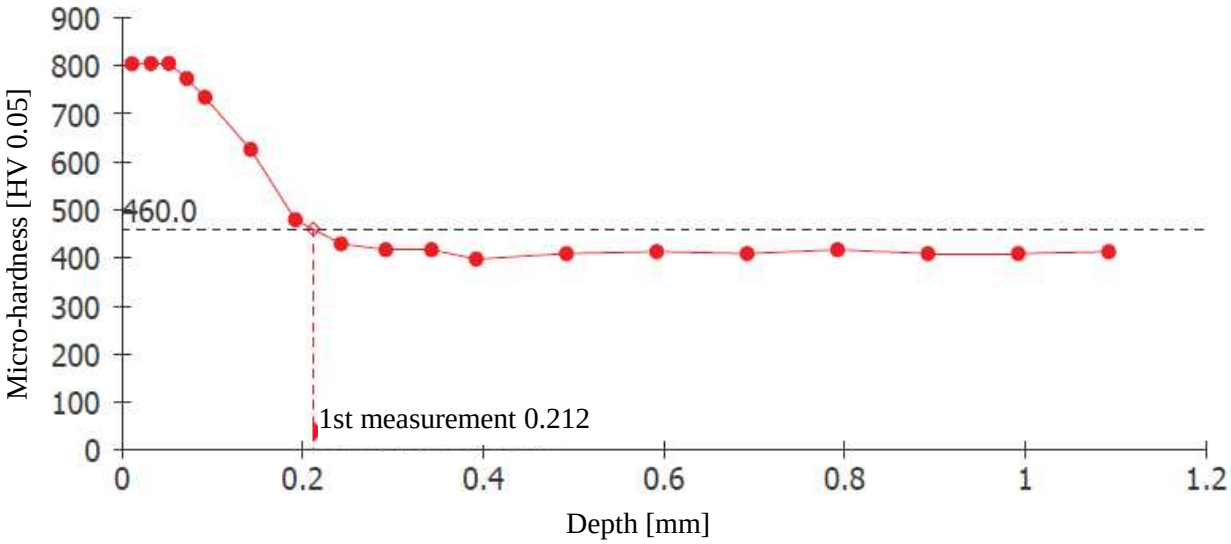

b)

Fig. 4 Micro-hardness of 50CrV4+QT , a) after 5 hours plasma nitriding, b) after 20 hours plasma nitriding

Tensile test was realised in the laboratories in University of Trencin using the experimental device INSTRON 5500R. Measured values are depicted in Tab. 7.

Tab. 7 Tensile strength and yield strength – untreated and plasma nitrided samples

Material **50CrV4+QT**	**R_m [MPa]**	**$R_{p0,2}$ [MPa]**
Basic state	1255	1200
5 hour nitriding	1211	1202
20 hour nitriding	1225	1205

Rotating beam fatigue test was carried out in the Laboratory of mechanical tests at the University of Defence in Brno, Czech Republic, using the experimental device INSTRON R.R.Moore in accordance with the Standard STN 42 0362. As testing bars, the smooth samples without notch loaded by rotating beam fatigue were used in accordance with the experimental device producer instructions and depended on the applied loading. The fatigue limits at 1.10^7 cycles, determined by the staircase method are shown in Table 8.

Tab. 8 Fatigue limits at 1.10^7 cycles

State	**σ_c at 1.10^7 (MPa), n = 9250 rpm => f = 154 Hz**
untreated	450
5 hour nitriding	650
20 hour nitriding	705

4 Discussion of results

Low-alloyed steel 50CrV4 has relatively higher content of chromium (Tab. 1) which leads to a better aptitude for nitriding. The structure consists of three zones: white layer, mixed phases ε ($Fe_{2-3}N$) and γ' (Fe_4N) of irregular depth ranging from 3 to 5 μm, diffusion layer made up of nitrogen solution in insertion and possibly of the fine nitride precipitate or carbo nitrides, structure of tempered martensite resulting from the preliminary heat treatment. The white layer consists of a mixture of γ prime and ε iron nitrides, is very hard and brittle and provides the tribological characteristics and corrosion resistance. The ε-nitride which has compact closely packed hexagonal structure and higher nitrogen content, exhibits better wear and corrosion resistance than γ′-nitride. White layer, considered for its good tribological properties, must have a reduced depth when the treated part is exposed to surface fatigue. This thickness being controlled by the process parameters (Tab. 3), decreases when the temperature and/or the duration period and/or

the nitrogen potential decrease. The white layer is very thin, its thickness is 4.22 μm (5 hour nitriding) and 3.72 μm (20 hour nitriding).

The underlying diffusion zone contains precipitated alloy nitrides and determines the strength of the nitrided layer. Diffusion layer considered as favourable for the fatigue endurance and thick of some tenth of millimetres (Tab. 6) where the nitrogen is inserted as a solid solution in the shape of carbo nitride or nitride precipitate. The plasma nitriding ensured a hardened layer of 193 μm (5 hour nitriding) and of 212 μm (20 hour nitriding) in depth (Fig. 3). The solid solution effect and precipitation of chromium nitrides induce coherent distortions and expansions of the matrix, by increase in volume, causing significant hardening (Tab. 5). A comparison of the surface hardness of the plasma nitrided sample and the samples that remained plasma untreated presents increases of 76% (HV1 after 5 hour nitriding) and 71% (HV1 after 20 hour nitriding), 131% (HV5 after 5 hour nitriding), 135% (HV5 after 20 hour nitriding), and 111% (HV10 after 5 hour plasma nitriding), 107% (HV10 after 20 hour nitriding), respectively, in plasma-treated samples.

The micro-hardness test measurements were conducted on the nitrided layer with a load of 0.05 kp (0.49 N) (HV 0.05) using a square-based pyramidal diamond indenter and an indentation time of 10s. The results characterise the physical properties of the case as a function of depth. The case depth defined as Nht 460 HV 0.05 as being 193 μm (after 5 hour nitriding) and 212 μm (after 20 hour nitriding), and hardness of the core (GH HV0.05) as being 399 (after 5 hour nitriding) and 408 (after 20 hour nitriding). The hardness of the nitrided layer decreased from the surface inwards as a result of the decreasing concentration of metal nitrides towards the core.

In order to determine the plasma nitriding effect the rotating bending test was applied to untreated and plasma nitrided samples. The stress applied to the plasma-untreated specimens was in the range from 800 to 450 MPa and for the plasma-nitrided specimens from 1050 to 705 MPa. The number of cycles was within 1.10^4–1.10^7. Under the operating conditions of 9250 rev min^{-1} (i.e. 154 Hz), Ra≤0.4 μm and the number of cycles Nc =1.10^7, fatigue limits σ_C for rotating bending were determined as being 450 MPa for the 50CrV4+QT steel specimens, 650 MPa for the 50CrV4+QT steel specimens plasma nitrided for 5 hours and 705 MPa for 20 hour plasma nitriding. The enhancing effect of plasma-nitriding on the fatigue limit was thus confirmed attaining an improvement of 44% (5 hour plasma nitriding) 57% (20 hour plasma nitriding). This improvement is predicated on the stabilised gradients of properties in the plasma-nitrided layer that occurred after cyclic relaxation. This resulted in a redistribution of the hardness and compressive residual stresses that are favourable to the fatigue life

5 Conclusion

In this paper the mechanical properties of steel 50CrV4 after plasma nitriding were examined. The main results can be summarized as follows:

- Plasma nitriding has led to formation of white layer (ε +γ´) and diffusion layer with thickness respectively equal to 4.22 and to 193 μm after 5 hours plasma nitriding and 3.72 and 212 μm after 20 hour plasma nitriding.
- Fatigue resistance improvement has been proved by an increase of fatigue limit, 450 MPa for untreated samples, 650 MPa for samples after 5 hour plasma nitriding and 705 MPa for samples after 20 hour plasma nitriding.
- The positive effect of plasma nitriding on fatigue resistance of low-alloy steel 50CrV4 has been in good harmony with plasma nitriding of similar steels presented in works [14-16].

References

[1] Hrubý V., Lipták P., Pokorný Z.: Plasma Nitriding of Cavities. RSdruk Rzeszów, Poland, 2013, 162 p. ISBN 978-83-63666-93-4.

[2] Hrubý V., Kadlec J.: Surface technologies (in Czech). Brno, VA, 1997, p. 120

[3] Jurči P.: Thermochemical processing of ledeburitic cold work tool steels, in Metal 2009, Ostrava. ISBN 978-80-87294-03-1.

[4] Pye D.: Practical nitriding and feritic nitrocarburizing. 2. Edition, Ohio: ASM International materials park, 2003, 256 p. ISBN 0-87170-791-8.

[5] Sevim, I.: Fracture Toughness of Spot-welded Steel Joints, Kovove Mater., 2005, 43(2), p 113–123

[6] Fragoudakis, R., Saigal, A., Savaidis, G., Malikoutsakis, M., Bazios, I., Savaidis, A., Pappas, G. and Karditsas, S.: Fatigue Assessment and Failure Analysis of Shot-peened Leaf Springs. Fatigue Fract. Eng. Mater. Struct., 2013, 36(2), p 92–101

[7] Penha, R.N., Canale, L.F. and Canale, A.C.: Modeling of Tempering Curves of Alloy Steels by Means of Neural Networks. 65th ABM International Congress, 18th IFHTSE Congress and 1st TMS/ABM International Materials Congress, , July 26 - 30, 2010 (Rio de Janeiro, Brazil), Associação Brasileira de Metalurgia, Materiais e Mineração, 2010, 3, p 2480–2487

[8] Eck, S., Prevedel, P., Marsoner, S., Ecker, W. and Illmeier, M.: Using Finite Element Simulation to Optimize the Heat Treatment of Tire Protection Chains, J. Mater. Eng. Perform. 2014, 23(4), p 1288–1295

[9] Jiang, X.-B. , Liang, Y.-L. and Liu, G.-D. : Fracture Analysis of 50CrVA Steel Spring and Its Solution, Jinshu Rechuli/Heat Treatment of Metals, 2011, 36(7), p 109–11

[10] Arndt, J. , Lehmann, G. and Lehnert, W.: Mechanisms in Fatigue Strength Improvement of Thermomechanically Manufactured Automotive Suspension Springs, Steel Res., 1998, 69(7), p 286–291

[11] H. Mizukami, K. Hanaori, K. Takahashi, A. Tange and K. Ando: 'Improvementfatiguelimit ofsteel containing asmallcrack-likesurface defect by overload effect', Int. J. Struct. Integr., 2010, 1, (2), 153–160.

[12] D.SinghandD.P.Mondal: 'Effectofquenchingandtemperingprocesses and shot peening intensity on wear behaviour of SAE-6150 steel', Indian J. Eng. Mater. Sci., 2014, 21, (2), 168–178.

[13] R. Zenker, H.-J. Spies, A. Buchwalder and G. Sacher: 'Combination of thermal surface treatment by high energy beams with thermochemical treatment and hard protective coating – state of the art', Proceedings – 15th IFHTSE – International Federation for Heat Treatment and Surface Engineering Congress, 2006, Leoben, Austria, ASMET.

[14] Ch. Zhou, M. Wang, W. Hui, H. Dong, L. Wang and R. Wuc: 'Rotating bending fatigue properties of two case hardening steels after nitriding treatment', Mater. Des., 2013, 46, 539–545.

[15] S. M. Y. Soleimani, A. R. Mashreghi, S. S. Ghasemi and M. Moshrefifar: 'The effect of plasma nitriding on the fatigue behavior of DIN 1.2210 cold work tool steel', Mater. Des., 2012, 35, 87

[16] D. Ch. Wen: 'Plasma nitriding of plastic mold steel to increasewearand corrosion properties', Surf. Coat. Technol., 2009, 204, 511–519.

Corrosion and wear resistance of plasma nitrided and duplex treated 42CrMo4 steel

David Kusmic[1], Doan Thanh Van [1]

[1]University of Defence, Department of Mechanical Engineering, Kounicova 65, 612 00 Brno, Czech Republic.E-mail: david.kusmic@unob.cz, thanhvan.doan@unob.cz

Plasma nitriding is generally used as a final operation to improve wear, corrosion resistance and fatigue limit of machine parts. The corrosion and wear resistance of nitrided steels can be further increased by converse coating. This paper reports the results of corrosion and wear tests of plasma nitrided and duplex treated (plasma nitriding and manganese phosphate coating) 42CrMo4 steel. Plasma nitriding was carried out at 500 °C in different nitriding atmosphere ratio of $3H_2$:$1N_2$ and $1H_2$:$3N_2$ for 15 hours. Plasma nitrided samples were subsequently manganese phosphated (without lubrication). The experimental samples were exposed to NSS, visually and gravimetric evaluated during and after removing corrosion products. The wear test "ball on disc" was carried out at temperatures of 21 ºC, 150 ºC, and 300 ºC, under a load of 20 N. The results confirmed the possibility of applying manganese phosphate coating to plasma nitrided steel to enhance its properties. X-ray diffraction phase analysis (XRD) found the different volumes of ε-$Fe_{2-3}N$, γ´-Fe_4N nitrides in the compound layers and hureaulite $Mn5\ (PO_3\ (OH))_2\ (PO_4)_2\ (H_2O)_4$ in the manganese phosphate coatings. The results were further supplemented by metallographical documentation, thickness measurements, and microhardness test.

Keywords: Plasma Nitriding, Duplex Treatment, Corrosion, Wear

1 Introduction

Plasma nitriding as a chemical heat treatment process is generally used to increase the surface hardness, fatigue strength and corrosion resistance [1]. According to some authors, plasma nitriding increase wear resistance [2], but it also reduces the notch toughness [3]. After nitriding process, a compound layer, which is usually composed of nitride phases γ´-Me_4N and/or ε-$Me_{2-3}N$, (supplemented by alloying elements like Al, Cr, Mo, V) [4], is created on the surface. The compound layer is characterised by increased hardness and good corrosion resistance, which can be decreased by porosity. An accepTab. way to suppress these pores is the post-oxidation process [5-9]. As well phosphating can be applied for increasing the corrosion resistance of steels, cast irons or zinc, magnesium, cadmium and often also aluminium [10-12]. Another purpose of phosphate converse coating is an improvement of running-in of rotating machine parts and decrease drag friction. The most frequently used process is zinc phosphating (coating formed mainly by hopeite $Zn_3\ (PO_4)_2\ (H_2O)_4$), zinc-calcium phosphate (formed by scholzite $Zn_2Ca(PO_4)_2\ (H_2O)_4$, so-called "three-cations" phosphating (formed by phosphophyllite) and manganese phosphating (formed usually by dense crystalline coating of hureaulite $Mn5\ (PO_3\ (OH))_2\ (PO_4)_2\ (H_2O)_4$). At elevated temperatures (160 °C ÷ 400 °C), it is necessary to consider the dehydration process of phosphates, which can affect the quality and structure of phosphate coating. Hureaulite (manganese phosphating) deals for the most thermal sTab. type of phosphating [13]. The manganese crystalline structure can be modified to moderate the grain size of phosphate crystals and thus further to increase the corrosion resistance [14].

This paper is focused on evaluation of corrosion and wear resistance of plasma nitrided and duplex treated (plasma nitriding and manganese phosphate coating) 42CrMo4 (AISI 4137/4140) steel and compared to tempered one. Plasma nitriding process was applied under $3H_2$:$1N_2$ and $1H_2$:$3N_2$ nitriding gas ratio for 15 hours. The corrosion resistance was tested using the NSS corrosion test according to ISO 9227 standard, visually and gravimetric evaluated. After removing the corrosion products, the surfaces were evaluated using the laser confocal microscopy. The wear tests "ball on disc'' were performed at temperature of 21 ºC, 150 ºC, and 300 ºC and a load of 20 N. The wear resistance and coefficient of friction during unlubricated sliding according to ASTM G99-95a standard was evaluated. Results of corrosion and wear tests were further supplemented by X-ray diffraction phase analysis (XRD), metallographic documentation and measuring of compound layer thickness. Thickness and microhardness of created layers were measured by Vickers microhardness method in accordance with DIN 50190 standard.

2 Experimental

For study 42CrMo4 (AISI 4137/4140) steel with the following chemical composition [in wt.%]: 0.40 C, 1.08 Cr, 0.63 Mn, 0.27 Si, 0.15 Mo, 0.10 Ni, 0.0019 S, 0.0012 P was used. Chemical composition was verified using the Q4 Tasman device, calibrated by the Fe 130 and Fe 140 standards. Experimental samples were heated to 850 °C for 20 min, oil quenched, tempered at 550°C for 40 min to attain martensitic-carbidic structure. All the surfaces of samples were ground to roughness Ra = 0.6 μm and degreased in ethyl alcohol prior the plasma nitriding and following duplex treatment (see Tab. 1).

Tab. 1 Plasma nitriding parameters (Rubig PN 60/60)

Process	Temperature [°C]	Duration [h]	Pressure [Pa]	Bias [V]	Gas flow [l/h] H_2	N_2
Plasma cleaning	480	0.5	80	800	20	2
PN1	500	15	280	530	24	8
PN2	500	15	280	530	8	24

The duplex treatment of plasma nitriding and manganese phosphate coating (marked as PN1+ Mnph and PN2+Mnph) were prepared in a standard solution containing H_3PO_4, MnO_2, and demineralised water. The mean value of measured thickness of Mnph coating was approximately 3.7±0.5 (μm) on plasma nitrided steel samples. The phase analysis was performed by XRD Rigaku Miniflex 600 device (Rigaku D/teX Ultra 250, Cu Kα radiation), using PDXL software with PDF-2 and Crystallographic Open Database for quantitative analysis. As can be seen in Fig. 1, crystalline hureaulite $Mn5\ (PO_3\ (OH))_2\ (PO_4)_2\ (H_2O)_4$) was created.

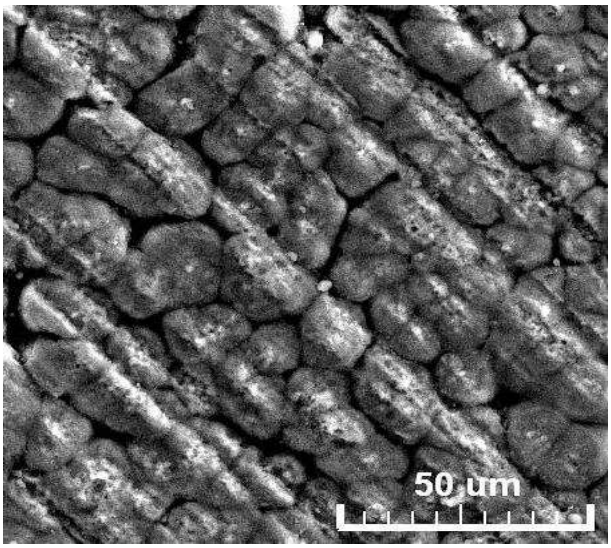

Fig. 1 Hureaulite (Mnph) coating (SEM 1000x Tescan Vega)

For metallographic testing, all samples were crosswise cut, wet ground using SiC paper with grit size from 80 to 2000, subsequently polished and finally etched by 2 % Nital,.

Prior to metallographic testing, nitride layer depth was evaluated by microhardness testing in accordance with DIN 50190 standard using the automatic microhardness tester LECO LM 247 AT equipped with the AMH43 software. The microhardness depth profile was characterised by 18 indentations at 50 g load and 10 s dwell. The nitride layer depth and the thickness of compound layer of nitrided and duplex treated steel samples are summarised in Tab. 2.

Tab. 2 Nitride layer characteristics

Process	Nitride layer depth [μm]	Compound layer (mean value) [μm]
PN1	200	6.6±0.4
PN2	240	8.9±0.6
PN1 + Mnph	180	4.4±0.4
PN2 + Mnph	200	8.8±0.6

The cross-structure documentation and compound layer thickness measuring were realised using the opto-digital microscope OLYMPUS DSX 500 (see Fig. 2 and Fig. 3). According to the X-ray phase analyses, it is evident, that increased ratio of N_2 to H_2 (l/h) in the nitriding atmosphere promotes the creation of ε-$Fe_{2\text{-}3}N$ nitrides (see phase analysis in Fig. 3).

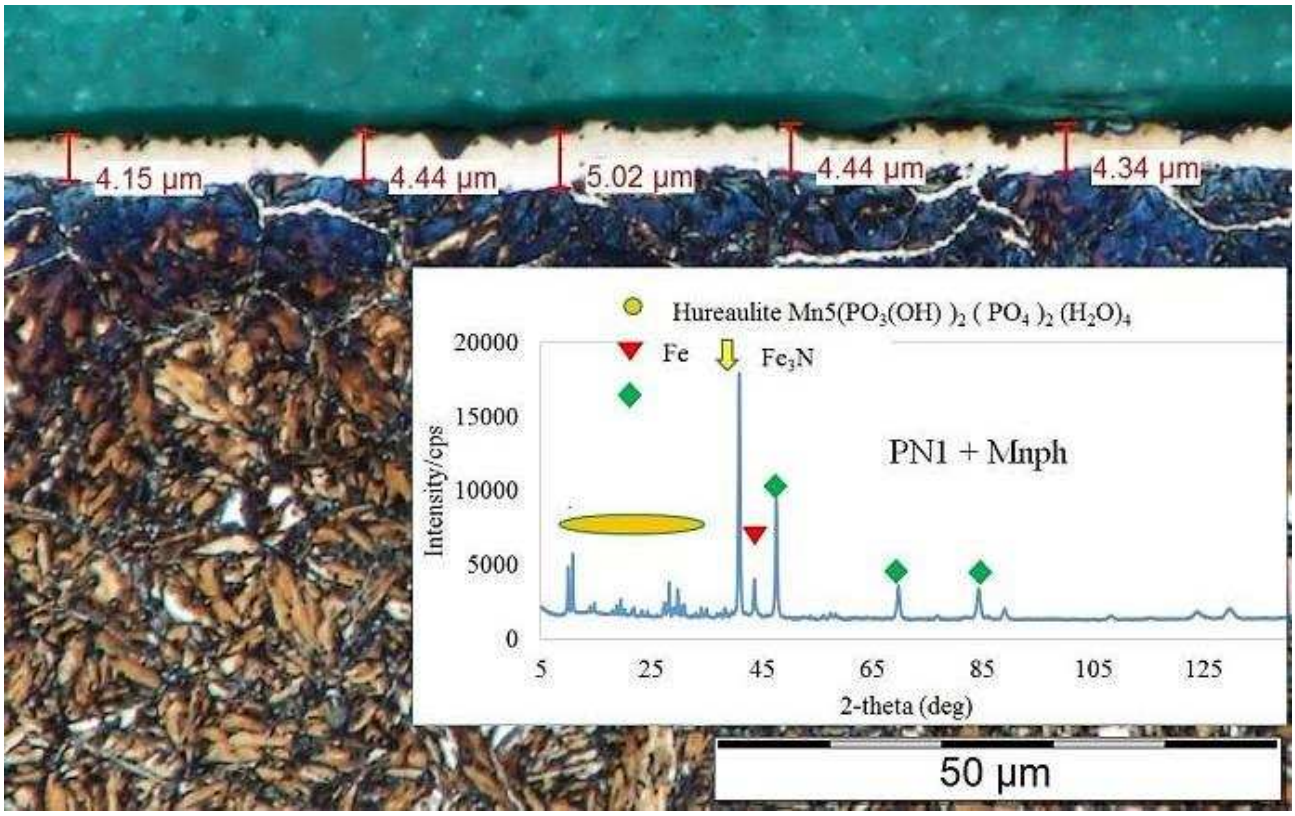

Fig. 2 Cross-sectional microstructure of PN 1+Mnph

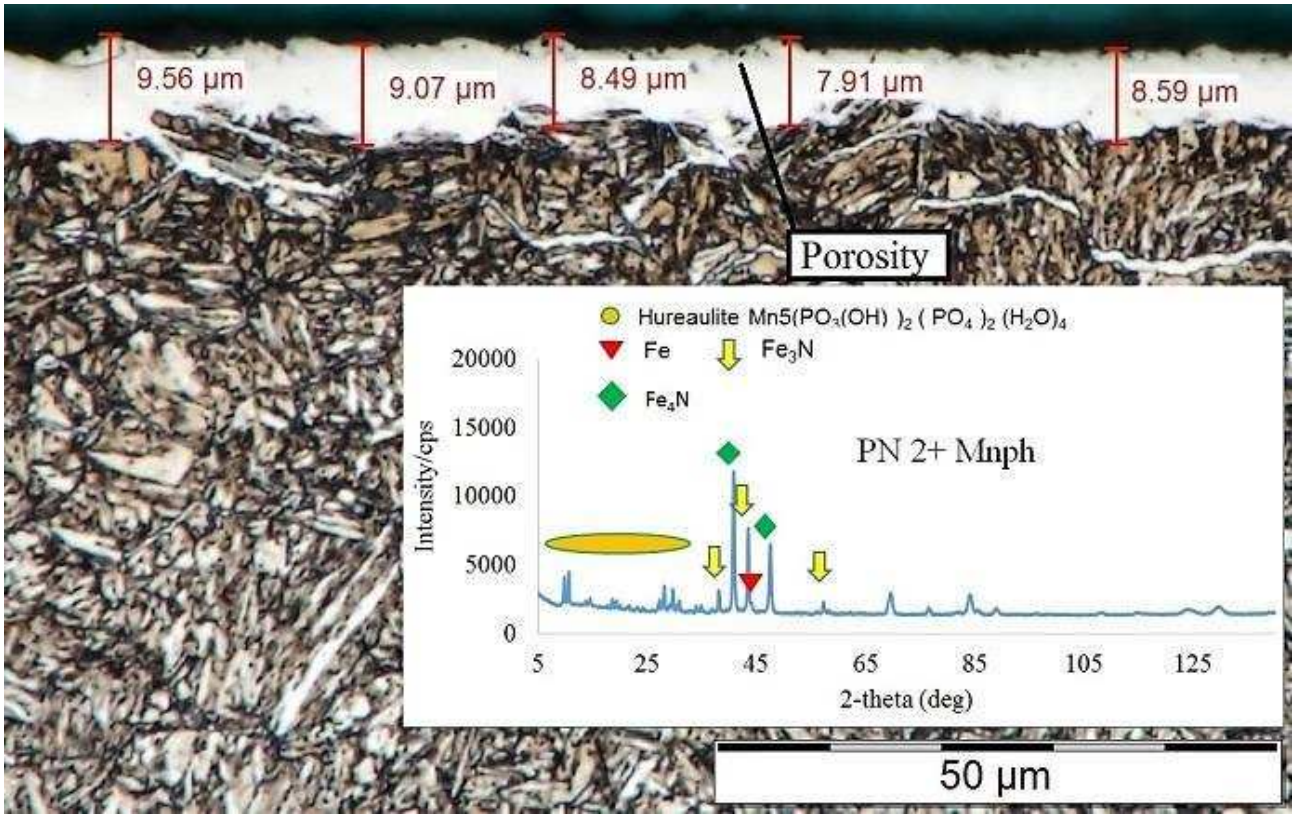

Fig. 3 Cross-sectional microstructure of PN 2+Mnph

2.1 Corrosion resistance

The corrosion resistance was visually and gravimetric evaluated during 2, 4, 8, 24, 48, 72, 96, 144 and 196 hours of exposition periods. The NSS Exposure corrosion tests in the 5 % neutral sodium chloride solution were performed in accordance with ISO 9227 standard in the VLM GmbH SAL 400-FL corrosion chamber. Prior the NSS Exposure

corrosion tests the samples were degreased by ethyl alcohol.

After defined exposition periods (2, 4, 8, 24, 48, 72, 96, 144 and 196 h) the exposited samples were dried and visually evaluated using the QuickPHOTO Industrial 2.3 software with phase analyses application and corroded surface (in %) calculated. The surface corrosion propagation (full lined) is summarised in Graph 1.

The corrosion resistance evaluation was supplemented by gravimetric evaluation, and the corrosion rates K_{corr} [mg.cm^{-2}.h^{-1}] were calculated, modified to weight gain (see dashed lines in Graph 1):

$$K_{corr} = \frac{m_t}{S.t}\left[mg.cm^{-2}.h^{-1}\right] \quad (1)$$

Where:
m_t...weight gain for period [mg],
S…surface area [cm^2],
t...evaluated period [h], (2, 4, 8, 24, 48, 72, 96, 144 and 196 hours).

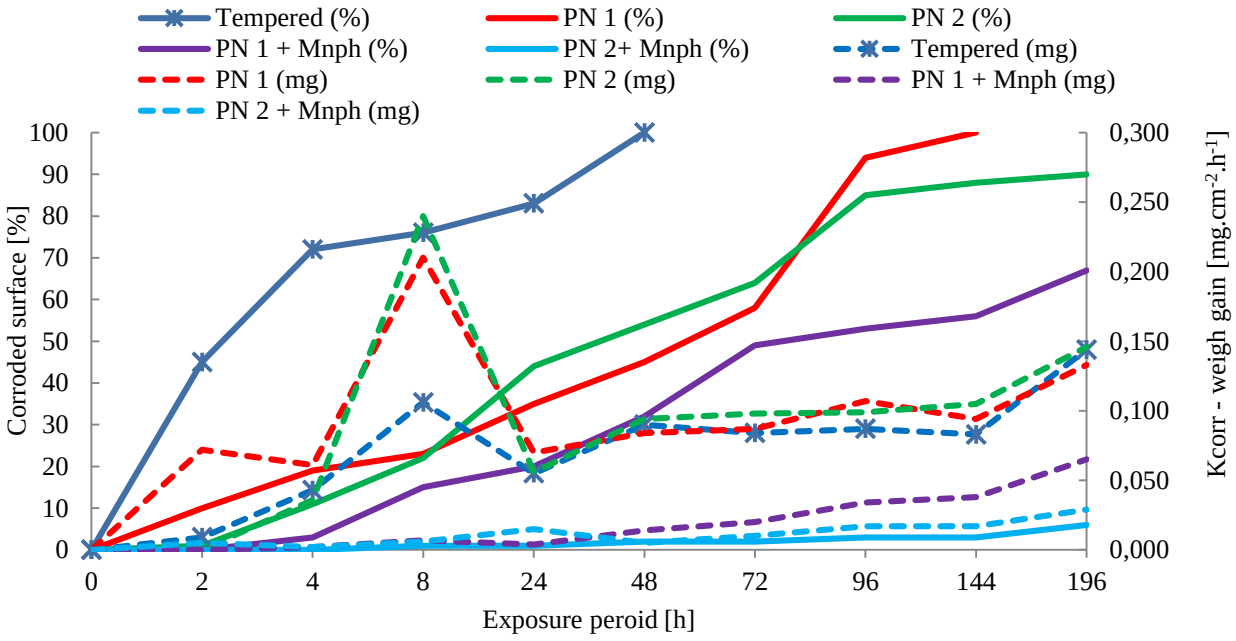

Graph 1 Corrosion propagation (NSS corrosion test)

As seen in Graph 1 significant reduction of corrosion propagation [in %] occurs after plasma nitriding PN1 and PN2 compared to not nitrided steel (Tempered). This corrosion propagation was further reduced by following converse manganese phosphate coating, see PN1+Mnph and PN2+Mnph steel samples. After 196 h of exposures the surface of sample PN1+Mnph was corroded of 67 % and sample PN2+Mnph of 6 %.

The visual evaluation after 196 h of exposure was compared to calculated K_{corr} [mg.cm^{-2}.h^{-1}] values (see Graph 1-- dashed lines). As seen in Graph 1, the values of the corroded surface [in %] and values of K_{corr} – weight gain [mg.cm^{-2}.h^{-1}] have not the same progress as awaiting. Generally, it is supposed, that with increased corroded surface, the weight gain will increase, too. It means that there is another type of corrosion attack on the steel surfaces contributing to the corrosion attack, as seen peaks after 8 h of exposure. Very good correlation was found for PN1+Mnph and PN2+Mnph. To clarify this finding, the corrosion products were cleaned according to ISO 8407 standard from the surface. Using the laser confocal microscopy (Olympus Lext OLS 3000) the corrosion free surfaces were examined and additionally localised type of corrosion attack determined. Localised type of corrosion penetrated deeper into the surfaces especially of plasma nitrided PN1 and PN2, thanks to increased porosity of compound layer (see Fig. 4), and thus the values of K_{corr} – weight gain increases. This phenomenon was suppressed by Mnph converse coating. The level of localised corrosion (pitting) can be expressed as so-called "Pitting factor" (PF) given by ISO 11463 standard, as a ratio of the deepest penetration to the average penetration of 10 measured penetrations. The value of PF = 1 represents the uniform type of corrosion and PF > 1, represents increasing of pitting.

After chemical cleaning, in accordance with ISO 8407 standard, the corrosion loss evaluation was expressed by Δm_x [mg.cm^{-2}]:

$$\Delta m_x = \frac{m_{int} - m_k}{S}\left[mg \cdot cm^{-2}\right] \quad (2)$$

Where:
m_{int}...initial weight [mg],
m_k… weight after removing corrosion products [mg],

S…surface area [cm^2],

The pitting factor values and total corrosion loss [$mg.cm^{-2}$] are summarized in Graph 2. As seen after application of plasma nitriding, localised type of corrosion rises and has a significant share of corrosion loss. Application of manganese phosphate converse coating this negative effect of plasma nitriding was reduced, see the reduction of corrosion loss and PF values in Graph 2 and Fig. 4.

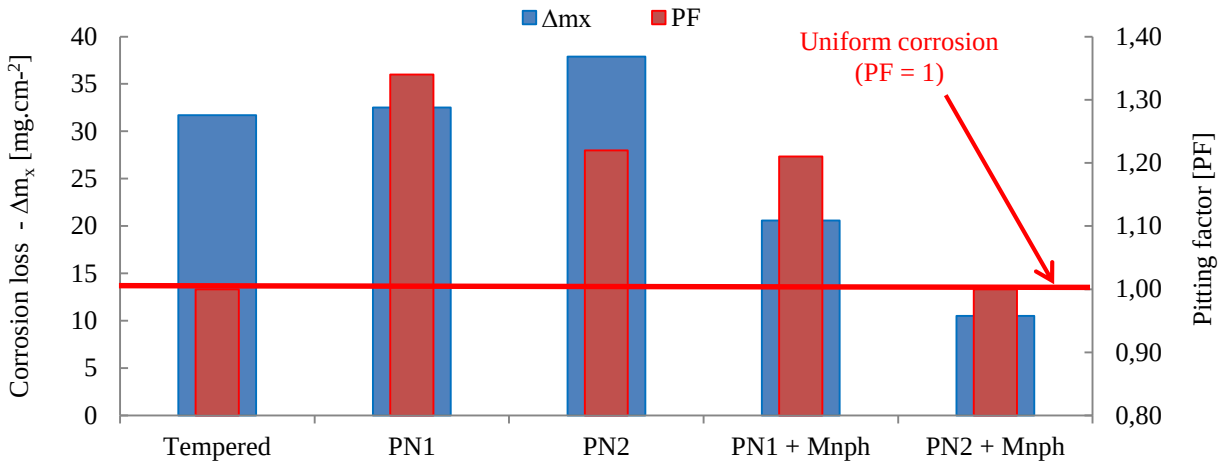

Graph 2 Corrosion loss and pitting factor values after removing corrosion products

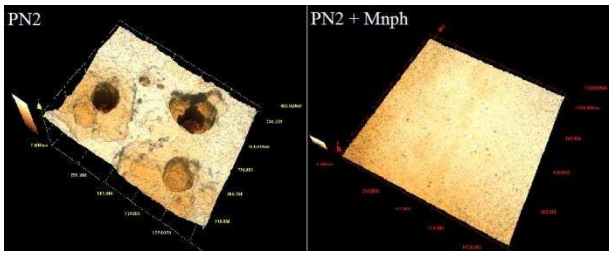

Fig. 4 3D surface evaluation of chemically cleaned samples – PN2(uniform and localized corrosion, PF = 1.21); PN2+Mnph (smooth surface, PF = 1)

2.2 Wear resistance

The samples for wear test were manufactured in the shape of round disk with a diameter of 70 mm and thickness of 6.6 mm. The heat treatment, plasma nitriding and following manganese phosphate converse coating were prepared according to corrosion tests samples.

The wear test "ball on disc'', corresponded to ASTM G99-95a, was carried out on the tribometer BRUKER UMT-3 with an indentor made of carbide wolfram of diameter 6.3 mm. Measurement parameters were set as following: a normal load of 20 N, the rotary speed of 500 rpm, track radius of 20 mm, test duration of 27 min, 13500 cycles. In order to gain a required temperature of 21 °C, 150 °C and 300 °C, the sample (disc) and indentor were heated in the testing chamber for 25 minutes and kept at this temperature for 10 minutes to attain a similar temperature of the testing sample and indentor.

After the wear test, the samples were air cooled and then cleaned in ethyl alcohol using an ultrasound cleaner for evaluation and measuring of the wear track (Fig. 5). The TALYSURF CLI 1000 profilometer was used to evaluate the wear depth and area of wear profile (see Fig. 6).

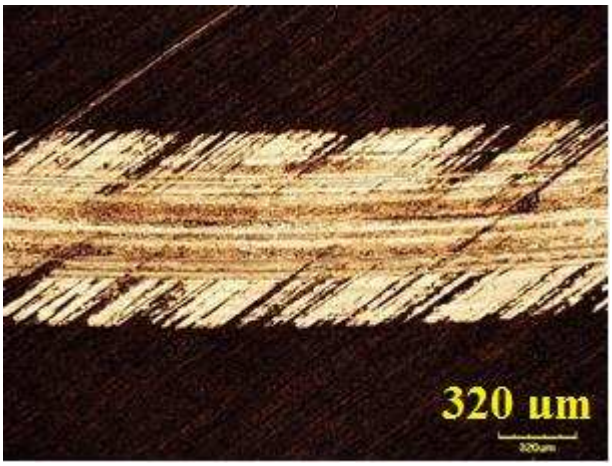

Fig. 5 *The wear track, sample PN 2, 21 °C (Olympus* Lext OLS 3000)

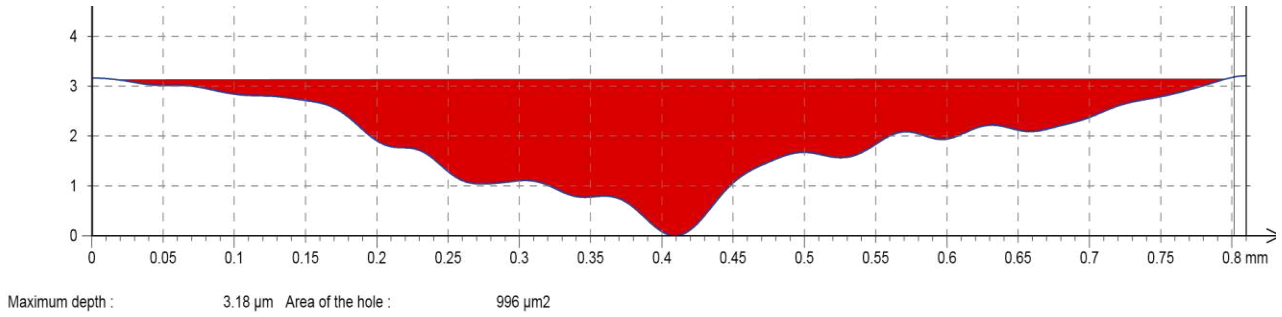

Fig. 6 Profile and area of wear profile measurement *using TALYSURF CLI 1000 (sample PN 2, 21 °C)*

Using the measured area of the wear profile the wear rates were calculated by the modified Archard´ equation (Tab. 3):

$$w = \frac{A}{F_N . \omega . t} \tag{3}$$

Where:
w – wear rate [$mm^{-3}.N^{-1}.m^{-1}$],
A – area of wear profile [mm^{-2}],
F_N – normal load [N],
ω – rotary speed [rpm],
t – measurement time [min].

Tab. 3 Wear rate and coefficient of friction

	Wear rate [$mm^{-3}.N^{-1}.m^{-1}$]			Coefficient of friction [-]		
Process	21 °C	150 °C	300°C	21 °C	150 °C	300°C
Tempered	7.99 ± 0.19	2.76 ± 0.42	5.78 ± 1.49	0.92 ± 0.12	0.95 ± 0.02	0.96 ± 0.03
PN 1	3.21 ± 0.43	5.07 ± 1.25	21.53 ± 10.14	0.79 ± 0.14	0.66 ± 0.08	0.55 ± 0.06
PN 2	3.78 ± 0.76	4.94 ± 0.91	18.85 ± 5.28	0.83 ± 0.03	0.55 ± 0.03	0.55 ± 0.03
PN 1+Mnph	2.54 ± 0.36	2.94 ± 1.19	10.23 ± 5.21	0.76 ± 0.06	0.59 ± 0.04	0.61 ± 0.03
PN 2+Mnph	3.42 ± 0.72	2.43 ± 0.43	7.91 ± 1.31	0.74 ± 0.07	0.61 ± 0.05	0.62 ± 0.09

Plasma nitriding significantly reduces the wear rate at ambient temperature compared to the tempered steel sample as seen in Tab. 3, which can be further reduced by manganese phosphate converse coating. With increased temperature to 150 °C the wear rates of plasma nitrided steel samples increases and duplex treated were almost unchanged, compared to decreased wear rate of tempered steel sample. At 300 °C the wear rate of tempered steel, was slightly increased but it was lower than at ambient temperature. It can be explained by a oxide layer formed on the surface, which plays a role as self-lubricant, thus the wear was decreased.

As seen in Tab. 3, the wear rate of plasma nitrided steel (PN 1 and PN 2) at 300 °C was rapidly increased, using of manganese phosphate was the wear rate reduced to more than 50 % of plasma nitrided steel samples.

The value of friction coefficient was considered of the sTab. section of friction coefficient measurement (as seen in Fig. 5) for testing temperatures and summarised in Tab. 3.

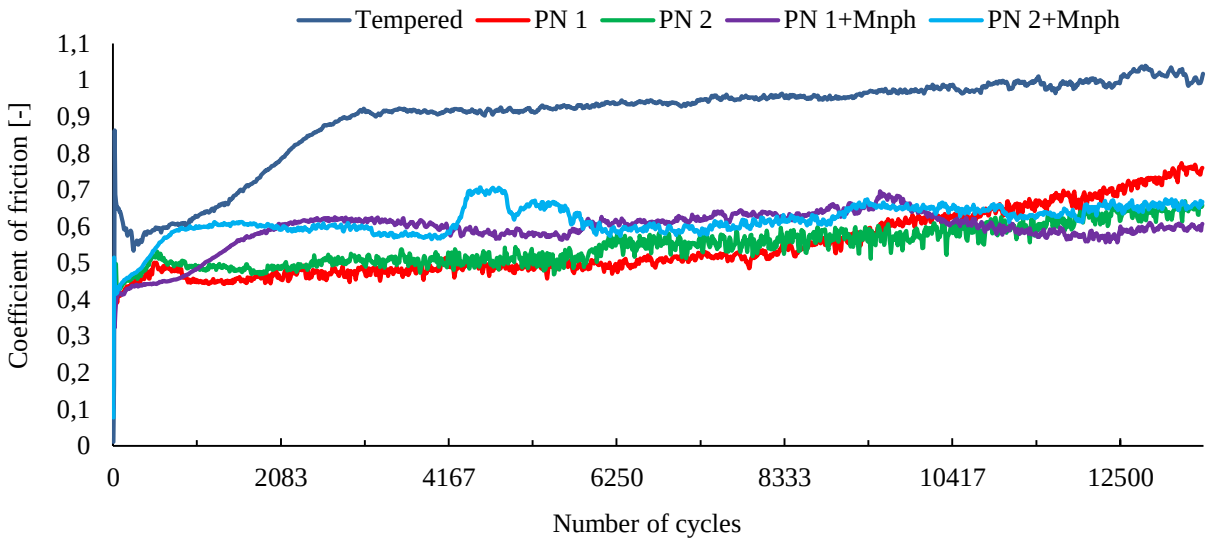

Fig. 5 *Friction coefficient measurement under temperature of 300 °C*

It is evident that tempered steel sample exhibits the greatest coefficient of friction, increased with temperature in the range of 21 °C ÷ 300 °C. Using of plasma nitriding significantly decreases the coefficient of friction for used temperatures and the lowest values were measured at 300 °C. At ambient temperature, manganese phosphate decreases the coefficient of friction of nitrided samples, however at elevated temperature duplex coating plasma nitriding + Mnph showed a higher coefficient of friction than substrate – nitrided surface (see Tab. 3). Increasing of the coefficient of friction for duplex treated steel samples can be attributed to dehydration of manganese phosphate [13].

3 Conclusions

The tempered, plasma nitrided and duplex treated (plasma nitrided and manganese phosphate coating) 42CrMo4 steel samples were prepared for corrosion and wear resistance evaluation. Prepared samples were exposed to NSS corrosion tests up to 196 hours, continuously visually and gravimetric evaluated.
The wear tests "ball on disc'' were carried at temperatures of 21 °C, 150 °C and 300 °C to investigate the coefficient of friction and the wear rate. The most relevant conclusion is as follows:

1) According to the visual evaluation the corrosion propagation [in %], which was significantly reduced after application of plasma nitriding, was further reduced by following manganese phosphate coating;

2) The gravimetric evaluation proved a discrepancy with visual evaluation thanks to the negative effect of compound layer porosity. This porosity caused increased ratio of localised type of corrosion, this fact was confirmed by surface evaluation after removing of corrosion products and expressed by increased "pitting factor", which was reduced by following manganese phosphate coating;

3) Plasma nitriding has significantly reduced the wear rate at ambient temperature compared to tempered steel sample, which was further reduced by manganese phosphate converse coating;

4) The wear rate of plasma nitrided and duplex treated steel samples was increased with increased temperature but the coefficient of friction has decreased.

5) The wear rate of tempered steel at elevated temperatures is smaller than at ambient temperature and smaller than nitrided or duplex treated samples, but on the view of corrosion resistance, tempered steel cannot correspond to the requirements of practical operation of machine parts.

Acknowledgement

The present research work was supported by the project The Development of Technologies, Design of Firearms, Ammunition, Instrumentation, Engineering of Materials and Military Infrastructure "VÝZBROJ (DZRO K201)" and "Surface technology in applications special techniques SV17-216".

References

[1] STUDENY, Z. (2015). Analysis of the Influence of Initiating Inclusions on Fatigue Life of Plasma Nitrided Steels. In: Manufacturing Technology, Vol. 15, No. 1, pp. 99-105. ISSN 1213-2489.

[2] DOAN, T.V., DOBROCKY, D., POKORNY, Z., KUSMIC, D., NGUYEN, V. T. (2016) Effect Of Plasma Nitriding On Mechanical And Tribological Properties Of 42CrMo4 Steel. In: ECS Transactions, Vol. 74, No. 1, pp. 231-238. ISSN 1938-5862.

[3] DOBROCKY, D. STUDENY, Z., POKORNY, Z., POSPICHAL, M. SMIDA, O. Effect of plasma nitriding on the notch toughness of spring steel. In: METAL 2016, 25th Anniversary International Conference on Metallurgy and Materials**.** Ostrava: TANGER 2016, pp. 1037-1044. ISBN 978-80-87294-67-3

[4] PYE, D. (2003): Practical nitriding and ferritic nitrocarburizing. 2nd edition, Ohio: ASM International Materials Park 2003, pp. 127-129.

[5] EBRAHIMI, M., HEYDARZADEH S. M, HONARBAKHSH R. A., MAHBOUBI, A. (2010) Effect of plasma nitriding temperature on the corrosion behavior of AISI 4140 steel before and after oxidation. In: Surface & Coatings Technology, Vol. 205, pp. 261-266, ISSN: 0257-8972**.**

[6] POKORNY, Z., HRUBY, V., STUDENY, Z. Effect of nitrogen on surface of layers (2016). In: Metallic Materials, Vol. 54, No. 2, pp. 119-124, ISSN 1338-4252.

[7] DONG-CHERNG, W. (2009). Plasma nitriding of plastic mold steel to increase wear and corrosion properties. In: Surface&Coatings Technology, 2009, vol. 204, pp. 511-519. ISSN: 0257-8972**.**

[8] YANG LI, LIANG WANG, DANDAN ZHANG, LIE SHEN (2010): Improvement of corrosion resistance of nitrided low alloy steel by plasma post-oxidation. In: Journal Applied Surface Science, Vol. 256, Issue 13, pp. 4149-4152, ISSN 0169-4332.

[9] BASU, A., MAJUMDAR, J. D., ALPHONSA, J., MUKHERIEE, S., MANNA, I. (2008). Corrosion resistance improvement of high carbon low alloy steel by plasma nitriding. In: Materials Letters, Voll. 62, Issue 17-18, pp. 3117-3120, ISSN:0167-577X.

[10] PASTOREK, F., BORKO, K., FINTOVA, S., KAJANEK, D., HADZIMA, B. (2016). Effect of surface pretreatment on quality and electrochemical corrosion properties of manganese phosphate on S355J2 HSLA Steel. In: Coatings, Vol. 46, Issue 6, 2016, Doi: 10.3390/coatings6040046, 9 p., ISSN 2079-6412, Switzerland.

[11] AMINI, R., VAKILI, H., RAMEZANZADEH, B. (2016). Studying the effects of poly (vinyl) alcohol on the morphology and anti-corrosion performance of phosphate coating applied on the steel. In: Journal of the Taiwan Institute of Chemical Engineers, Vol. 58, pp. 542–551, ISSN: 1876-1070.

[12] DAYYARI, M. R., AMADEH, A., SADREDDINI, S. (2015). Application of magnesium phosphate coating on low carbon steel via electrochemical cathodic method and investigation of its corrosion resistance. In: Journal of Alloys and Compounds, Vol. 647, pp. 956-958, ISSN: 0925-8388.

[13] POKORNY, P., SZELAG, P., NOVAK, M., MASTNY, L., BROZEK, V. (2015). Thermal stability of phosphate coatings on steel. In: Metalurgija, Vol. 54, Issue 3, pp. 489-492, ISSN 0543-5846.

[14] GUANGYU L., LIYUAN N., JIANSHE L., ZHONGHAO J. (2004). A black phosphate coating for C1008 steel. In: Surface and Coatings Technology, Vol. 176, pp. 215-221, ISSN: 0257-8972**.**

Posuzování technické bezpečnosti speciální techniky při zavádění do rezortu MO

Kamil Liška[1], Radek Tolar[1]

Ministerstvo obrany, Sekce dozoru a kontroly, odbor státního dozoru, Generála Píky 1, 160 00 Praha 6, Česká republika, E-mail: liskak@army.cz, tolarr@army.cz

1 Státní odborný dozor v podmínkách Ministerstva obrany

Státní odborný dozor (dále jen „SOD“) nad bezpečností a ochranou zdraví při výkonu vojenské činné služby v působnosti rezortu Ministerstva obrany (dále jen „MO“) je prováděn dle § 2 zákona č. 45/2016 Sb., o službě vojáků v záloze a § 100 zákona č. 221/1999 Sb., o vojácích z povolání ve znění pozdějších předpisů. SOD nad bezpečností vojenského materiálu, technických zařízení a bezpečností jejich provozu je prováděn na základě § 7 písm. d) zákona č. 219/1999 Sb., o ozbrojených silách České republiky ve znění pozdějších předpisů a dle prováděcí vyhlášky MO č. 273/1999 Sb., kterou se vymezují určená technická zařízení používaná s vojenskou výstrojí, vojenskou výzbrojí, vojenskou technikou a ve vojenských objektech a provádění zkoušek určených technických zařízení.

Další základní právní předpisy, vztahující se k uvádění výrobků na trh jsou např. zákon č. 22/1997 Sb., o technických požadavcích na výrobky a o změně a doplnění některých zákonů, ve znění pozdějších předpisů; zákon č. 102/2001 Sb., o obecné bezpečnosti výrobků a o změně některých zákonů, ve znění pozdějších předpisů, zákon č. 309/2000 Sb., o obranné standardizaci, katalogizaci a státním ověřování jakosti výrobků a služeb určených k zajištění obrany státu a o změně živnostenského zákona nebo nařízení vlády č. 378/2001 Sb. kterým se stanoví bližší požadavky na bezpečný provoz a používání strojů, technických zařízení, přístrojů a nářadí včetně příslušných technických norem a Českých obranných standardů.

V rámci MO je výkonem SOD v této oblasti pověřen Odbor státního dozoru Sekce dozoru a kontroly MO (dále jen „OSD“), jehož působnost a oprávnění jsou vymezeny zejména rozkazem ministra obrany (dále jen „RMO“) č. 92/2015 Věstníku MO, Organizační řád MO, RMO č. 28/2002 Věstníku MO, Státní odborný dozor v rezortu Ministerstva obrany a normativním výnosem MO (dále jen „NV MO“) č.76/2013 Věstníku MO, Základní požadavky k zajištění bezpečnosti určených technických zařízení a jejich provozu.

Další vnitřní předpisy rezortu MO k zavádění speciální vojenské techniky jsou NVMO č. 100/2015 Věstníku MO, Zavádění vojenského materiálu do užívání v rezortu Ministerstva obrany, RMO č. 117/2014 Věstníku MO, Nabývání majetku v rezortu Ministerstva obrany a NVMO č. 119/2014 Věstníku MO, Obsah souhrnné specifikace majetku.

Další činností OSD je:

- výkon inspekce práce v rozsahu ustanovení § 3 odst. 1 písm. c) a d) v případech dle § 6 odst. 2 věty druhé zákona č. 251/2005 Sb.;
- prověřování odborné způsobilosti fyzických osob k zajišťování úkolů v prevenci rizik v oblasti BOZP a vydává jim osvědčení dle zákona č. 309/2006 Sb.;
- výkon státní kontroly v oblasti energetiky dle zákona č. 458/2000 Sb., a č. 406/2000 Sb., č. 165/2012 Sb., ve znění pozdějších předpisů, a RMO č. 11/2016;
- výkon kontrolní a správní činnosti na úseku územního plánování a stavebního řádu dle zákona č. 183/2006 Sb. podle § 16 odst. 2 písm. a) a podle § 15 odst. 1 písm. a) v rozsahu § 43 zákona č. 49/1997 Sb. ve znění pozdějších předpisů;
- výkon požárního dozoru v souladu s ustanovením § 85a, v rozsahu § 31, zákona č. 133/1985 Sb., ve znění pozdějších předpisů, vyhlášky č. 246/2001 Sb. a v souladu s RMO č. 38/2016;
- řízení a koordinaci bezpečnosti a ochrany zdraví při práci občanských zaměstnanců podle § 101 a 102 zákona č. 262/2006 Sb., bezpečnosti a ochrany zdraví při výkonu služby vojáků v činné službě podle zákona č. 45/2016 Sb. a § 98 a 99 zákona č. 221/1999 Sb. a RMO č. 11/2009;
- poradenská činnost a technická pomoc ve výše uvedených oblastech.

OSD dozírá, zda dokumentace staveb, určených technických zařízení a technologií, včetně pojízdné, převozné a přenosné vojenské techniky a dalšího materiálu, splňuje požadavky bezpečnosti určených technických zařízení. Dále OSD posuzuje textové části specifikace nabývaného majetku z hlediska bezpečnosti a ochrany zdraví při práci a výkonu vojenské činné služby, určených technických zařízení, požární bezpečnosti a hospodárného nakládání s energiemi podle postupů a zásad stanovených RMO a vydává k nim stanoviska.

Při posuzování prototypů určených technických zařízení OSD vydává odborná stanoviska, která dokládají, zda při projektování, konstrukci, výrobě, montáži, provozu, obsluze, opravách, údržbě a revizi určených technických zařízení byly splněny požadavky na bezpečnost technických zařízení. Manažer projektu v součinnosti s uživatelem a OSD určuje, které technické parametry a takticko-technické parametry, stanovené ve smlouvě, budou předmětem ověření v

rámci kontrolních zkoušek, vojskových zkoušek, nebo zkrácených vojskových zkoušek podle NVMO č. 100/2015.

2 Zjištění z činnosti v oblasti posuzování speciální techniky při zavádění do rezortu MO.

Vojenským materiálem je vojenská výstroj, vojenská výzbroj, vojenská technika a určená technická zařízení používaná k plnění úkolů ozbrojených sil ČR. Určená technická zařízení jsou zařízení se zvýšenou mírou rizika ohrožení majetku, života a zdraví osob. Pro jejich výrobu, montáž, revize, zkoušky, provoz a údržbu jsou stanoveny zvláštní požadavky.

Provozovatel je povinen zajistit, aby stroje, technická zařízení, dopravní prostředky, přístroje a nářadí byly z hlediska bezpečnosti a ochrany zdraví při práci vhodné pro práci, při které budou používány. Stroje, technická zařízení, dopravní prostředky, přístroje a nářadí musí být vybaveny ochrannými zařízeními, která chrání život zaměstnanců, čímž se rozumí vojáci z povolání, vojáci v záloze, ve službě, státní zaměstnanci, zaměstnanci ve správních úřadech, občanští zaměstnanci.

Častým nedostatkem při posuzování specifikací nabývaného majetku v rámci zavádění do rezortu MO je obecně nízká odborná úroveň zpracování, chyby v platnosti právních a vnitřních předpisů, neznalost technických norem, v podrobných popisech chybějící odkazy na splnění technických podmínek stanovených Českými obrannými standardy, např. elektrická zařízení v pojízdných a převozných prostředcích, protipožární ochrana - způsob a lhůty kontrol provozuschopnosti a údržby automatického hasicího zařízení. Chybí požadavky na bezpečný vstup do nástavby techniky (stupačky v protiskluzovém provedení, madla), výhled z kabiny osádky, eliminace ostrých hran a rohů, které mohou být zdrojem rizika pro osádku, opakuje se potřeba posuzovat opravené specifikace. V soupisu dokumentace v rámci dodávky chybí prohlášení o shodě a stanovené Nařízením Evropského parlamentu a Rady Evropské unie, certifikát k přezkoušení typu, výsledky technických zkoušek příslušné autorizované osoby, upřesňující technický výkres a správná technická norma.

Při posuzování způsobilosti prototypů určených technických zařízení vojenské techniky v rámci zavádění do užívání se při podnikových zkouškách v některých případech objevily nedostatky prokazující nesplnění požadavků platných vyhlášek o Mezinárodní úmluvě o bezpečnosti kontejnerů a ČSN ISO norem – např. akreditovaná zkouška kontejneru na přepravu nebezpečných látek. Často chybí technická dokumentace výrobce, návody k obsluze a bezpečnostní informace v českém jazyce, a jasné, srozumitelné a snadno pochopitelné označení ovládacích prvků. U prototypů vojenské techniky nejsou dokládány výchozí typové revize, které musí být ve smyslu ČOS 615001 3v na elektrickém zařízení provedeny zkušebním komisařem odborného technického dozoru v rezortu MO. Výrobcem nejsou uvedeny postupy stanovené nařízením vlády č. 116/2016 Sb. při posuzování shody a ochranných systémů určených k použití v prostředí s nebezpečím výbuchu při jejich dodávání na trh, při uvádění výrobků na trh a nařízením vlády č. 118/2016 Sb., o posuzování shody elektrických zařízení určených pro používání v určitých mezích napětí při jejich dodávání na trh.

U vojenského materiálu, který se nabývá jako dar, se vykonávají v rámci zavádění materiálu do užívání vojskové zkoušky nebo zkrácené vojskové zkoušky. Problémem je, že darovaný materiál byl ve většině případů vyroben mimo území EU, předložená dokumentace uživatele neodpovídá požadavkům národní legislativy ani Nařízení Evropského parlamentu a Rady Evropské unie. V takových případech je vydáno nesouhlasné závazné stanovisko OSD s výčtem některých podmínek pro doplnění:

- průvodní dokumentace v českém jazyce,
- EU prohlášení o shodě nebo jiný dokument potvrzující shodu,
- elektrické schéma zapojení, výchozí revizní zpráva elektro,
- ochrana zásuvek proudovým chráničem,
- rozměrový náčrtek, údaje o tloušťce stěny pláště a dna brzdových vzduchojemů,
- schéma zapojení vzduchového systému vozidla, apod.

U kontejnerů vyrobených mimo EU jsou instalovány elektrické zásuvkové systémy SCHUKO, na které nelze připojit spotřebiče systému dvoupólových zásuvek a vidlic s kolíkem 230V, zavedených v ČR. Zařízení není konstruováno pro připojení na vnější zdroj elektrické energie s jakýmkoli způsobem ochrany před úrazem elektrickým proudem.

3 Závěr

Prvním krokem každého akvizičního procesu je identifikace potřeby, která řízeně přechází v konečnou specifikaci požadovaných výrobků nebo služeb a nákladů na jejich životní cyklus. Role a odpovědnost osob v akvizičním systému jsou jasně definovány schvalovacím řízením. Odborně způsobilí pracovníci (inspektoři) OSD v dané fázi akvizičního procesu posuzují textové specifikace pořizovaného vojenského materiálu, komunikují s projektovými manažery a vydávají souhlasná, případně nesouhlasná závazná stanoviska k pořízení vojenského materiálu. V další fázi procesu fyzicky kontrolují v rámci kontrolních zkoušek u výrobce a podnikových zkoušek u akreditované zkušebny, zda pořizovaný vojenský materiál splňuje bezpečnostní požadavky k provozu určených technických zařízení. Přestože je dělba odpovědnosti akvizičního procesu vymezena na jednotlivé osoby, není úroveň zpracování posuzovaných dokumentů na patřičné úrovni, chybí obecné legislativní vědomí, znalost technických norem a vazba na vojenské

předpisy STANAG a ČOS. U některých pořizovaných komodit se opakují nedostatky již z dříve vydaných stanovisek ke specifikacím. Jako vojenský materiál je také pořizován na trhu dostupný levnější komerční výrobek, který nesplňuje všechny požadavky ČOS a neměl by být z těchto důvodů používán k vojenským účelům. ČOS stanovuje požadavky na výrobky a služby nebo na postupy při činnostech v oblasti operační, logistické a administrativní, které slouží k zajištění obrany státu podle zákona č. 309/2000 Sb., o obranné standardizaci, katalogizaci a státním ověřování jakosti výrobků a služeb určených k zajištění obrany státu. Někteří provozovatelé nakupují levnější komerční výrobky a požadavky ČOS obchází dodatečnými opatřeními, kterými se snaží vytvořit takové podmínky, které jsou při konkrétním způsobu provozu daného technického zařízení akceptovatelné.

V rámci posuzování textových částí specifikací a následné verifikace splnění těchto parametrů u vyrobených prototypů dochází k celkovému zkvalitňování akvizičního procesu a ke zvyšování bezpečnostních parametrů při zavádění a modernizaci vojenského materiálu a techniky do rezortu MO. Pozitivním přínosem odborné složky OSD jsou detailní znalost problematiky, provázanost vojenských předpisů, obecně platných technických předpisů a požadavků národní a evropské legislativy. Cílem posudkové činnosti OSD v procesu zavádění je bezpečné užívání techniky a materiálu zadavatelem po celou dobu jejich životnosti, což zajistí pouze úplná průvodní dokumentace k provozu, revizím, údržbě, opravám a omezení pořizování cenově podhodnocených komerčních výrobků, které nevyhovují požadavkům pro nasazení techniky při vojenských cvičeních a v rámci plnění mezinárodních závazků Severoatlantické aliance NATO.

Wear and tool life investigation of cutting inserts when face milling of steel Armox 500

Jozef Majerík[1], Igor Barényi[1]
[1]Faculty of Special Technology, Alexander Dubcek University of Trencin. Pri Parku 19, 911 05 Trenčín. Slovak Republic. E-mail: jozef.majerik@tnuni.sk, igor.barenyi@tnuni.sk

Presented authors article deals with experimental investigation of coated carbide cutting inserts type SNHF 120408EN-SR-M1when hard face milling of steel Armox 500. This work was supported by the Slovak Research and Development Agency under the contract No. APVV-15-0710". All realized measurements and tests have been performed at Department of Engineering in Trencin. It also includes support and cooperation with the University of Defence in Brno, Department of mechanical engineering. The main aim of this work is to focus measurement on the influence of the various applied values of feed rates per tooth during hard machining of steel Armox 500. All tested workpiece material are investigated with variable cutting parameters of feed rate per tooth, whereas the cutting speed and depth of cut were specified as the constant parameters. Practical part of presented article also includes some figures of worn flank faces of carbide cutting inserts, microstructure of workpiece material Armox 500 and graphical dependences of tool wear and tool life curve in logarithm graph as the results of these realized experimental investigation.

Keywords: Hard face milling, Tool life, Wear, steel Armox 500, Mechanical properties, Carbide inserts

1 Introduction

Rough face milling technology of hard materials has become a great contribution for for the recent years. Especially hard finish milling can potentially be an alternative to planar grinding technology with the possibility to improve productivity, flexibility, wokpiece quality, capital expenses, and reduced environmental waste [11]. Planar grinding can be divided into the cutting processes which are always the final finishing operations of hardened steels. Some of the hard machining processes have been considered as the great alternative to traditional grinding operations. It is possible to say that hard machining process can reach the same surface quality as planar grinding while required cutting conditions, cutting temperature are defined [5]. Nowadays the hard machining presents a significant alternative instead of grinding for hard steels, because it can improves surface quality, reduces production costs, improves production efficiency and eliminates the environmental influenece of coolant. The main factors which can affect the reliability of hard machining processes are surface integrity and tool wear [2]. One of the existing problems in this hard machining process is early tool wear, and its influence on the machinability of hard steels. After the heat treatment application the final shape od workpiece has to be machined. Apart from abrasive technological processes, the face milling with geometrically defined cutting edges is established to machine hardened steel components as a substitution technology. The benefits of hard machining with defined cutting edge compared to grinding technology are high level of material removal rates and reduced machining times.. But aleready exists also the disadvantages of hard machining such as increased tool wear compared to machining materials in none hardened state. The reason for that is the fact, that hardened steels are exposed to high loads, the surface quality and surface integrity already must present required characteristics. For that reason, the tool wear has a significant effect on the surface integrity. Face milling process of hardened steels has a important role for mould and die manufacturing sphere due to the high strength of machined material. One of the existing main disadvantages is the tool wear, which is a result of the high thermo-mechanical stress on the cutting tool. The flank wear rate can generally be impacted by the cutting edge geometry and surface coatings. This article investigates hard face milling of Armox 500 steel with milling cutter with regard to the flank wear. Tool life is also an important factorr in investigating the cutting performance of coated carbide inserts. Flank wear significantly affects the shape of edge geometry of the cutting inserts and it is also one of the most important criteria in determining tool life [3]. When the cutting insert reaches tool wear criterion then the cutting edge fails and cannot be used further. Many machining investigations have been realized on hardened steel (with HRC = 48 and more) due to analyse the influence of flank wear onto tool life of the PVD coated carbide cutting tools. Current investigation aims to improve the tool life in hard face milling. In addition to the selection of the cutting insert and the machining conditions, can be said tehat the geometric shape of the cutting edge influences the behavior of the flank wear [6].Generally the tool wear is a gradual process and wear rate depends on cutting tool and workpiece materials, tool geometr, coolant, process parameters and also machine-tool characteristics. Mainly flank wear in hard machining affects the tool life and it is one of the most important criterion in determining tool life. In addition to progressive tool wear, until gradual tool fracture or excessive chipping and surface roughness also significantly affect tool life. The tool wear criteria for face milling operations depends on the following values which are considered from ISO Standard 3685 for tool life testing [8, 11].

2 Materials and methods

From the point of view of the economy of machining, it is advantageous to machine with the cutting tool until its disastrous wear. The wear time of the cutting tool for selected wear criteria under particular cutting conditions is called

the tool life T [min]. If the influence of the cutting parameters on the tool life of the cutting tool is analyzed, it can be delimited by the Taylor equation (1).

$$T = \frac{C_T'}{v_c^m \cdot a_p^{xT} \cdot f_z^{yT}} [\text{min}] \quad (1)$$

Where:
C_T'...Constant [-],
T…Tool life [min].
m, x_T, y_T…Experimentally determined exponents [-].

In the process of realized experiments is monitored the dependence of $T = f(f_z)$. Then it can be used simplified Taylor equation (2).

$$T = \frac{C_T'}{f_z^{yT}} [\text{min}] \quad (2)$$

In this article, all realized experimental investigations were carried out by hard milling process. Machining tests are performed with the aim of study the performance of cutting parameter such as feed rate with consideration of multiple responses viz. volume of material removed, tool wear, tool life and flank face appearance to evaluate the performance of PVD coated carbide inserts and milling cutter. It has been observed through the Tescan Vega 5135 scanning electron microscope of type REM as the authors [7]. Flank wear appearance of cutting insert can be seen in Fig. 3 and Fig. 4.

2.1 Basic Information

Armox steels are ultra high strength martensitic steel used as a armor material and protection for vehicles, mobile containers and other components in armament as well as civil applications. Ballistic resistances of these steels are given by combination of high hardness and strength with optimal value of toughness in a view of materials characteristics. Armox steel were used in Slovakia for construction of Aligator army vehicle body, demining system Bozena or mobile army containers for modular communication system Mokys. Scientific research and development in production of those steels allows to reduce active thickness of armor on 50 % with the same ballistic resistance.
Armox steels production process consists of few important steps to reach their required mechanical properties. First step is continuous casting of slab with using of ore with high chemical purity. The next step is the controlled rolling of the slabs at high temperature about 1250 °C to refine austenitic grains. Then the slabs are solution annealed at temperature about 850 °C. Most important for result high strength and hardness are two final steps – quenching and tempering. The slabs are quenched in continuous furnace from the temperature about 1000°C with very rapid cooling (fig. 1) in water to harden the steels and finally low tempered at about 200 °C in order to make hardened steels tougher [4]. The micro-structure resulting from this treatment is fine tempered martensite.

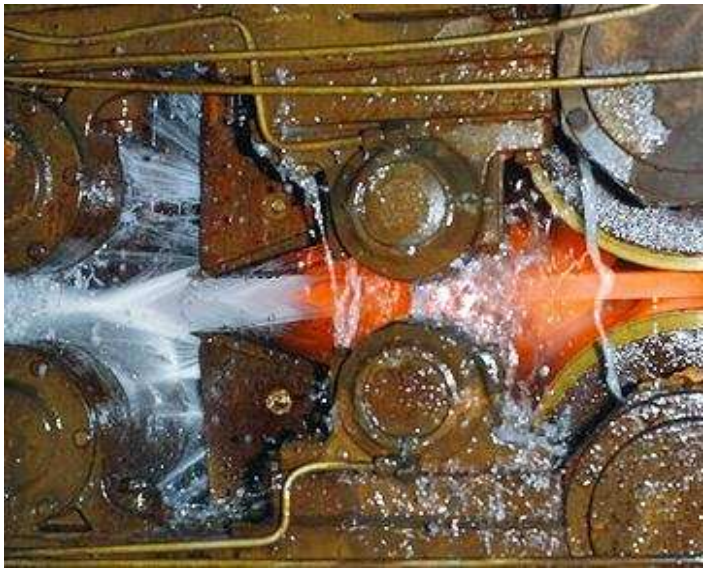

Fig. 1 Rapid quenching of Armox steel by water [4]

The producer of Armox steels recommend their secondary processing (machinig, cutting, welding etc.) at lower temperatures than tempering temperature due to accidental over tempering and degradation of mechanical properties in heat affected zone [1]. Specific properties of Armox steels require special tools for secondary processing of Armox steels by machining. Due to very high surface hardness, and therefore to high wear of used tool, the cutting edge

made by cemented carbide and coated by PVD nano AlTiCN+TiN coating is required to mill the Armox steels.

2.2 Basic properties of Armox 500 steel

Middle class of Armox high strength steels - Armox 500 was chosen as experimental material. Its basic mechanical characteristics and chemical composition are described in the table 1. Showed mechanical properties were evaluated by standard tensile strength test (EN ISO 6892-1), Charpy impact test (EN ISO 148-1) and Brinell hardness test (EN ISO 6506-1). Chcemical composition was measured by spectral analyzer Spectrolab Jr CCD.

Table 1 Chemical composition and mechanical properties of examined steel Armox 500 [2]

Chemical composition [wt. %]	C	Si	Mn	P	S	Cr	Ni	Mo	B
	0.27	0.23	1.10	0.014	0.009	0,81	1,58	0.7	0.004

Mechanical properties	Tensile strength R_m [MPa]	Yield strength $R_{p0.2}$ [MPa]	Toughness KCU [J]	Hardness [HBW]	Elongation A_5 [%]
	1638	1422	25	516	9

Basic microstructure of this steel is shown in Fig. 2. The microstructure consists of tempered martensite with assumed small amount of retained austenite. There are observed some carbides as a product of tetragonal martensite transformation to cubic tempered martensite during tempering.

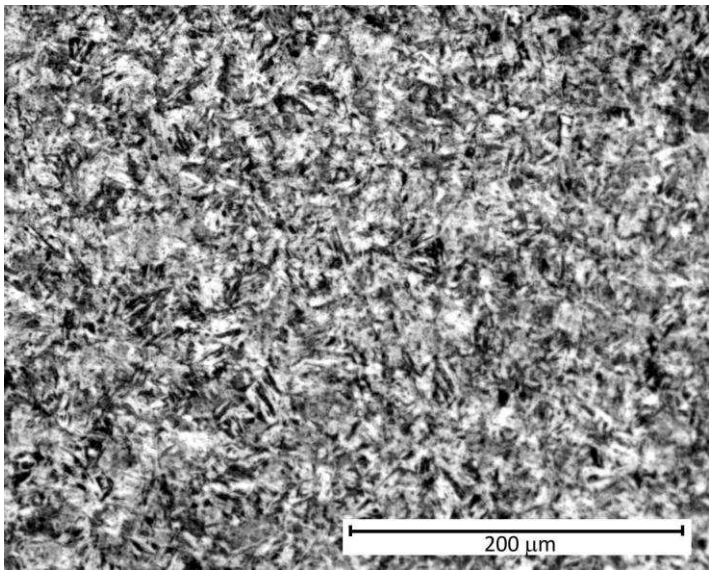

Fig. 2 Microstructure of material Armox 500, etch. nital, **[2]**

3 Experimental details

In the process of machining experiments were used PVD coated carbide cutting inserts for applying rough face milling process. Geometry of each cutting insert was SNHF 1204EN-SR-M1 and cutting material was cemented carbide type 8230 (P30 was tested) with PVD coating of TiAlCN + TiN type. These cutting inserts were used in the processes of all realized experimental tests of rough milling of the hard steel Armox 500. As cutting tool was selected PN222460.12 dia. 50 mm milling cutter type was used with the following geometry of cutting edge z = 4; χ_r = 75º; γ_o = -7º; α = 7º, λ_S = - 4º; (made by NAREX). Cutting tool geometry for this investigation was chosen according to ISO 3685 norm – Tool Life Testing of Cutting Tools [8, 12]. All types of changeable carbide cutting inserts, which are investigated, have a normalized shape which was mentioned above. All used cutting parameters were determined according the manufacturer recommendations, which was the DormerPramet Company. Numerical values of cutting parameters were chosen for testing these types of cutting materials and can be seen in Table 2.

Table 2 Cutting parameters

Cutting parameters				
Feed rate per tooth	f_z [mm.tooth^{-1}]	0.06	0.08	0.11
Spindle speed	n [min^{-1}]	500		
Cutting speed	v_c [m.min^{-1}]	78.5		
Depth of cut	a_p [mm]	2		

The processing of the individual values of the dependence of the tool life and feed rate per tooth can be realized by a graphical or analytical method. Each coordinate point is gradually drawn into the prepared diagram of the T_1-f_{z1} to T_3-f_{z3}

(can be seen in Fig. 6). The value of the exponent y_T is determined as the tangent of the angle α, and the value of the constant Cv is substracted from the axis of the feed rate where the created line T-f_z intersect this axis (this is the feed rate value for the tool life T). The value of the C_T' constant cannot be read from the graphical processing and therefore is calculated from the already determined values C_T' and y_T, therefore $C_T = C_V^{yT}$.

During hard milling process realization, all these obtained values of machining times were achieved: t_{As1} = 6.3 min, t_{As2} = 4.5 min, t_{As3} = 3.2 min and averaged values of tool lives were as follows: T_1 = 118 min; T_2 = 83 min; T_3 = 59 min.

4 Results and discussion

Experimental dermination of dependence of tool life on feed rate T = f (f_z) at constant values of depth of cut a_p = 2 mm, and width of cut a_e = 40 mm, at determined wear criteria VB_k = 0,2 mm, without coolant (dry machining), with the constant value of cutting speed v_c = 78.5 m.min^{-1} and speindle speed n = 500 min^{-1}, were directly realized with high strength steel Armox 500 and with the milling cutter of type NAREX PN 222460.12 with number of teeth z = 4. Machining experiements were realized on the FA3V machine tool. The required values are calculated and processed in the Table 3. Graphical dependence of tool wear of used changeable cutting inserts is recorded in the Fig. 5.

Table 3 The calculation table to the tool life T [min] determination

N	T_i	f_{zi}	log T_i	log f_{zi}	log T_i . log f_{zi}	$\log^2 f_{zi}$
1	130.8	0.056	2.11661	-1.25181	-2.64959	1.56703
2	91.6	0.08	1.96190	-1.109691	-2.15202	1.20321
3	56.3	0.112	1.75051	-0.95078	-1.66435	0.90398
1	105.1	0.056	2.02113	-1.25181	-2.53007	1.56703
2	73.5	0.08	1.86629	-1.09691	-2.04715	1.20321
3	60.8	0.112	1.78390	-0.95078	-1.69609	0.90398
Σ	-	-	11.5003	-6.5990	-12.74008	7.3484

Note: where N is the number of all realized measuremens

$\sum \log^2 f_{zi} = -6.5990$ $\quad (\sum \log f_{zi})^2 = (-6.5990)^2 = 43.5468$

To determination of the specified T = f (f_z) dependence not only with the conditions v_{cmax} = 2,5 and v_{cmin} [6] also tool wear criterion of VB_k = 0,2 mm is to be executed. Each research and investigation is conducted twice with the same cutting parameters and after modification of the position of each cutting, which also meets the general recommendations from the literature sources [9, 10]. As was mentioned above, the obtained results of flank wear and achieved tool life can be seen in Tab. 3 and in the resulting dependenc can be seen in Fig. 5. All realized face milling experiments were performed at these values of feed rates: f_{z1} = 0.06 mm.tooth^{-1}, f_{z2} = 0.08 mm.tooth^{-1}, and f_{z3} = 0.11 mm.tooth^{-1}. In this presented experimental work a criterion of average flank wear VB_k = 0.2 mm was selected for the tool life measurement. After each cutting tool path, tool wear measurements on applied cutting insert were executed to measure tool wear and then define the progress of flank wear.

By using the analytical method we express exponent y_T directly from the equation (2). Finally we get the form of equation (3) by means of the calculations. Replacing the competent values from Table 3 into Equation (3) for the exponent (y_T) then we obtain this following numerical value:

$$y_T = \frac{N.(\sum \log T_i . \log f_{zi}) - \sum \log T_i . \sum \log f_{zi}}{N.\sum \log^2 f_{zi} - (\sum \log f_{zi})^2} = \frac{6.(-12{,}74008) - (-6{,}599.11{,}5003)}{6.7{,}3484 - 43{,}5468} = -1{,}011 = -b \qquad (3)$$

The C_T' constant can be determined by substituting the computed value for exponent y_T into the Equation (4) and than we obtained this following form and by fitting the values of this equation we get the following result:

$$\log C_T' = \frac{\sum \log T_i + y_T . \sum \log f_{zi}}{N} = \frac{11{,}5003 + 1{,}011.(-6{,}5990)}{6} = 0{,}80478 \qquad (4)$$

then $C_T' = 10^{\log C_T} = 10^{\acute{}1{,}011} = 10{,}25$

The obtained graphical dependence of T = f(f_z), acquired from measurements and calculated through the method of least squares in logarithmic coordinate system is presented in Fig. 6. The final form for tool life equation T = f (f_z) is represented by the: y_T = 1, 011 = tg α

α = arctg 1,011 = 45,33º = 45º 20´ Accordingly the final version is: $T = \frac{C_T'}{f_z^{y_T}} = \frac{10{,}25}{f_z^{1{,}011}}$

In the process of realized investigations were selected three points of measurement in T = f (f_z) according to the relevant equation, determining the profile of the obtained curves as linear in the logarithmic coordinates. For the computation are available values from Table 3. Tool life dependence of the f_zT curve can be seen in Fig. 6.

The tool wear process is a very complicated phenomenon that depends on many factors (physical and mechanical

properties of machined and tool material, type of machining operation, tool geometry, working conditions, cutting fluid, etc.), and in which many different physico-chemical phenomena (wear mechanisms). The most commonly used and quantified criterion is the flank wear VB which can be defined as the width of the wear on the flank face of cutting insert. In practice, methods of direct measurement of basic wear criteria are most commonly used for measuring the wear of the cutting tool. VB values are measured using a small workshop microscope so that the so-called crosshair is set to the base position at the line representing the rake face and then moves to the position where it meets the measured wear criterion. Measured values are taken into dependencies VB = f (time). Worn flank faces appearance of used cutting inserts were investigated by REM microscopy of type Tescan Vega 5135 (can be seen in Fig. 3 and Fig. 4). Surface quality of the machined surfaces mainly depends on specified cutting parameters and maintained a significant task in the fatigue life and functionality of the machined surfaces. The monitoring of flank wear was realized after 12 min; 18 min; 24 min; 30 min; 40 min; 50 min; 70 min; 90 min; 100 min; 115 min; 125 when setting values of feed rates f_{z1} to f_{z3}.

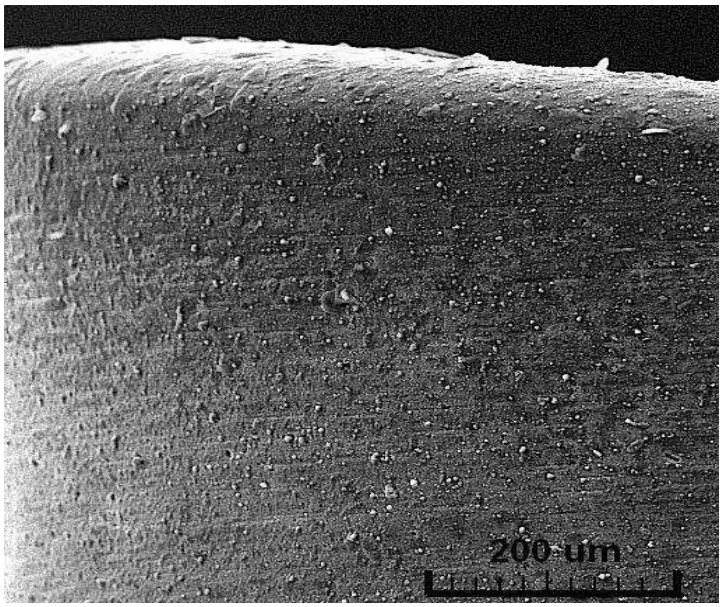

Fig. 3 REM image of cutting edge before hard milling (exp. 250x).

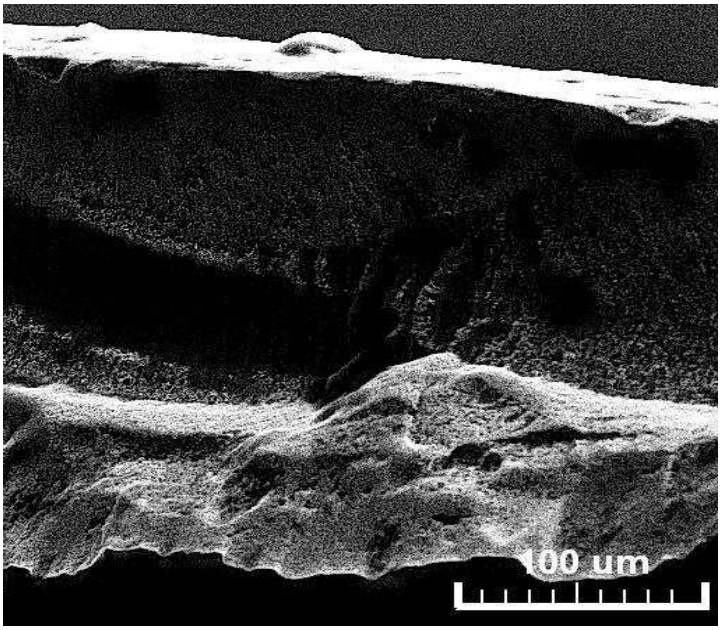

Fig. 4 REM image of surface morphology of worn cutting edge at T = 91,6 min and f_z = 0.08 mm.tooth^{-1}(exp. 500x)

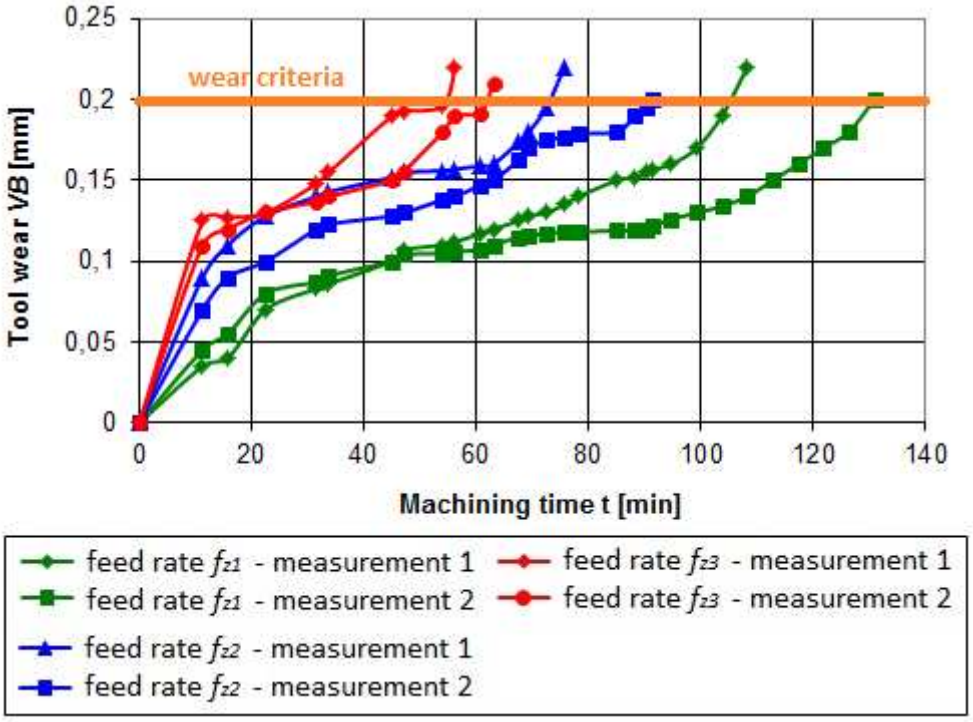

Fig. 5 Graphical presentation of dependence of tool wear in hard milling of Armox 500 steel to determine the dependence of $T = f(f_z)$

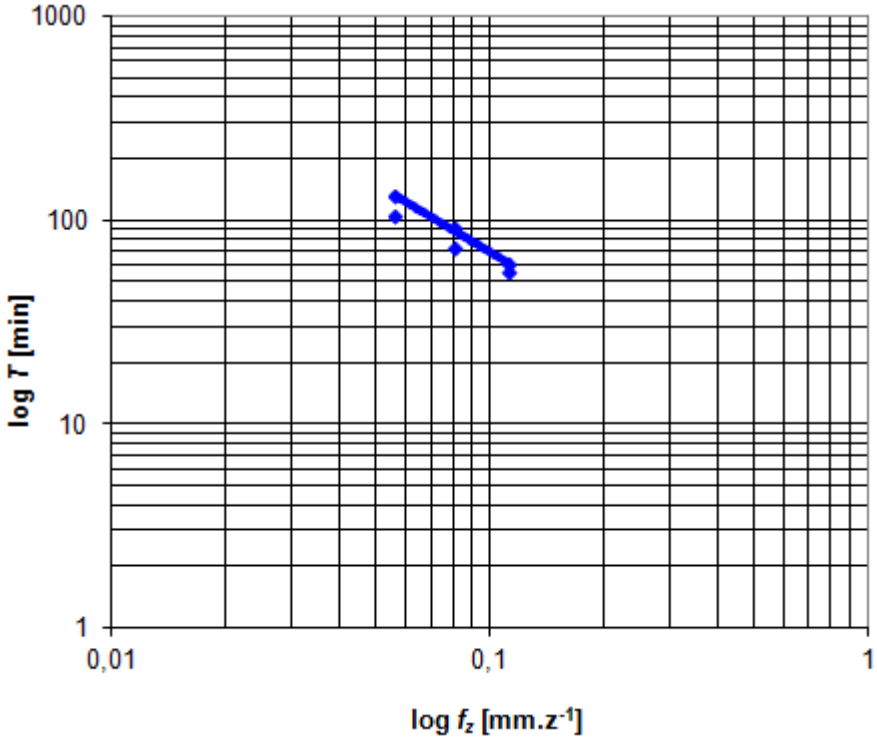

Fig. 6 Tool life testing of f_zT curve in hard face milling of Armox 500 steel

5 Conclusion

All realized experimental investigation in authors presented article is focused on the fundamental relations between tool wear and tool life. In the process of experiments also deals about the cutting inserts and workpiece material Armox 500 and its mechanical properties. The acquired results and findings are summarized in the following points:

(1) The main aim of this presented study is the investigation and measurement of the tool life depending on the feed rate per tooth according to Taylor equation when hard face milling of steel Armox 500.

(2) Feed rate per tooth f_z (selected machining parameter) also has comparatively significant influence on the flank wear (as well as cutting speed v_c).
(3) The investigated and obtained results were statistically processed by the linear regression analysis according to the method of the least squares.
(4) In the process of realized experiments authors also evaluated chemical composition of worpiece material measured by spectral analyzer Spectrolab Jr CCD.
(5) In the microstructure study, authors realized production of metallographic samples. Based on her assessment, the authors state that the observed microstructure consists of tempered martensite with assumed small amount of retained austenite. There are also observed some carbides as a product of tetragonal martensite transformation to cubic tempered martensite during tempering.
(6) The study of the size and location of the flank wear in worn cutting carbide inserts has been also observed through the REM type Tescan Vega 5135 scanning electron microscope. Changes on substrate material were widened during machining, and can be said that was caused by the increase of cutting temperature. Analysis of the worn area also confirmed that there is high dependance of the workpiece sample on the cutting inserts face in concerning the temperature growth, causing the formation of seizure areas on the rake and flank faces of carbide inserts.

In terms pf already in the past researches, authors note that the most significant impacts have cutting speed v_c, and then the feed rate f_z. However some other parameters of tool life as for example $T = f(a_p)$, have not yet been studied, which gives a new opportunity for further experimental investigation. Further experiments with respect to the dependence $T = f(a_p)$ on different cutting parameters with respect to wear behaviour and surface integrity will be conducted in the future.

Acknowledgement

This work was supported by the Slovak Research and Development Agency under the contract No. APVV-15-0710.

References

[1] BARÉNYI, I. (2016). Microstructure changes in cut face obtained by plasma and laser cutting of selected high strength steels. In:UPB Scientific Bulletin, Series D: Mechanical Engineering, vol.78, No.1(2016), p.233-240.

[2] BARÉNYI, I. (2017). Changes of material characteristics of high strength martensitic steels at their cutting and welding / Scientific monograph, TnUAD, 2017. - 131 s. - ISBN 978-80-8075-774-8.

[3] FLEISCHER, J., BECKE, C., PABST, R. (2008). Improving tool life by varying resilience and damping properties in close proximity of the cutting edge. In: Production Engineering, Vol. 2, Issue. 4, pp. 357 – 364.

[4] General Product Information: Weldox, Hardox, Armox and Toolox. SSAB [online]. (2016). Available in: http://www.ssab.com/Global/Plate/Brochures/en/041_SSAB_plate_general_product_information_UK.pdf

[5] KOLESNYK, V., KRYVORUCHKO, D., HATALA, M., MITAL, D., HUTYROVA, Z., DUPLAK, J., ALOWA, M. (2015). The effect of cutting temperature on carbide drilling life in the process of CFRP steel stacls drilling. In: Manufacturing Technology, Vol. 15, No. 3, pp. 357 – 362.

[6] MAJERÍK, J., BARÉNYI, I. (2016). Experimental investigation into tool wear of cemented carbide cutting inserts when machining wear resistant steel Hardox 500. In: Engineering Review, Vol. 36, Issue. 2, pp. 167 – 174. University of Rijeka.

[7] POKORNÝ, Z,, HRUBÝ, V., STUDENÝ, Z. (2016). Effect of nitrogen on surface morphology of layers. In: *Kovové Materiály*, Vol. 54, Issue. 2, pp. 119 – 124. Slovenska Akademia Vied.

[8] SCANDIFFIO, I., DINIZ, A. E., DE SOUZA, A. F. (2016). Evaluating surface roughness, tool life and machining force when free form shapes on hardened AISI D6 steel. In: International Journal of Advanced Manufacturing Technology, Vol. 82, Issue. 9-12, pp. 2075 – 2086. Springer Verlag London.

[9] TAN, L., YAO, C., REN, J., ZHANG, D. (2017). Effect of cutter path orientations on cutting forces, tool wear and surface integrity when ball end milling TC17. In: International Journal of Advanced Manufacturing Technology, Vol. 88, Issue. 9-12, pp. 2589 – 2602. Springer Verlag London.

[10] VASILKO, K. (2015). Machining with plastic cutting wedge. In: Manufacturing Technology, Vol. 15, No. 5, pp. 951 – 957.

[11] ZETEK, M., ZETKOVÁ, I. (2017). Influence of the workpiece quality on the cutting tool life when gear wheel are machined. In: Manufacturing Technology, Vol. 17, No. 1, pp. 121 – 125.

[12] ZHANG, S., Li, J.., LY, H. (2014). Tool wear and formation mechanism of white layer when hard milling h13 steel under different cooling/lubrication conditions. In: Advances in Mechanical Engineering, Article number 949308, Hindawi Publishing Corporation.

Evaluation and Measurement of Surface Texture

Karel Maňas[1], Emil Svoboda[1], Ondřej Klanica[1], Jakub Hnidka[1], David Dobrocký[1]
[1]Faculty of Military Technology, University of Defence. Kounicova 65, 662 10 Brno. Czech Republic. E-mail: karel.manas@unob.cz, emil.svoboda@unob.cz, ondrej.klanica@unob.cz, jakub.hnidka@unob.cz, david.dobrocky@unob.cz

The paper describes the analysis of selected parameters of profile roughness and surface texture measured with 2D and 3D systems on real work pieces. Comparison, evaluation and application of both systems is provided as well. The measurement of a profile roughness was performed with 2D roughness checker Surtronic 25, while the surface topography was investigated with 3D surface profiling system Talysurf CLI 1000.

Keywords: surface analysis, 2D surface profile, 3D surface topography, surface structure

1 Introduction

Surface texture or surface finish, and properties of the surface layer are a result of a manufacturing process and are influenced by a machining process. Objective assessment and evaluation of surface finish can be performed with variety of parameters, typically divided by the spacing between occurred irregularities. Surface waviness is characterized by greater spacing between irregularities and positions of surfaces [3]. This paper focuses on a surface roughness, which is a measure of finely spaced irregularities. The surface roughness is a result of a technological process and the measured values are compared with the values defined in the technical documentation. If the roughness is not specified, the investigation of roughness is conducted in compliance with set principles for periodic or aperiodic profile roughness [1] [2].

2 Evaluation of surface roughness

The paper describes surface texture assessment by 2D profile roughness and 3D texture analysis applied to samples marked by numbers (1, 2, 3, 4, 5, 6, 7, 8, 9, 10). The samples are manufactured parts, produced during real manufacturing process. The measurement was performed with measurement instrumentation Surtronic 25 and Talysurf CLI 1000. For data evaluation and assessment of measured values of investigated parameters of both profile and surface roughness, the software provided with the instrumentation was used [3].

Tab. 1 Defined values of surface roughness

No.	Selected samples		
	Shape of the sample	Ra [µm]	Surface finish
1.	Pump lid	0.04	Grinding
2.	Insert	0.02	Lapping
3.	Threaded rod	0.04	Grinding
4.	Pump piston	0.04	Polishing
5.	Ring	0.08	Grinding
6.	Shaft with a wheel	0.20	Grinding
7.	Cube	0.20	Grinding
8.	Surface ring	0.20	Grinding
9.	Injector	0.08	Grinding
10.	Brass ring	0.80	Turning

The conditions of the measurement followed the ČSN EN ISO 4288 [2], with regard to the possibilities of the measurement instrumentation and its software capabilities. The samples were divided into two groups based on the roughness defined in the technical documentation and are listed in Table 1. Both groups have to be evaluated differently, because based on the ČSN EN ISO 4288 the measurement have to be performed under different conditions – e.g. the cut-off wavelength, sampling length, and evaluation length all vary. The first group of samples (1, 2, 3, 4 and 5) was measured with the sampling length of 0.25 mm and the evaluation length of 1.25 mm. For 3D surface texture evaluation, the total area of 1.25 mm x 1.25 mm was investigated.

The second group of samples (6, 7, 8, 9, and 10) was measured with the sampling length of 0.80 mm and evaluation length of 4 mm. For 3D surface texture evaluation, the area of 4 mm x 4 mm was investigated.

Measurement of both groups of samples was performed on three randomly selected areas and in total five measurements of 2D profile and three measurements of 3D texture surface were conducted. Measurement was performed on following measurement instrumentation:

- Talysurf CLI 1000 performed surface texture analysis (3D) and absolute roughness surface profile (2D).
- Surtronic 25 performed relative roughness surface measurement (2D).

3 Results and discussion

The parameter Ra is the arithmetic average of absolute values of the profile deviations from the mean line of the roughness profile. The parameter SaR is the arithmetic mean height of the surface, calculated after applying a correction for the waviness. Both parameters of Ra and Sa are commonly-used parameters to evaluate a surface texture. They feature low sensitivity to valleys and peaks, which is why they produce stable results.

The graph displayed in Figure 1 demonstrates that measured values of 2D and 3D parameters used to evaluate the surface roughness show steady growth. These values are greater that their relative counterparts. The growth of measured values of surface roughness is linear with certain deviations, because the surfaces measured were of parts manufactured in a real manufacturing process. This is also the main reason of observed deviation between measured values of surface roughness and surface texture.

Tab. 2 Measured values of surface roughness Ra and surface texture SaR of samples 1 to 5

Surface roughness Ra and SaR							
Measured range of surface roughness 0.02 µm < Ra < 0.10 µm		2D				3D	
		Relative		Absolute			
		Ra [µm]		Ra [µm]		SaR [µm]	
Sample	Surface finish	ø	±	ø	±	ø	±
No. 2. Insert	Lapping	0.021	0.004	0.037	0.002	0.094	0.004
No. 3. Threaded rod	Grinding	0.035	0.006	0.043	0.005	0.091	0.002
No. 4. Pump piston	Polishing	0.040	0.006	0.049	0.005	0.099	0.005
No. 1. Pump lid	Grinding	0.043	0.008	0.056	0.004	0.099	0.002
No. 5. Ring	Grinding	0.075	0.006	0.088	0.004	0.116	0.006

A result of evaluation (2D) of surface roughness is a graph, which shows a profile of surface roughness – Figure 2. The surface roughness profile does indicate how different the actual roughness in different parts of the profile is and what the multiplicity of the observed irregularities in the observed area is. The result of 3D surface texture investigation is a surface shown in Figure 2. The obtained surface clearly shows the difference in different parts of the area. Figure 2 shows the surface texture and the roughness profile of a pump lid (sample No. 1). The surface shows obvious injuries in form of peaks and valleys on both the evaluated surface and the profile. These valleys and peaks influence the values of investigated parameters of surface roughness and surface texture.

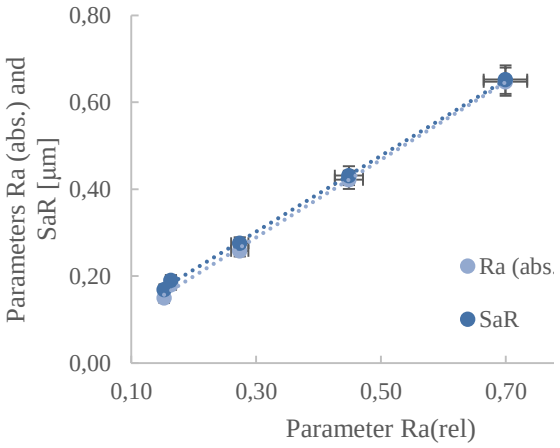

Fig. 1 Parameters of surface roughness SaR and profile roughness Ra

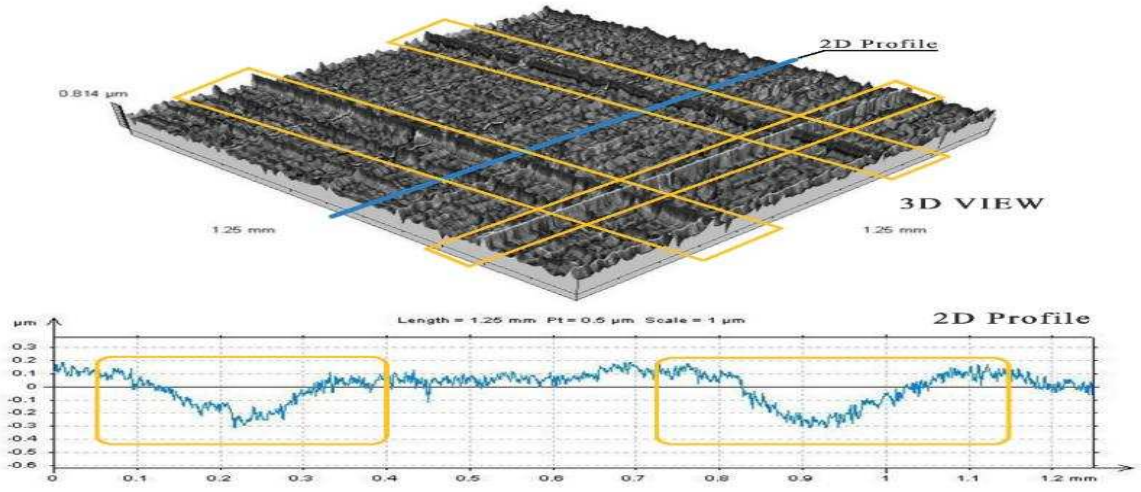

Fig. 2 Surface of sample number 2 Pump Lid

The group of samples (6, 7, 8, 9 and10) has the similar average value of parameters SaR and Ra measured both relatively and absolutely with exception of small deviations. Samples are listed in the Table 3. The Figure 3 shows the relation between parameters of surface roughness measured with relative method and surface roughness measured with absolute method. The graph clearly states that the measured values feature linear behaviour – e.g. with the relative roughness growing, the parameter of surface roughness measured with absolute method as well as parameters of surface texture grow proportionally.

Tab. 3 Measured values of surface roughness Ra and surface texture SaR of samples 6 to 10

Surface roughness Ra and SaR							
Measured range of surface roughness 0.10 µm < Ra < 2 µm		2D				3D	
		Relative		Absolute			
		Ra [µm]		Ra [µm]		SaR [µm]	
Sample	Surface finish	ø	±	ø	±	ø	±
No. 6. Shaft with a wheel	Grinding	0.153	0.050	0.150	0.016	0.169	0.006
No. 7. Cube	Grinding	0.164	0.010	0.180	0.009	0.190	0.011
No. 8. Surface ring	Grinding	0.274	0.031	0.258	0.029	0.276	0.028
No. 9. Injector	Grinding	0.449	0.048	0.422	0.062	0.431	0.013
No. 10. Brass ring	Turning	0.700	0.025	0.647	0.041	0.652	0.014

The largest difference from the linear behaviour were observed on the sample No. 7 (cube) and sample No. 9 (injector). Figure 4 shows the measured surface of the sample No. 9 (injector), where there are observable injuries in form of valleys and peaks on both measured surface (3D) and surface profile (2D). These valleys and peaks influence the values of measured parameters of surface roughness. In the Figure 4 on the roughness profile (2D profile), there are apparent more significant valleys in left and right part of the graph. It is not possible to assess the multiplicity of these injuries on the measured area. In a 3D view it is possible to detect even more significant valleys. The valleys and peaks in measured area were caused by the imperfections of the surface of the sample originated in the manufacturing process.

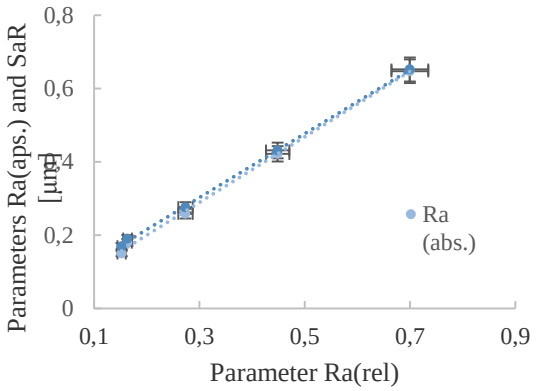

Fig. 3 Parameters of roughness SaR and Ra

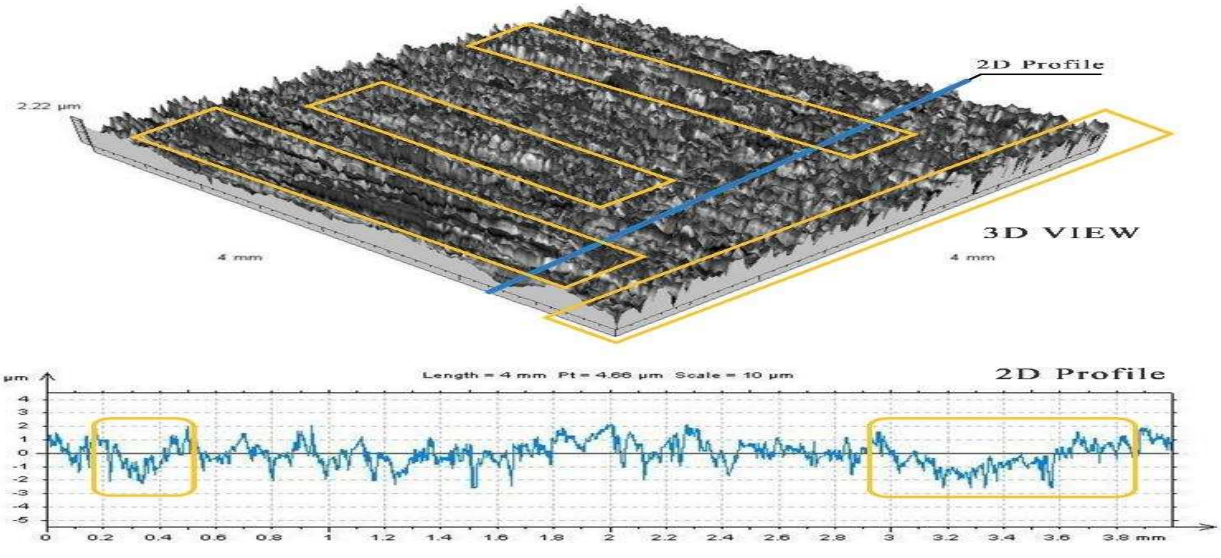

Fig. 4 Surface of the sample number 9 Injector

Parameters Sa and Ra belong to the most common group of parameters used to evaluate the surface roughness. Application of the 3D topography improves and extends the possibilities of the evaluation of the surface finish. In order to further investigate the 3D parameters, a relation between selected 2D and 3D parameters was observed. It is widely believed that the surface parameters (marked by "S") tend to have larger values. Obtained data from 3D topography proves that larger values of roughness is achieved when the surface roughness is in range 0.02 μm < Ra < 0.10 μm. If the surface roughness is in range 0.10 μm < Ra < 2 μm then the values of the parameters – with very few exceptions – are similar.

The 3D topoghraphy proves as and extended analytic tool, used to evaluate the surface as a functional area. It is also suitable for detailed investigation of the surface nature.

Acknowledgment

This work was completed thanks to the successful cooperation within a project DZRO K-205 "Podpora činnosti letectva AČR v lokálních konfliktech".

The paper has been prepared using the results of the research DZRO K 201 VÝZBROJ "Rozvoj technologií o oblasti konstrukce zbraní, střeliva, přístrojového vybavení výzbroje, materiálového inženýrství a vojenské infrastruktury" as well as SV16-216 "Povrchové technologie v aplikacích speciální techniky„ and is a component in solving these research issues.

References

[1] ČSN EN ISO 4287 - Geometrical Product Specifications (GPS) - Surface texture: Profile method -Terms, definitions and surface texture parameters

[2] ČSN EN ISO 4288 - Geometrical product specification (GPS) - Surface texture: Profile method -Rules and procedures for the assessment of surface texture

[3] MAŇAS, Karel, SVOBODA, Emil, DVOŘÁKOVÁ, Renata. Measuring of surface structure and their analysis. In 13th International Research/Expert Conference Trends in the Development of Machinery and Associated Technology TMT 2009. Hammamet : Universita Zenica, 2009, s. 761-764. ISSN 1840-4944.

Influence of projectile impact velocity and steel armour hardness on breakage of projectile 14.5 x 114 API/B32

Regina Mikulikova[1], Radek Ridky[2], Stanislav Rolc[1], Jan Krestan[1]
[1]Military Research Institute. Veslarska 337/230, 637 00 Brno. Czech Republic. E-mail: mikulikova@vvubrno.cz, rolc@vvubrno.cz, krestan@vvubrno.cz
[2]SVS FEM, s.r.o. Skrochova 3886/42, 615 00 Brno. Czech Republic. E-mail: rridky@svsfem.cz

The goal of this article was focused on study of projectile breakage after impact on steel armour depending on projectile impact velocity and steel armour hardness. Steel armour samples of hardness HBW500 and HBW600 were impacted by steel core projectile 14.5 x 114 API/B32 using three different impact velocities. The depth of projectile penetration into witness steel armour of hardness HBW400, which was placed 65 mm behind the steel armour samples, was measured. The projectile remains after each impact were searched. For better visualization of projectile breaking process after impact on steel armour the numerical simulations were performed. Experimental and numerical results were compared and combined in graph showing dependence of depth of penetration on projectile impact velocity for two different steel armour hardnesses and with indication of projectile coherence after impact.

Keywords: projectile breakage, impact velocity, hardness, depth of penetration

1 Introduction

Requirements to enhance the ballistic protection level of armoured vehicles still increase. One of the higher protection levels is K4 according to STANAG 4569, AEP-55, Volume 1, Edition C. The ballistic protection level K4 is represented by projectile 14.5x114 API/B32 with steel core and standardized impact velocity 911 ± 20 m/s [1]. Projectile weight is 64 g and the steel core weight is 40 g.

One of the mechanisms of armour to defeat the projectile is to break the projectile core and stop the projectile remains. For research and development of enhanced armour protection it is very useful the knowledge of the projectile breaking conditions. Projectile behaviour after impact on the armour is influenced by many factors. Two of main factors are the armour material hardness and the projectile impact velocity [2, 3].

In some cases of projectile / armour material interactions the specific phenomenon called „shatter-gap“ occurs. The classical shatter-gap is exhibited when the projectile core is shattered and thereby defeated by the armour when impacted at relatively high velocities. At lower velocities, the projectile could however defeat the armour because the impact energy is insufficient to break the projectile core. This usually results in projectile / armour combinations having multiple ballistic limit values. The classical shatter-gap phenomenon is most common with ceramic armour systems [1].

Nevertheless, armour steel is still the most common armour material, so the goal of this work was the study of projectile breakage after impact on steel armour depending on projectile impact velocity and steel armour hardness.

2 Methodology

2.1 Experimental testing

Steel armour plates were impacted by projectile 14.5 x 114 API/B32 with hardened steel core using three different impact velocities: 690 ± 20 m/s, 911 ± 20 m/s and 980 ± 20 m/s. Three following set-ups of steel armour plates of different Brinell hardness (HBW) were tested (plate thickness is behind slash):

- Set-up 1: steel armour plate HBW 400 / 50.7 mm
- Set-up 2: steel armour plate HBW 500 / 8.3 mm + air gap / 65 mm + steel armour plate HBW 400 / 50.7 mm
- Set-up 3: steel armour plate HBW 600 / 8.3 mm + air gap / 65 mm + steel armour plate HBW 400 / 50.7 mm

The scheme of general experimental set-up is shown on Fig. 1. The distance of target from the muzzle was 18 m.

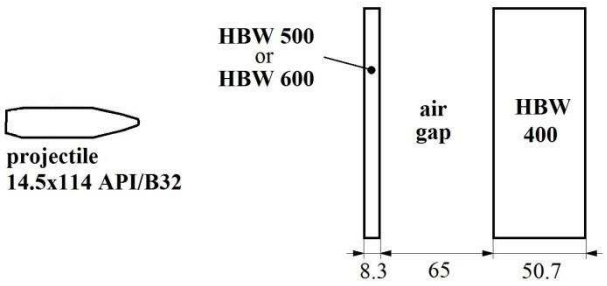

Fig. 1 Experimental set-up

The depth of projectile penetration into steel armour of hardness HBW 400 was measured. The projectile remains after each impact were searched. Unfortunatelly, not all the projectile remains during experimental tests were found.

Some of shots were repeated to confirm the results. Repeated shots were not averaged, each shot was included into table and graph separately.

2.2 Numerical simulation

The numerical simulations were performed by LS-Dyna software package, the software for non-linear dynamic finite element analysis. The numerical modelling was performed for all the three different steel armour set-ups mentioned in chapter 2.1. For each velocity range only one impact velocity was chosen and simulated. At the start of simulation the projectile was situated just in front of the first plate of the armour set-up with defined impact velocity. Simulations for Set-ups 2 and 3 were performed for two yaw angles from projectile flight path, i.e. 0° and 3°. The depth of projectile penetration into steel armour of hardness HBW 400 and projectile residual mass were evaluated.

For the projectile as well as the armour steel parts the Johnson-Cook material model was used, i.e. the empirical constitutive relation used to capture large strains and high strains rates as well as the damage evolution and failure of the metal materials [4, 5, 6, 7].

3 Results and discussion

3.1 Set-up 1

Experimental and numerical results for the Set-up 1 "steel armour plate HBW 400 / 50.7 mm" are stated in Tab. 1 and Fig. 2.

Tab. 1 Results for the Set-up 1

Projectile impact velocity [m/s]	Experimental testing	Numerical simulation for yaw angle 0º	
	Projectile depth of penetration [mm]	Projectile depth of penetration [mm]	Projectile residual mass [g]
689.5	22.6	19.5	34.8
926.8	28.0	27.6	28.9
988.3	27.5	30.0	27.8

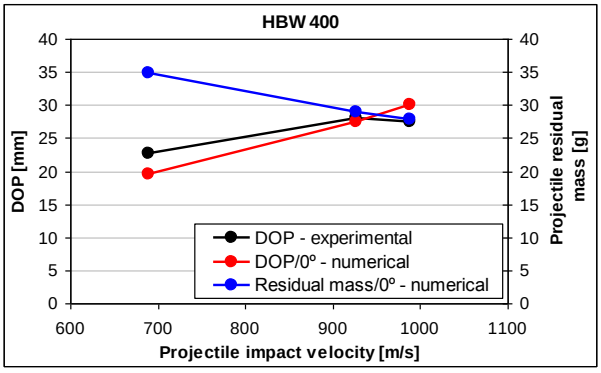

Fig. 2 Dependence of projectile depth of penetration (DOP) and projectile residual mass on projectile impact velocity for the Set-up 1

According to experimental results shown in Tab. 1 and Fig. 2 the depth of projectile penetration (DOP) increases with increasing impact velocity from 23 mm for velocity 689.5 m/s to 28 mm for velocity 926.8 m/s. For the highest projectile impact velocity 988.3 m/s the DOP stays similar.

According to numerical results the dependence of the DOP on the projectile impact velocity is almost linear. The residual mass of the projectile is almost linear too and corresponds to the DOP dependence, that means the higher projectile impact velocity, the higher DOP and the lower projectile residual mass. For the lower velocity the residual mass is only about 5 g lower than original weight of projectile core, for middle and higher velocities the residual mass is about 11 - 12 g lower than original weight of projectile core.

The numerical results of projectile residual mass were confirmed by experimental tests. Fig. 3 shows the projectile core remains for the lower and middle impact velocity. At the lower velocity the projectile core was not broken, at the middle velocity the core was broken probably into two or three parts.

Fig. 3 Remains of projectile 14.5x114 API/B32, which were found after impact on the Set-up 1

Resulting models of the numerical simulation of projectile impact into the Set-up 1 are shown on Fig. 4.

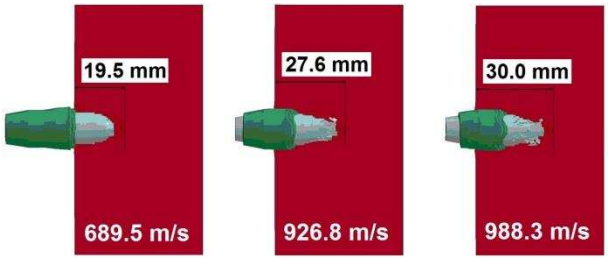

Fig. 4 Numerical simulation for the Set-*up 1 for yaw angle 0°*

Experimental testing and numerical modelling of the Set-up 1 was performed with regards to have a reference for comparison with Set-ups 2 and 3.

3.2 Set-up 2

Experimental and numerical results for the Set-up 2 "steel armour plate HBW 500 / 8.3 mm + air gap / 65 mm + steel armour plate HBW 400 / 50.7 mm" are stated in Tab. 2 and Fig. 5.

Tab. 2 Results for the Set-up 2

Projectile impact velocity [m/s]	Experimental testing	Numerical simulation for yaw angle 0°		Numerical simulation for yaw angle 3°	
	Projectile depth of penetration [mm]	Projectile depth of penetration [mm]	Projectile residual mass [g]	Projectile depth of penetration [mm]	Projectile residual mass [g]
511.7	10.0	-	-	-	-
673.0	15.5	-	-	-	-
690.1	18.5	7.3	36.8	4.7	29.7
907.8	4.6	-	-	-	-
916.9	2.6	-	-	-	-
930.1	2.6	7.8	6.8	8.4	4.1
983.0	9.0	9.0	14.7	10.3	7.5

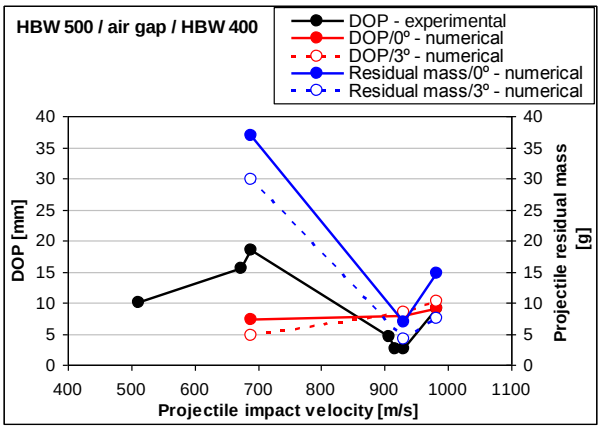

Fig. 5 Dependence of projectile depth of penetration (DOP) and projectile residual mass on projectile impact velocity for the Set-up 2

According to experimental results shown in Tab. 2 and Fig. 5 there is a fall of DOP at velocity 911 ± 20 m/s. The DOP fall was confirmed by two another shots at the same velocity range. Because of this non-linear dependence even lower impact velocity around 500 m/s was tested. Whole curve for experimental DOP indicates the shatter-gap influence. That means that for the velocity around 690 m/s the projectile has higher ballistic efficiency and for the velocity

around 911 m/s the projectile has lower ballistic efficiency. Projectile ballistic efficiency at velocities around 500 m/s and 980 m/s is similar.

According to found projectile remains shown on Fig. 6 the projectile starts to break at impact velocity around 673 m/s. Projectile breakage could be also influenced by the yaw angle from the impacting projectile flight path. In this case the projectile at velocity 690 m/s was probably not broken due to yaw angle cca 0° and the projectile at velocity 673 m/s could be broken due to yaw angle greater than 0°.

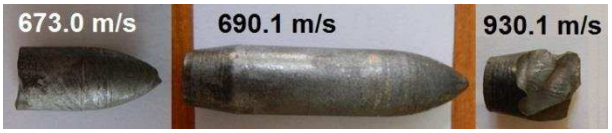

Fig. 6 Remains of projectile 14.5x114 API/B32, which were found after impact on the Set-up 2

The greater yaw angle can be estimated from the shape of hole in frontal armour plate caused by projectile perforation. If the yaw angle is cca 0° the hole is round. If the yaw angle is greater than 0° the ideal round shape of the hole is deformed.

The hole after perforation of the projectile at velocity 690 m/s is almost round (see Fig. 7), which means that the yaw angle was cca 0° and the projectile did not break (see Fig. 6), moreover it made greater DOP. Vice versa the hole after perforation of the projectile at velocity 673 m/s is deformed (see Fig. 7), which means that the yaw angle was greater than 0° and the projectile broke (see Fig. 6) and made lower DOP.

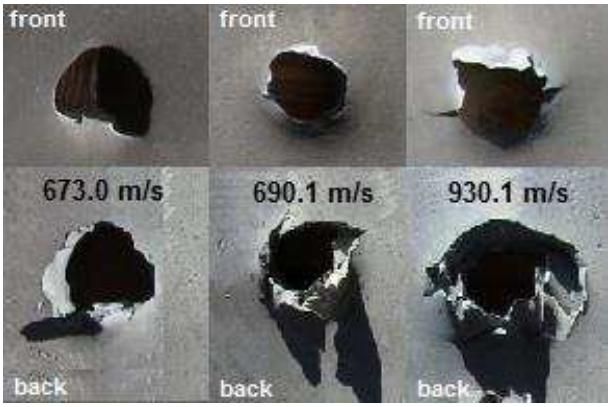

Fig. 7 Perforation of steel armour plate HBW 500 / 8.3 mm after projectile impact

According to numerical results the dependence of the DOP on the projectile impact velocity is almost linear, which does not correspond with experimental results. On the other hand the trend of projectile residual mass curve copies the trend of experimental DOP curve and also corresponds to size of found projectile remains (see Fig. 6).

Resulting models of the numerical simulation of projectile impact into the Set-up 2 are shown on Figs. 8 and 9, for yaw angles 0° and 3° respectively. Numerical modelling confirmed the influence of the yaw angle on the projectile breakage. In case of projectile impact velocity 690 m/s and yaw angle 0° the projectile did not break (see Fig. 8), in case of projectile impact velocity 690 m/s and yaw angle 3° the projectile broke down (see Fig. 9).

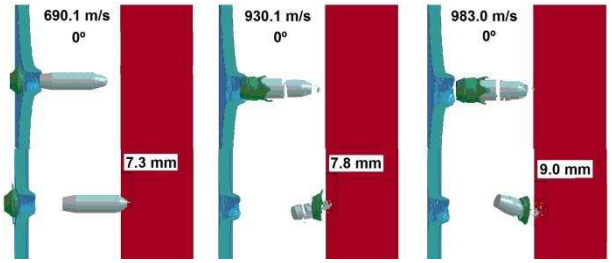

Fig. 8 Numerical simulation for the Set-*up 2 for yaw angle 0°*

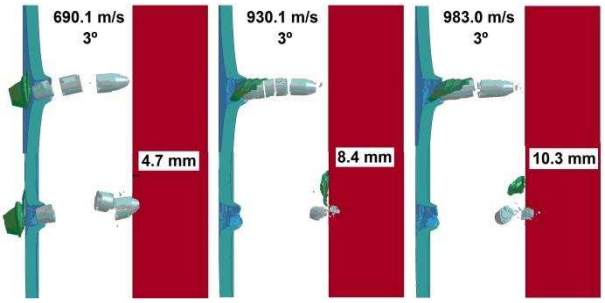

Fig. 9 Numerical simulation for the Set-*up 2 for yaw angle 3°*

3.3 Set-up 3

Experimental and numerical results for the Set-up 3 "steel armour plate HBW 600 / 8.3 mm + air gap / 65 mm + steel armour plate HBW 400 / 50.7 mm" are stated in Tab. 3 and Fig. 10.

Tab. 3 Results for the Set-up 3

Projectile impact velocity [m/s]	Experimental testing	Numerical simulation for yaw angle 0°		Numerical simulation for yaw angle 3°	
	Projectile depth of penetration [mm]	Projectile depth of penetration [mm]	Projectile residual mass [g]	Projectile depth of penetration [mm]	Projectile residual mass [g]
503.3	1.3	-	-	-	-
671.7	2.5	-	-	-	-
688.5	0.9	-	-	-	-
689.6	1.5	7.1	35.4	3.2	23.4
910.1	1.9	-	-	-	-
926.0	3.0	4.1	10.8	5.4	4.4
982.5	5.0	7.4	8.4	6.2	3.2

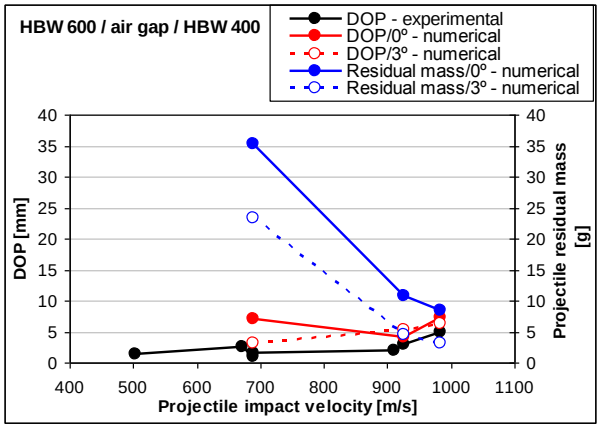

Fig. 10 Dependence of projectile depth of penetration (DOP) and projectile residual mass on projectile impact velocity for the Set-up 3

Because the goal of this work was to find the projectile impact velocity, when the projectile starts to break and because the projectile at impact velocity 671.7 m/s broke down, also even lower impact velocity around 500 m/s was tested. Fig. 11 shows that the projectile was broken even at such low velocity.

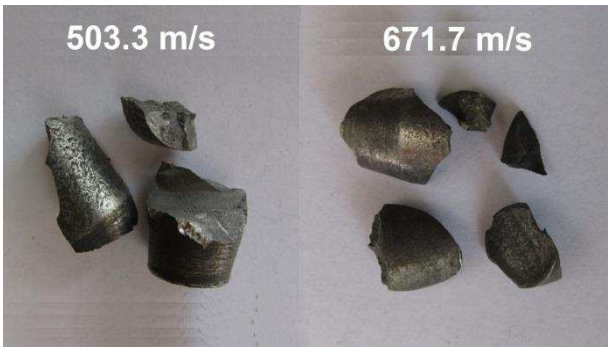

Fig. 11 Remains of projectile 14.5x114 API/B32, which were found after impact on the Set-up 3

According to experimental results shown in Tab. 3 and Fig. 10 the DOP increases very slightly with increasing projectile impact velocity.

Numerical values of the DOP are more or less similar to the experimental ones, especially for the yaw angle 3°. Projectile residual mass decreases quite fast and almost linearly with increasing projectile impact velocity.

Resulting models of the numerical simulation of projectile impact into the Set-up 3 are shown on Figs. 12 and 13, for yaw angles 0° and 3° respectively. On the Fig. 12 we can see difference from experimental results with regard to projectile breakage. According to numerical simulation the projectile with impact velocity 689.6 m/s and yaw angle 0° does not break. Within experimental testing the projectile was broken at impact velocity 671.7 m/s and also 503.3 m/s (see Fig. 11).

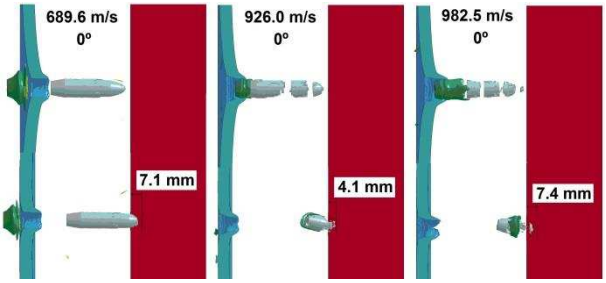

Fig. 12 Numerical simulation for the Set-*up 3 for yaw angle 0°*

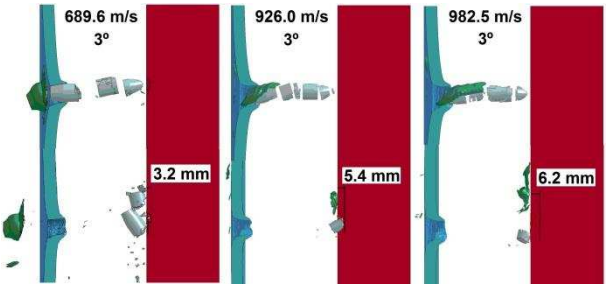

Fig. 13 Numerical simulation for the Set-*up 3 for yaw angle 3°*

4 Conclusions

Three set-ups of steel armour plates of different Brinell hardness (HBW 400, HBW 500 and HBW 600) were ballistically tested by steel core projectile 14.5 x 114 API/B32 using three different impact velocities: 690 ± 20 m/s, 911 ± 20 m/s and 980 ± 20 m/s. The depth of projectile penetration (DOP) into steel armour of hardness HBW 400 was measured. The projectile remains after each impact were searched. The experimental results were supplemented, combined and compared with numerical simulations.

For the Set-up 1 „steel armour plate HBW 400 / 50.7 mm“ it was found out that the DOP values correspond to numerical values. The dependences of the DOP and the residual projectile mass are more or less linear. The higher impact velocity, the greater DOP and the smaller projectile residual mass. The projectile starts to break down at impact velocity range 911 ± 20 m/s.

For the Set-up 2 „steel armour plate HBW 500 / 8.3 mm + air gap / 65 mm + steel armour plate HBW 400 / 50.7 mm“ it was found out that the DOP values do not correspond to numerical values. The experimental DOP curve indicates the shatter-gap influence. That means that for the velocity range 690 ± 20 m/s the projectile has higher ballistic efficiency and for the velocity range 911 ± 20 m/s the projectile has lower ballistic efficiency. Projectile ballistic efficiency

at velocities around 500 m/s and 980 m/s is similar. The projectile starts to break at impact velocity around 673 m/s in case, if the yaw angle is greater than 0°. The trend of numerical projectile residual mass curve copies the trend of experimental DOP curve, that means that the projectile residual mass as well as the DOP are the lowest at velocity range 911 ± 20 m/s. According to combination of experimental and numerical results it could be stated that the ballistic efficiency of steel armour plate of hardness HBW 500 and thickness 8.3 mm is the highest at 911 ± 20 m/s and the lowest at 690 ± 20 m/s.

For the Set-up 3 „steel armour plate HBW 600 / 8.3 mm + air gap / 65 mm + steel armour plate HBW 400 / 50.7 mm“ it was found out that the numerical values of the DOP are more or less similar to the experimental ones, especially for the yaw angle 3°. The DOP increases very slightly with increasing projectile impact velocity. Projectile residual mass decreases quite fast and almost linearly with increasing projectile impact velocity. Within experimental testing the projectile was broken at impact velocity 671.7 m/s and also 503.3 m/s.

Acknowledgement

The work was supported by the Ministry of Defence of the Czech Republic in connection with project OFVVU20150004.

References

[1] NATO STANDARD AEP-55 (2014). Procedures for evaluating the protection level of armoured vehicles - kinetic energy and artillery threat, Vol. 1, Ed. C, NSA, Brussels.

[2] BUCHAR, J., VOLDŘICH, J. (2003). *Terminální balistika*, pp. 340. Academia, Praha.

[3] RYAN, S., LI, H., EDGERTON, M., GALLARDY, D., CIMPOERU, S.J. (2016). The Ballistic Performance of an Ultra-High Hardness Armour Steel: An Experimental Investigation. In: International Journal of Impact Engineering, Vol. 94, pp. 60 – 73.

[4] LS-DYNA Keywords User's Manual (2013). Materials models, Vol. II, revision 3372.

[5] JOHNSON and COOK (1983). A constitutive model and data for metals subjected to large strains, high strain rates and high temperatures. In: Proceeding of the Seventh International Ballistics Symposium, pp. 541 – 547. The Hague.

[6] JOHNSON and COOK (1985). Fracture characteristics of three metals subjected to various strain, strain rates, temperatures and pressures. In: Engineering Fracture Mechanics, Vol. 21, No. 1, pp. 31 – 48.

[7] RIDKY, R., BODISOVA, K., KRESTAN, J., POPOVIC, M., KOPKANE, D., ROLC, S. (2015). Simulation as a reliable tool for predicting the degree of armor damage. In: International Conference on Military Technologies. IEEE, Brno.

The effect of mechanical features of a compound on a tire wear

Pavol Mikus[1], Ivana Mikusova[2]
[1] Trenčín Alexander Dubček University in Trenčín, Faculty of Special Technology, Pri parku 19, 911 06 Trenčín-Záblatie, E-mail: pavol.mikus@tnuni.sk, 00421 327 400 245
[2] Trenčín Alexander Dubček University in Trenčín, Faculty of Special Technology, Pri parku 19, 911 06 Trenčín-Záblatie, E-mail: ivana.mikusova@tnuni.sk, 00421 327 400 216

This article deals with the effect of the mechanical properties of the compound on the tire wear. For detection purposes the samples of 13 kinds of rubber compounds were made having been used and processed in practice. The hardness was measured with pocket Durometer of IRHD type; tensile strength and ductility were carried out at a universal testing facility Instron 4466. Rapid wear test was conducted on a roller abrasive machine. All measurements were assessed and compared.

Keywords: Tire, hardness, effect, testing sample, wear

1 Introduction

The tires play a non-substitutable role in an automotive industry and therefore their quality is very important. A level of a production technology and quality of a tire-casing used to be dependent on testing methods, used to test particular indicators. The testing methods should take into consideration above all the ultimate objective, which is the product and the purpose to which it is to be used. For these reasons, there is a requirement to choose new testing methods operating in a different way of wear for heavy loaded vehicle tire crown compounds working in extreme terrain surface conditions than conventional road and laboratory testing on elastomeric abrasion.

2 Production of samples

Testing samples for all kinds of tests were prepared by mould-pressing on a hydraulic vulcanizing two-storey 400x400 type press. The shape and dimensions of the testing samples meet applicable standards. Curing time and temperature were determined by rheology. After pressing the elements were cast off for more than 16 hours, as stated by the standard. There are pressed and vulcanized bodies in the picture (Fig. 1 and 2) for a preparation of samples for a quick wear testing and some plates to take measures of hardness.

Fig. 1 The plates to cut the blades

Fig. 2 The bodies for a preparation of samples for a quick wear testing

3 Taking measures of IRHD hardness

A characteristic being measured is the depth of the impression of a specified indenter by a set force into a material under defined conditions. A pocket IRHD durometer was used during measurements. Thickness of a testing body had to be as minimum 6 mm aiming to define hardness with the pocket durometer. The testing procedure was as follows. The testing body was placed on a flat, hard surface. Durometer was placed on the testing sample so that the centre of the durometer testing point was at least 12 mm from the edges of the testing body. Support foot was as fast as possible applied on a testing body so it was parallel to the surface of the testing body, and in order to ensure that the indentor

heads for perpendicular to the surface of the elastomer. There were 5 measurements carried out on each kind of compound, in which a mean hardness was defined for each compound. The result of test has been expressed as an integral number. All results are shown in the Tab. 1 and plotted in the Fig. 3.

Tab. 1. The measured values of the hardness of particular compounds

COMPOUND	1. VALUE	2. VALUE	3. VALUE	4. VALUE	5. VALUE	Median
189	59	61	60	60	60	**60**
672	54	55	54	53	54	**54**
163	87	87	86	85	85	**86**
164	67	70	68	68	67	**68**
SME	60	59	62	60	60	**60**
693	61	63	62	63	62	**62**
671	66	66	66	67	66	**66**
165	75	77	77	74	76	**76**
134	54	53	52	54	53	**53**
112	58	59	59	56	58	**58**
2546	61	60	62	61	62	**61**
137	64	65	66	66	64	**65**
092	88	86	89	89	88	**88**

The lowest hardness was measured for samples Nr. 134 and Nr. 672 and the highest hardness was achieved for samples Nr. 163 and Nr. 092.

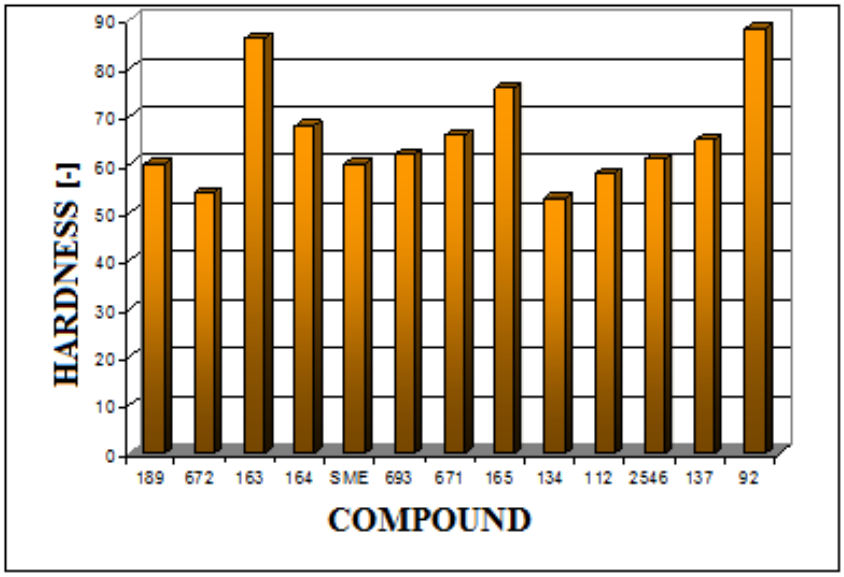

Fig. 3 IRHD hardness

4 Measuring of tensile strength and ductility

All 13 compounds were taken to measure the tensile strength and for each compound 5 pieces of double-sided blades were produced, which have undergone measurement. The blades were produced by mould-pressing in a laboratory 2-storey vulcanizing press.

As a testing bodies there were defined the both-sided blades of type 1, 115mm long and a length of a working zone was 25mm. They were cut out with a dies with the material sense. Measurement was carried out in accordance with ISO 37 standard. Measurement was performed on 23 March 2016 at FPT in Púchov. The results of measurements of the tensile strength are recorded for each compound in Tab. 2, and plotted (see Fig. 4).

Tab. 2 The measured values of tensile strength

Compound type	**189**	**672**	**163**	**164**	**SME**	**693**	**671**
Tensile strength [MPa]	7,76	20,01	8,25	10,96	16,01	9,92	18,12
Compound type	**165**	**134**	**112**	**2546**	**137**	**092**	-
Tensile strength [MPa]	14,11	18,52	14,02	15,21	16,47	10,09	-

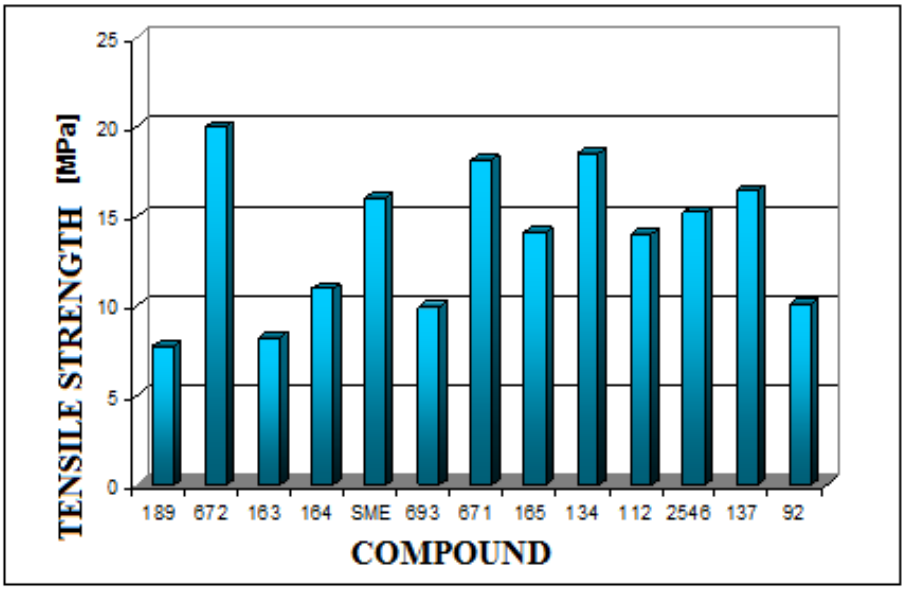

Fig. 4 Tensile strength

The results of measurements of ductility are recorded in Tab. 3 and plotted in Fig. 5. Tensibility is a tensile strain of a working length of a testing body in a breaking point. It is designated as E_b and it is expressed in percentage. There are particular courses of a tensile test (see Fig. 6) for each compound.

Tab. 3 Measured values of tensibility

Compound type	**189**	**672**	**163**	**164**	**SME**	**693**	**671**
Tensibility [%]	259,9	1211,06	588,81	574,09	1158,24	839,57	1098,45
Compound type	**165**	**134**	**112**	**2546**	**137**	**092**	-
Tensibility [%]	466,56	1289,96	1072,81	1056,61	893,83	240,18	-

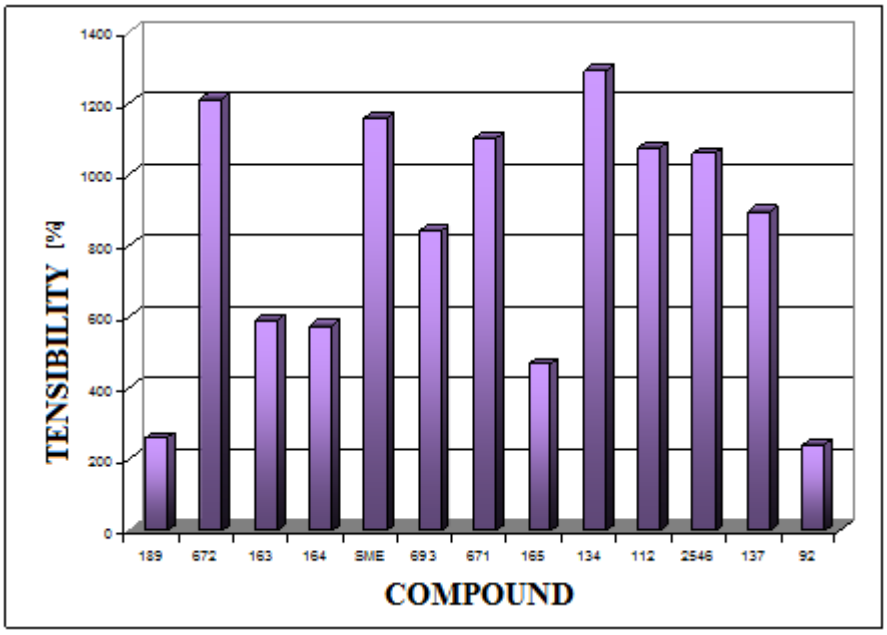

Fig. 5 Tensibility

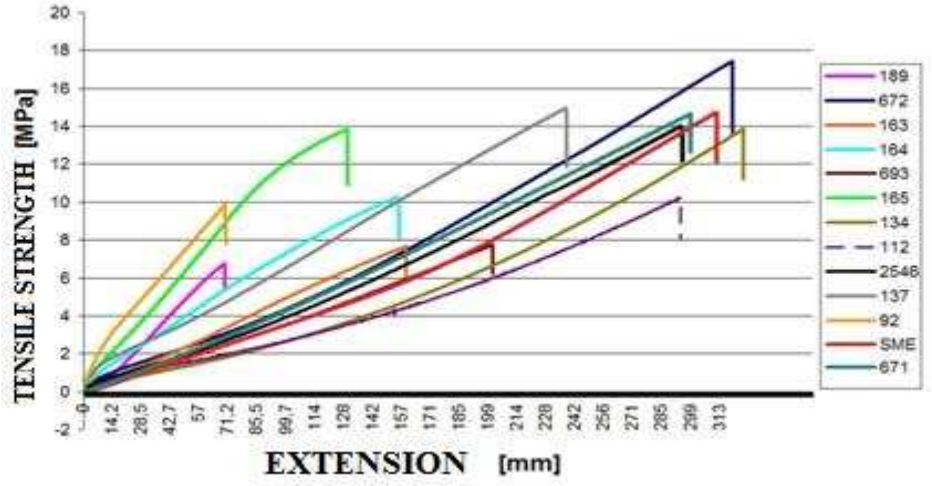

Fig. 6 Relation of tensile strength and extension

5 A quick wear test

The testing bodies are cylindrical shapes with a diameter of 16 mm and 15mm. They were prepared from the mould bodies with dimension 150x30mm with a hollow drill. The test was performed at standard laboratory temperature. Abrasion of the surface temperature during the test increased, but for the purposes of determining the weight loss composition comprises the temperature rise negligible. Temperature of a surface being worn has increased during the test, but for the purposes of determining the weight loss of the compound, these temperature increases are negligible. Before each test, it was necessary to remove the rubber powder from the abrasive cloth, after the previous test. The test was conducted with a rotating testing body. The testing body was weighed with 1 mg accuracy. Subsequently it was mounted in the holder so as to protrude 2 mm, this length was checked.

A holder of a testing body and the slide were placed in the starting position and a controlled test was launched. Vibrations of a testing body holder were monitored. If excessive vibration had been present, reliable results would have not been achieved. Test run stopped automatically after reaching the abrasive distance of 40 m.

Three tests were made for each compound. The testing bodies and testing device are shown in the picture (Fig. 7 and 8).

After each test cycle the testing body was weighed with 1 mg accuracy. Sometimes small shreds hanging from the testing bodies had to be removed before weighing. All courses followed one after the other. The measured values were compiled and assessed. The measured values of weights of particular samples are recorded in Tab. 4 and they are plotted (Fig. 9).

Fig. 7 The samples for a rapid wear test

Fig. 8 The device for a rapid wear testing

Tab. 4 Calculated values of weight reduction

COMPOUND	Differences in weight [g]			Median
	Sample Nr. 1	Sample Nr. 2	Sample Nr. 3	
189	**0,289**	**0,325**	**0,319**	**0,319**
672	**0,178**	**0,206**	**0,171**	**0,178**
163	**0,449**	**0,467**	**0,452**	**0,452**
164	**0,370**	**0,375**	**0,399**	**0,375**
SME	**0,180**	**0,161**	**0,181**	**0,180**
693	**0,328**	**0,320**	**0,322**	**0,322**
671	**0,192**	**0,205**	**0,160**	**0,192**
165	**0,350**	**0,380**	**0,392**	**0,380**
134	**0,125**	**0,152**	**0,144**	**0,144**
112	**0,326**	**0,429**	**0,378**	**0,378**
2546	**0,246**	**0,211**	**0,227**	**0,227**
137	**0,276**	**0,339**	**0,353**	**0,339**
092	**0,815**	**0,654**	**0,658**	**0,658**

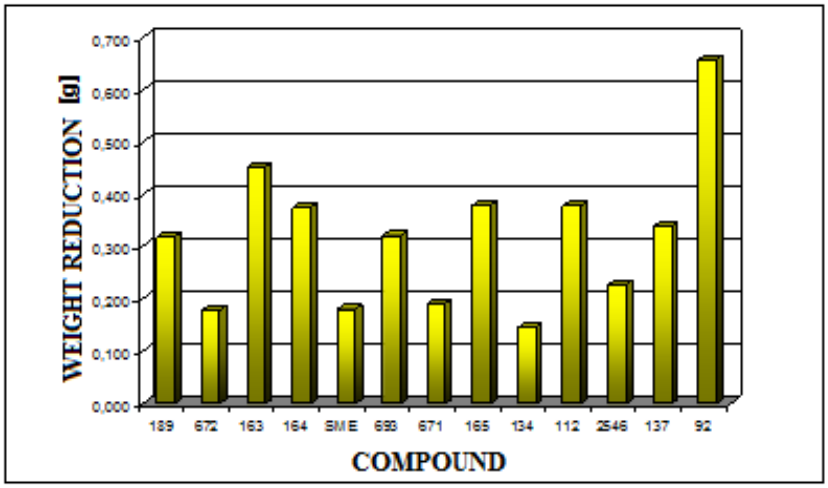

Fig. 9 Weight reduction of particular compounds

6 Interpretation

The most suitable method how to define the quality and lifetime of the tire is testing in terms of future application of the product in practice. However, the time interval of practical testing is long, as tires have a significantly longer lifetime than other industrial products. Therefore it is necessary to verify the quality parameters of tires at more frequent intervals in order to make technical and technological adjustments and avoid the risk that a large number of products would be produced with an error.

Hardness

High hardness values were determined for compounds Nr. 092, 163, 165 which are also compounds of the lowest wear resistance. Very low hardness was measured in the compounds Nr 134 and 672, which also showed the lowest wear. It meets also the expectations of the material behavior. Greater hardness makes "a compound crumbling" easier, while a tougher material will better resist to wear.

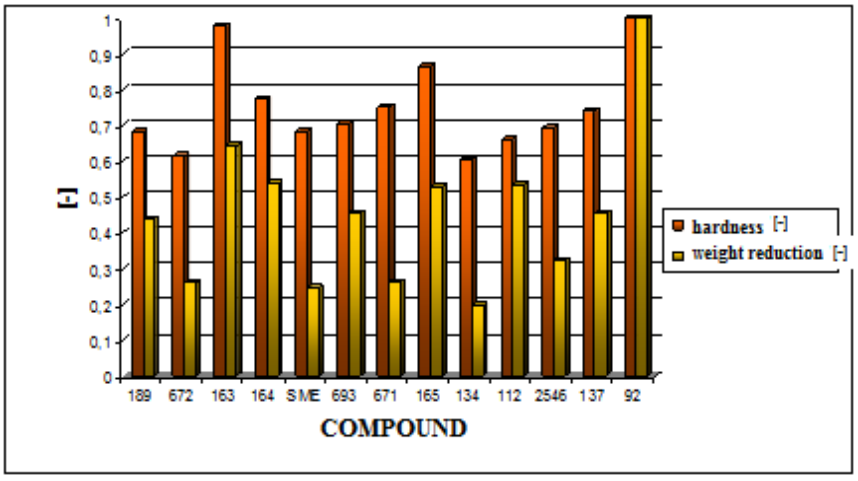

Fig. 10 Hardness and wear comparison

For further comparison, the values of so called hardness product were calculated, it means a product of hardness and ductility. The results of such comparison are shown in Fig. 11.

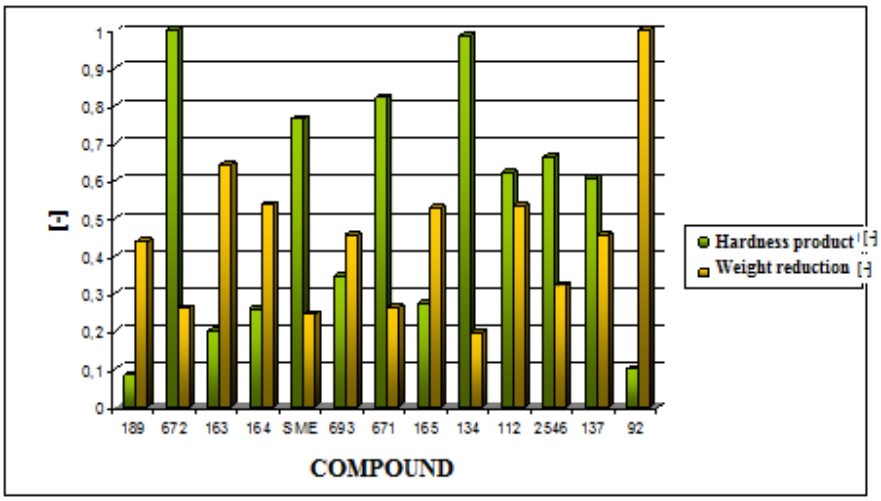

Fig. 11 Comparison of a hardness product and a wear

The measured values result in following:

- The best results were achieved in a set of measured values for wear in compounds 672 SMEs, 671, 134, which also showed the highest value of so called hardness product,
- The higher resistance to a reviewed type of wear was achieved in compositions that showed a lower hardness,
- wear increased in all reviewed cases evenly with time and over the time duration of the test, in regard with a fact, that the properties of the compound are affected by the composition (by a type and by representation of the components), therefore the wear was affected by composition of a compound.

7 Conclusion

This article discusses an issue of a wear of highly stressed parts from an elastomer, particularly tire treads. Set of measurements was conducted involving tensile testing (tensile strength, ductility) and hardness tests.

A test of rapid wear on a rotating cylindrical device forms a significant part of this work. On this device there was made a set of measurements on testing bodies made of thirteen kinds of different types of tread compounds assigned for a production of highly stressed tire treads for vehicles of special equipment and various technical vehicles.

The results of all measurements were recorded and evaluated. Then they were compared with the wear of a tread compound. The analysis has led to an interesting relationship between the degree of wear observed on the testing device and some mechanical properties. The relationship between hardness and wear can be considered as relevant– the harder was a sample, the higher was a wear.

The relationship between hardness and wear has not been established, that is the wear rate showed no clear relationship to the hardness of a sample. It seems to be a relation between ductility and a rate of wear based on measured values.

Rapid tests for wear of tread compounds can be carried out on the rotary device at very low operating costs and test duration. After the test, we get obtain a rough idea about the behavior of a given compound.

References

[1] ISO 2393: 2014 Rubber test mixes - Preparation, mixing and vulcanization -- Equipment and procedures

[2] ISO 37:2010 Rubber, vulcanized or thermoplastic - Determination of tensile stress-strain properties

[3] ISO 7619-2: 2010 Rubber, vulcanized or thermoplastic - Determination of indentation hardness -- Part 2: IRHD pocket meter method

[4] ISO 4662:2009 Rubber, vulcanized or thermoplastic - Determination of rebound resilience

[5] ISO 4649:2010 Rubber, vulcanized or thermoplastic - Determination of abrasion resistance using a rotating cylindrical drum device

Analysis of residual stress of the martensitic stainless X12Cr13 steel after machining with blunt mill

Ondrej Pilch[1], Vojtěch Hrubý[1], Petr Faltejsek[1]
[1]University of Defence, Faculty of Military Technology, Department of Mechanical Engineering, Kounicova 65, 662 10 Brno, Czech Republic,. E-mail: ondrej.pilch@unob.cz

Plasma nitriding is a great thermochemical treatment, widely used in many technical applications as a final operation to improve the mechanical, tribological and corrosion properties of steel. This paper is focused on plasma nitriding treatment of martensitic stainless steel X12Cr13. The plasma nitriding process was performed using two stage nitriding procedures. The analysis was performed by measuring depth profiles of residual stress by X-ray difraction. To identify critical areas in terms of surface integrity was used Barhausen noise analysis. The verification of material chemical composition was carried out by OES Oxford FOUNDRY-MASTER device. The objective was to verify the nature of the residual stress before and after thermochemical treatment. The samples before and after thermochemical treatment have significant differences in the directions of the measured residual stress which may be caused machining with blunt tool, what has significant influence on the creation of plasma nitride layer.

Keywords: Residual Stresses, Plasma Nitriding, Barkhausen noise

1 Introduction

The paper describes issues stainless steels machining in terms of chemical composition, physical and mechanical properties. This paper also deals with specification of stainless steels and corrosion resistant materials and cutting conditions. The issue of the machinability of stainless steels is in terms of their specific features interesting area.

Stainless steels are often regarded as 'difficult to machine' and classified a single group of steels, based on experience with the most common austenitic types. The machinability of the stainless steels i.e. austenitic, ferritic, duplex, martensitic and precipitation hardening is however different. It is important to consider these properties differences when selecting machining parameters and conditions are used [1].

In order to ensure the functional properties of the products, it is necessary to choose technological methods in their production which assume that their required shape, size and physical-mechanical properties, which correspond to the requirements of the operating conditions, will be ensured. These properties depend on the properties of the used material and on the interaction of this material with the material of the tool, which mainly influences the properties of the surface layer [2,3].

The surface layer of a component that was created after being machined by some of the technological operations can be evaluated from two aspects. From a visual point of view (external evaluation) and in terms of changes that occurred in the materials from the surface of the functional surface to the core of the material. Both of these directions of evaluation clearly lead to the observation and evaluation of the failures that have arisen on the functional surface of the component. These are defects that have only occurred in a thin surface layer and disturbances that occur at depths below the surface [3,4].

Subsurface failures include cracks occurring during machining and may extend to greater depth than the considered bandwidth affected by the work-up effects. In these cases, these will be disturbances resulting from the concentration of stresses on obstacles preventing movement of dislocations. The resulting subsurface failure occurs by the sum of the stress peaks from the load and residual stresses generated after the technological operation. When assessing the impact of technological processes on the properties of the surface layer of the workpiece, it is necessary to take into account the intensity and types of energies used to convert the semifinished product to the finished component [4,5].

The stresses which remain even after the causes that have caused them, are called residual stress. The external causes created by the technological operations are distributed unevenly. Only in a certain volume of the material (layer) of the component [5,6].

2 Experimental part

The analysis os residual stresses was maked on the wheel blades of turbocharger stator see **Fig. 1**. These individual blades were milled using blunt and sharp shank mill under same cutting conditions. The Turbocharger stator wheel blade is displayed in **Fig. 2**. The material of wheel is martensitic stainless steel X12Cr13. The X12Cr13 stainless steel is in used for steam valves, pump shafts, bolts and miscellaneous parts production requiring corrosion resistance and moderate strength up to 500°C.

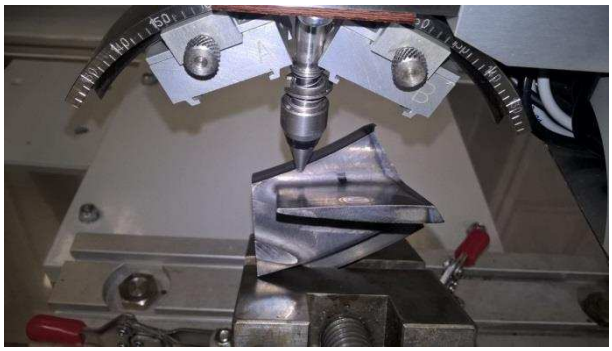

Fig. 1 Turbocharger stator wheel blade

The parameters of the plasma nitriding process were designed according to used component and selected martensitic stainless steel. The plasma nitriding process was performed using two stage nitriding procedures. After plasma cleaning procedure at 515 °C for 45 min the first stage nitriding procedure was performed at 520°C for 16 hours and followed by second stage of nitriding procedure, which was performed at 525°C for 4 hours. Plasma nitriding process was performed in RÜBIG PN 70/120 device. The process parameters are listed in Tab. 1[7,8].

Tab. 1 PN parameters

Nitriding process	**Temperature [°C]**	**Nitriding duration [h]**	**Voltage [V]**	**Pressure [Pa]**
Plasma cleaning	515	3/4h	800	80
1. stage of PN	520	16h	530	270
2. stage of PN	525	4h	540	250

Determination of the chemical composition was performed on the Oxford FOUNDRY-MASTER optical emission spectrometer. The results represent the composition of the core in the cross-sectional and are shown in the Tab. 2 [9].

Tab. 2 Chemical composition of samples

C	**Si**	**Mn**	**Cr**	**Ni**	**Mo**	**P**	**S**
(1.4006): EN 10088-2-2005							
0.08 - 0.15	max 1	max 1.5	11.5 - 13.5	max 0.75	0.15 - 0.25	max 0.035	max 0.035
Chemical composition of NPN sample							
0.14	0.51	0.37	12.7	0.07	0.594	0.011	0.003
Chemical composition of PN sample							
0.02	0.49	0.43	12.9	0.09	0.534	0.016	0.014

For the PN sample, the lower carbon content is probably the result of technological decarburization. Deeper grinding before the diffractometric measurement was a threat to thermal influence.

Examination of Barkhausen noise was carried out using the Rollscan 300 analyzer, the gear sensor S1-164-15-04 (toothed pole sensor with serial number 5425, new type S1-14-15-05). The individual measurements were made in three positions along the blade length on both sides (see **Fig. 2**). The location with the highest Barkhausen noise value corresponds to the location with the highest residual stress resp. with the smallest hardness. Found sites showing these parameters were subjected to residual stresses measurements by X-ray diffraction [10].

Fig. 2 The measurements on the left side

The measurements on the left side were the same as on the right side (0 cm on the left corresponds to 0 cm on the right). The arrow in the figure shows the direction of measurement. The sites for further analysis were determined on the blade surface. The measured values are shown in the graph for the left side, where the individual curves (red, black, purple) correspond to the curves of the MP (Amplitude of Barkhausen noise) values for the positions (0, 1.5, 3) measured in the direction indicated from the root of the blade to the face (see **Chyba! Nenalezen zdroj odkazů.**). The highest MP value is found on the blade surface at position 3 on the left side[6,10].

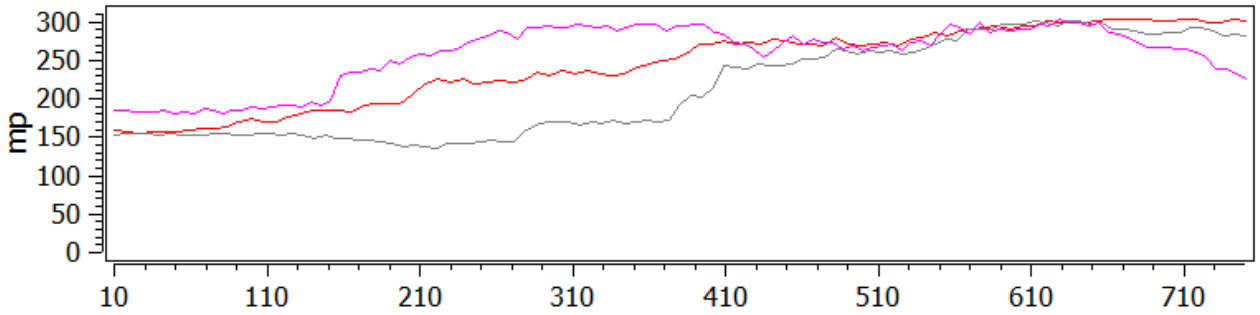

Fig. 3 Barhausen noise analysis

The measurements on the left side were the same as on the right side (0 cm on the left corresponds to 0 cm on the right). The arrow in the figure shows the direction of measurement. The sites for further analysis were determined on the surface of the blade and on the radius. The measured values are shown in the graph for the left side, where the individual curves (green, black, blue) correspond to the curves of the MP values for the positions (0, 1.5, 3) measured in the indicated direction from the root of the blade to the face (see **Chyba! Nenalezen zdroj odkazů.**). The highest MP value is found on the blade surface at position 0 and at the radius at position 3 on the left side [11].

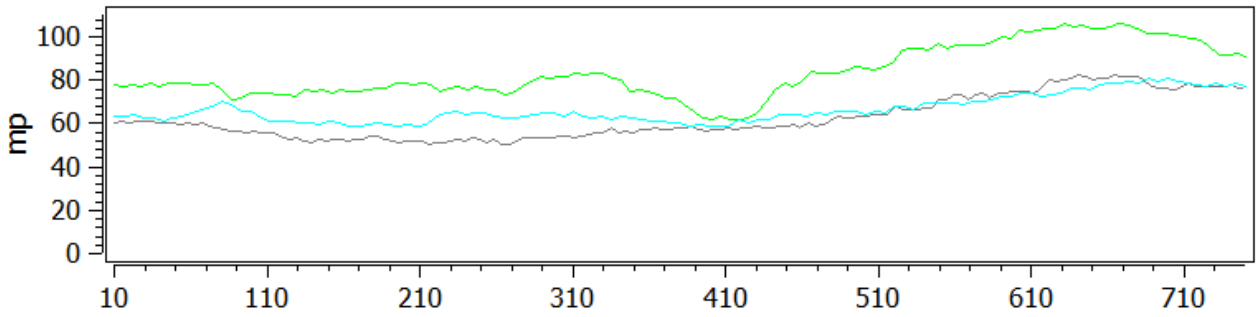

Fig. 4 Barhausen noise analysis

Residual stress measurements were performed on a Stresstech Xstress 3000 G2R diffractometer. The measurement sites were determined using a previous Barhausen noise analysis. The residual stress was determined in two directions (Fig. 5) [6,11].

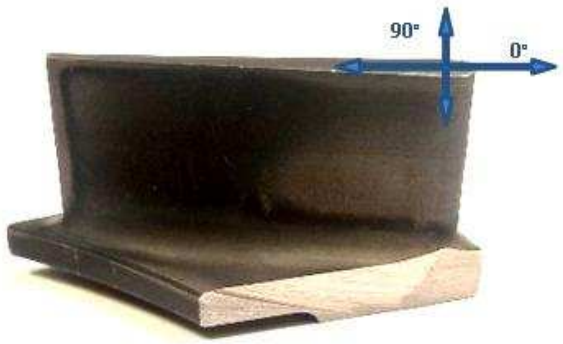

Fig. 5 The directions of residual stress measuring

Direction 0° is indicated in the following residual stress graphs and shown in a red line, and the 90° direction is shown in blue. In this way, measurements were taken on all samples. The results of measurements are shown in individual graphs of dependence of residual stress at depth below the surface. The results of measurements are showed in **Fig. 6** and **Fig. 7**.

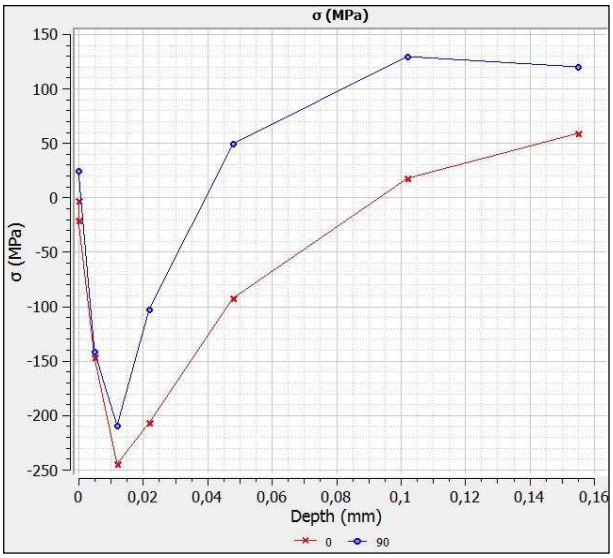

Fig. 6 Residual stress of NPN sample

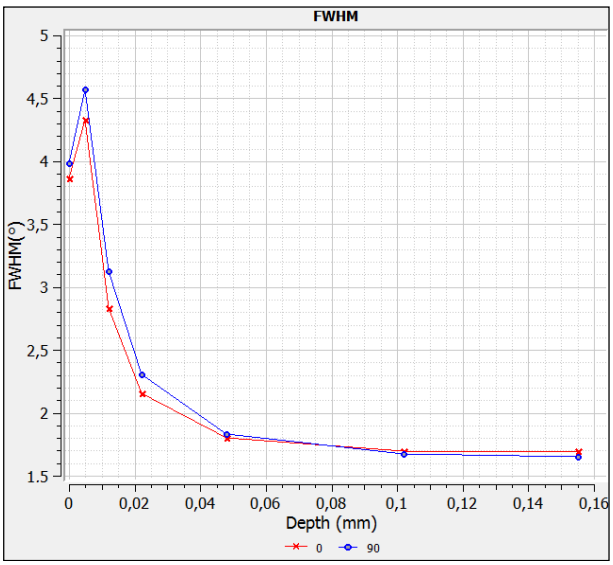

Fig. 7 FWHM of NPN sample

Another measured magnitude is the width of diffraction peak at half maximum (Full Width at Half Maximum-FWHM). This parameter is dependent on the structure of the monitored material, reflecting information on material hardness and micro-stress. FWHM values are shown in the secondary graphs as a dependency of FWHM on the depth, see **Fig. 8** and **Fig. 9** [10,11].

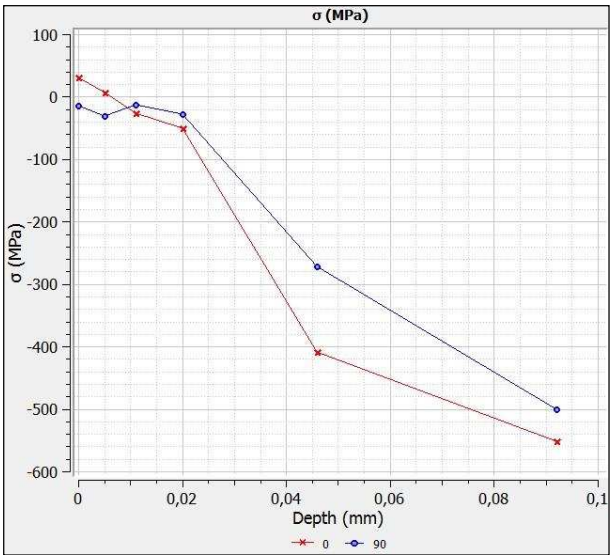

Fig. 8 Residual stress of PN sample

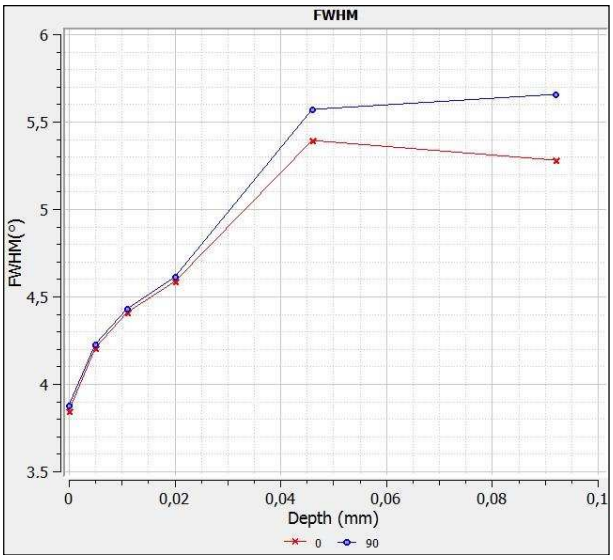

Fig. 9 FWHM of PN sample

3 Conclusion

From the dependence of residual stress and the depth below the surface it can be seen that the stress in the near subsurface layers is a significant pressure stress (200-500 MPa). These stresses reach equilibrium (± 100 MPa) at a depth of 50 microns. When comparing the sample before and after the chemical heat treatment, there are significant differences in the measured residual stress directions which may be caused by machining influences. From the FWHM dependence on the depth, it is obvious that the hardness of the surface of the layers at a depth of about 50 μm decreases rapidly and corresponds to the values of the heat-treated part.

Acknowledgement

The paper has been prepared thanks to the support of the project "The Development of Technologies, Design of* Firearms, Ammunition, Instrumentation, Engineering of Mat*erials and Military Infrastructure VÝZBROJ (DZRO K201)." and "Surface technology in applications special techniques SV16-216."

References

[1] FATTAH, M., MAHBOUBI, F. Comparison of ferritic and austenitic plasma nitriding and nitrocarburising behaviour of AISI 4140 low-alloy steel. Materials and Design. 2010, 31, 8, s. 3915 – 3921. ISSN 0261-3069.

[2] VASILKO, K. Teória a prax trieskového obrábania, Prešov 2009, ISBN 978-80-553-0152-5

[3] PŘIKRYL, Z., MUSÍLKOVÁ, R. Teorie obrábění. Praha: SNTL, 1982, 235 s.

[4] ABEDI, H.R., A. ZAREI HANZAKI, Keng-Liang OU a Chih-Hua YU. Substructure hardening in duplex low density steel. Materials & Design. 2017, vol. 116, p. 472-480. ISSN 02641275.

[5] JERSÁK, J., GANEV, N., KOVALČÍK, J., DVOŘÁČKOVÁ, Š., KARÁSEK, J., HOTAŘ, A. Surface integrity of hardened bearing steel after milling. Manufacturing Technology, 2010, vol. 10, p. 80 - 87. ISSN 1213-2489,

[6] SUOKNUUTI, J., SUOMINEN, L., WOJTAS, A. S. New more flexible portable goniometer to measure residual stresses. Strojírenská technologie, 2006, vol XI. no. 3, 32-37, ISSN 1211-4162.

[7] DOBROCKY, D., KUSMIC, D. The Effect of Plasma Nitriding Process on the Change of Dynamic Parameters of Steel DIN 1654/4. Manufacturing Technology, 2015, vol. 15, no. 1, p. 14-20. ISSN 1213-2489.

[8] POKORNÝ, Z., KADLEC, J., HRUBÝ, V. et all. HARDNESS OF PLASMA NITRIDED LAYERS CREATED AT DIFFERENT CONDITIONS. *Chemické listy*, 2011, vol. 2011, no. 105, p. 717-720. ISSN 1213-7103.

[9] PAYLING, R.; JONES, D.; BENGTSON, A. Glow Discharge Optical Emission Sepctometry. England: John Wiley & Sons Ltd. 1997. ISBN 0-471-96683-5.

[10] STEWART, D. M., STEVENS, K. J., KAISER, A. B. Magnetic Barkhausen noise analysis of stress in steel. Current Applied Physics, 2004, no. 4, p. 308-311, ISSN 1567-1739.

[11] J. Gauthier, T.W. Krause, D.L. Atherton, Measurement of residual stress in steel using the magnetic Barkhausen noise technique, NDT&E Int., vol. 31, no. 1 (1998), p. 23–31. ISSN 0963-8695.

Influence of chemical composition on layer properties

Zdenek Pokorny, Zbynek Studeny, David Dobrocky
Faculty of Military Technology, University of Defence, Kounicova 156/65, 662 10 Brno, Czech Republic. E-mail: zdenek.pokorny@unob.cz, zbynek.studeny@unob.cz

This article deals with influence of chemical composition on depth of diffusion layers and porosity of compound layers after gas nitriding. Experiments are focused on using of gas nitriding processes for surface treatment. Gas nitriding technologies were applied to steels C 35 (sample A1), 34Cr4 (sample A2) and steel 42CrMo4 (sample A4), which were subsequently evaluated by electron microscopy, GDOES, XRD and microhardness methods. The results of measurement showed characteristics of chemical composition of alloying elements in core of material and in created nitrided layer after chemical-heat treatment process. Main task was to compare the porosity in compound layer after gas nitriding and finally the surface hardness and the depth of diffusion layer. Gas nitriding process were applied for increasing of surface hardness of material in depth and improve mechanical properties. Mechanical properties of tested material were significantly increased.

Keywords: gas nitriding; microhardness; nitrided layer; porosity.

1 Introduction

Non-equilibrium structure is due to redistribution of alloying elements in crystal lattice more suitable for diffusion process. The aim of this paper is to achieve an enhanced surface hardness and reduced friction coefficient with low occurrence of porosity. During nitriding process the nitrides of iron are primarily created. These type of nitrides caused low increasing of microhardness. Alloying elements which caused increasing of mechanical properties are described in this paper. During gas nitriding process, two layers can be effectively created. The compound layer created on the surface of steel is consisted of ε-Fe2-3N and γ-Fe4N phase [2]. Ratio of individual phases is dependent on carbon concentration in steel [1]. The compound layer has been very hard and brittle with good friction and anticorrosion properties [2]. After gas nitriding process the porosity is very often presented in these surface compound layers. There are many possibilities which are applicable to pores, especially subsequent oxidation. The thickness and hardness of γ´-Fe_4N (diffusion layer) depends on quantity and quality of alloying elements [3]. This article describes the influence of selected alloying elements on thickness of diffusion layer and the porosity of compound layer. The porosity is presented in surface layer and be able to have bad influence on mechanical properties, esp. the wear resistance. Chemical composition of steel was verified by GDOES/Bulk method on LECO SA 2000 spectrometer and local measurement of composition was carried out on SEM microscope Hitachi Tabletop 3000. Microstructure was evaluated by electron microscopy method on Hitachi Tabletop 3000. Thickness and microhardness of nitrided layers were measured by microhardness method in accordance with DIN 50190 standard on automatic microhardness tester LECO LM 247 AT [4].

2 Sample preparation

Steel C35 (sample A1), 34Cr4 (sample A2) and 42CrMo4 (sample A4) in untreated state were heat-treated. Quenching and tempering was performed due to reach two different microstructures with different parameters of initial microhardness and different redistribution of atom in crystal lattice.

Tab. 1 Temperatures of heat-treated steels

Steel	Sample	Procedure	
		Quenching/20´	Tempering/30´
C35	A1	860 °C, water	600 °C, air
34Cr4	A2	840 °C, water	600 °C, water
42CrMo4	A4	850 °C, oil	600 °C, water

The steel microstructure was evaluated by electron microscopy on SEM Hitachi Tabletop 3000 before and after chemical heat-treatment. The structure after quenching is displayed in Fig. 1. The conditions of heat-treatment process are given in Tab. 1.

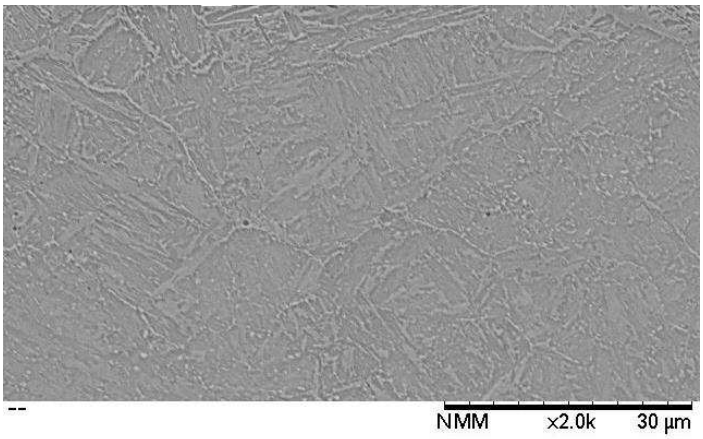

Fig. 1 The chemically etched SE cross-sectional structure of tempered steel, magnification 2000x

The microhardness of steel was evaluated by Vickers microhardness method on the automatic microhardness tester LM 247 AT LECO. Load set at 50 g and 10 s dwell time. This method was used for evaluation of initial surface microhardness before chemical-heat treatment and finally for the measurement of thickness of diffusion layer after gas nitriding process. The initial surface microhardness of heat-treated samples is displayed in Tab. 2.

Tab. 2 Initial microhardness of core of steel after heat-treatment

Steel	Sample	Initial surface microhardness HV 0.05	
		Quenched	Tempered
C35	A1	499±31	266±6
34Cr4	A2	660±29	328±11
42CrMo4	A4	645±24	335±22

The initial microhardness of steel after quenching is usually decreased during process of chemical-heat treatment to tempered values (see Fig. 2). The values of surface microhardness of diffusion layer was determinate by microhardness method and was measured as a higher in case of quenched samples (Fig. 2).

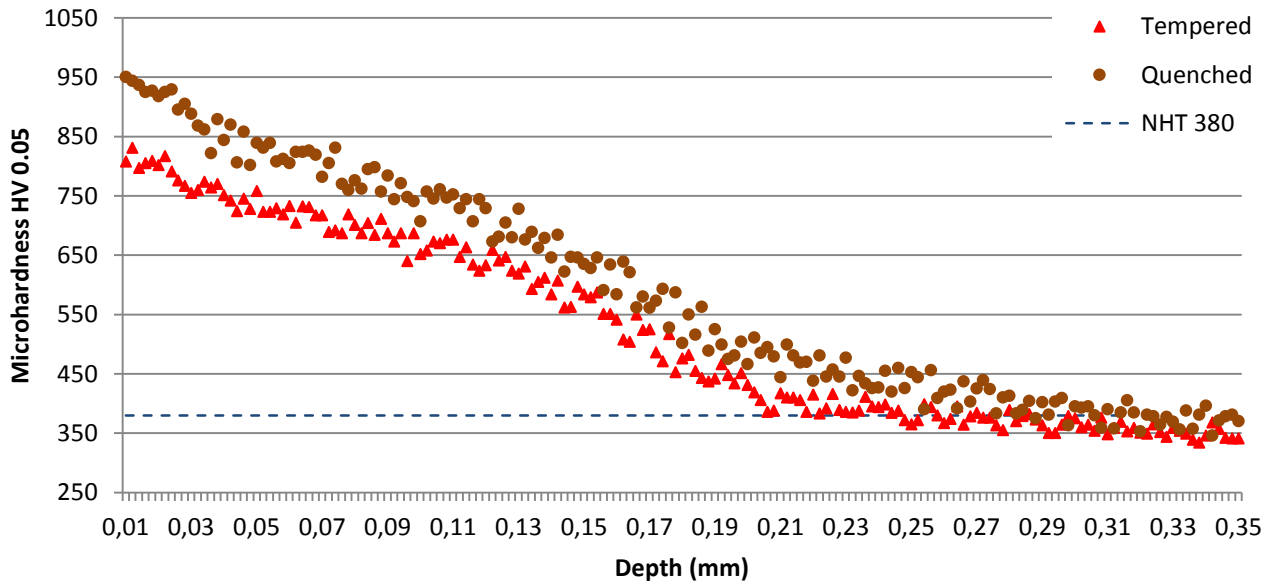

Fig. 2 Microhardness depth profile of A4 sample; gas *nitriding process 490°C/6h*

After preparation and nital etching, the electron microscope Hitachi Tabletop 3000 was used for observation of cross-sectional structure, thickness of compound layer (Fig. 3) and especially the documentation of porosity present in

the top of compound layer (Fig. 4a-c). The porosity was measured by using SE method and magnification 5000x (fig. 5).

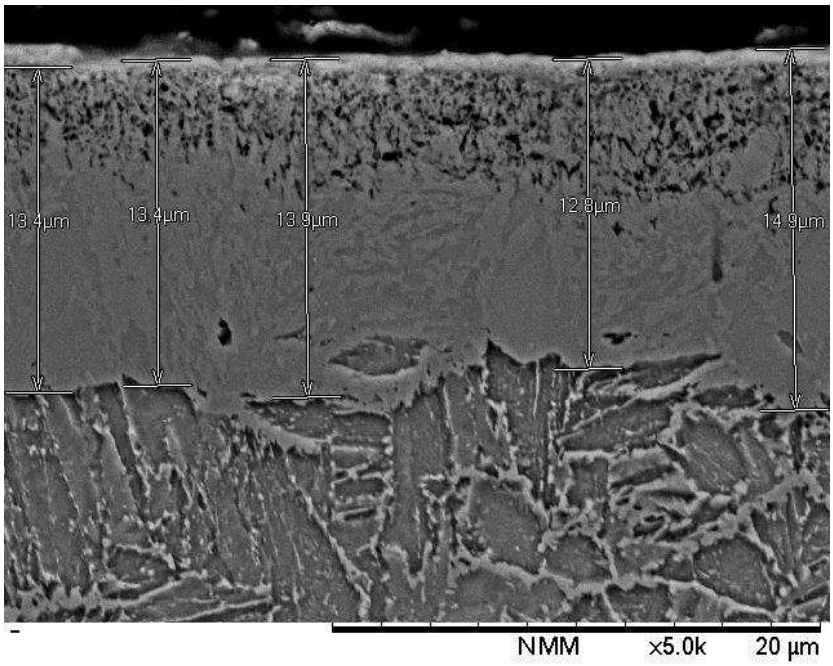

Fig. 3 The chemically etched SE cross-sectional structure of tempered steel A2, the measurement of thickness of compound layer, magnification 5000x

Chemical composition of material was measured by GDOES/Bulk method (Tab. 3). Glow discharge optical spectroscopy (GDOES) measurements were performed in LECO SA-2000, with argon glow discharge plasma excitation source, calibration of nitrogen: JK41-1N and NSC4A standards.

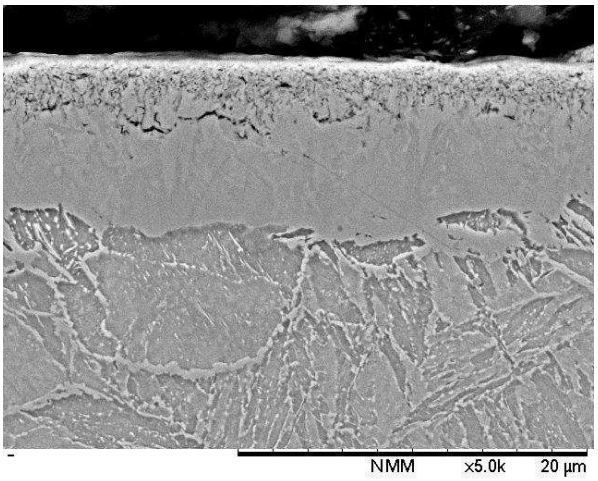

Fig. 4a The chemically etched SE cross-sectional structure of tempered steel A1, compound layer with porosity (top of surface) and diffusion layer below, magnification 5000x

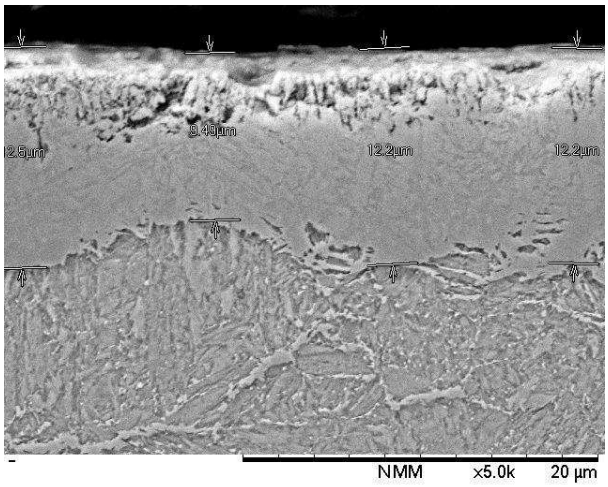

Fig. 4b The chemically etched SE cross-sectional structure of tempered steel A2, compound layer with porosity (top of surface) and diffusion layer below, magnification 5000x

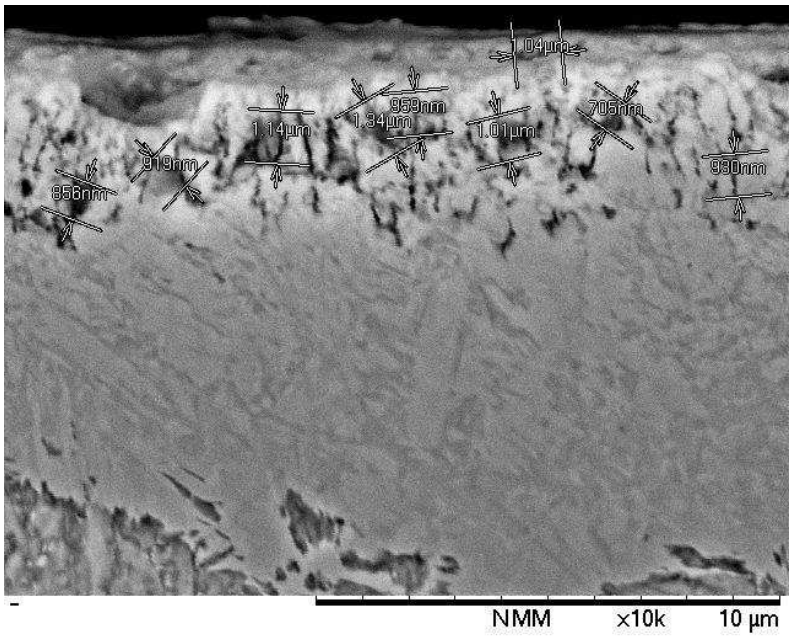

Fig. 5 The chemically etched SE cross-sectional structure of tempered steel A4, documentation of porosity, magnification 10000x

Tab. 3 Parametres of nitrided layers

Sample	Compound layer thickness [µm]	Depth of diffusion layer [mm]	Porosity [nm]
A1	9.2	0.02	370-610
A2	9.7	0.20	280-890
A4	10.2	0.19	390-970

Tab. 4 Chemical composition of A1, A2 and A4 steel measured by GDOES/BULK method

	Concentration [wt. %]						
Sample	C	Mn	Si	Cr	Ni	Mo	Al
A1	0.36	0.68	0.33	0.08	0.04	-	0.003
A2	0.35	0.70	0.35	**1.06**	0.05	-	0.035
A4	0.38	0.81	0.35	**1.09**	0.06	**0.19**	0.019

Steel A2 contents about 1 alloying element more than sample A1. The concentration of alloying elements Mn, Si and interstitial element C is similar (tab. 4). The same ideology is applied to the other steels A4 (tab. 4). Due to the same conditions of gas nitriding process there is possible to evaluate the influence of substitution elements on creation of surface hardness of diffusion layer and depth of nitriding (thickness of diffusion layer).

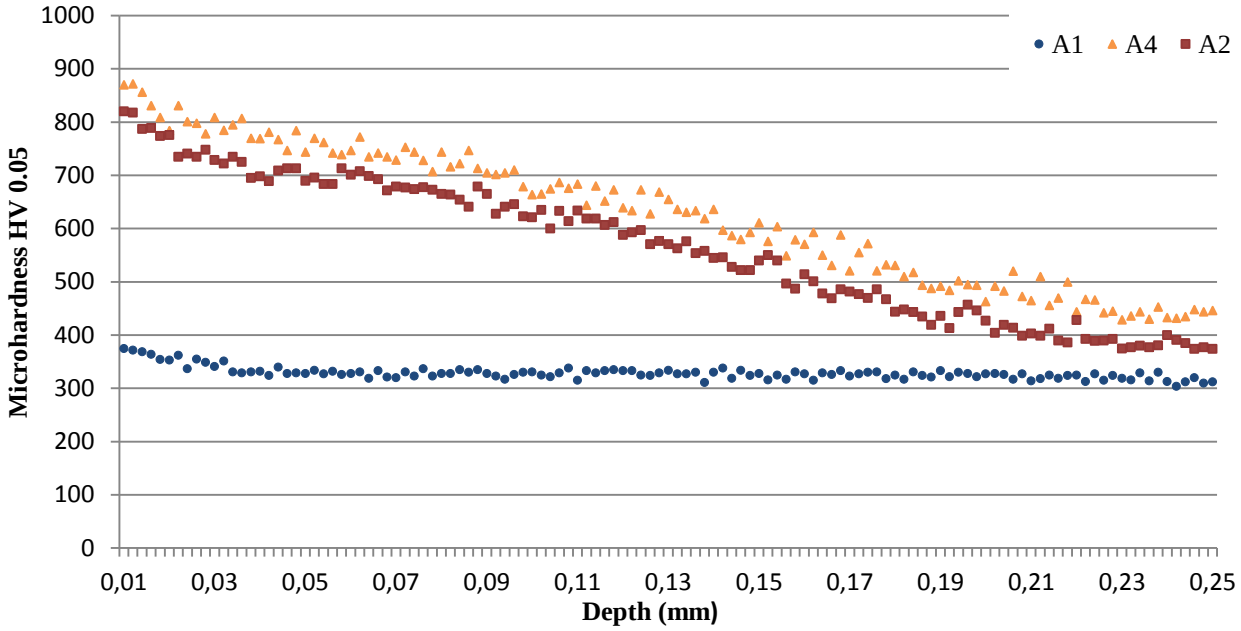

Fig. 6 Influence of alloying elements on surface hardness and depth of nitriding

3 Results

The initial microhardness after quenching was decreased during process of chemical-heat treatment due to high temperature close to A_1 curve Fe-Fe_3C (Fig. 2). There was reached higher values of microhardness after quenching than tempering (Fig. 2). The reason is the different type of redistribution of ionts in crystal lattice. Experiments showed that alloying elements as Cr and Mo caused the increasing of surface microhardness after chemical-heat treatment (fig. 6). The depth of diffusion layer was increased by increasing concentration of Cr and Mo (Fig. 6). By increasing concentration of alloying elements the depth of diffusion layer was increased. The thickness of compound layer was evaluated by SEM method on electron microscope Hitachi Tabletop 3000 and all results are displayed in table 3. The lowest thickness of compound layer was measured on A1 sample but the difference of all measured thicknesses is very close. There is possible to consider as the same.

The porosity of compound layer was evaluated by using electron microscopy (fig. 4a, b). The size of pores was measured on electron microscope by magnification 10000x and the results are displayed in tab. 3. The influence of chemical composition on size of pores was not confirmed. Porosity was present only in top part of compound layer.

4 Conclusions

Evaluated steel with different chemical composition were used for experiments concern porosity, microhardness and thickness of compound layer. The basic steel C35 is not suitable for application of diffusion processes due to non-effective increasing of mechanical properties. Elements as Mo and Cr cause increasing of microhardness and has remarkable influence to microhardness and depth of diffusion layer. The influence of these elements to thickness of compound layer was not confirmed. The most of pores was created in top part of compound layers in all tested steels. The chemical composition of steel has no influence on porosity. The sizes of pores (porosity) is depend on selected technology of chemical-heat treatment.

Acknowledgement

The present research work was supported by the project The Development of Technologies, Design of Firearms, *Ammunition, Instrumentation, Engineering of Materials and Military Infrastructure "VÝZBROJ (DZRO* K201)" *and "Surface technology in applications special techniques SV17-216".*

References

[1] JONSTA, P., MARSALEK, P., HAVLIK, J., JONSTA, Z., VALICEK, J. Influence of Spur Gears Hardened Method to Allowable Stress Numbers for Bending. Key engineering materials, Vol. 607 (2014), pp 11-14, (2014) Trans Tech Publications, Switzerland, doi:10.4028/www.scientific.net/ KEM.607.11

[2] POKORNY, Z., HRUBY, V., BARBORÁK, O. Characteristics of plasma nitrided layers in deep holes. KOVOVE MATERIALY-METALLIC MATERIALS, 2012, vol. 3, no. 50, p. 209-212. ISSN 0023-432X.

[3] POKORNY, Z, KADLEC, J., HRUBY, V. Mechanical Properties of Steels after Plasma nitriding Process. Journal of Materials Science and Engineering A 1, 2011, vol. 2011, no. 6/2011, p. 42-45. ISSN 1934-8959.

[4] ČSN ISO 14577-1 METALIC MATERIALS – Instrumected indentation test for hardness and materials parameters – Part 1: Test method.

Ocele, diagnostika ich stavu a metódy opráv trupov plavidiel

Danka Rakusova[1], Peter Liptak[1]
[1]Fakulta špeciálnej techniky, Trenčianska univerzita A. Dubčeka, Pri parku 19 Záblatie, 91106 Trenčín, Slovenská republika. E-mail: danka.rakusova@tnuni.sk, peter.liptak@tnuni.sk

Plavebné prostriedky ako pontóny v armáde a riečne lode sa vyrábajú zo špeciálnych ocelí [1]. Po mnohých rokoch prevádzky prišiel čas na ich opravu. Základným materiálom na výrobu a opravu plavidla je oceľ a pre riečno-námorné lode je to nízko uhlíková oceľ. Na opravu silne zaťaženého a namáhaného trupu sa používajú oceľové platne so špeciálnymi fyzikálnymi a fyzikálno-mechanickými vlastnosťami ako aj súčasti odliate z ocele. Zliatiny poskytujú lepšie charakteristiky a používajú sa v mnohých častiach riečnych plavidiel, [2] avšak treba zohľadniť náklady [3] pri rozhodovaní o ich aplikácii počas opravy. Príspevok sa zaoberá metódami použitými na diagnostiku stavu trupu lode a diagnostickými prístrojmi, ktoré boli vyvinuté a účinne použité vo viacerých krajinách.

Kľúčové slová: vlastnosti ocele, diagnostika trupu, skenovanie hrúbky, korekčná oprava, spoľahlivá prevádzka

1 Ocele používané na stavbu trupu plavidiel

Kostra lode je určená poslaním lode a plánovanej prevádzky. Železné konštrukcie nahradili drevené trupy v druhej polovici 18.storočia, po nich nasledovala oceľ. Odvtedy boli námorné a vnútrozemské lode konštruované s viacerými druhmi a tvarmi ocele. Ocele sú najbežnejšie materiály používané pri stavbe a oprave lodí. Tieto ocele spĺňajú presnejšie prísne požiadavky ako pevnosť, pružnosť, vysoká schopnosť spracovania, zvárania, náklady a opraviteľnosť, atď. Ocele používané pri stavbe lodí tiež vyžadujú vysokú odolnosť voči chladu, dobré charakteristiky pri zváraní a zvýšené lomové napätie. Tieto vlastnosti určujú veľkosť lode, zložitosť [4] a funkciu konštrukčných zložiek. V závislosti od časti plavidla sa používajú rôzne materiály, ale trup plavidla sa vyrába hlavne z ocele. Pri výbere značky materiálu, ktorý sa použije na stavbu akéhokoľvek produktu lode (detail trupu, mechanizmus, zariadenie), predpisy stanovené registrom, štátom, odvetvové normy poskytujú základné požiadavky na produkty používané počas prevádzky plavidla. [5].

Ocele vyzerajú rovnako, avšak keď sú použité v konštrukcii lode, o moc väčšie záťaže sú kladené na špeciálnu oceľ, teda záťaže, ktoré by pravdepodobne nevydržala, ak by ju chybou nahradila konvenčná oceľ.

K špeciálnym oceliam patria:

1.1. Oceľové platne na termomechanické riadené procesy (TMCP) pre kontajnerové lode

1.2 Antikorózne oceľové platne (NAC5). NAC5 (Nová antikorózna oceľ č.5), ktorá predlžuje životnosť platní paluby asi o 5 rokov, s použitím lodného základu. NAC5 má vynikajúce vlastnosti pri zváraní, čo je významná vlastnosť u materiálov na stavbu lodí.

1.3 K potrubným výrobkom patrí JFE-MARINE-COP na antikorózne potrubia pre ropné tankery

1.4 Platne z plátovej ocele.

1.5 Platne s pozdĺžnym profilom (LP)

1.6 Oceľové platne pre zváranie s vysokou vstupnou teplotou (EWEL)

Obr.1 *Ľadoborec Krupina*

Hlavné charakteristiky ocelí používaných pri stavbe a oprave lodí.

Základným materiálom na stavbu a opravu lodí je uhlíková oceľ [5]: Pre mnohé námorné a riečne lode je to oceľ s nízkym obsahom uhlíka, ktorá je charakterizovaná vyššou pevnosťou a trup lode vyrobený z nej je ľahší. Počas opráv plavidla potrebné informácie poskytuje norma GOST 5521-67.

Oceľové platne lodí, v závislosti od základných vlastností a určenia sú označované nasledovnými značkami:

Uhlíková oceľ- C, VMStZsn (podľa normy GOST 380-71)
Nízko zliatinová 09G2, 09G2S, 10G2S1D, 10XSND (podľa normy GOST 5521—67).
Okrem ocele VMStZsp metalurgické závody vyrábajú ocele: VMStZps, VMStZkp, VKStZsp, VKStZps, VKStZki (v súlade s normou GOST 380—71).
Uhlíková oceľ značky S sa používa na stavbu a opravu lodí, uhlíková oceľ VMStZsp bežnej kvality – na lode pre vnútrozemské a kombinované (rieka-more) plavby.
Oceľové platne lode by mali byť:
odolné voči korózii (vo vode a na vzduchu);
vydržať spracovávanie v horúcich a studených podmienkach;
dať sa zvárať elektrickým oblúkom;
vydržať ohýbanie do 180° za studena podľa ohýbacieho tŕňa.

Nízko zliatinové ocele (hore uvedené značky) sa odlišujú nízkym obsahom uhlíka (nie viac než 0,12%); Uhlíkové ocele sa líšia malým obsahom uhlíka (0, 14—0,22%), síry a fosforu – lámavosťou za studena (nie viac než 0,05% každého). Síra dodáva kovu lámavosť za horúca, a fosfor – lámavosť za studena. Pri lámavosti za horúca kov puká a láme sa v zohriatom stave, lámavosť za studena je schopnosť kovu znižovať viskozitu pri nižších teplotách legujúcich prvkov: kremíka, mangánu, chrómu, nikla pridaných do ocele.Oceľ (podľa normy GOST 5521—67) sa vyrába vo forme oceľových platní a profilovej ocele; tiež sa rozlišujú ocele ako hrubá oceľová platňa (hrúbka platne je v rozmedzí od 4—56 mm); tenká oceľová platňa (hrúbka oceľovej platne je v rozmedzí od 0,9—3,9 mm); profilová oceľ rovnoramenná, nerovnoramenná, nosníky, ocele tvaru U, I, hlavičková oceľ, symetrická hlavičková oceľ, ocele s polkruhovými prierezmi.Ďalšie druhy ocelí so špeciálnymi fyzikálno-mechanickými charakteristikami sa používajú pri stavbe a oprave lodí – tvárnené ocele na výrobu drobných detailov, uhlíková a liatinová oceľ – na kované časti lode, nehrdzavejúce ocele. Posledne menované sú vysoko odolné voči korózii, dajú sa dobre zvárať, avšak sú drahé, preto je ich využitie obmedzené.

Aj keď je uhlíkový ekvivalent (Ceq) dôležitou charakteristikou ocele pri stanovení jej zvárateľnosti v triedach lodných ocelí, v triedach lodných ocelí sa používa hodnota Pcm (citlivosť na lámavosť za studena) na základe vzorca Pcm = % C + % Si/30 + % Mn/20 + % Cu/20 + % Ni/60 + % Cr/20 + % Mo/15 + % V/10 +5* % B. Hodnota uhlíkového ekvivalentu pre lodné ocele sa určuje podľa vzorca :

$$Ceq = C + \frac{Mn}{6} + \frac{Cr+Mo+V}{5} + \frac{Ni+Cu}{15} \quad (\%) \qquad (1)$$

Oblasť pod hornou palubou okolo komína výfukových plynov z dieselového motora je vystavená zmesi atmosféry výfukových plynov a sírovodíka H2S unikajúceho z nafty. Nakoľko táto oblasť podlieha cyklickej kondenzácii a vyparovaniu síry počas dňa a noci, objavuje sa špecifický typ korózie charakteristickej pre podpalubné oblasti, nazývaný korózia parného priestoru. Priemerná miera korózie v parnom priestore je asi 0.1 mm/za rok. Ak berieme životnosť ropných plavidiel asi 20 rokov, pravdepodobnosť nahradenia palubnej platne vzrastá [6]. Bez nahradenia palubnej platne, náklady ktorého sú veľmi vysoké, výsledná spoľahlivosť loby by bola nižšia.

2 Diagnostika lode

Pri uskutočňovaní meraní trupu lode v podmienkach skúmania na mori sú samozrejme určité problémy. Charakteristiky lodnej vrtule ako aj vplyv poveternostných podmienok majú vplyv na namerané výsledky v porovnaní so štandardnými podmienkami v suchom doku [7]. Diagnostické merania by sa mali vykonávať nepretržite, v určitých časových bodoch, napr. po ukončení stavebných prác na lodi, po oprave prvkov [8]. Merania sa vykonávajú na plavidle, aby sa vyhodnotili súčasné prevádzkové parametre využívaného plavidla. Bez ohľadu na cieľ meraní, treba poznamenať, že plavidlo vždy pláva v odlišných podmienkach a tieto podmienky môžu ovplyvniť kvalitu a spoľahlivosť meraní. Zmena podmienok pre pohyb plavidla je vyvolaná parametrami, ktoré sú spojené s:

- Plavidlom, zaťažením plavidla, používaním rezerv (zmeny v rozmiestnení), zmenou v stave trupu, lodných vrtúľ, motorov, atď.
- Hydro- meteorologickými podmienkami
- Regiónom, v ktorom je plavidlo prevádzkované [9]

Rovnako ako trup, lodné vrtule pracujú v značne sa meniacich podmienkach [10]. Špeciálne to platí pre zmeny v ťahu lodnej vrtule, vyplývajúceho z výtlaku, stálej zmene výtlaku a uhla prichádzajúcej a odchádzajúcej vody pri smere vlny, ako aj zhoršení podmienok plochy lopatky lodnej vrtule (zvýšená nerovnosť). Aby sme vyhodnotili podmienky, v ktorých funguje lodná vrtuľa v zadnej časti trupu lode, je dôležité poznať vzťah súčinnosti medzi trupom lode a vrtuľou. Na obrázku 2 sú vidieť vzorové charakteristiky vrtule v prevádzke v zadnej časti trupu lode [11].

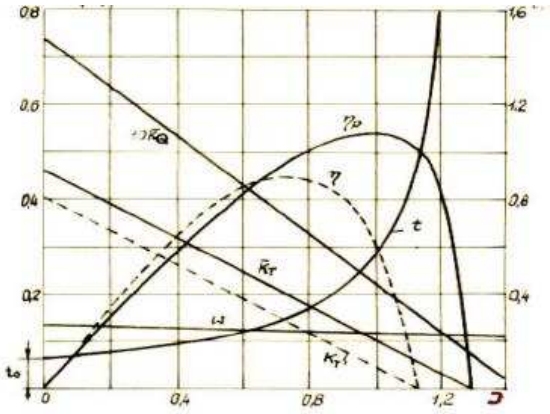

Obr. **2** *Hydrodynamické* chrakteristiky lodnej vrtule: charakteristiky voľnej vrtule v *pokojných vodách; charakteristiky fungujúcej vrtule za trupom lode*

3 Oprava lode

Moderná oprava lode zahŕňa výrobu zložitej oceľovej štruktúry, do ktorej je upevnený celý rad vyrobených zariadení. Dnes je hlavnou surovinou oceľová platňa a schéma modernej lodenice je usporiadaná tak, aby uľahčila tok ocele prijatej z oceliarní cez rôzne procesy zhotovenia, rezania, ohýbania, zvárania, výroby montážnych podskupín a konečné rozostavenie celkov prefabrikátov do trupu lode a nadstavby.

V niektorých vysoko pevnostných oceliach, napríklad kalených a tvrdených oceliach, prívod tepla pri zváraní, ktorý by bol akceptovateľný pre bežnú oceľ, by drasticky znížil pevnosť špeciálnej ocele v zóne ovplyvnenej teplom.

Obr. 3 *Výmena oceľovej platne na trupe lode*

Na riečnom ľadoborci sú miesta v určitej úrovni a v určitej šírke asi 0,5m , ktoré vykazujú vyššie opotrebenie a mali by byť nahradené po celej dĺžke plavidla v strednej časti lode, nakoľko hrúbka ocele je menšia než je prípustná hodnota zostávajúcej hrúbky t zb i pre oceľovú platňu ľadoborca.

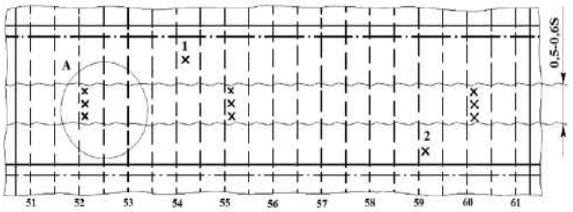

Obr. 4 Poškodená oceľová platňa, x – body merania zostávajúce hrúbky oceľovej platne.

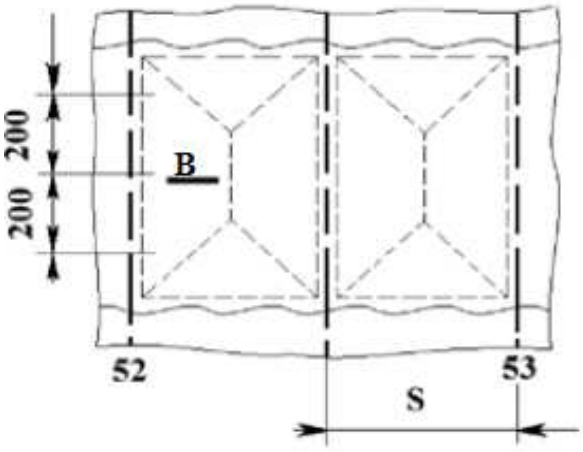

Obr. 5 B- *schéma najopotrebovanejších úsekov; hraničná čiara opotrebovanej časti oceľového listu*

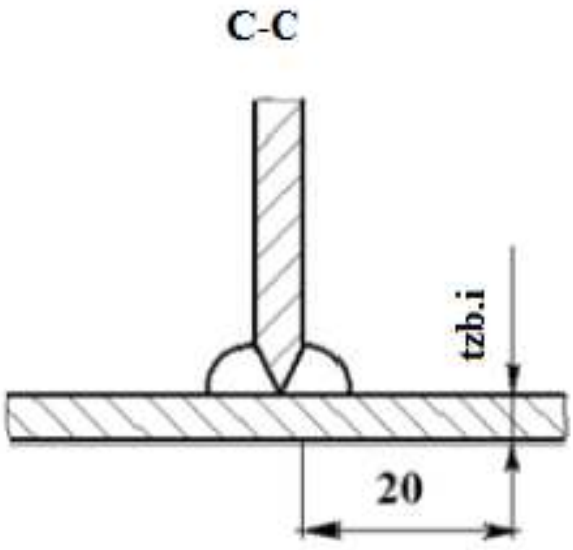

Obr. 6 *Zbytková hrúbka na úseku so zvýšeným opotrebením*

Zistíme, aká je zostávajúca hrúbka na úseku so zvýšeným opotrebnení. Poškodená oceľová platňa a schema deštrukcie na najviac opotrebovaných úsekoch je uvedená na obrázku 6 . Sú spracované prísné postupy pri zváraní , ako napr. v tabuľke 1, aby sa zabránilo chybám pri stracovaní.

Tab. 1 *Oprava vložením platne*

Detail	Norma opravy
Oprava vložením platne 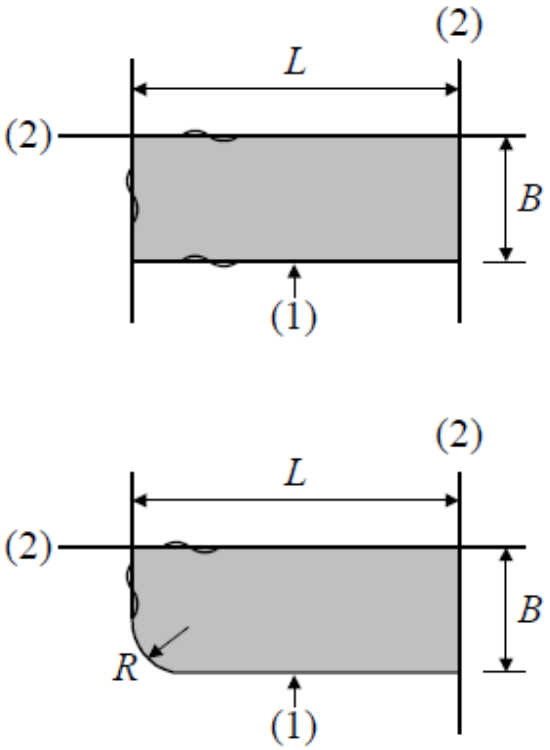	L=300 mm minimálne B=300 mm minimálne R=5t mm, 100 mm minimálne (1) Najprv treba zvariť spoj s vloženým kusom (2) Musí sa uvoľniť pôvodný zvar a prevariť na minimálne 100 mm
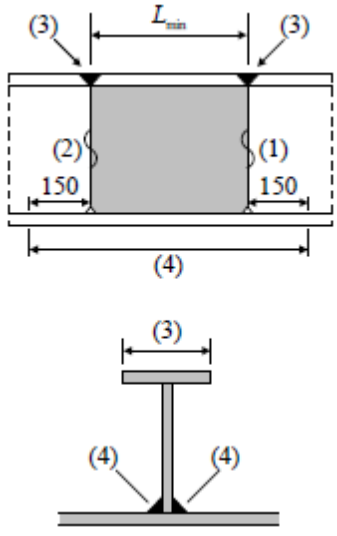	Lmin ≥ 300mm Poradie zvárania (1)→ (2)→ (3)→ (4) Okraj spojového zvaru jadra treba vyplniť počas posledného prechodu (4)

4 Metódy testovania

Metódy na zistenie povrchových nedokonalostí uvedené v tejto práci sú vizuálne testovanie (VT), testovanie prenikania tekutín (PT) a testovanie magnetických častíc (MT). K metódam na detekciu vnútorných nedokonalostí patrí testovanie ultrazvukom (UT) a rádio grafické skúšanie (RT).

Použiteľné metódy na testovanie rôznych typov zváraných spojov sú uvedené v tabuľke 2.

Tab. 2 Použiteľné metódy na testovanie zvarových spojov

ZVÁRANÉ SPOJE	HRÚBKA POVODNÉHO MATERIÁLU	POUŽITEĽNÁ TESTOVACIA METÓDA
Tupé zvary s úplnou difúziou	Hrúbka ≤ 10mm	VT,PT,MT,RT
	Hrúbka > 10 mm	VT,PT,MT,UT,RT
T-spoje, rohové spoje a krížové spoje s úplnou difúziou	Hrúbka ≤ 10mm	VT,PT,MT
	Hrúbka> > 10 mm	VT,PT,MT,UT
T-spoje, rohové spoje a krížové spoje bez difúzie a prúžkové zvary	Všetky	VT,PT,MT,UT

5 Záver

Plavidlo je dlhodobá investícia. Avšak, lode, prevádzkované v riečnych a námorných podmienkach v zime akými sú ľadoborce trpia ťažkými a neustále sa meniacimi podmienkami, ktoré spôsobujú, že na niektorých miestach a oblastiach sa hrúbka trupu zmenšuje. Pravidelné nátery dokážu predĺžiť obdobie prevádzky, ale ak sa nerobia, takéto zanedbávanie môže spôsobiť zmenšenie hrúbky trupu a po dlhej dobe dokonca aj potopenie plavidla a obrovské škody na majetku a životnom prostredí. Medzinárodné dôsledky spojené s blokovaním plavby by boli veľké. Strojová časť sa pravidelne kontroluje a rovnako treba kontrolovať a udržiavať aj trup plavidla. Investície do kontroly a čiastočnej obnovy trupu stoja za to, a naviac, ak máme vlastné kapacity v riečnom suchom doku so skúsenými pracovníkmi.

Literatúra

[1] LIPTAK,P, RAKUSOVA, D. Need for mechanical protection of Gabcikovo ship lock, 2015. In: Recent advances on mechanics, materials, mechanical engineering and chemical engineering: Proceedings of the international conference on mechanics, materials, mechanical engineering and chemical engineering Barcelona, Spain. - Sofia : Institute for Natural Sciences and Engineering, 2015. - ISBN 978-1-61804-295-8. - p.88-97.

[2] RAKUSOVA, D.; LIPTAK, P. Operation of Danube ports supported by specialized equipment, 2015.In: Deterioration, Dependability, Diagnostics: Monograph. - Brno: University of Defence, 2015. - ISBN 978-80-7231-431-7. - p. 265-270

[3] STODOLA, J., RAKUSOVA, D.: Methodology of risk analysis: In: University review. - ISSN 1339-5017. - Vol.8, No.3-4(2014), p.90-93.

[4] RAKUSOVA, D.-Water treatment facilities on a vessel. Proceeding of the 21st International Scientific Conference.Transport Means 2017.

[5] RAKUSOVA, D. – Pumps and piping systems in a vessel operation and crisis situations. –Proceeding of the 21st International Scientific Conference. Transport Means 2017.

[6] KOPECKÝ, I, LIPTÁK, P, RAKÚSOVÁ, D.-Renewable sources of electric energy for mobile logistic means Iso 1c containers .In: Transport means 2014 : Proceedings of the 18th international conference. - Kaunas : Technologija, 2014. - ISSN 2351-4604. - s.211-214.

[7] BREZNICKA, A., STODOLA,P., STODOLA,J., Currently concept of risk and application. 11th International Conference on Intelligent Technologies in Logistics and Mechatronics Systems, ITELMS 2016 , pp. 31-37.

[8] STODOLA,P, BREZNICKA, A., STODOLA, J.-.Reliability analysis and testing of special technique. Intelligent Technologies in Logistics and Mechatronics Systems, ITELMS 2015 - Proceedings of the 10th International Conference

[9] KARDASZ, P.- The potential use of waste oil. Journal of Ecological Engineering. Volume 14, Issue 3, 2013, Pages 77-82, Open Access, ISSN: 2081139X, DOI: 10.5604/2081139X.1056050

[10] LIPTAK, P, KOPECKY, I. RAKUSOVA, D.-Variability of application, special equipment operation using renewable sources of energy .In: Materiály a technologie ve výrobě speciální techniky. - Brno : BVV, 2015. - ISBN 978-80-7231-999-2. - s.72-78, CD ROM.

[11] LIPTAK,P., STODOLA,J.-Errosion wear.- Transport Means - Proceedings of the International Conference, 2014-January, pp. 335-338.

The quality issue of spare parts for the road transport means

Dariusz Rudnik[1], Andrzej Świderski[1], Ewa Dębicka[1], Marcin Ślęzak[1]
[1]Motor Transport Institute, Jagiellonska 80, 03-301 Warsaw. Poland. E-mail: info@its.waw.pl

The article discusses the issues concerning the system of classification and labelling of spare parts for the road transport means from the point of view of their quality. It also discusses the results of tests conducted at the Motor Transport Institute, whose purpose was, among the others, to evaluate the quality of the components in the commercial circulation. It presents statistical data on accidents due to technical reasons. Attention was paid to the legal situation related to the admission to trading of spare parts which are not subject to the type-approval procedure. The problems arising from poor quality of parts, were confronted also with the new requirements of the European Union implementing the principles of closed-circuit economy.

Keywords: Spare Parts, Quality, Admitting To Commercial Circulation, Closed-Circuit Economy

1 Introduction

An interest in quality has grown dynamically over the last years. It was proved that organizations which achieved success in the world market have assurance quality systems implemented according to the international standards. In their operation methods they have developed to perfect elements of detailed planning, realization and monitoring of all processes which occur in the company. Science contributed to the development of these issues, elaborating new diagnosis methods for quality assurance state. Without reliable diagnosis, it is impossible to make a rational business, development and technological decisions. Decisions which have improved quality of realized processes produced product and provided service [1] [2] [3] [4].

If we talk about the quality of the spare parts of the road transport means, the first thing which comes to our minds is the safety of road users, including safety of vehicles, in which the parts have been used. An intensive development of the automotive industry led to a sharp increase in the number of vehicles in use. Also the structure of the vehicle fleet has changed - the number of different makes, models, variants and varieties is ever growing. Accordingly, the number of different parts manufactured, despite an ongoing unification of parts within the companies and between corporations, also increases rapidly.

A user leaving the vehicle at the service company for repairs or doing it himself should be aware, that the original parts that were used for production, as a result of wear or failure no longer meet the requirements, will be replaced with others. At this point he faces a dilemma - which parts to use? This problem also applies to transport means for special purposes.

In connection with the adapting of the Polish law to the requirements in force in the European Union, as of 1 May 2004 there expired in Poland system of mandatory type-certification of automotive parts and components. The number of manufacturers and distributors who certified their products declined by more than 90%, and in some important areas from the point of safety, there was a total lack of applications for certification. The safety certification was replaced by the certification of conformity conducted based on the accredited testing laboratories and certification bodies.

The new situation in the area of certification of spare parts resulted in a total lack of information about their quality (parts not subject to type-approval). Therefore, the Motor Transport Institute, which is the accredited entity to certify compliance of replacement parts (including notification to conduct type-certification tests), has completed development project entitled: "Developing the testing and evaluation system of parts, components and fluids used in motor vehicles to ensure the safety of their use" [6]. Its purpose was, among other things, to evaluate the quality of selected parts of "comparable quality" and "substitutes", "that may pose a significant risk to the correct functioning of systems that are essential for the safety of the vehicle or its impact on the environment" [5]. For the purposes of the project there were selected several parts of different makes and models of the road transport means, from the systems that are essential for safety of vehicle: braking, steering, suspension. Also selected were fluids: brake, radiator and washer.

The results of this project have been used in the article.

2 The quality of parts and vehicle's safety, legal regulations

One of the causes of road accidents is the technical condition of vehicles. However it is a small percentage in the police statistics of the causes of accidents (Tab. 1).

To this statistics, there should be added accidents caused by fire of the vehicle (the electric, fuel, exhaust systems failures, etc.), as well as many of the cases referred to as „Undetermined causes".

However, these numbers probably do not reflect the real scale of the problem of improper technical condition of vehicles. The reason is in not being possible to conclude that it was a technical defect that led to a traffic incident.

At the scene of the accident, the police may interview the participants and witnesses of this event, and inspect the scene of an accident and the vehicles taking part in it. Based on this they can only find obvious technical shortcomings and faults of the vehicle, visible without the use of additional test equipment. The policeman is not a specialist, who is

able to correctly assess the technical cause of the accident in every case. It should be noted that even specialists of automotive technology, in many cases, would also not be able to clearly identify the causes of technical failure without additional testing at the laboratory, though, even there in specific cases, unambiguous answer might be very difficult to achieve or even impossible.

Tab. 1 The number of accidents due to technical reasons in Poland in the years 2009-2015

	2009	**2010**	**2011**	**2012**	**2013**	**2014**	**2015**
The total number of accidents	44196	38832	40065	37046	35847	34970	32967
The number of accidents for technical reasons	101	66	80	55	53	88	65
Technical malfunction unrelated to the vehicle *	83	94	88	100	91	81	106
Glaring by another vehicle, the sun	33	21	27	22	29	28	30
TOTAL - technical reasons	217	181	195	177	173	197	201
	0,49%	0,47%	0,49%	0,48%	0,48%	0,56%	0,61%

* Unserviceability, which directly contributed to the accident
Source: Police Headquarters Statistics in Poland

Some damage to the lighting and excessive tire wear, as well as the brake system malfunctions, manifested by worn brake discs and/or brake pads or brake fluid leaks, are visible in the course of making a cursory inspection. By contrast, it is more difficult to determine the cause of failure of the brake system, caused by water in the brake fluid (approx. 2 years of normal operation of the vehicle), or which is attributable to the too low boiling point of the fluid resulting from the use for its production improper components. In both cases, brake fluid boiling at too low temperature, produces steam lock in the brake system or momentary total loss of the possibility of effective braking. After cooling, the fluid shows no signs of poor quality. The only possibility to find too low boiling point is the use of special testing equipment. An additional difficulty in the diagnosis of this phenomenon is uneven water accumulation of the fluid in different places of the system, and uneven heating of the fluid in the system during braking of the vehicle.

One should also mention cases of cracking the old and corroded metal brake lines, which occur during the technical inspection of the vehicle at a vehicle control station. During the brakes effectiveness test a very hard brake pedal pressure is applied, corresponding to emergency braking, which virtually rarely occurs in traffic. The high fluid pressure in the brake system causes rupture of the corroded pipes. In the event of such a failure in traffic, the probability of an accident is nearly 100%.

Similar situation is with the steering and suspension defects - during a routine inspection one can only spot backlash e.g. of the steering. Unfortunately, under road conditions, during the inspection of the vehicle after the accident, in the case of total destruction of these elements, it is not possible to clearly determine whether the rupture of, e.g., poor quality ball joint (material defect, the use of inappropriate materials for the production, the use of inappropriate technologies, etc.) was the cause of the accident or the rupture happened as a result of vehicle impacting the obstacle.

Police quotes the following technical causes of accidents:

- lighting deficiencies,
- tires deficiencies,
- brake system malfunctions,
- steering faults,
- other defects.

It is possible to observe that most of established faults with vehicles are those which are easily identifiable by visual inspection (Fig. 1).

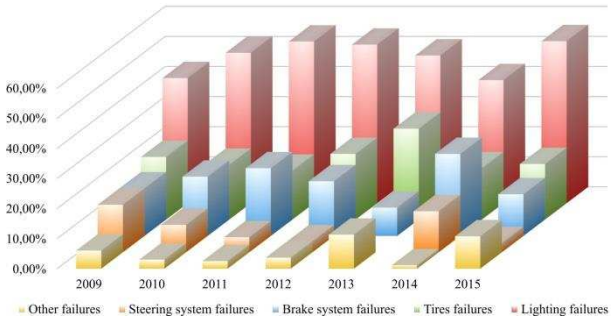

Fig. 1 Defects of vehicles causing accidents in Poland in 2009-2015
Source: own study based on statistics of the Police Headquarters in Poland

In accordance to the regulations of the European Economic Commission of the United Nations or the corresponding EU directives, in order to admit into the commercial circulation on the territory of the Republic of Poland, the selected items of equipment or parts installed in the vehicles, it is necessary to obtain type-approval certificate. These requirements relate mainly to the elements "for the first assembly" (partial type-approval and Full-Vehicle type-approval), while only a few spare parts available in the trade are covered by these regulations (e.g. bulbs or brake pads).

The second group represents "parts that could pose a significant risk to the correct functioning of systems that are essential for the approval of the vehicle to be technically safe, in this also as regards its impact on the environment". These parts, in accordance with the Article 31 of the Directive of the European Parliament and of the Council 2007/46/EC of 5 September 2007 [5] establishing a "framework for the type-approval of motor vehicles and their trailers and systems, components and separate technical units intended for those vehicles", must obtain a permit for introduction to commercial circulation. A list of these items of equipment and parts which are not covered by the type-approval should be given in Annex XIII of the Directive.

The problem is that the procedure for obtaining the authorization for placing components and sub-assemblies on the market is not actually used because, so far, there has not been prepared a list of the spare parts for Appendix XIII. There is also no plan of the European Commission for legislative action in this area.

The market left to itself is capable, to some extent, to make self-regulation by eliminating the sale of products of poor quality. This also applies to spare parts market. If an auto repair facility used for repairs some poor quality part, which resulted in a complaint reported by the client, the effect of which was another repair, it will not again use the part coming from the same source. However, the knowledge about the quality of replacement parts, gained through trial and painful - prestigiously and economically - error, should not satisfy anyone. On the other hand, the demand for the cheapest parts possible will not disappear because in many cases such parts are used to "eliminate" defects in vehicles prepared for sale by unscrupulous dealers. It is also hard to imagine the mechanisms of market self-regulation regarding the impact of spare parts and fluids on human health and the environment. Therefore, in this area it is necessary for the state to step in, based on independent expertise.

3 Own research

Spare parts can be selected from three groups of quality:

"O" parts - new spare parts, original, made by the vehicle manufacturer. In the nomenclature of the EU, these parts are marked as OEM - Original Equipment Manufacturer).

"Q" parts - new spare parts, of the same quality as the parts coming from the vehicle manufacturer (manufactured according to specifications and production standards established by the vehicle manufacturer), manufactured by the same manufacturer that supplies the vehicle manufacturer with parts for the assembly of vehicles or just spare parts (also known as parts equivalent to the original). In the EU nomenclature, these parts are marked OES - Original Equipment Supplier.

„P" parts - new spare parts, aftermarket, of comparable quality, warranted by the manufacturer, testifying that they are of the same quality as the components which are or were used for the assembly of the vehicles.

An attempt to put in order the spare parts market was taken up with the entry into force of the provisions of Commission Regulation (EC) No. 1400/2002 of 31 July 2002. (GVO) [8]. This document included definitions of spare parts, which covered the aspect of their quality. Parts are divided into two groups:

- original spare parts,
- spare parts of comparable quality.

In Poland, at the time, there were regulations on the mandatory certification of parts and automotive components in force, which could pose a significant risk to the correct functioning of systems that are essential for regarding the vehicle to be technically safe, including its impact on the environment, entitling the manufacturer (or importer) to marking its product with "B" safety mark, belonging to the competence of the Minister of Economy. So, there was an opportunity for objective verification of the quality of spare parts entering the market, based on both, the results of their

laboratory tests as well as the results of the audit of production conditions and periodic inspections as monitoring the issued certificate. This concerned mainly the "comparable quality" parts, which were produced based on other technologies than those used for the original parts.

In 2005 the insurance companies and distributors of spare parts developed a Single Information System on the Quality of Spare Parts. Parts were divided into eight groups with respect to their quality:

O - original part marked with the vehicle manufacturer's logo or in packaging with the logo of the vehicle's manufacturer,
Q - original parts marked with the parts manufacturer's logo or in packaging with the logo of the parts manufacturer, supplying given element for the first assembly,
PC - Part of comparable quality, which has a quality certificate issued by a certifying entity Centro Zaragoza (Spain),
PT - part of a comparable quality, which has a quality certificate issued by the certification body Thatcham (UK),
PJ - part of a comparable quality, especially recommended by the supplier (distributor),
P - parts of comparable quality - spare parts, whose manufacturer certifies that they are of the same quality as the components which are or were used for the assembly of motor vehicles,
ZJ - replacement of higher quality, recommended by the supplier (distributor),
Z - other substitutes.

Commission Regulation (EC) No. 1400/2002 was in force until 31 May 2010. It was replaced by Commission Regulation (EU) No. 461/2010 of 27 May 2010, in which there was no definition of spare parts. Uniform Information System on the Quality of Spare Parts used in Poland remained unchanged.

Material tests (chemical composition, structure, mechanical properties) in the course of the project and studies of the functional properties of metal elements were performed using the following research equipment [6]:

- Metallographic examinations (microstructure) on the elements cross-sections - using an optical microscope OLYMPUS type PMG 3 and scanning electron microscope JEOL JSM-6360LA with X-ray type EDS micro-analyzer;
- Verifying analysis of the chemical composition of steel - using a spectrometer - type ARC MET 930SP by METOREX company (Finland), using optical emission spectrometry (OES), with intermittent arc induction by direct current;
- Hardness tests - using nanoindenter by CSM Instruments (including universal hardness (Hit), Vickers hardness (HV), reduced Young's modulus (EIT) in the micro-regions) and durometer by STRUERS Duramin 500 (Rockwell-Vickers-Brinell);
- Strength tests - servo-hydraulic strength machines, of single- and dual-axis: INSTRON model 8802 (100 kN), INSTRON model 8874 (25 kN), and electromechanical testing strength machine - Instron Electropuls E 10 000;

In the case of service fluids, the assessment covered their following properties [6]:

- Brake fluids:
  - boiling point;
  - boiling point of fluid with water content;
  - kinematic viscosity at +100°C;
  - kinematic viscosity at -40°C;
  - pH;
  - stability - determining changes in boiling point of the brake fluid caused by:
    - long warming up of the fluid sample at an elevated temperature, which is characterizes thermal stability of the fluid tested;
    - mixing a sample of the fluid tested with a reference fluid, which characterizes the chemical stability of the fluid tested.
  - corrosive action on metals;
  - appearance and low temperature fluidity;
  - evaporativeness;
  - resistance to water;
  - miscibility with the reference fluid;
  - resistance to oxidation;
  - effect on the SBR seal.
- Coolant concentrates and car radiators fluids:
  - crystallization temperature;
  - boiling point;

- pH;
- water content in the concentrate;
- incineration residue;
- alkaline reserve;
- density at 20°C;
- tendency to foam;
- colour, appearance;
- miscibility with hard water;
- corrosion under heat transfer.

The parts and fluids of different manufacturers selected for tests were bought at random stores and wholesalers of automotive parts. These parts were then tested for compliance with the requirements of the relevant technical conditions. Conducting tests allowed to determine not only product defects visible to the naked eye, but also a comprehensive assessment of parts, components and fluids with regards their fabrication (used materials and technologies) and properties.

The results of tests of automotive parts gave a negative image of the quality of parts, components and service fluids offered in trade, which are used for repairs and used in the operation of cars. Based on the analysis of the results obtained, it was found that depending on the inventory group, approx. 50% and 70% of the purchased and analysed vehicle parts and various types of service fluids, including brake ones, is of the quality that directly jeopardizes safety of the operation.

For individual product groups, the following significant differences were found in relation to the requirements of technical conditions and standards in question [6]:

A. Brake systems parts (Fig. 2 - 4)

All tested pumps, cylinders and brake callipers did not meet the requirements.

The metal materials (cast iron, aluminium alloys) of the bodies of tested pumps and brake cylinders were found to have unacceptable material defects in the form of discontinuities, cracks and other subsurface defects, while steels were found to have excessive degree of contamination non-metallic inclusions.

The rubber elements of pumps, cylinders and brake callipers were found to have incorrect percentage change in volume and diameter of their seals and shrouds after aging in the reference brake fluid, excessive change in hardness (IRHD) of gaskets and “O” rings after aging in air at elevated temperatures and excessive average percentage change in tensile strength of shrouds samples after aging in air at elevated temperature;

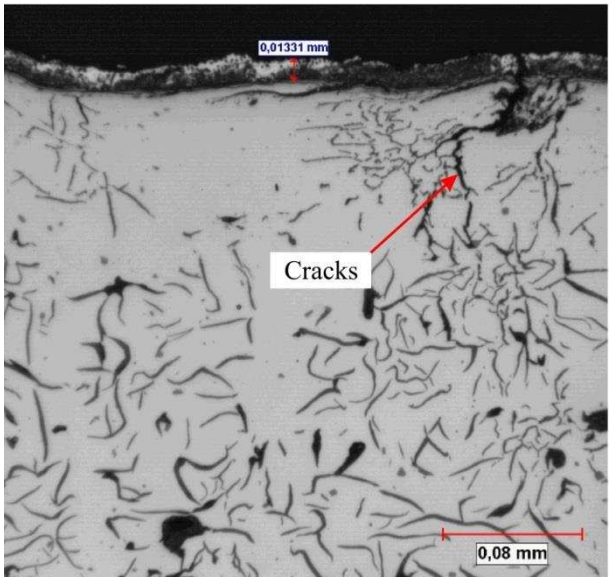

Fig. 2 Body of the steel brake cylinder, unetched condition, ordinary lighting, magn. 200x

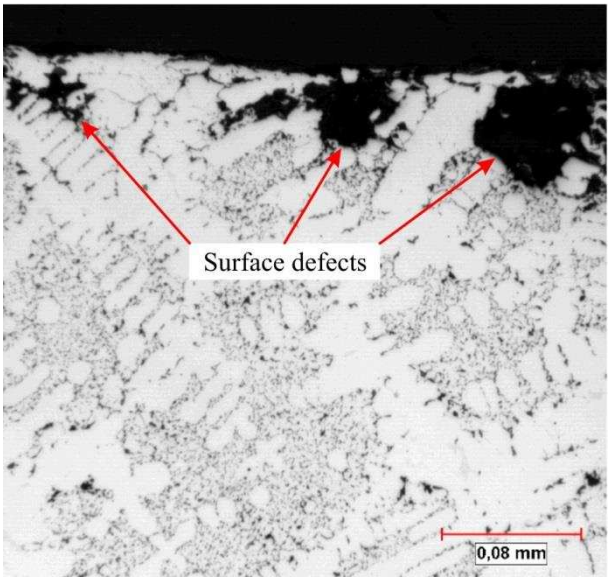

Fig. 3 Body of the steel brake cylinder, unetched condition, ordinary lighting, magn. 200x

Fig. 4 Rubber parts of the brake cylinder: A - seals B - shrouds

B. Rods and steering ball joints (Fig. 5 and 6)

The individual elements of the rods and ball joints of steering systems, namely: ball pins, joints casings, joints clamping bolts, joint pin nuts were found to have an unacceptable material defects in the form of cracks, improper structure, incomplete decarbonising, incorrect grain size and wrong hardness.

The abnormal thread profiles and excessive roughness on the surfaces of conical pins were also observed. The functional studies have shown insufficient angle values of the extreme deflections of the pin and excessive values of friction rotating torques of the pin in the housings.

In some cases it was found that improper materials were used for the production.

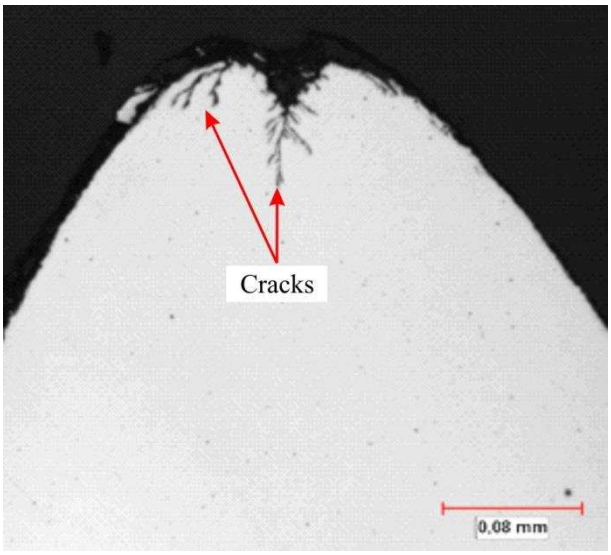

Fig. 5 Steering rod- thread cracks, conventional lighting, magn. 200x

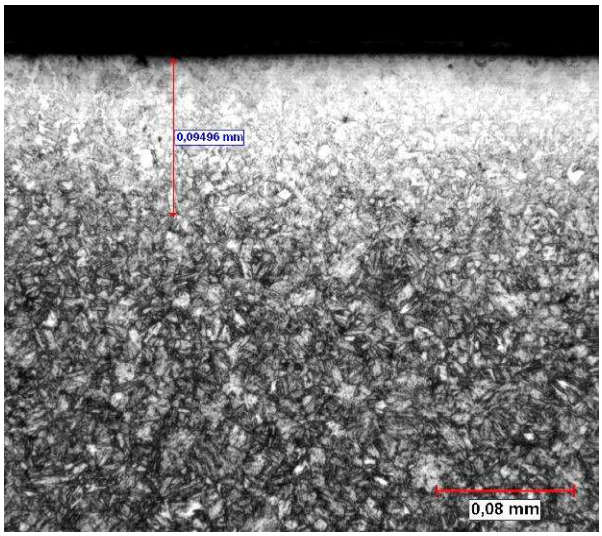

Fig. 6 Steering rod joint nut - incomplete decarbonising, unetched condition, conventional lighting, magn. 100x

C. Suspension systems parts (Fig. 7 - 9)

The suspension systems parts tested: control arms, arms joints, stabilizer rods, coil springs, steering ball pins, wishbone bushings, reaction bars, were found to have significant material defects in the form of abnormal material structure, excessive degree of contamination with non-metallic inclusions, lowered hardness of hardened layers, the occurrence of intergranular corrosion and incomplete decarbonisation.

In some cases it was found that inappropriate grade of steel was used for the production.

The functional studies have found lowered tensile strength of welded joints in the stabilizer rods, greatly insufficient tear off strength of the pins from the joints sockets and incorrect thread profiles.

Also numerous signs of surface corrosion were observed on the components of reaction rods for trucks.

Fig. 7 In the stabilizer link, during welding process, the material of the joint housing was excessively overheated resulting in reduction in tensile strength of the joint

Fig. 8 In the stabilizer link the use of improper material caused breaking at too low force

Fig. 9 Corrosion traces on the surfaces of the reaction rods ball pins

D. Hub and wheel nuts (Fig. 10)
Some of the tested bolts and wheel hubs nuts were found incompatible with the requirements of hardness, fracture and with incorrect thread profiles.

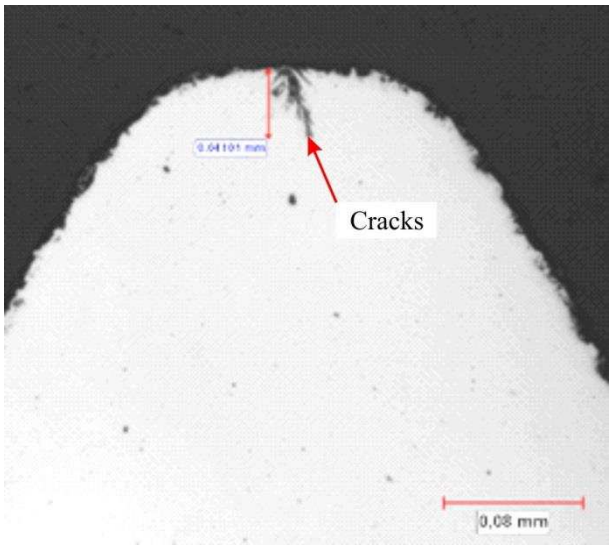

Fig. 10 *Crack of the bolt's thread, conventional lighting, magn. 200x*

E. Alloy wheels (aluminium alloy) (Fig. 11)
In all tested wheel rims made of aluminium alloys there have been found numerous material discontinuities.

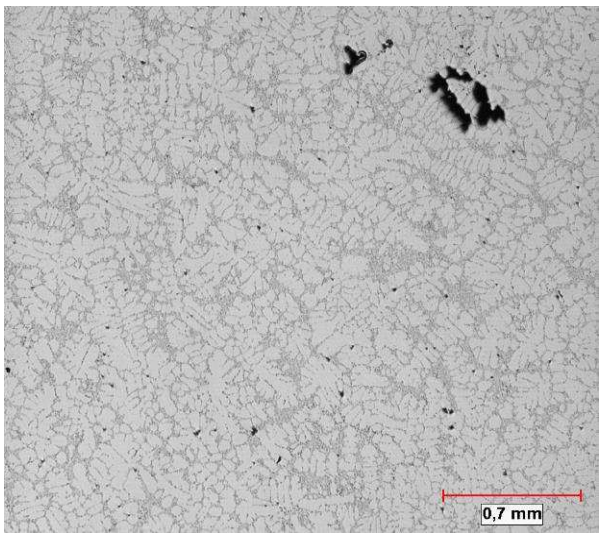

Fig. 11 Wheel rim, unetched condition, conventional lighting, magn. 25x

F. Battery isolators, jump leads
The battery disconnectors tested, which did not meet safety requirements, were found to have improper voltage drop and current overload while the sets of jump cables, current overload incompatible with the requirements and incorrect marking.

G. Service fluids
In the tested service fluids, that did not meet safety requirements, the irregularities were found, concerning:

- in DOT 4 brake fluids: reacting of the fluid on the SBR rubber gaskets; corrosive action on the brake system components (master cylinder, pistons, cylinders), the boiling point;
- in the fluid concentrates and car radiators coolants: the crystallization temperature, corrosive effects under the heat transfer conditions, tendency to foam, water content, pH;
- in the washer fluids: the crystallization temperature, fluid reacting on the wiper rubber, reacting with paint.

The irregularities found in the materials used and the workmanship of spare parts, as well as improper recipes of fluids, are a reflection of the activity of manufacturers associated with the desire to achieve the greatest profits by drastically reducing production costs, which directly reflects negatively on the quality of manufactured parts and fluids. Producers are "saving" by:

- using cheaper materials that do not meet the requirements,
- simplifying technological processes,

- simplifying or even skipping quality control in the subsequent stages of the production process and final inspection.

These actions result in the fact that finished products being used in a vehicle represent a real threat to the health and lives of all road users.

Inadequate quality of new parts introduced to the trade circulation becomes even more relevant in the context of the re-use of spare parts obtained from the end of life vehicles. These parts are used for normal maintenance repairs and post-accident ones, therefore, if the quality of new parts from the very beginning was inappropriate, their reuse will be a big threat to road safety.

In order to subsequently safely reintroduce the components from dismantling, the following organizational solutions and procedures can be proposed:

- preparation of the list and qualifying the individual parts to an appropriate group taking into account the criterion of user safety;
- following dismantling, an initial verification and classification of the technical condition of parts;
- for parts that do not have significant impact on safety, such as various types of covers and interior accessories of the vehicle - based on the examination - directing them for re-use or transferring for disposal;
- for the part relevant to the safety - a detailed verification of the technical condition using advanced non-destructive methods. In case of qualifying for reuse, if necessary making a repair or reconditioning in accordance with specific methods (technologies) as described in the relevant normative documents.

4 Summary

The quality of parts and components used in the repair of road transport means should be such as to ensure the safety of vehicles, i.e. the safety of all road users. Indisputable is also aspect of environmental protection, waste minimization and rational use of natural resources, which is especially emphasized in the assumptions of the closed circuit economy. Accordingly, the materials used for the production of parts and technologies should allow their re-use without additional processes or remanufacturing and these parts should continue to ensure adequate safety.

To ensure this, critical spare parts and fittings of a vehicle should be tested and evaluated by independent, objective entities. By creating such a system one must include in it already functioning mechanisms of the conformity assessment of products. Performing tests by the laboratories accredited by national accreditation systems allows to use the existing procedures to supervise the correctness of the tests conducted. The same applies to entities providing products certification based on, among the others, tests conducted. The credibility of such evaluations is supported by separating the process of products testing and evaluation process.

The system should also protect manufacturers and distributors of high quality parts from unfair competition. On the other hand, it should be subtle enough not to interfere with competition and no favour to the monopolization of the market. Parts manufacturer should be responsible for its quality, and the customers should be able to relatively easily assert their rights.

The quality of spare parts used to repair vehicles takes on a whole new meaning in the context of the European economic model of a closed circuit economy, so-called Circular Economy [9], whose plan was adopted by the European Commission on 2 December 2015. If a new spare part does not meet the technical requirements at the onset, then even if it does not get rapidly destroyed during operation (and becomes waste/material), its value as an element which can undergo remanufacturing, will be questionable. Attention ought to be drawn to the fact that industrial remanufacturing processes are based on standard procedures and reproducible technologies. Only this way it could be ensured that the performance of the element following reconditioning will not differ from the properties of the new parts. But going through this process with parts, the original manufacturing process, which involves using wrong materials may lead to the creation of the item, whose operation will represent a danger to life and health of all road users.

Acknowledgement

The research were carried out within the project No. N R10 0017 06/2009 with financial support from the Ministry of Science and Higher Education of Poland.

References

[1] FOLTIN, P., GONTARCZYK, M., ŚWIDERSKI, A., ZELKOWSKI, J. (2015). Evaluation model of companies operating within logistic network, pp. 21-33. Archive of Transport. Polish Academy of Sciences Committee of Transport, Volume 36, issue 4.

[2] LEGÁT, V., ALEŠ, Z., HLADÍK, T. (2017). Maintenance Audit: the Tool for Maintenance Management Quality of Manufacturing Equipment. Manufacturing Technology, Vol. 17, No. 1, ISSN 1213–2489.

[3] ŚWIDERSKI, A. (2007). Quality assurance prototyping of technical transport means, pp. 99-110. Archive of Transport. Polish Academy of Sciences, Committee of Transport, Volume 19, issue 4.

[4] ŚWIDERSKI, A. (2011). The selected aspects of the quality assessment of transport services, pp. 651-658. Journal of KONES Powertrain and Transport. European Science Society of Powertrain and Transport Publication, Volume 18, No. 1.

[5] Directive of the European Parliament and of the Council 2007/46/EC of 5 September 2007 establishing framework for the type-approval of motor vehicles and their trailers, as well as systems, components and separate technical assemblies intended for these vehicles (Framework Directive).

[6] Developing system of tests and evaluation of parts, components and service fluids used in motor vehicles in order to ensure safety of their use. Development project No. N R10 0017 06/2009 (report).

[7] Commission Regulation (EU) No. 461/2010 of 27 May 2010 on the application of art. 101 section 3 of the Treaty on the Functioning of the European Union to the categories of vertical agreements and concerted practices in the motor vehicles sector.

[8] Commission Regulation (EC) No. 1400/2002 of 31 July 2002 on the application of art. 81 section 3 of the Treaty to the categories of vertical agreements and concerted practices in the motor vehicles sector.

[9] http://europa.eu/rapid/press-release_MEMO-15-6204_pl.htm

Influence of heat treatment on mechanical properties and microstructure of the tool steel D2

Stanislav Tobolik[1]
[1]Faculty of Military Technology, University of Defence in Brno. Kounicova 65, 662 10 Brno. Czech Republic. E-mail: stanislav.tobolik@unob.cz

This article deals with the mechanical properties and microstructure after heat treatment of tool steel D2. This steel is often found in practical applications where is required high wear resistance and the operating temperature does not exceed about 200 °C. Overall were carried out 12 different modes of heat treatment. The heat treatment modes were chosen generally recommended quenching and tempering temperature. One mode of heat treatment included after hardening cooling to -180°C. Subsequently were evaluated hardness, abrasion resistance, toughness, the amount of residual austenite and the grain size. The results indicate the benefits of heat treatment of the primary hardness. Due to higher amount of retained austenite after heat treatment of the primary hardness tested steel may keep good toughness with excellent wear resistance.

Keywords Ledeburitic steel D2, metallographic analysis, hardness, toughness, abrasion resistence

1 Introduction

Tools which are made from ledeburitic steel are often subject to contradictory demands. This means, for example, high strength and hardness with sufficient toughness of the tools. AISI D2 steel is in group of cold work tool steels. There are high chromium carbides in the microstructure of these alloys due to the presence of high chromium (~12 wt%) and high carbon (1.5–2.35 wt%) contents that cause excellent wear resistance and high strength properties. To maximize the working potential of ledeburitic steels, they have to always be heat treated. Heat treatment consists of gradual heating to the austenitizing temperature, maintaining it at that temperature and subsequent cooling under the conditions resulting in the martensite structure, but the tool does not break due to high internal stress. After each hardening, multiple tempering is followed as soon as possible. This heat-treated steel can be subjected to a working load. Some of the typical industrial applications of D2 steel include punches, piercing and blanking dies, spinning tools, shear blades, slitting cutters, as well as a variety of wood working tools. [1-3]

2 Experimental

D2 is a ledeburitic chrome-vanadium steel for cold work. It is characterized by high resistance to abrasive and adhesive wear. Chemical compositions of test samples are measured by using spectrometer PMI Master Pro Oxford Instruments. Measured values are shown in tab. 1. The chemical compositions are consistent with the values specified by the manufacturer [4].

Tab. 1 Table of measured chemical composition

Elements	C	Mn	Si	Cr	Mo	V
Content [%]	1,55	0,45	0,36	11,6	0,84	0,9

Heat treatment was made in an electrical atmosphere furnace. Cooling from the austenitizing temperature was done in a cooling chamber with the aid of pressurized nitrogen. Tempering of test samples was carried out in a shaft tempering furnace with circulating atmosphere by a fan at the bottom of the furnace.

The heat treatment regime was chosen generally recommended quenching and tempering temperature, depending on the resultant hardness - primary or secondary. There was performed the tests when the hardening temperature was chosen for secondary hardness, but subsequent tempering temperature corresponded to primary hardness (groups 10 to 12). In one case was conducted cooling to -180 °C immediately after quenching and subsequent tempering at 200 °C (the third group). All modes of heat treatment are shown in tab. 2

The charpy impact test was performed by 150 J hammer. For each test were available 6-7 samples. Samples had normalized shape 10 x 10 x 55 mm and were provided at the U notch with a depth of 2 mm, placed perpendicular to the direction of molding material. The results of the tests are shown in the graph 1.

Determination austenite grain size and microstructure evaluation was carried out in the metallographic laboratory by light microscope Carl Zeiss Axio Vert.A1. The size of the austenitic grain was determined according to ASTM E112-13 [5] (oxidation method). Samples for light microscopy were prepared in conventional method, the samples were etched with nital 3% or Vilella Bain, observations were made with 100x and 500x magnification.

Abrasion test was carried out according to CSN 01 5084 [6]. For the test were made standard cylinders with a diameter of 10 mm and a length of 60 mm. Each group of test samples containing one sample.

The resulting values of residual austenite were determined by the diffractometer XSTRESS3000. Measurement underwent 12 broken samples after impact test.

Hardness test was carried out according to standard EN ISO 6508-1 [7]. On a selected sample in each group was 4 times measured hardness after quenching and tempering. Surface pattern before the measurement had to be cleared of decarburized layer.

Tab. 2 Process of heat treatment

Test	Hardening temperature / time	Tempering temperature / time
1.	1015°C / 30 min	200°C / 120 min
2.	1015°C / 30 min	2x 200°C / 120 min
3.	1015°C / 30 min	-180°C / 240 min; 200°C / 120 min
4.	1020°C / 20 min	400°C /120 min
5.	1020°C / 20 min	2x 400°C /120 min
6.	1020°C / 20 min	3x 400°C /120 min
7.	1015°C / 20 min	350°C / 120 min
8.	1060°C / 25 min	2x 555°C /120 min
9.	1035°C / 25 min	535°C / 120 min
10.	1040°C / 25 min	200°C / 120 min
11.	1060°C / 25 min	200°C / 120 min
12.	1060°C / 25 min	200°C / 120 min; 400°C / 120 min

3 Results

Impact test

The graph 1 shows that the average impact energy for all groups of samples is relatively low. In some cases the substantial standard deviation of 5, 8 and 9. The highest impact values of the samples showed the seventh group. To the resulting comparison was taken an average impact values with regard to the standard deviation.

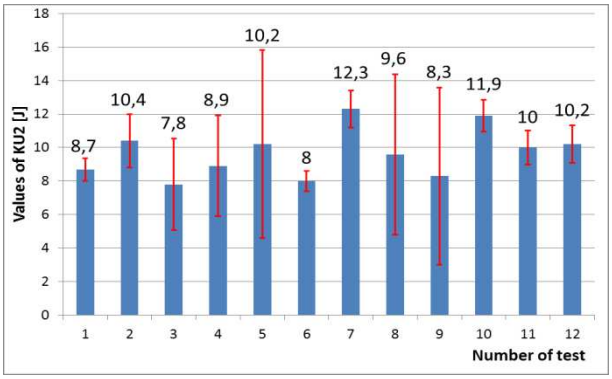

Graph 1 Values of impact energy

Microstructure and austenite grain size

For all samples, the average grain size of austenite was determined by comparative method. In each case equal number 7. We can see that in all structures is apparent at first glance a considerable number of large, irregularly shaped primary carbide that are channeled after forming in lines. Furthermore, in addition of primary carbides can be seen eutectic carbides, which are also arranged in rows in the direction of forming. Microstructure fig. 1a-b was formed on the heat treatment regime primary hardness, specifically hardening from a temperature 1015 °C and subsequent tempering at 200 °C. The matrix is composed of tempered martensite. The boundaries of the original austenite grains are not significant. In the matrix, there are very fine secondary carbides of alloying elements, which are evenly distributed in the whole volume. Special carbide precipitation due to the technique were noted. As will be demonstrated hereinafter, it participates in the structure of the certain amount of residual austenite.

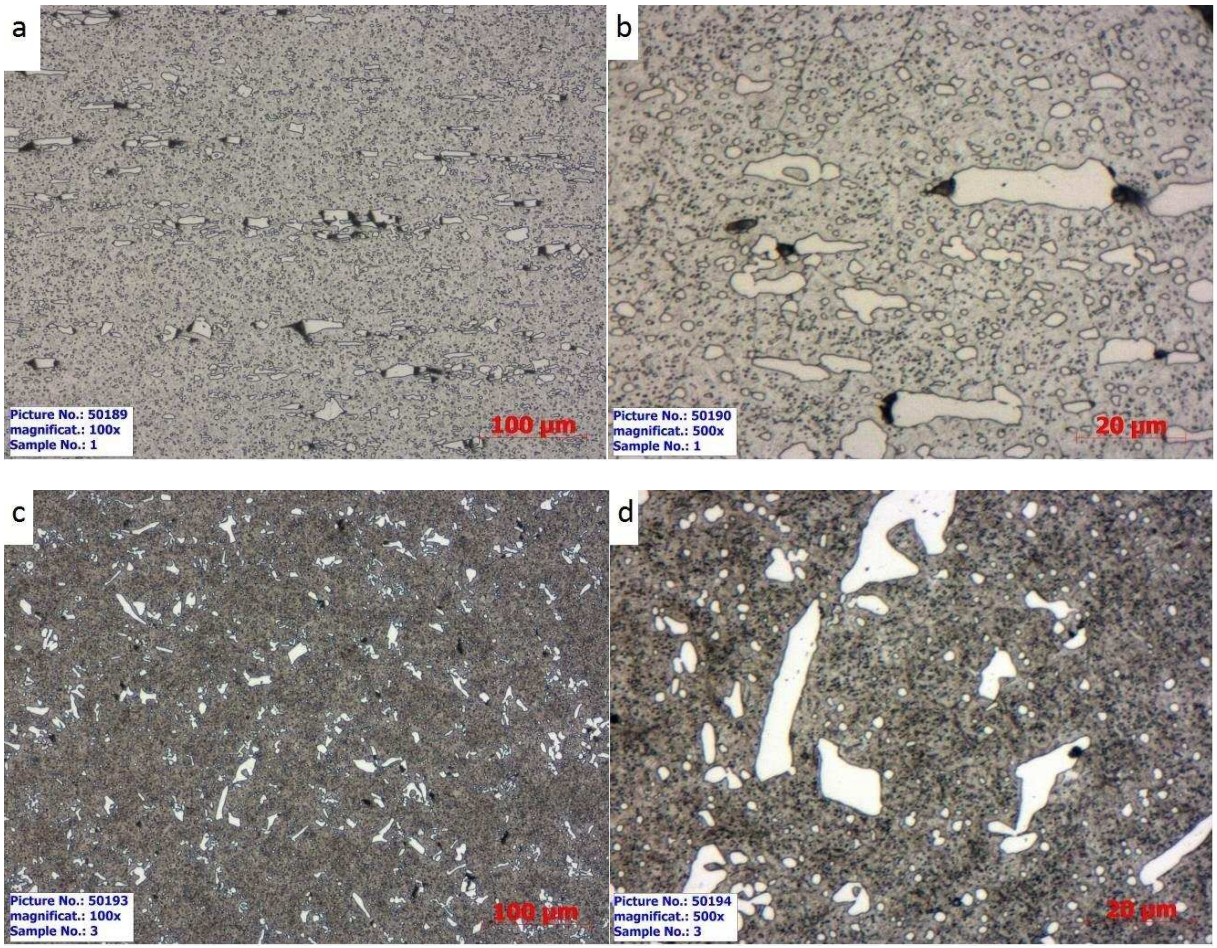

Fig. 1 Optical micrographs of heat treated specimen a)-b) hardening *1015°C; tempering 200°C; c)*-d)hardening *1015°C*; cooling to *-180°C; tempering 200°C*

At the fig. 1c-d can be seen the structure of the prepared treatment regime to the primary hardness. Temperature of quenching from 1015 °C immediately after hardening was performed at freezing temperature of -180 °C and tempered at 200 °C. Again, there are no clear boundaries of the original austenite grains. In the matrix of tempered martensite are present, evenly distributed small secondary carbides, which is in this case larger quantities than in the samples of the first.

Fig. 2a-b shows the structure of the prepared secondary heat treatment hardness. The samples were quenched from a temperature of 1060 °C and tempered two times from a temperature of 555 °C. The shape and distribution of primary and secondary carbides remained unchanged. The matrix consists of tempered martensite thicker needles between which there are fine carbides of alloying elements with an even distribution. Grain boundaries were not particularly significant. In this case one could consider a very small proportion of residual austenite in the structure occurring. The latest example of the structure of work in this section is shown in fig. 2c-d. In this group of samples was selected hardening temperature of 1060 °C, which is typical for secondary hardness. However, the tempering was carried out only at 200 °C which is usual for primary hardness. Then form a matrix of fine needle tempered martensite along with small carbides. There was also a highlight grain boundaries.

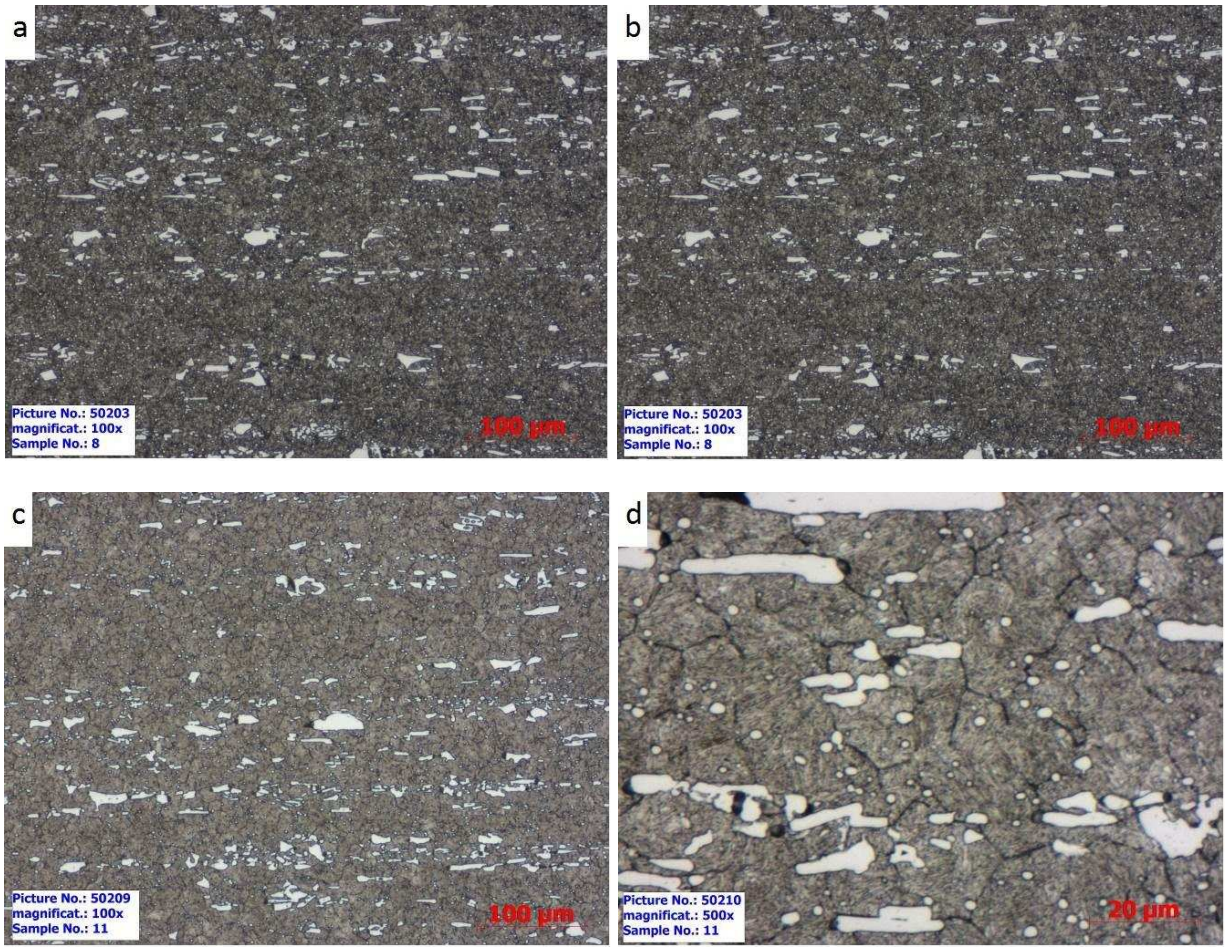

Fig. 2 Optical micrographs of heat treated specimens a)-b) hardening 1060°*C; tempering 2x 555°C; c)*-d)hardening 1060°*C; tempering 200°C*

Wear rezistence

High abrasion coefficient has five groups of samples which exceeded or equaled the value of relative wear resistance ψ = 2,8. Surprisingly, resistance to abrasive wear showed a clear dependence on the tempering temperature. Higher temperature during the tempering showed lower wear resistance of the samples. This dependence is shown in graph 2. In the case of group 3 can not be clearly said that the cryogenic treatment has an effect to improve the wear properties of steel. To confirm this, it would be necessary to test more specimens.

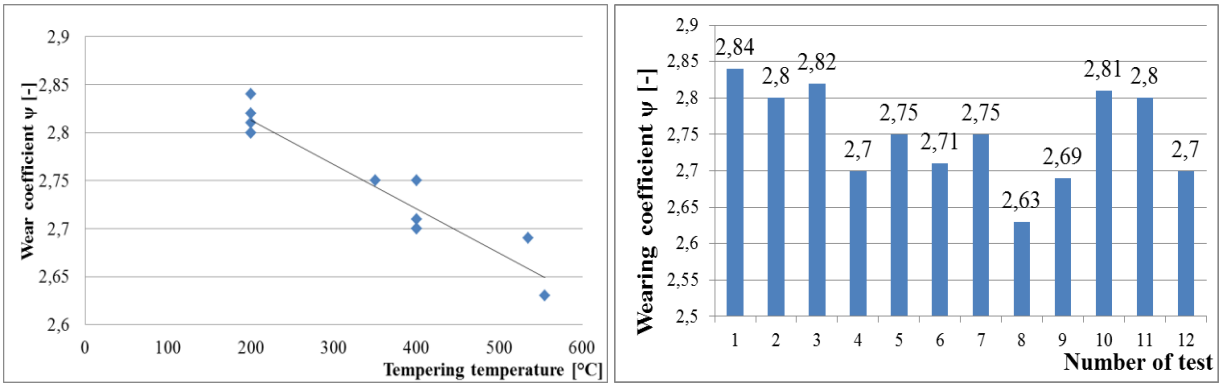

Graph 2 Values of wear coefficient.

Retained austenite

The measurement results after electrolysis are written in tab. 3. Before cleaning the measuring point of samples had a higher amount of retained austenite. Measured values may be distorted by the dirt on the surface, therefore a further description and considerations is commented only results that were observed after electrolysis of the sample surface.The highest amount of retained austenite was measured for the samples of group 1 – 13,2% with a deviation of ± 1,3%. The lowest amount of samples were 8 and 9, which was below 1%. Measurements confirmed a rule that says that at a sufficiently high temperature tempering is transformed residual austenite to martensite, whereby the retained austenite from the structure almost removed. Cryogenic treatment aimed at reducing the content of residual austenite. This fact can be observed between the groups of samples 1, 2 and 3, in which the quenching and tempering temperature but identical samples of group 3 underwent immediately after quenching, cooling to -180 °C.

Tab. 3 Amount of retained austenite and hardness

Test	Retained austenite [%]	Hardness after hardening [HRC]	Hardness after quenching [HRC]
1.	13,2 ± 1,3	61 - 62	60 - 60,5
2.	10,6 ± 0,2	61 - 62	59 - 61
3.	3,1 ± 0,6	61 - 62	59 -59,5
4.	3,8 ± 0,1	61 - 62	59 -60,5
5.	7,3 ± 0,9	61 - 62	58,5 - 60
6.	12,1 ± 1,0	61 - 62	59 - 61
7.	11,4 ± 0,7	60 - 61	60 - 61
8.	<1 ± <1	61 - 62	57 - 60
9.	<1 ± <1	62 - 63	59 - 61,5
10.	4,3 ± 1,0	61,5 - 62	57 - 57,5
11.	8,9 ± 1,5	60 - 62	60 - 62
12.	10 ± 0,4	60 - 62	58 - 59,5

Hardness

The measured values can be seen at a glance that the heat treatment on the primary or secondary hardness can achieve the same hardness.(tab. 3) Proof of this are the same hardness values between group 2, the heat treating primary hardness and group 9, the heat treating secondary hardness. Cryogenic treatment was not reached higher hardness values compared to the classical heat treatment carried out on specimens of group 1 and 2.

4 Discussion

In this article were determined selecting characteristics of ledeburitic chrome-vanadium tool steel 1.2379, which is used for cold working tools. A total of 12 groups of the samples were evaluated, 11 had undergone a conventional heat treatment, and the third group of samples was subjected to heat treatment with a cryogenic cooling to a temperature -180 °C. Primary or secondary hardness character was achieved by conventional procedures. Certain regimes of heat treatment consisted of a higher austenitizing temperature, which is typical for secondary hardness and lower tempering temperature. Both types of heat treatment can achieve hardness in the range 58 ± 1 HRC, which is most commonly recommended for knives used in practice.

Results of impact energy of some groups were highly unequal, exemplified by such groups 5 and 9. The lowest impact strength of samples has groups 8 and 9. These samples were processed for secondary hardness and tempering temperature was moved above 535 °C. The highest impact values have samples of 7 and 10 groups; the tempering temperature should not exceed 350 °C. The hardness of these samples has a primary character. Steel, which is engaged in such work, has a lower impact values with increasing tempering temperature. The described behavior is not quite common among tool steels, steel producer writes in his catalog [4] opposite behaviour, the toughness values decreasing on the tempering temperature. In older literatures [8] can be read precepts of higher toughness of tool steels with increasing tempering temperature. On the other hand, the book of tool steels ledeburitic type [3] confirms the behavior determined by experiment, and it also explains the increased proportion of retained austenite in the structure. This fact was confirmed in the group of samples 8 and 9, which have in their structure, as measured by less than 1% retained austenite and showed the lowest value of impact energy.

Values of relative abrasion resistance show a linear dependency on the amount of tempering temperature, as schematically indicated in graph 2. With increasing tempering temperature decreases abrasion resistance of steel. There is believed that despite the elimination of special precipitation of carbides of alloying elements and the transformation of retained austenite to martensite matrix decreases the ability to resist abrasion, because it increases the degree of tempering martensitic structure resulting after hardening.

Cryogenic heat treatment had a significant effect on reducing the value of the residual austenite in comparison with the groups of samples 1 and 2. In the work Stratton [9] states that the cryogenic heat treatment of steel 1.2379 tool abrasion may increase by up to 817%. The results of my work but do not confirm any improvement in wear resistance. The microstructure contains larger amounts of fine carbides in the matrix compared to a conventional heat treated structures.

Metallographic observation was found in all samples carbide banding. Carbides in rows are mostly primary and eutectic origin, not participating in the heat treatment and therefore can not be removed. With the growth of the hardening temperature grows brilliance grain boundaries. In the structure of the group 10 or 11 which have been quenched from a temperature of 1060 °C were most pronounced grain boundaries. Basic tempered martensitic matrix of the higher tem-

perature, the coarser and stronger unlike tempered martensitic structure at a lower temperature, which caused homogeneously without significant martensite laths. For all samples was consistently determined grain size, thus hardening temperature in the range 1015 °C to 1060 °C did not affect the change in grain size.

5 Conclusion

In this work was investigated ledeburitic tool steel 1.2379 which is used for tools for cold working. The aim of this work was to design an optimal mode of heat treatment. This served to results of the tests on the basis of which can be summarized findings make several points.

- Desired hardness of tools can achieve primary and secondary heat treatment.
- Toughness was higher for primary tempering hardness than after secondary tempering hardness.
- The amount of retained austenite in the structures after tempering above 535 °C and higher, is reduced to less than 1%.
- Abrasion resistance is linearly decreasing with increasing tempering temperature.
- Cryogenic heat treatment had a significant positive effect on assessed property.
- In the interval hardening temperature from 1015 °C 1060 °C do not change grain size.
- In the microstructure occur carbide phase is rectified in the rows that can not be removed by heat treatment, the properties of the material are directionally dependent.

The submitted fact implies a clear conclusion. The most appropriate method for heat treatment of 1.2379 steel for cold working tools seems quenching from a temperature of 1040 °C and tempering at 200 °C - group 10. It should be appreciated that in this mode will not achieve maximum hardness of the steel.

References

[1] ROBERTS, George, George KRAUSS a Richard KENNEDY. Tool steels. 5th ed. Materials Park, OH: ASM International, 1998. ISBN 16-150-3201-0.

[2] ASM Handbook Volume 1: Properties and Selection: Irons, Steels, and High-Performance Alloys (06181). 10th editon. 1993. ISBN 978-0871703774.

[3] JURČI, Peter. Ledeburitic tool steel. Prague: Czech Technical University in Prague, 2009, 221 s. ISBN 978-80-01-04439-1.

[4] Information on http://www.bohler-edelstahl.com/media/productdb/downloads/K110DE.pdf

[5] ASTM E112-13. Standart Test Methods for Determining Average Grain Size. ASTM International, 2013.

[6] ČSN 01 5084. Determination of metal material resistance against wear by abrasive cloth. Prague: Czech Standards Institute, 1973.

[7] ČSN EN ISO 6508-1. Metallic materials - Rockwell hardness test - Part 1: Test method. Prague: Czech Standards Institute, 2015

[8] JECH, Jaroslav. Heat treatment of steel: metallographic manual. 4. issue. Prague: SNTL, 1983, 342 p.

[9] Stratton, P. F.: Proc. of the 1st Int. Conf. on Heat Treatment and Surf. Engng. of Tools and Dies, Pula, Croatia, 8.-11.6.2005, 11.

Consequences of incorrect heat treatment of high-strength low-alloy steel

Milan Vnouček[1], Petr Beneš[1], Antonín Kříž[1]

[1]Faculty of Mechanical Engineering, University of West Bohemia. Univerzitní 8, 306 14 Plzeň. Czech Republic. E-mail: vnoucek@kmm.zcu.cz, pbenes@kmm.zcu.cz, kriz@kmm.zcu.cz

This investigation concerns high-strength low-alloy steel plates. The material is subjected to a temperature that exceeds manufacturer's recommendations. It was examined with respect to changes in the microstructure and mechanical properties. The decline in the mechanical properties of this type of material can be very dramatic. This high-strength steel has an initial microstructure that consists of martensite and is alloyed with a higher amount of nickel. This may be the reason why the decrease of its mechanical properties is not monotonic with changes of the heat treatment temperature. The maximum thermal load permitted for this steel is 150°C for 20 minutes, if it is to retain specified mechanical properties. The steel was annealed at temperatures of 180ºC, 240ºC and 300ºC for 2 hours.

Keywords: Mechanical properties, high-strength low-alloy steel, heat treatment

1 Introduction

High-strength low-alloy steels are optimal materials for special equipment that operates under severe conditions and high stresses. These steels possess high ultimate strength combined with sufficient processability. Since the special equipment is usually of robust construction and/or produced on a mass scale, there is an advantage in the low alloy content of these steels (below 5 percent). In order to obtain high mechanical properties, the steels must be thermomechanically treated [1, 2, 3]. The application studied herein required maximum hardness and toughness. Therefore, the material had to possess martensitic structure achieved through appropriate chemistry and thermal and mechanical processing. Experiments were carried out on 5-mm-thickness sheet metal. The as-received material was specified to have a hardness of 58-63 HRC, an offset yield strength Rp0.2min of 1250 MPa and a notch toughness KCVmin of 12 J at -40ºC. Its chemical composition is given in Table 1.

Tab. 1 The prescribed chemical composition of the material [%]

C	Si	Mn	P	S	Cr	Ni	Mo	B
0.46	0.16	0.7	0.007	0.001	0.5	2.09	0.341	0.001

According to the manufacturer, the sheet metal is not intended for heat treatment. The manufacturer specifies a maximum permitted thermal exposure at 90ºC and an ultimate maximum of 150ºC for 20 minutes. In this experiment, the material was heat-treated to customer specifications. The heat treatment sequence consisted of annealing at 180, 240 and 300ºC for 2 hours. It was followed by cooling in still air to room temperature. Because the as-received material had been controlled-rolled, the annealed material was examined on both transverse and longitudinal cross sections (with respect to the rolling direction) in order to detect possible anisotropy. It was also mechanically tested and metallographically examined [4].

2 Metallographic investigation

Specimens were prepared for observation under the optical microscope. Metallographic observation did not confirm the expected anisotropy (Fig. 1). The material had a very fine needle-like martensite microstructure. For this reason, the magnification of 500× was mainly used. Lower magnifications were not useful, as evidenced by Fig. 1.

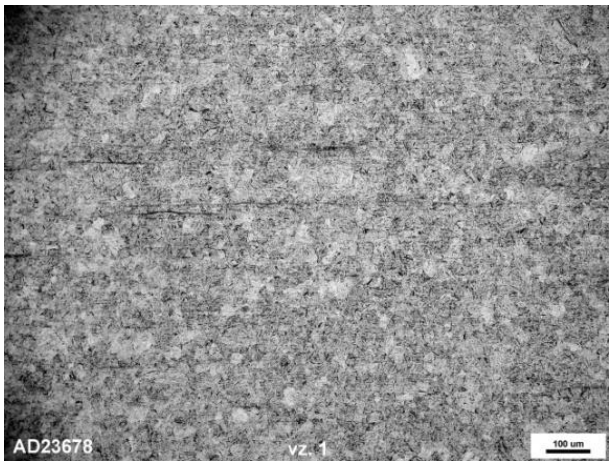

Fig. 1 Micrograph of the specimen surface; as-received condition; indications of the rolling direction are visible, *whereas anisotropy is not. Magnification 100×*

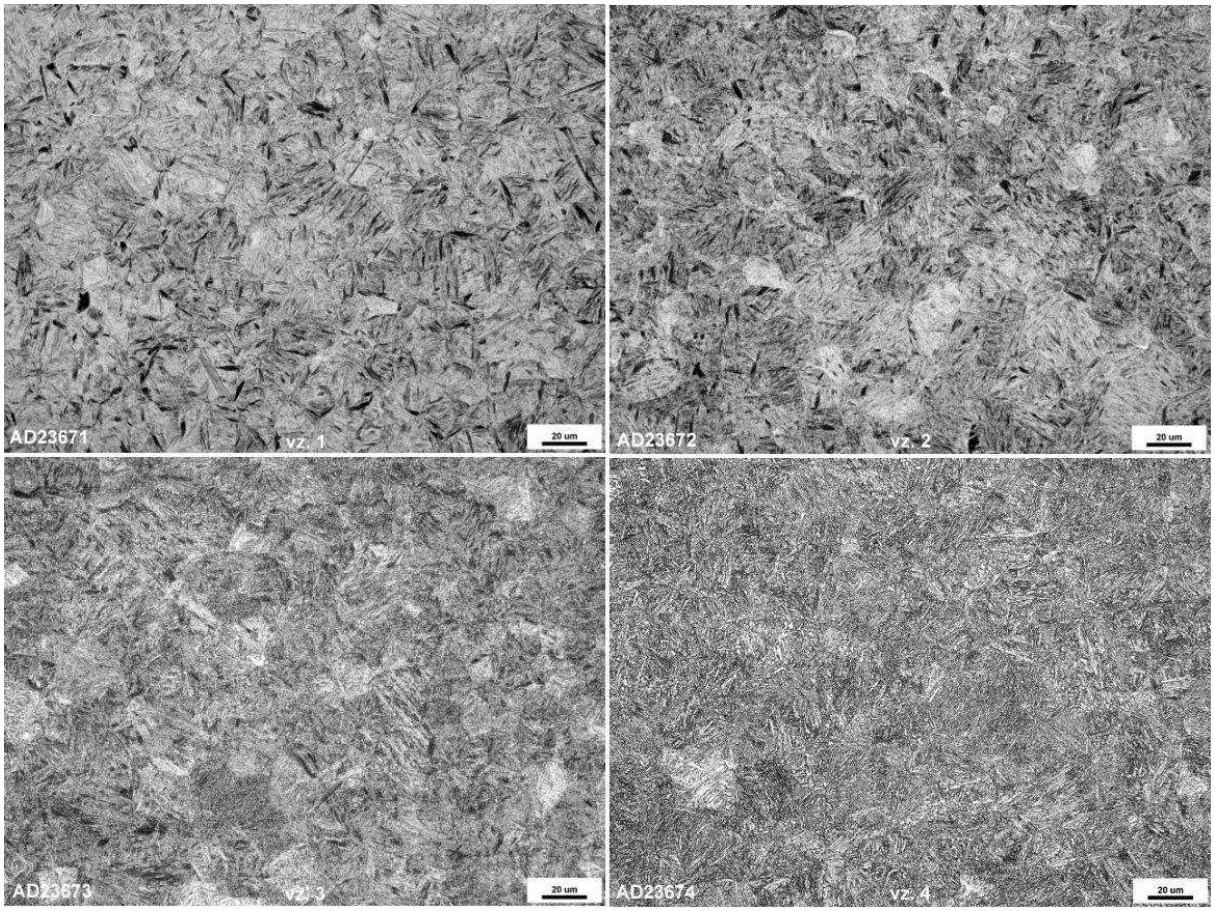

Fig. 2 Micrographs of specimen surfaces before and after heat treatment; as-received condition: AD23671, annealed at *180ºC: AD23672, annealed at 240ºC: AD23673, annealed at 300ºC: AD23674, magnification 500×*

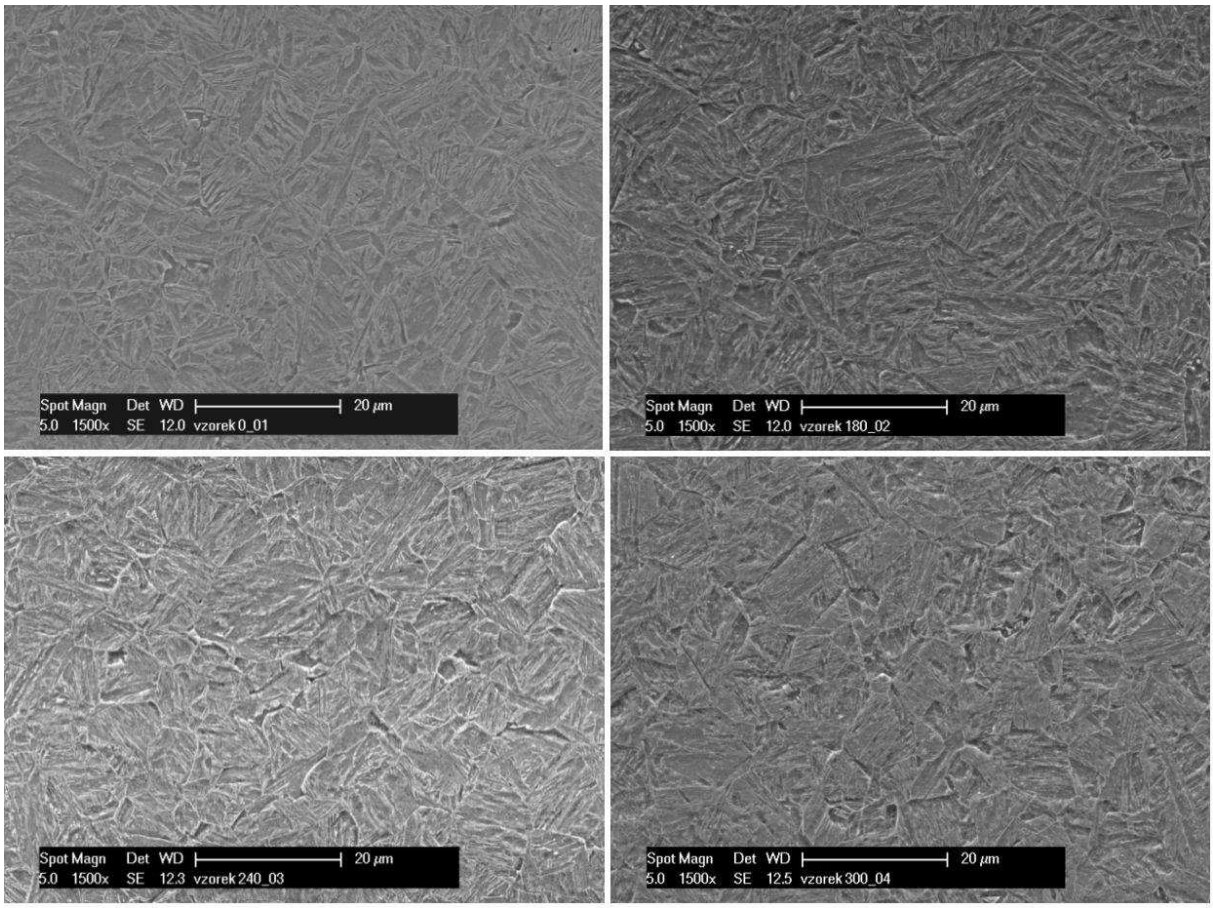

Fig. 3 Scanning electron micrographs of specimen surfaces before and after heat treatment: as-received condition, *annealed at 180ºC, annealed at 240ºC, annealed at 300ºC, magnification 1500×*

Annealing had a minimal impact on the microstructure. The most extensive changes occurred upon annealing at 300ºC (Fig. 2) which obliterated prior austenite grain boundaries. The changes were easier to observe using higher magnifications in a scanning electron microscope.

According to the theory presented in [2], the main effect in the microstructure is the precipitation of carbides and redistribution of carbon and/or boron. At 1500× magnification, i.e. an ordinary magnification of metallographic microscopes, it was impossible to resolve any precipitates in the scanning electron microscope. The particles which precipitate in the fine martensitic matrix are smaller than 0.5 µm, see Fig. 4.

The microstructural changes, predominantly the redistribution of carbon and boron, are reflected in mechanical properties. The latter were therefore measured in the next stage of the experiment. Brinell and Rockwell hardness measurement and tensile and impact toughness tests were carried out. The response of mechanical properties was expected to be similar to that of artificially-aged aluminium alloys in which notch toughness and strength decrease whereas ductility increases with increasing temperature.

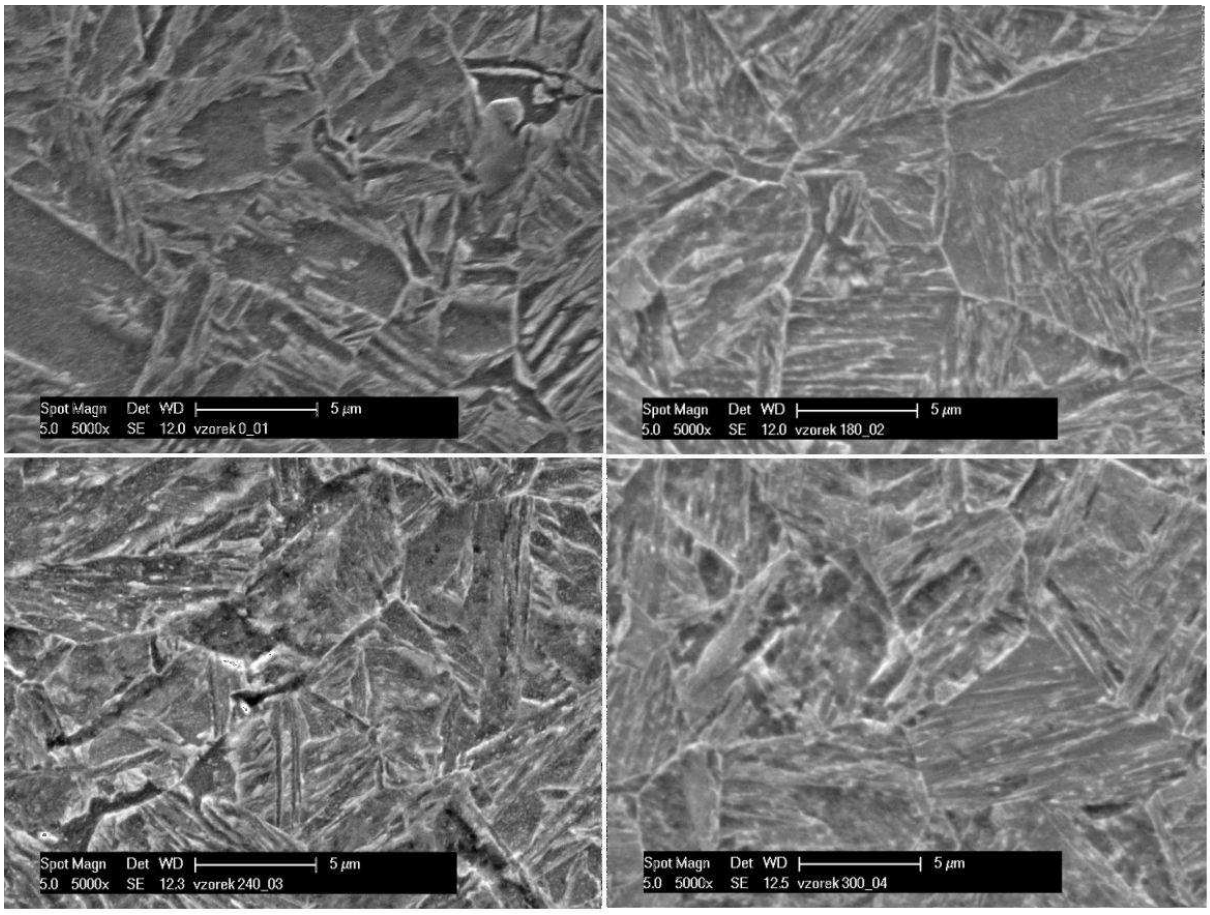

Fig. 4 Scanning electron micrographs of specimen surfaces before and after heat treatment: as-received condition, *annealed at 180ºC, annealed at 240ºC, annealed at 300ºC, magnification 5000×*

3 Mechanical testing

Specimens taken from as-received and annealed blanks were machined into test bars for mechanical testing. For each test, 5 bars were manufactured. As chip cutting of this material is difficult, the specimens were cut using water jet. Notches caused by cutting limited the options for the as-received specimen. For this reason, the edges of all test bars were ground.

Longitudinal and transverse strengths were identical: the direction of rolling has no substantial impact on strength. Yield strength is impossible to measure due to brittleness of the material. Therefore, the offset yield strength Rp0.2 was determined. An extensometer attached to the specimen was used. Stress and strain characteristics are given in Table 2. Specimen codes: temperature – specimen number; the values in Table 2 apply to the longitudinal direction, i.e. parallel to the direction of rolling.

Elongation and reduction of area were low in the as-received material due to its brittleness. Specimens after annealing at 180, 240 a 300ºC showed higher values of reduction of area: twice as high as in the as-received material. The ultimate strength decreased monotonically with increasing annealing temperature. Other properties, such as yield strength and elongation, changed as well but their dependence on temperature was impossible to identify [4].

Tab. 2 Tensile test values

Annealing temperature – specimen number	Resulting values				Comment
	(MPa)		(%)		
	Rp0.2	Rm	A	Z	
X - 01	–	2039	–	–	Premature fracture in a notch in the neck region
X - 02	–	2477	4.76	6.51	Without extensometer
X - 03	1458	2404	7.11	27.48	
X - 04	1505	2478	5.85	8.88	
X - 05	1513	2494	7.18	22.17	
Average	**1492**	**2378**	**6.23**	**16.26**	
180 - 01		2015	8.25	33.19	Without extensometer
180 - 02	1554	2012	7.99	37.04	
180 - 03	1533	1988	8.4	38.98	
180 - 04	1559	2014	7.83	34.58	
180 - 05	1560	2013	8.1	38.69	
Average	**1552**	**2008**	**8.11**	**36.50**	
240 - 01	–	1828	7.39	47.28	Without extensometer
240 - 02	1537	1839	7.59	46.29	
240 - 03	1522	1821	7.7	47.5	
240 - 04	1525	1827	8.07	49.97	
240 - 05	1510	1808	7.92	50.16	
Average	**1524**	**1825**	**7.73**	**48.24**	
300 - 01	–	1677	8.4	46.47	Without extensometer
300 - 02	1425	1652	5.86	52.23	
300 - 03	1440	1668	8.3	44.91	
300 - 04	1443	1672	8.41	47.3	
300 - 05	1442	1667	8.33	47.65	
Average	**1438**	**1667**	**7.86**	**47.71**	

Hardness, which dictates the wear behaviour, decreased with increasing annealing temperature. The decrease was not dramatic. Hardness was measured using Brinell HBW 10/3000/10 and Rockwell HRC methods. The latter is better suited for testing quenched materials. Brinell hardness testing, which was required by the customer, reaches its capability limit in this application but offers more accurate measurement than Rockwell hardness testing. Table 3 shows the decrease in hardness with increasing annealing temperature.

Tab. 3 Rockwell and Brinell hardness values

	No annealing	Annealing 180°C	Annealing 240°C	Annealing 300°C		No annealing	Annealing 180°C	Annealing 240°C	Annealing 300°C
Measurement 1	634	587	538	499	Measurement 1	58.3	56.1	52.5	50.2
Measurement 2	632	584	538	499	Measurement 2	59.2	57.3	53.5	50.5
Measurement 3	632	584	538	499	Measurement 3	58.5	55.9	52.8	52.7
Measurement 4	637	584	538	497	Measurement 4	58.7	56.7	52.9	51.4
Measurement 5	634	584	538	499	Measurement 5	58.7	55.8	52.8	50.3
Average HBW	**634 ± 2**	**585 ± 1.5**	**538 ± 0.0**	**499 ± 1**	**Average HRC**	**58.7 ± 0.3**	**56.4 ± 0.6**	**52.9 ± 0.4**	**51.0 ± 1.1**

Hardness decreased relatively slowly with increasing temperature: by approximately 2.5 HRC or 50 HBW per 60ºC. Up until 220─250ºC, mechanical properties were decreasing but still remained within the basic specification range for ordinary structures from this material. However, in the special application considered in this article, this decrease would already cause catastrophic failure of the equipment. Some mechanical properties were decreasing but others were increasing with increasing annealing temperatures. This is evidenced by notch toughness levels. As this property is sensitive to thermomechanical treatment, it was measured in both longitudinal and transverse directions.

Tab. 4 Notch toughness in transverse and longitudinal directions

Transverse direction	No annealing	Annealing 180°C	Annealing 240°C	Annealing 300°C	Longitudinal direction	No annealing	Annealing 180°C	Annealing 240°C	Annealing 300°C
Measurement 1	31.3	40.3	28.9	28.4	Measurement 1	29.5	37.1	28.1	29.7
Measurement 2	33	37.8	26.6	28	Measurement 2	33.4	39.1	28.4	29.9
Measurement 3	29	39	27.1	27.2	Measurement 3	32.2	35.9	28.4	29.4
Measurement 4	33	35.1	26.7	28.9	Measurement 4	27.2	35.6	27.7	29.2
Measurement 5	31.5	37.8	28.1	29.4	Measurement 5	17.3	37.8	30.6	31.7
Average	**31.5**	**38**	**27.5**	**28.4**	**Average**	**27.9**	**37.1**	**28.6**	**30**

As shown in Table 4, the highest notch toughness values were found in the specimen annealed at 180°C. The initially higher transverse notch toughness becomes equal to the longitudinal notch toughness at approx. 210─220°C. At higher temperatures, it remains higher than the values for the longitudinal direction. This is plotted in Graph 1. These changes are not reflected in the microstructure or in other mechanical properties.

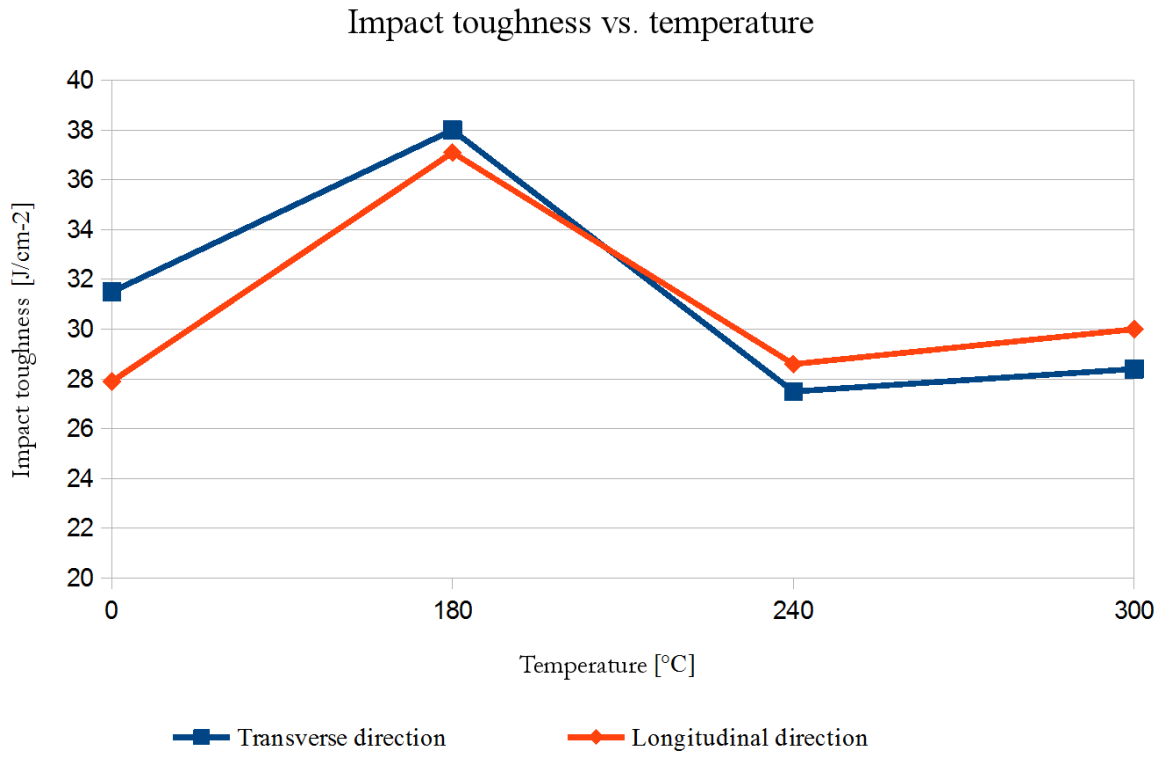

Graph 1 Nnotch toughness in two directions upon annealing at various temperatures

4 Conclusion

Annealing at low temperatures causes changes in low-alloy materials, particularly in some mechanical properties. Other mechanical properties only show minimal variation. The property which serves as the main design criterion ─ yield strength ─ remains practically constant. Other values decrease only slightly or reach their maximum at around 180°C. Annealing at 180°C delivers no additional improvement in a specific application of high-strength low-alloy materials for special equipment. Observation of microstructure under the optical microscope at 500× magnification does not reveal enough information for understanding the processes that take place in the material and their relation to mechanical properties. Substantial findings can only be obtained using electron microscopy. It is therefore rather complicated to detect whether thermal stress limits specified by the manufacturer have been exceeded. A slight decrease of approx. 2 HRC below the specified hardness level is very difficult to measure under the operating conditions of the

special equipment, whereas metallographic observation is downright impossible.

Acknowledgement

This article was prepared under the student project SGS-2015-016 "**Analysis of Surfaces of Structural Details and Tools by Surface Integrity Method, and Impacts on End-Use Properties**".

References

[1] Jirková, H., Kučerová, L., Průcha, V., Mašek, B. Effect of advanced thermomechanical treatment on mechanical properties of low alloyed high strength steels, 21st International Conference on Metallurgy and Materials, METAL 2012; Hotel Voronez I Brno; Czech Republic; 23-25 May 2012 pp. 532-538, 2012.

[2] Masek, B., Kucerova, L., Jirkova, H., Klauberova, D., THE ROLE OF A COOLING RATE IN THERMO-MECHANICAL TREATMENT WITH INCORPORATED Q-P PROCESS, 20th Anniversary International Conference on Metallurgy and Materials, May 18-20, 2011, Brno, Czech Republic, pp. 474-479, 2011

[3] Jirkova, H., Kucerova, L., Q-P process on steels with various carbon and chromium contents, 8th Pacific Rim International Congress on Advanced Materials and Processing 2013, PRICM 81, pp. 819-824, 2013

[4] Coufal V: Vliv tepelného zpracování na terminálně balistické vlastnosti nízkolegované vysokopevné oceli, (Bachelor's thesis), University of West Bohemia, 2016

Perspektívy špeciálnej techniky v obrannom a krízovom manažmente

Peter Liptak[1],
[1]Faculty of Special Technology, Trencin University of Alexander Dubcek, Pri parku 19 Zablatie, 91106 Trencin, Slovak Republic. E-mail: peter.liptak@tnuni.sk,

V krízových situáciách sú potrebné prístroje a zariadenia charakteru špeciálnej techniky. V článku je uvedená súčasná charakteristika pojmu ŠPECIÁLNA TECHNIKA, predpokladaná kategorizácia špeciálnej techniky, možné smerovanie jej vývoja z pohľadu vedeckej a odbornej činnosti. Východiská vychádzajú z orientácie a smerovania potrieb aliančných uskupení, predurčených pre obranných obranné potreby, pre potreby riešenia neštandardných situácií, v rámci ktorých je predpoklad vývoja, prevádzkovania a nasadenia špeciálnej techniky. Zvláštna pozornosť je venovaná mobilite špeciálnej techniky. Riešený kontajnerový program je poňatý nielen z hľadiska prevozu ale i nakladania a stability. Táto technika vyžaduje balistickú ochranu a balistické zodolnenie. Táto problematika je riešená špecifikou materiálov a strojárskych technológií pre spracovanie na účely balistického zodolnenia. Ďalej je v článku riešená problematika zabezpečenia elektrickou energiou a vody pre kontajnerové pracoviská špeciálnej techniky. V článku sú uvedené konkrétne príklady nových zariadení, konštruovaných v spolupráci Fakulty špeciálnej techniky s konkrétnymi zariadeniami a inštitúciami na Slovensku [2].

Keywords: Crisis situations, renewable sources of energy, photovoltaic collectors, logistic container, power systems, mobile assets of crisis management

1 Úvod

Pre zabezpečenie základných ľudských potrieb pri riešení obranných operácií a krízových situácií je potreba zabezpečenia postihnutej oblasti energiami a vodou. Autori v rámci výskumného programu riešili toto zabezpečenia s predpokladom zasadenia techniky v rôznych prostrediach a s využitím okrem tradičných vstupných energetických a napájacích zdrojov i energiou slnečného žiarenia a veternou energiou. Pri riešeniach bolo navrhované mobilné riešenie, to znamená zabudovanie prístrojov a zariadení do kontajnerov, prepraviteľných do miesta nasadenie vrtuľníkom, automobilom alebo loďou.

Katedra automobilov a špeciálnej techniky Fakulty špeciálnej techniky Trenčianskej univerzity Alexandra Dubčeka v Trenčíne venovala v uplynulom období v rámci vedeckej práce a kontaktov s praxou pozornosť oblastiam:

- Zodolňovanie mobilných a prepravných systémov skvalitňovaním balistickej ochrany.
- Kontajnerový program mobilnosti zariadení špeciálnej techniky.
- Vývoj vysokoenergetických materiálov v rámci úlohy Slovenska pri začlenení do NATA v rámci programu tímu EOD – práca s muníciou a výbušninami.
- Ekologické a nezávislé zdroje elektrickej energie ako súčasť mobilných zariadení.
- Toto smerovanie vychádzalo a vychádza zo súčasných potrieb logistického a výzbrojného zabezpečenia krízových situácií.

2 Potreby krízového manažmentu z pohľadu technického zabezpečenia špeciálnou technikou

Z pohľadu potrieb krízového manažmentu špeciálnou technikou sme riešili potreby:

- Prístupu a dostupnosti, priechodnosť vo vode, teréne blatistom, teréne horskom a lesnom, cesty, vzduchom.
- Mobility a doprava zariadení a systémov.
- Zodolnenie mobilných pracovísk formou balistickej ochrany.
- Zabezpečenie elektrickou energiou.
- Zabezpečenie pitnou a úžitkovou vodou.
- Zdravotnícke a lekárske zabezpečenie.

Pre účely tohto článku doložíme možné riešenie zabezpečenia elektrickou energiou, pitnou a úžitkovou vodou a kontajnerový systém dopravy zariadení a systémov.

3 Prístupy ku riešeniu mobility pracovísk pre špeciál a ich balistické zodolnenie

Činnosti spojené s kontajnermi sú stále aktualizované podľa požiadaviek zákazníka, čo možno poukázať aj s meniacimi sa požiadavkami na ich rozmery, kvalitu a vybavenie.

Pri pohľade na rozmach kontajnerizácie v globálnej distribúcii tovarov bol jej prienik do oblasti vojenstva a krízového manažmentu očakávaný a tiež mnohými armádami žiadaný. Použitie prepravnej jednotky so

štandardizovanými rozmermi je výhodné z mnohých hľadísk a to najmä pri kooperácii spojeneckých síl v zahraničných misiách. Vojenská logistika kontajnerových systémov NATO, čo sa týka dopravných prostriedkov, spočíva na leteckej alebo lodnej preprave a následnej preprave prostredníctvom kolesových vozidiel. Na tieto vozidlá sú tak kladené vysoké nároky na jazdný dosah, nosnosť, rýchlosť pri pohybe po spevnených komunikáciách, priechodnosť členitým terénom atď. Moderné špeciálne kolesové vozidlo na prepravu kontajnerových systémov musí byť vybavené hydraulickým zariadením na samostatnú nakládku a vykládku kontajnera a balistickou ochranou podľa požadovanej úrovne ochrany.

Podľa normy ISO 830 sú všetky kontajnery postavené do rádu a je im definovaná nosnosť a rozmery. Ďalej je normou stanovená plošina kontajnera. V podmienkach špeciálu sa najčastejšie používajú kontajnery ISO 1C a 1D, prípadne ich varianty z rozdielnou výškou a tiež špeciálne kontajnery – najmä v armádach NATO tzv. „Flatrack“ čo je vlastne zváraná plošina s rozmermi kontajneru ISO 1C, ktorá je štandardizovaná v norme STANAG 2413.

Preprava kontajnerov na miesto určenia je mnohokrát komplikovaná, vyžaduje si aj logistickú potrebu. Zaisťuje sa to pomocou rôzneho druhu presunu s využitím cestnej, železničnej, lodnej a leteckej dopravy. K tomu je tiež potrebné využívať prekladiská, ktoré nazývame terminály.

Výhodou cestnej dopravy je doprava kontajnera na miesto určenia, alebo k jeho maximálnemu priblíženiu. K využitiu sú možné všetky druhy pozemných komunikácií v rámci zjazdnosti. Využívame pri tom vozidlá so špeciálnymi nadstavbami. Nevýhodou tejto dopravy je preprava menšieho množstva kontajnerov.

Obr. 1 *Príklad riešenia nosiča kontajnera TATRA 815 8x8 vybaveného zariadením pre bočnú nakládku a vykládku* kontajnera s kontajnerom. [1].

Výhody železničnej dopravy spočívajú v možnosti prepravovať veľkého množstva kontajnerov jedným dopravným prostriedkom, čo nie je možné dosiahnuť pri cestnej doprave. Dôsledkom sú nižšie náklady na prepravu a lepšia cena. Výhodou je i možnosť prepravy aj veľmi ťažkých zásielok. Nevýhodou je potreba dostupnosti železničnej trate, nevhodnosť pre prepravu v zložitejšom teréne dlhší čas prepravy na miesto určenia, malá flexibilita, možné nedodržanie časových harmonogramov a pomalosť manipulácie. Tento spôsob si vyžaduje vytvorenie priestoru na nakládku a vykládku, kde sa vytvára predpoklad ďalšieho zvyšovania nákladov. Železničná doprava je naviazaná na cestnú dopravu, preto sa vytvárajú miesta nazývané kombinovaná doprava. [2]. Na dopravu kontajnerov po vode existujú dva druhy vodnej dopravy – riečna a námorná. Preprava kontajnerov po rieke nie je tak využívaná ako preprava po mori. Využitie dopravy po moriach a oceánoch je efektívnejšie. Námorná doprava je nosným systémom v rámci medzikontinentálnej prepravy tovarov a jej využitie sa spája najmä s kontajnerovými prepravami. Len v rámci námornej dopravy je možné prepraviť zásielku medzi kontinentmi za prijateľné náklady. Cestná a železničná doprava túto možnosť nedovoľujú s výnimkou Európy a Ázie, kde sa v poslednom období uvažuje najmä o možnosti využitia železničnej dopravy. Významnou prednosťou je možnosť prepravy veľkých zásielok a veľkého množstva tovaru. Jednoznačnou nevýhodou vodnej dopravy je dlhý čas prepravy, s ktorým treba počítať pri návrhu dopravného riešenia. [2]. Leteckú dopravu kontajnerov môžeme chápať v usporiadaní – kontajner umiestnený v nákladnom lietadle, v transportnom lietadle, napr. typu – C 130, AN 124, IL 76, A 400M a kontajner umiestnený v podvese vrtuľníka. Obidve sa využívajú i v práci so špeciálnou technikou, napr. prevoz náhradných dielcov a delaborovanej techniky na miesto nasadenia, ktoré je vybavené letiskom, poľným letiskom, napr. Kandahár alebo doprava kontajnera opráv, zdrojových sústav, čističiek vody v podvese vrtuľníka priamo na miesto nasadenia v teréne.

Fakulta špeciálnej techniky riešila a rieši v rámci svojej vedeckej a výskumnej činnosti dva okruhy problémov- zodolnenie kontajnerov balistickou ochranou a prepravu a nakladanie kontajnerov na prepravu kolesovou technikou.

Na FŠT bolo riešené umiestnenie a nakladanie kontajnera na vozidle TATRA 815-7 10x10. Podvozok tatra 815-7 je navrhnutý ako ťažký nákladný automobil s využitím v armáde ale aj civilnom sektore. [3]. Rám vychádza z konceptu pôvodnej Tatry 817, teda jej základom je centrálna nosná rúra kombinovaná s priebežným rámom. Riešenie zavesenia náprav je principiálne rovnaké so staršími modelmi, teda s výkyvnými polonápravami s nezávislým zavesením. Podvozok bol rozšírený pridaním piatej nápravy, pričom štvrtá a piata náprava je schopná zatáčania. Modernizáciou prešiel systém pruženia, ktorý je v tomto prípade riešený pomocou pneumatických vakov. Vďaka tomu je možné regulovať výšku vozidla podľa potreby. Zároveň je podvozok vybavený centrálnym dofukovaním kolies s možnosťou zmeny tlaku, ovládaný z miesta vodiča. Všetky tieto prvky spolu umožňujú veľmi dobre prekonávať náročný terén Kabína prešla v tomto prípade taktiež zmenou, čím sa dosiahlo jej zníženie. Vďaka tomuto riešeniu je zároveň možná preprava vozidla lietadlom C-130 Herkules v rámci spolupráce NATO. Zníženie a zjednodušenie kabínovej časti umožnilo použitie balistickej ochrany v prípade potreby. Ako hlavnú výhodu vozidla Tatra 815-7 10x10 je nutné uviesť veľmi dobrú prejazdnosť terénom a zdolávania prekážok. Veľkou výhodou je aj tuhosť celého rámu a zavedenie vozidiel značky Tatra v armáde. Ako nevýhodu je možné uviesť zložitejšiu konštrukciu pohonu kolies, ktorá je jednak cenovo náročnejšia (z dôvodu vysokých výrobných nákladov) a zároveň zložitejšia pri opravách.

Obr. 2 *Príklad ideového návrhu podvozku nosičov kontajnerov s manipulátorom na nakladanie, resp. vykladanie* kontajnerov v *teréne.* [2].

Balistické zodolnenie Z hľadiska smerovania vývoja špeciálnej techniky pre potreby obrany štátu môžeme ako východiská aplikovať závery charakterizované ako trendy obranných spôsobilostí [6]:

- Vývoj a uplatnenie nových technológií.
- Nárast efektivity a ničivej sily asymetrických hrozieb, predovšetkým aktívnych teroristických skupín.
- Riešenie post-konfliktných situácií.
- Zvyšujúci sa podiel vedenia boja v zastavanom teréne a mestách.
- Používanie vysoko presných a účinných zbraní na ciele v prostredí s civilným obyvateľstvom.
- Šetrenie ľudských zdrojov ako prioritu pri plánovaní operácií.
- Postupná robotizácia bojovej činnosti.

V ďalšom uvádzame prehľad vlastností východiskových materiálov ARMOX. Vyšší obsah legujúcich prvkov (Cr, Ni) v pancierovej oceli typu ARMOX je potrebný na dosiahnutie požadovaných vlastností. Oceľ musí mať nízky obsah inklúzií (vtrúsenín), [8]. Tab. 7.1.1 prezentuje mechanické vlastnosti a smerné chemické zloženie vybraných pancierových plechov typu ARMOX.

Tab. 1.1. *Mechanické vlastnosti a smerné chemické zloženie vybraných plechov z pancierových ocelí ARMOX [8], [9],* [10]

Typ	Charakteristika									
Armox 440T	Smerné chemické zloženie (významné legúry) [%]									
	C	Si	Mn	P	S	Cr	Ni	Mo	B	
	0,21	0,-0,5	1,2	0,01	0,01	1,0	2,5	0,7	0,005	
	Mechanické vlastnosti									
	Tvrdosť [HBV]		KV-40^0 C [j]		Medza klzu [Mpa]		Pevnosť v ťahu [Mpa]		Ťažnosť [%]	
									A5	A50
	420-480		min.30		min.1100		1250-1550		10	12
Typ	Charakteristika									
Armox 500T	Smerné chemické zloženie (významné legúry ([%]									
	C	Si	Mn	P	S	Cr	Ni	Mo	B	
	0,32	0,1-0,4	1,2	0,015	0,010	1,0	1,8	0,7	0,005	
	Mechanické vlastnosti									
	Tvrdosť [HBV]		KV-40^0 C [j]		Medza klzu [Mpa]		Pevnosť v ťahu [Mpa]		Ťažnosť [%]	
									A5	A50
	480-540		min.20		min.1250		1450-1750		8	10
Typ	Charakteristika									
Armox 600T	Smerné chemické zloženie (významné legúry) [%]									
	C	Si	Mn	P	S	Cr	Ni	Mo	B	
	0,47	0,1-0,7	1,0	0,01	0,005	1,5	3,0	0,7	0,005	
	Mechanické vlastnosti									
	Tvrdosť [HBV]		KV-40^0 C [j]		Medza klzu [Mpa]		Pevnosť v ťahu [Mpa]		Ťažnosť [%]	
									A5	A50
	570-640		min.12		1500		2000		7	x

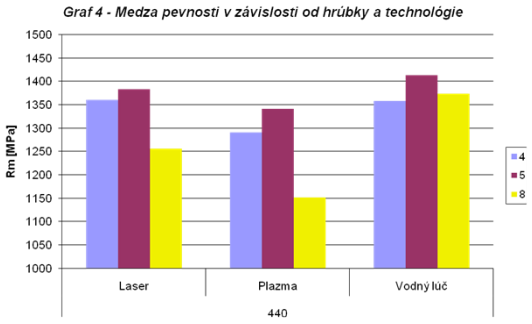

Obr. 3 Medza pevnosti v *závislosti od hrúbky materiálu a technológie rezania pre materiál ARMOX 440T [8]*

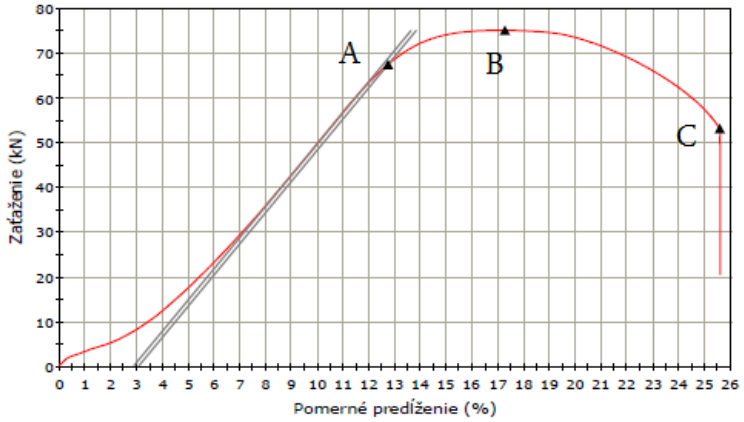

Obr. 4 *Ťahový diagram pre materiál ARMOX 440T s podobnosťou pre hrúbky 4 mm, 5 mm, 8 mm*

Na základe uvedených experimentov boli pre výrobné účely na špeciálnu techniku typu KONTAJNER SO ZABEZPEČENOU BALISTICKOU OCHRANOU odporúčané austenitické ocele. Technológia delenia vodným prúdom nemá vplyv na zmenu mechanických vlastností materiálu

4 Zabezpečenie elektrickou energiou

V súčasnej dobe je stále aktuálnou témou využívanie obnoviteľných zdrojov elektrickej energie. Tento trend preniká aj do mobilných zariadení a jeho využitie by bolo prínosom aj v kontajneroch ISO 1C využívaných ako mobilné logistické prostriedky. Na základe analýz elektrickej spotreby logistických prostriedkov používaných v misiách Ozbrojených síl Slovenskej republiky, bolo zostavené variantné využitie mobilných nekonvenčných zdrojov elektrickej energie.

Využitím nekonvenčných zdrojov by mobilný logistický prostriedok nebol závislý iba na vonkajšej elektrizačnej sústave, alebo na elektrickom zdrojovom agregáte, ale mal by vlastné variantné riešenie získavania elektrickej energie. [7].

Problematika vyčerpateľnosti zásob ropy a fosílnych palív je veľmi zásadná a hľadanie alternatívnych zdrojov je dnešnou prioritou. Energetická potreba technologického vybavenia mobilných kontajnerových prostriedkov je rôzna a preto je dôležité vedieť k nej priradiť aj optimálny zdrojový súbor. K návrhu optimálneho zdrojového súboru obnoviteľných zdrojov elektrickej energie bol spracovaný funkčný model ostrovného systému obnoviteľných zdrojov energie.

Využitím vytvoreného funkčného modelu ostrovného systému obnoviteľných zdrojov energie ktorý bol realizovaný s cieľom mať k dispozícii experimentálny zdroj elektrickej energie mimo dosah energetických rozvodných sietí umožňuje analýzu prevádzkových parametrov v konkrétnych podmienkach. Funkčný model obr. 6 obsahuje fotovoltaický panel a veternú turbínu, ako predstaviteľov najčastejšie používaných obnoviteľných zdrojov energie (OZE), ďalej akumulátor energie, mikropočítačový riadiaci a monitorovací blok a tiež náhradný zdroj energie a voliteľné spotrebiče energie.

Obr. 6 *Príklady funkčných modelov mobilného energetického zariadenia*
1-*veterná turbína, 2-fotovoltický panel, 3-akumulátor energie, menič energie, meracia časť*

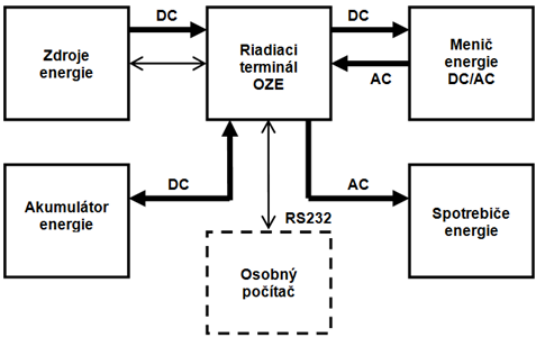

Obr. 7 *Bloková štruktúra funkčného modelu mobilného energetického zariadenia z obnoviteľných zdrojov elektrickej* energie [7].

5 Zámysel riešenia zabezpečenia pitnou a úžitkovou vodou

Dostatočné zásobovanie vodou vyžaduje obrovské množstvo kapitálu, investície do infraštruktúry, ako je potrubná sieť, čerpacie stanice a úpravovne vody. Obzvlášť je dôležité riešiť zásobovanie úžitkovej a pitnej vedy v krízových situáciách. Pre riešenie týchto úloh je potrebné zamerať pozornosť na:

- Prieskum zdrojov vody a diagnostika jej kvality.
- Doprava a preprava vody.
- Úprava vody.
- Spracovanie, úpravu a doprava kalu ako zostatkového materiálu po čistení vody.

Pre potreby krízového programu bol riešený kontajnerový program. Technologické procesy úpravy vody a samotná upravená voda musí spĺňať rôzne požiadavky:

- voda musí mať vyhovujúcu akosť,
- musí byť dodávaná v dostatočnom množstve
- celkové výrobné náklady musia byť minimálne.

Akosť upravenej vody musí zodpovedať príslušným normám alebo smerniciam. Pre pitnú vodu platí Vyhláška SR č. 354/2006 Z. z. o požiadavkách na vodu určenú na ľudskú spotrebu a kontrolu kvality tejto vody.

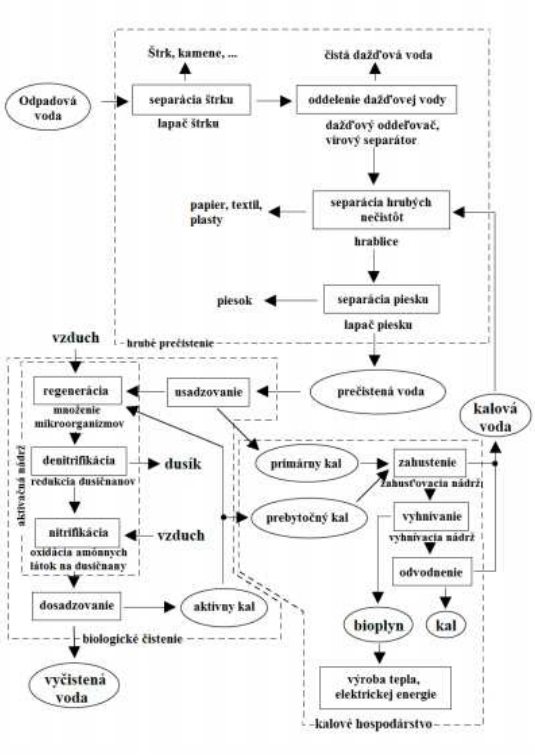

Obr. 9 *Bloková schéma čističky odpadových vôd [11]*

6 Smerovanie vývoja FŠT z pohľadu možného zapojenia sa do projektov

Práce na Katedre automobilov a špeciálnej techniky FŠT TnU AD v Trenčína v oblasti vedecko výskumnej činnosti predpokladáme do budúcna smerovať na pokračovanie v riešení:

- Kontajnerového programu z pohľadu dopravy a manipulácie, zodolňovaní balistickou ochranou pre krízový manažment a potreby obrany štátu.
- Štúdie a navrhovanie inteligentných obnoviteľných zdrojov elektrickej energie zabudovaných na mobilných prostriedkoch.
- Zámysel riešenia zabezpečenia pitnou a úžitkovou vodou mobilnými prostriedkami.
- Práca s vysokoenergetickými materiálmi ako predurčenými pre potreby krízového manažmentu a pre potreby obrany štátu.

Do budúcna je predpoklad navrhnúť a podať projekty so smerovaním:

- Návrh budovania Výskumného a vývojového centra zbraňových systémov Trenčianskej univerzity Alexandra Dubčeka v Trenčíne, DMD GROUP, A.S. a Konštrukty-Defence, A.S. v Dubnici nad Váhom.
- Návrh a riešenie zodolneného mobilného prostriedku na bázy ľahkého a stredného kolesového bojového vozidla ako nosiča riediaceho variabilného systému.
- Návrh a riešenie logistického vybavenia mobilného topografického pracoviska riadenia a vyhodnocovania krízovej situácie s využitím moderných prostriedkov informatiky a kumunikácií.

7 Záver

Potreba vedy, výskumu a vzdelávania v oblasti špeciálnej techniky je evidentná. Snahám premenovať špeciálnu techniku iným spôsobom môžeme predísť jej komplexným definovaním, zodpovedajúcim súčasným potrebám vedy, výskumu a praxe. Následne na to spracovaním a vydaním vhodnej encyklopedickej publikácie monografického typu, v ktorej bude problematika špeciálnej techniky komplexne charakterizovaná. Vzájomná spolupráca Trenčianskej univerzity Alexandra Dubčeka v Trenčíne so školami a zariadeniami na Slovensku a v zahraničí je predpokladom rozvoja špeciálnej techniky v komplexnom poňatí. Problematika materiálov a technológií pre špeciálnu techniku má v zahraničí i na Slovensku historické korene a v minulosti aj úspešnú históriu spolupráce. To je základ otvorenia riešenia ďalších, nových projektov riešených na medzinárodnej úrovni.

Predpoklady práce v oblastiach súvisiacich so špeciálnou technikou sú pomerne široké a je zrejmé, že autori ale aj fakulta, na ktorej pôsobia, v nich nájdu svoje miesto realizácie.

Literatúra

[1] Tatra MULTILIFT T – 815 8x8, [2014.11.12; 18:25]. Dostupné na internetehttp://www.mil.sk/6462/

[2] Podmienky bezpečnej manipulácie s kontajnermi, [cit. 2015.1.6; 12:00] Dostupnéna internete : http://www.vectura.sk/sk/files/manipulacia.pdf

[3] KOLMAŠ, Vojtěch – KOHOUTEK, Jaroslav – VYMĚTAL, Jindřich : Katalog automobilní a pásové techniky používané v AČR : Ministerstvo obrany České republiky – AVIS, Praha, 2007. 220 s. ISBN 978-80-7278-382-3

[4] CZE-Tatra-815-6MWR8T-45-324-12x12-1R, [cit. 2015.03.04; 11:45]. Dostupné na internete : https://forum.valka.cz/topic/view/36161/CZE-Tatra-815-6MWR8T-45-324-12x12-1R

[5] CZE-Tatra-815-6ZVR8T-43-400-10x10-1R, [cit. 2015.03.04; 11:45]. Dostupné na internete : https://forum.valka.cz/topic/view/34928/CZE-Tatra-815-6ZVR8T-43-400-10x10-1R

[6] Lipták, P.: Deterior. Dependability. Diagnostics. University of Defence. Brno 2015. ISBN 978-80-7231-431-7. P.135-140.

[7] Lipták, P., Kopecký, I.: Deterior. Dependability. Diagnostics. University of Defence. Brno 2015. ISBN 978-80-7231-431-7. P.127-134.

[8] Lipták, P., Barényi, I., Híreš, O.: Heat Affected Zone after Cutting of ARMOX Steels by Unconventional Technologies. In: Machine Modeling and Simulations 2011. - Trenčín : TnUAD, 2011. - 486s. - ISBN 978-80-8075-494-5. - p.367-372 AFD

[9] Lipták, P.: Aktivity FŠT v spolupráci na rôznych prezentáciách neuniverzitných organizácií FST activities in coordination with the various presentations of non-university organizations. Vyžiadaná prednáška. In: Trenasfer 2011. Elektronický zborník prednášok, 2011, Trenčín: TnU AD: 2011 – ISBN 978-80-8075-505-8, EAN 9788080755058

[10] Bačík, S. – Híreš, O. – Barényi, I. – Lipták, P. –Heděnec, J.: Degradation ofmechanical properties of ARMOX 500 Steel at welding. In: Trenasfer 2011. Elektronický zborník prednášok, 2011, Trenčín: TnU AD: 2011 – ISBN 978-80-8075-505-8, EAN 9788080755058

[11] Lipták, P., Kopecký, I., Krchňavý, M., Binka, I.: Projekt Investícia do budúcnosti. Firma BOST SR, a.s. Trenčín. Trenčín 2015.

Possibilities of materials improving for a ballistic protection of an individual

Peter Liptak[1], Ivan Kopecký[1]
[1]Faculty of Special Technology, Trencin University of Alexander Dubcek, Pri parku 19 Zablatie, 91106 Trencin, Slovak Republic. E-mail: peter.liptak@tnuni.sk, ivan.kopecky@tnuni.sk

The paper deals with possibilities in improving mechanical features of ballistic materials used for a ballistic protection of an individual. At present time these materials include materials as Kevlar and ceramics. A change in their features e.g. mechanical ones as well may occur after having irradiated them with accelerated electrons. So in a practical application it would be possible to improve a ballistic protection of a bullet-proof vest as well as to decrease a weight of a vest meanwhile keeping the protection class. The achieved results that are presented in the paper, can be used also in other applications, e.g. protective clothes used in industry.

Keywords: ballistic protection, mechanical features, kevlar, ceramics

1 Characteristics of a bullet-proof vest

Bullet-proof vest is a protective clothes designed so that it provides protection for its wearer against any kind of violent attacks. They are developed so that act as a shield against shrapnel debris from explosion, against hits from small arms, from an attack with a knife, a shell [1]. The vests are produced from many layers of a laminated or special woven fiber, resulting in an improved protection of a wearer. In some cases ceramics or metal is used, which with a soft layer provides a sufficient protection against larger calibres [2]. In a proposal for an advanced armor,there is a bullet-proof vest in combination with some other components, as e.g. combat helmets. Additional ballistic protective means for sides and shoulders are used in armed forces. Pyrotechnical units use heavy vests with helmets and a backbone protection [2].

Obr. 1. Kevlar vest with a helmet [3]

Ballistic bullet-proof vest is divided in two main cathegories: heavy and light bullet-proof vests. Heavy bulletproof vests act similarly as armours worn by medieval knights. These vests are rather heavy, however they provide for a better protection than soft bullet-prood vests. Individuals can wear this type of protection mainly in a high risk of attack, but for a daily routine it is more suitable to wear more flexible kinds of protection such as light vests.

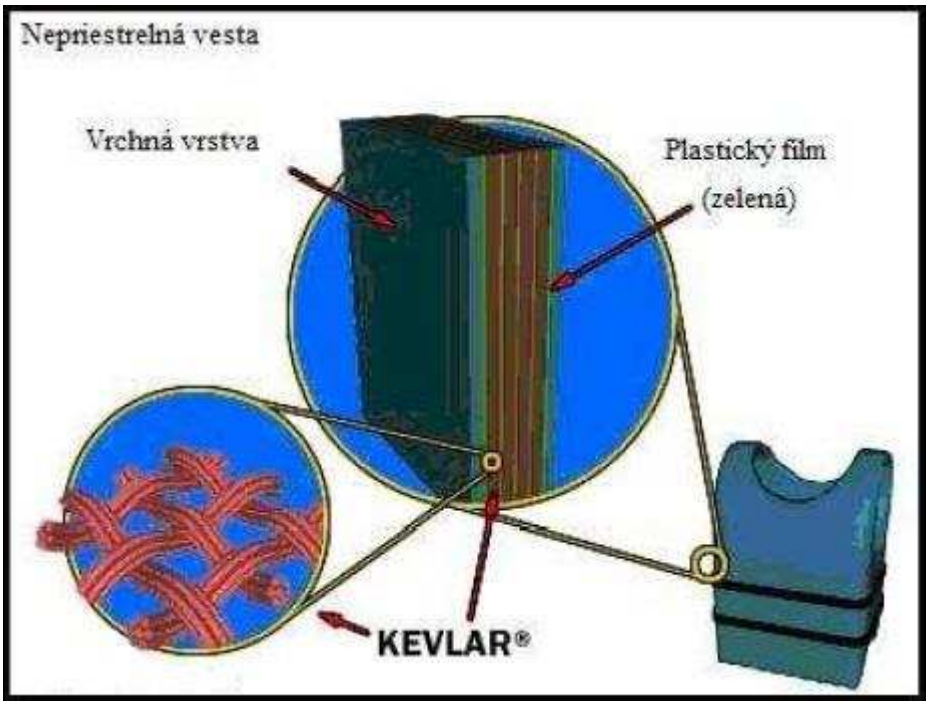

Fig. 2 Structure of a bullet-proof vest [3]

2 Structure and materials used in development of a bullet-proof vest

In the past various metallic and non-metallic materials were used for protective purposes. Special plastic materials are mostly used as special protective materials for further processing (into a form of textile fabric). They are of a high strength, resistance to dynamic impact effects, high tenacity, that predetermine them for an application as a ballistic protection. These materials have several times lower mass that steel while providing a high level of protection. There are semi-products produced from their fibers for manufacturing of protective clothes.

The synthetic protective materials being used are aramid and a special polyethylene. They are produced under various trade marks and they differ with their mechanical features. Nowadays the protective vests (bullet protection) is produced from the followig kinds of special protective textiles: Kevlar, Twaron, Dyneema, Spectra, GoldFlex.**WOVEN FABRIC**

Woven fabric is a sheet textile, which is formed through a reciprocal rectangular binding of warp and weft yarns. One set of yarns is arranged lengthwise and is called a warp. A warp is bond with another one, which is a perpendicular set, called a weft. The werf goes broadwise a woven fabric, from one edge to the other one. Thread count – firmness of a textile is a number of warp or weft yarns per 10mm (in softer woven fabrics) or on 100 mm (in thicker woven fabrics). Softness nad density of a woven fabric depends on a thread count.

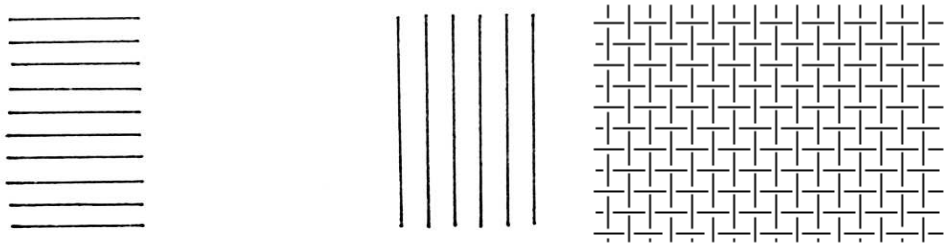

a) **b)** **c)**

Fig. 3 Basic set of yarns [10]

a) weft, b) warp [5], c) binding of a weft with a warp (tabby weave) [6]

Mechanical features of special textiles are, in addition to the material features, effected with a way of binding a werf and warp set of threads when woving (examples of binding a weft and warp are shown in Fig. 9), with an orientation of yarns of a protective layer and with folding of particular layers of a protective textile on each other. Synthetic materials being used are able to resist to projectiles with a velocity below 700 $m.s^{-1}$ in keeping textile´s features.

Three basic kinds of weave -tabby weave, twilled weave, basket weave, are used for woven special bullet-proof textiles (Twaron), or there are also their modifications.

NON-WOVEN TEXTILES

Non-woven textiles are textile products manufactured through more advanced manufacturing procedures. The most often their production is based on fibred layers. .Knitting and weaving are avoided in a manufacturing procedures as they are expensive operations. They are replaced by mechanical and chemical processes of the strengthening of fibred layers.

Advantages of non-woven textiles reside in a possible overlaying the textile and non-textile units and in a possible regulation of a fibred ratio and its form in a resulting product.

Textiles from a special polyethylene (Spectra and Dyneema) are not woven, two layers of parallelly aranged fibres are laid on each other, whereby they are reciprocally swivelled in 90°. The both layers of fibers are inserted between foils. Protective capability of Spectra, Dyneema does not change in different impact of a projectile. Kevlar, Twaron are more sensitive to a different impact angle of a projectile. Some authors point at some small blunt shock when Spectra, Dyneema were used in comparison with textiles made of Kevlar, Twaron [7].

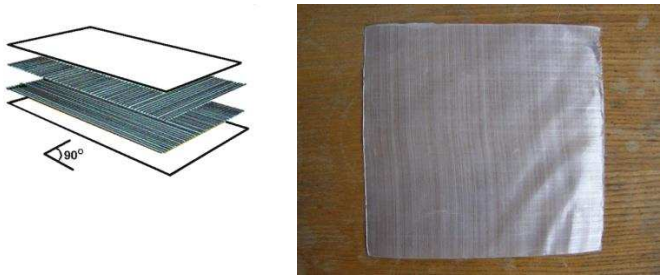

a) b)

Fig. 4 SpectraShield Protective material [10]
a) schematic representation of layers, b) spectraShield

ARAMID FIBRES

Aramid fibres are synthetic fibres resistant to heat, that are of a high tensile strength at an excellent ratio to its weight. They are used for a production of protective ballistic testiles and as a replacement of asbestos. The aramid assignment has risen as acronym from: „aromatic polyamide“ [9].

Aramides are generally created through a reaction between an amine and carboxyl groups of elements creating AABB polymere. This liquid chemical compound is then transformed into its solid form through twisting with the sulphur acid, which can be transformed into fibers, powder or cellu**lose during annealing treatment** [4]**.**

Features:

Aramid is sensitive to UV radiation, it has got a good abrasive resistance, it is resistant to effects of organic solutions and heat degradation. It is sensitive to humidity and salt. It is non conducting and it is lightly flammable [9]. Para-aramide fibres used for protective vests have a different structure comparing with original aramide material. Yarns are of a high ductility and a high Young´s modulus of elasticity. Specific volume weight of aramid is 1,4 g.cm^{-3} [10].

Kevlar

Kevlar is a synthetic para-amid fiber with a specific volume weight about 5-times higher that the one of steel. Kevlar is a type of an aramid, consisting of long polymere chaines with a paralel orientation. Strength is derived from intermolecular hydrogene bonds and aromatic stacked interactions among aromatic groups in adjacent yarns. These interactions are much more stronger than Van der Vaals interactions, that can be found in other synthetic polymeres. Para-aramid material is Twaron, as well.

Kevlar is an organic fibre, with combination of features enabling a high strength with a low weight, a high chemical resistance and a high resistance to slitting. Kevlar is non-flamable, it does not solve, and submerging into water has no effect on a yarn.

Kevlar is pretty resistant to high temperatures, it keeps its strength and flexibility even at cryogenic temperatures (-196 °C), it is little bit stronger at low temperatures. Tensile strength is reduced at high temperatures by 10 ÷ 20 %, and its strenght henceforth decreases as early as after several hours. For example at 160 °C a decrease in strength by 10 % becomes evident after 500 hours. At 260 °C a 50 % decrease expresses after 70 hours. At temperature of 450 °C kevlar sublimates. Kevlar is not resistant to UV radiation. Ultraviolet component of solar radiation degrade and disintegrate Kevlar therefore a protection against UV radiation must be used. In case, that Kevlar is convoluted, the fiber has a high tensile strength (about 3000 MPa), relative density of 1,44 g/cm^3 and it does not corrode.

Fig. 5 Kevlar vest [1]

Tab. 1 Comparison of features of ballistic materials [7 - 9]

Material		Maximum strength (MPa)	Flexibility module (GPa)	Density (g/cm^3)	Start of a thermal degradation (°C)
Kevlar	Kevlar 29	3600	80.0	1.44	450
	Kevlar 49	3600	130.0	1.44	450
	Kevlar 149	3400	146.0	1.47	450
Twaron	Twaron 900	2800	65.0	1.44	450
	Twaron 930	3000	125.0	1.45	450
Nomex		700	17.3	1.40	350
Dyneema	Dyneema SK60	2800	88.0	0.97	152
	Dyneema SK76	3500	125.0	0.97	152
Spectra	Spectra 1000	3000	170	0.97	147

3 Irradiation of samples with accelerated electrons

Experiment results from knowledge on a modification of mechanical features of non-metallic materials, that had been exposed to irradiation through a linear electron accelerator and from official documents of the DuPont Company, that had executed a similar experiment on their Kevlar material.

Irradiation with electrone beam includes modification of materials through an electrone accelerator. The accelerators use similar technology as the first televisions using catode tubes (CRT).

Modification with electrone beam is used in industry mainly for:

- Spinning of polymere materials, to improve mechanical, thermic and chemical features**.**
- Degradation of materials due to recycling**.**
- Sterilization of medical and pharmaceutical products.

Spinning polymers in processing with an electron beam changes a thermoplastic material into thermoset. If the polymers are spinned, the molecular movement is prevented, so resistance to high temperature increases. This molecule lockout is an origin of all advantages of spinning, including improvement of the following features:

- Thermal resistance to higher temperatures, ageing, etc.

- Mechanical increase of tensile strength, resistance to abrasion, increased resistance to pressure, resistance to creep, etc.
- Chemical resistance to fatigue cracks, etc. [4].

Spinning is biding of adjacent molecules with bounds network induced in irradiation with an electron beam. Processing of thermoplastic materials through accelerated electrons results in improvement of these materials, e.g. increase of tensile strength and resistance to abrasion etc.

The polymers, that are usually bound through an irradiation process with beam of electron rays include polyvinylchloride (PVC), thermoplastic polyurethanes and elastomers (TPU), polybutyleneterephtalate (PBT), polyamids/nylon (PA66, PA6, PA11, PA12), polyvinylidenefluoride (PVDF), polymethylpentene (PMP), polyethylene (LLDPE, LDPE, MDPE, HDPE, UHMW PE), and ethylene copolymers, as ethylene-vinyl acetate (EVA) and ethylene-tetrafluoretylene (ETFE). Some additives are added into some polymers so that the polymer spins more easily through irradiation [5].

Irradiation was performed on the UELR-5-1S industrial accelerator.

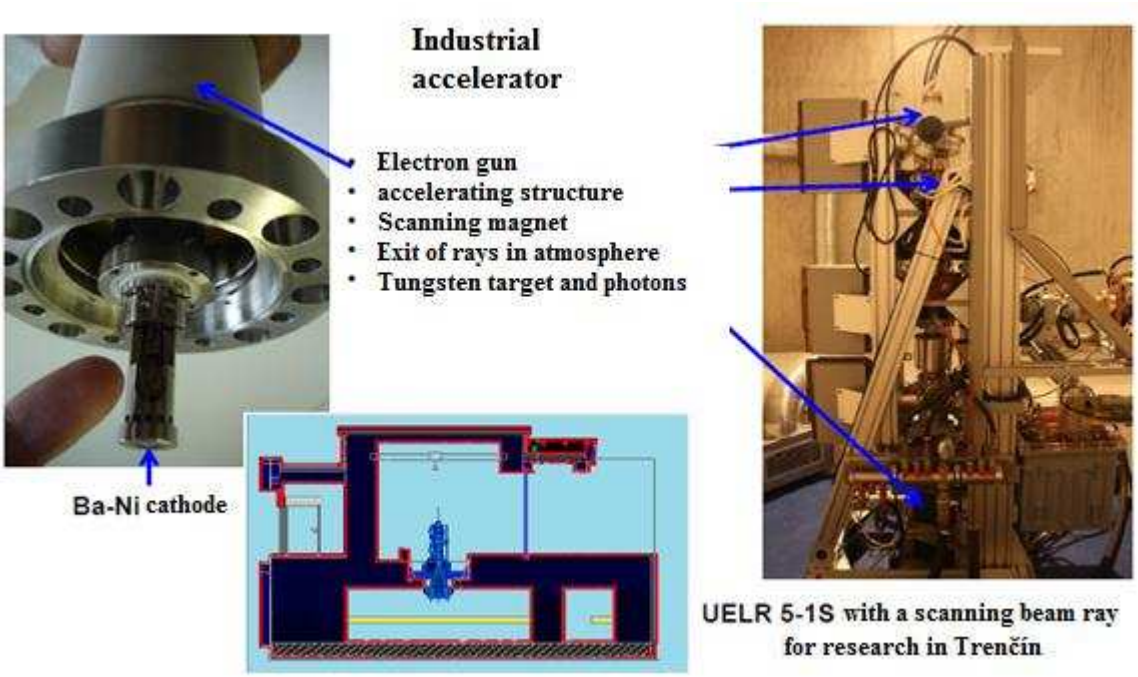

Fig. 6. UELR-5-1S accelerator with description of main parts [6, 8]

A precondition was defined as 4 levels of doses - 100, 300, 500 and 1000kGy.

4 Results of an experiment

The results from measurements were recorded for each level of dose irradiation in Table 2 and they are visualized in Fig. 7 and 8.

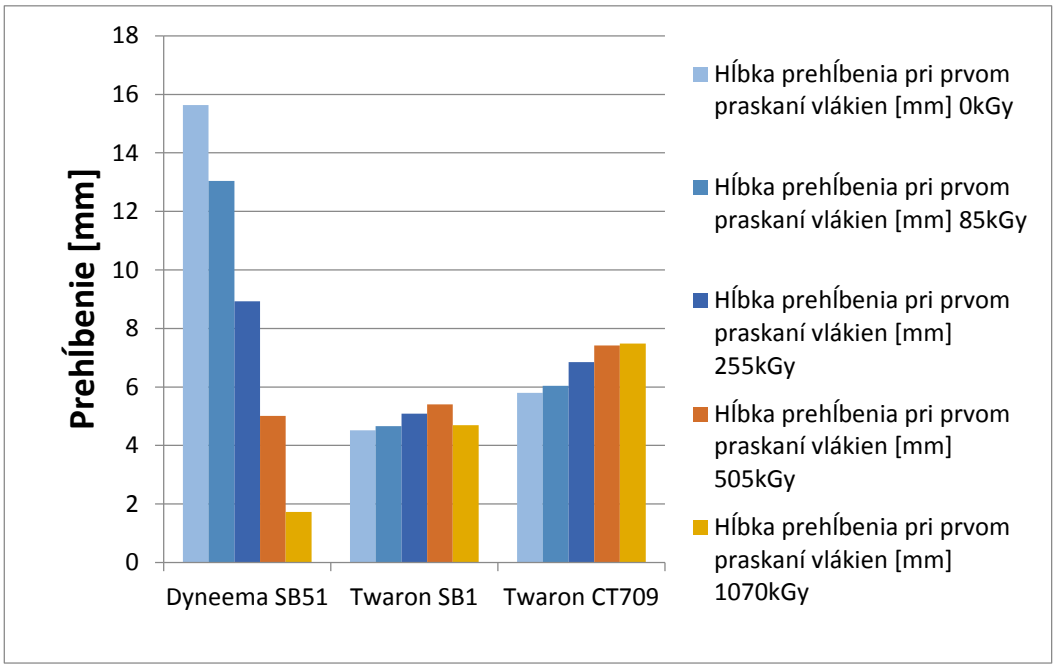

Fig. 7 Graphic comparison of measurements – Depth of a cavity in the first crack of fibres

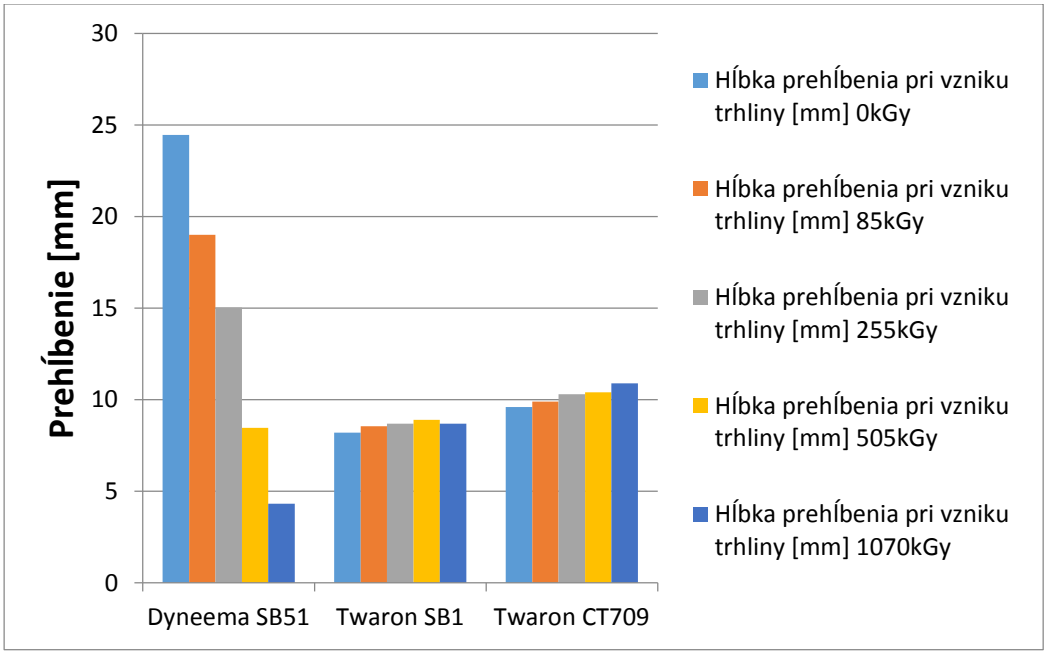

Fig. 8 Graphic comparison of measurements – Depth of a cavity in a crack rise

Tab. 2 Results of testing measurements by Erichsen for all levels of irratiation

Tabuľka nameraných hodnôt základných materiálov (bez ožiarenia)						
Druh materiálu	Hĺbka prehĺbenia pri prvom praskaní vlákien [mm]			Hĺbka prehĺbenia pri vzniku trhliny [mm]		
	Meranie č. 1	Meranie č. 2	**Median**	Meranie č. 1	Meranie č. 2	**Median**
Dyneema SB51	15,9	15,4	**15,6**	24,7	24,2	**24,5**
Twaron SB1	4,8	4,3	**4,5**	8,6	7,8	**8,2**
Twaron CT709	5,6	6,0	**5,8**	9,4	9,8	**9,6**
Tabuľka nameraných hodnôt ožiarených materiálov 85 kGy						
Druh materiálu	Hĺbka prehĺbenia pri prvom praskaní vlákien [mm]			Hĺbka prehĺbenia pri vzniku trhliny [mm]		
	Meranie č. 1	Meranie č. 2	**Median**	Meranie č. 1	Meranie č. 2	**Median**
Dyneema SB51	12,9	13,2	**13,0**	19,8	18,2	**19,0**
Twaron SB1	4,9	4,4	**4,7**	8,7	8,4	**8,6**
Twaron CT709	6,1	6,0	**6,0**	9,7	10,1	**9,9**
Tabuľka nameraných hodnôt ožiarených materiálov 255 kGy						
Druh materiálu	Hĺbka prehĺbenia pri prvom praskaní vlákien [mm]			Hĺbka prehĺbenia pri vzniku trhliny [mm]		
	Meranie č. 1	Meranie č. 2	**Median**	Meranie č. 1	Meranie č. 2	**Median**
Dyneema SB51	8,8	9,1	**8,9**	14,8	15,3	**15,0**
Twaron SB1	5,0	5,2	**5,1**	8,6	8,8	**8,7**
Twaron CT709	6,8	6,9	**6,9**	10,2	10,4	**10,3**
Tabuľka nameraných hodnôt ožiarených materiálov 505 kGy						
Druh materiálu	Hĺbka prehĺbenia pri prvom praskaní vlákien [mm]			Hĺbka prehĺbenia pri vzniku trhliny [mm]		
	Meranie č. 1	Meranie č. 2	**Median**	Meranie č. 1	Meranie č. 2	**Median**
Dyneema SB51	5,1	4,9	**5,0**	8,7	8,3	**8,5**
Twaron SB1	5,4	5,4	**5,4**	8,7	9,1	**8,9**
Twaron CT709	7,1	7,7	**7,4**	10,3	10,5	**10,4**
Tabuľka nameraných hodnôt ožiarených materiálov 1070 kGy						
Druh materiálu	Hĺbka prehĺbenia pri prvom praskaní vlákien [mm]			Hĺbka prehĺbenia pri vzniku trhliny [mm]		
	Meranie č. 1	Meranie č. 2	**Median**	Meranie č. 1	Meranie č. 2	**Median**
Dyneema SB51	1,8	1,6	**1,7**	4,4	4,2	**4,3**
Twaron SB1	4,8	4,6	**4,7**	8,6	8,8	**8,7**
Twaron CT709	7,4	7,6	**7,5**	10,6	11,2	**10,9**

5 Conclusions

The paper and a performed experiment were aiming to verify possibilities how to achieve features of materials being used in production of bullet-proof vests. It will enable an increase of a protection of a ballistic vest and a decrease of the vest weight, whereby the resistance class will remain the same. Achieved knowledge has proved a presumption, that irradiation can improve mechanical features of some chosen materials. A working place of authors is ready to go on in research in form of experiments in improving not only mechanical features of materials after having irradiated them with accelerated electrons. Application of such adjusted materials for practice is wide, e.g. reconnaissance equipment, automation equipment etc.

References

[1] KELIAR M.: Advanced ceramics for ballistic protection, Doksem 2013 – Technológ 2013 [konferenčný zborník]. Žilina: Žilinská univerzita, 03/2013, s. 117 – 120, ISSN 1337-8996.

[2] KELIAR M.: Inovations in the area of ballistic protection, Transfer inovácií 25/2013 - [konferenčný zborník], s. 150 – 152, ISSN 1337-7094.

[3] KELIAR M., MIKULČÍK J.: Tatraruv 250, ELENEM 2013: 1. Medzinárodná vedecká konferencia Aplikácia elektroniky, energetiky, einformatiky a mechatroniky v špeciálnej technike a krízovom manažmente. Trenčín: TnUAD, 2013. ISBN 978-80-8075-601-7.

[4] ZDENĚK JONŠTA.: „Technické materiály II", 126, 2012, ISBN 978-80-248-2574-8.

[5] JORMA JUSSILA.: „Wound ballistic simulation: Assessment of the legitimacy of law enforcement firearms ammunition by means of wound ballistic simulation." Helsinki: Academic Disertation, 2005, 112s, ISBN 952-10-2209-.

[6] PETR KLUČINA, ANDREJ ROMAŇÁK.: "Člověk, zbraň a zbroj v obraze doby 2: 17.-20. Století", 1. vyd. Praha: Naše vojsko, 1984,

[7] <https://www.iamtheironman.com/body-armor-materials.htm, [online], [citované 8.1.2014]

[8] <http://inventors.about.com/library/inventors/blforensic3.htm [online], [citované 29.12.2013]

[9] <http://www.safeguardarmor.com/articles/body-armor-materials/[online], [citované 4.2.2014]

[10] Šprync, E., Foltýn, J. „Textilné materiály", Bratislava: Alfa, 1991.351p.ISBN 80-05-00796-5.

OLYMPUS®

Your Vision, Our Future

Videoskop IPLEX NX

Ideální kombinace vysoce kvalitního obrazu s intuitivním uživatelským prostředím, ergonomického designu a odolnosti - to je nový videoskop Olympus IPLEX NX. Umožňuje měření hloubky defektu použitím stereoskopického zobrazení, disponuje různými měřícími nástroji pro efektivní hodnocení kontroly. Maximální komfort obsluhy, jednoduchost a ergonomie z IPLEX NX činí ideální nástroj pro časově náročné inspekce.

LEXT OLS 4100

je unikátní, přesný 3D laserový měřící konfokální mikroskop s rozsahem zvětšení 50x až 17.280x. Vytváří ostré a kontrastní snímky díky funkci super HDR (High Dynamic Range). Umožňuje provádět vysoce spolehlivé, opakovatelné měření v osách X, Y a Z s garantovanou přesností měření 12 nm. Je ideální volbou pro sledování textury povrchu včetně plnohodnotného měření drsnosti, disponuje kalibračním certifikátem.

OLYMPUS OMNISCAN MX2

Nedestruktivní testování materiálů s odolným a snadno přenosným OmniScan MX2 PA2 s Phased Array modulem druhé generace umožňuje rychlé skenování i záznam dat a nabízí výkonné softwarové funkce pro nedestruktivní zkoušení PA i TOFD současně. Přináší další výrazný posun v efektivitě zkoušení při zachování preciznosti v pokročilých AUT i ve standardních aplikacích jako je defektoskopie tavných svarov ých spojů, zkoušení kompozitů, testování korozního poškození apod.

Optodigitální mikroskopy DSX

Vytváří nový standard pro materiálové aplikace, který umožňuje získání výsledků na špičkové úrovni v minimálním čase a s minimálními nároky na obsluhu, včetně garantované přesnosti měření vzorků a to i ve 3D. Inteligentní automatizace systému včetně Nomarského diferenciálního kontrastu, polarizace či unikátní kombinace světlého a temného pole a jednoduchost a přesnost kalibrace celého systému je základem přesných a opakovatelných výsledků měření odpovídajících mezinárodním standardům a certifikátům.

Scientific Solutions Division

Olympus Czech Group, s.r.o., člen koncernu

Evropská 176/16, 160 41 Praha 6 | Tel.: +420 221 985 211 | info-industrial@olympus.cz | www.olympus.cz